Winter 12-15-2022

# The Impact of Nucleolar Stress on Thymocyte Development and T Cell Acute Lymphoblastic Leukemia Transformation

Joseph Ryan Krambs
*Washington University in St. Louis*

WASHINGTON UNIVERSITY IN ST. LOUIS

Division of Biology and Biomedical Sciences
Molecular Genetics and Genomics

Dissertation Examination Committee:
Daniel C. Link, Chair
Grant A. Challen
Timothy J. Ley
Laura G. Schuettpelz
Hani S. Zaher

# The Impact of Nucleolar Stress on T Cell Acute Lymphoblastic Leukemia Transformation

by
Joseph Ryan Krambs

A dissertation presented to
The Graduate School
of Washington University in
partial fulfillment of the
requirements for the degree
of Doctor of Philosophy

August 2022
St. Louis, Missouri

# Table of Contents

# List of Figures

# Acknowledgments

The completion of this Ph.D. thesis work and doctoral dissertation was an impossible undertaking made possible by the immeasurable support and encouragement I received from countless individuals and institutions over the last thirty years.

The fact that this document exists is a testament to Ludwig and Karin Krambs; Joseph and Delores Smid; Sabine and Mathew Smid; Katrin Schöffler; Kenny, John, and Terry Smid; Sarah, Brandon, Leiah, and Parker Vogel; Mary Henry, Alexander Krambs, Juda and Elijah Hayes, Abel Henry, and James Rowe; Emelia and Austin Reinoehl; Natalya and Justin Pack; Hannah Smid; Melanie, Wayne, and Linda Sparks; Martha Sparks; Kathleen Snyder; Richard and Janet Snyder; Trey Bonner; Greg, Valerie, Joshua, and Lizzie Dunn; Renee Sears; Josh Jang; Luis Sandoval; Jessica Palacios-Gomez; Jantz Chapel; Cecil Cole; Florian Stroich; Rene, Kathrin, and Pierre Behrendt; Cathy Smid; Kenny, Gina, and Robert Link; Martín Morales; the Texas Rangers search-and-rescue team; Mrs. Dietz; Herr Riele; The Long Beach Homeless Shelter; Angel Martinez; Mrs. Zarzicki; Mr. Robertson; the Johns Hopkins University Center for Talented Youth; The Bread of Life Rescue Mission; Roane State Community College; James Condon; Middle Tennessee State University; Brian Robertson; John Vile; Philip Phillips; Susan Lyons; Marsha Litchfield; Washington University School of Medicine; Jim Skeath; John Majors; Peter and Bonnie Burgers; Roberto Galletto; Melanie Relich; Dana Kharibian; Grazia Abou Ezzi; Terrence Wong; Alun Carter; Michael Zhang; Robin Yao; Amy Schmidt; Jun Xia; Darlene Monlish; Hani Zaher; Grant Challen; Timothy Ley; Laura Schuettpelz and especially Daniel C. Link.

I was raised by my resilient eternally optimistic parents, Sabine and Mathew, alongside my five fiercely independent sisters, Sarah, Mary, Emelia, Natalya, and Hannah. To make ends meet,

we lived an itinerant lifestyle, moving from Kansas to Texas, Iowa, Germany, California, Nevada, Arizona, and Tennessee, never living in any one location more than a year. More often than not, we went without food or basic amenities; several times we were homeless; several more, I was made a ward, placed under the guardianship of strangers, to pursue my education, living away from my family for part of my formative years. Across more than ten states, I attended nine elementary schools, five middle schools, three high schools, and three colleges, working while homeless to pursue my education. As a first-generation American and first-generation college student, I experienced many missteps and setbacks in college. After only one semester of college, I could not continue my education because of a financial hold on my transcripts. With my academic pursuit on indefinite hold, I experienced varying levels of depression and shame. Ultimately, I worked three jobs, including twelve-hour shifts at a factory, to purchasing my academic transcript and continue in college. Needless to say, the path to my Ph.D. was never easy, and often uncertain.

I mention all of this to acknowledge and highlight the immense effort of so many people who have worked to make this a reality, and it starts with my family.

All of the good in who I am, and everything about the person I want to be, is a direct reflection of my family – my grandparents, mom, dad, sisters, wife, in-laws, aunts, and uncles. I have been blessed with a family that has been everything I have ever needed and more. My family is resilient, nurturing, gentle, dysfunctional, insightful, observant, patient, generous, strong, sentimental, passionate, driven, creative, inspiring, and so much more.

Mom, thank you for being my shelter and refuge when I was young. I am so awe-inspired by you. I don't know how you managed it all. I can barely keep up with my family of two, but you raised six well-grounded independent (rebellious) kids while working from sunrise to sunset.

I know you sacrificed a lot to make sure we were taken care of, and I can't thank you enough for protecting and comforting us. Thank you for making sure we were always able to pursue every opportunity given to us and thank you for giving me the freedom to try, literally, everything skateboarding, surfing, snowboarding, swimming, guitar, basketball, track and field, football, chess club, math club, theater, spelling bees, odyssey of the mind, baking, cooking, student government, and community service. No matter what my interests, you were always right beside me cheering me on. I worked hard and believed I could be the best, because you told me I was the best. You showed me what it means to work hard, and you helped me reimagine my potential. What's more, you showed me the good work we can do in others' lives. You are the most giving person I know; I have yet to see a depth to your generosity. You routinely drop everything you're doing to make sure others are okay, even if it means putting yourself in danger (ehhhm, answering the phone while balancing on top of a ladder when you're afraid of heights, because you thought you kiddo was in trouble). You are the most nurturing, caring, compassionate, benevolent person I know, and you have always been that way in the face of so much adversity. Thank you for setting the standard for me to strive toward and for being the reminder of how much good there is in the world.

Dad, thank you for always challenging me at my level, pushing me to always be better. I wish I had your tact and insight; you always knew exactly how to motivate me, to help me understand and think about things outside of myself, to take stock of what others are feeling, and to accept necessary consequences. I owe my sense of curiosity to you. Thank you for reading to me (even if it was out of an encyclopedia sometimes) and thank you for entertaining every hairbrained scheme I ever had – from throwing away all of your personal items when you first moved in to using perforated edges to pay for ice cream. Dad, I miss your lectures, and I know

that, even without the PhD or college degree, you will always be smarter than me. That's why I have to keep working, because learning any new thing brings me closer to you.

Opa, ich habe seit langem vorgehabt, mich hinzusetzen und Dir einen Brief zu schreiben, auch wenn es spat ist. Ich hatte nie die Chance, mit dir zu sprechen, als ich klein war. Ich wünschte, Mama hätte uns Deutsch beigebract, aber ich verstehe, dass es schwierig war. Ich möchte die verlorene Zeit aufholen, was noch wichtiger ist, ich möchte dich kennen lernen. Ich habe mein ganzes Leben damit verbract, Dich zu bewundern, aber ich weiß nicht viel über dich. Ich möchte gerne mehr über Deine Erfahrungen und Deine Erlebnisse erfahren. Ich weiß, dass du sehr großsügig bist und du deine Familie immer an erster Stelle setzt. Du bist einer der fleißigsten Personen, die ich kenne, trotzdem nimmst Du Dir Zeit für die Liebe und die Familie. Ich habe seit langem, mich einfach hinsetzen wollen, um mit dir zu sprechen. Nichts würde mich glücklicher machen im Leben, also eine Flasche Rum oder ein paar Bier mit dir zu teilen und zu hören, was du zu sagen hast, und das ohne Verständigungsprobleme. Opa, ich möchte dir danken. Dir ist es vielleicht nicht bewußt, aber deine Anwesenheit und die Art, wie du bist, gab mir Kraft, also ich jung war. Ich bin mir nicht sicher, ob Mutter dir damals sagte, wie es in unserem Haus zuging, aber du sollst Wissen, daß mitten in all der Unsicherheit während meiner Kindheit, gabst Du mir Trost und Hoffnung. Wann immer du um uns herum warst, fühlte ich mich geborgen, und du gabst mir das Gefühl der Sicherheit. Ich lebe das Beispiel, das Du mir damals vorlebtest, das Beispiel von Respekt, Großzügigkeit, Richtung und Geduld. Vor allem du zeigtest mir, dass es gute Menschen in der Welt gibt. Es mag sein, daß ich nun sehr sensibel klinge, aber ich liebe dich. Ich liebe dich mit meinem ganzen Herzen, und ich kann mir nun vorstellen, wie du dies mit einem Lächeln und einer Handbewegung abschüttelst. Opa, du verdienst es geliebt und verehrt zu warden von deiner ganzen Familie. Du arbeitest unermüdlich daran, uns zu unterstützen, und du

unternimmst alles, um für uns da zu sein. Ich weiß, dass ich ohne dich nicht so wäre wie ich es heute bin. Also ich ohne Richtung war, geschweige denn ohne Lebenserfahrung, kamst Du und Du gabst mir Hoffnung. Du zeigtest mir, was es bedeutet gütig zu sein, und du gabst mir etwas wo nach ich leben konnte. Ich kann nicht alles vermitteln, was ich in diesem Brief sagen möchte, aber ich hoffe, dass Du aus diesem Brief erkennst, daß es sonst niemand in diesem Leben gibt, den ich mehr Achtung schenke als Dich.

Melanie, you are the better scientist. Unintentionally (or maybe intentionally), you show me my limitations and help me exceed them. Somehow you always manage to break through my stubbornness, and it is always to my benefit. I know that the scientist, husband, gardener I am capable of being today is only possible because of you. I know it's a cliché, but you complete me. Rather, you make me the best version of myself and show me how to be better. You are patient when I am restive. You are calm when I am overwhelmed. You are my voice when I need an advocate. You might point out these shortcomings, but it is while you're simultaneously lift that burden from me. You have given me so much love and support without batting an eye. You have been here, reassuring me, since my first failed graduate school course, and you were the driving force behind continuing my education in medical school. You cried with me and held me when my dad and Opa died, and you never hesitate when my family needs a place to stay. You have blessed my life, and you have made all of this possible today. Thank you for letting me grow together with you. I know I don't always make life easy. Sometimes (most times), I make the worst decision we could have made, but you let me make that decision. You are my pillar, and I know that we can accomplish anything together – I just might be a few years behind you.

I am always so inspired by my sisters, Sarah, Mary, Emelia, Natalya, and Hannah. They bear burdens that to me are unimaginable, and they are still able to pour love into everything they

do. Their love and patience is evident in the sweet innocent demeanor of my nephews and niece, and it's evident in the time they take to make spontaneous phone calls and their showing interest in the things I like (even though I'm a giant nerd and like some of the most convoluted stuff around). The thanks I owe to your love, care, and support is incalculable. You have encouraged me from the beginning, and you have continued to support me throughout my time in college and graduate school. Thank you so much for helping me realize a dream of mine that seemed so uncertain. You were there in the beginning, and you have always been my biggest advocates. I think most siblings would jump at the chance to pick on a nerdy one, but you have always supported me, and your enthusiasm in what I pursue has never waned. I love you Sarah, Mary, Emelia, Natalya, and Hannah! I think we have an awesome relationship, but I'm still so inspired by you to be better – a better man, brother, and uncle.

Lastly, I would like to personally thank Dan for welcoming me into his lab so many years ago (and putting up with me ever since). Dan you are, of course, an outstanding scientist, as you have provided seminal work to the field of hematology. As well as being a world-class scientist, you are an genuine mentor, advocate, friend, and cheesehead (I won't fault you for that). In fact, one of my favorite times to be in lab is during football season. It's unfortunate that the Packers and the Titans never made it to the Super Bowl during my time in lab, but it was great watching them play during the regular season, knowing that you were probably cursing and celebrating the Packers as much as I was the Titans. Besides football, I know you enjoy watching the St. Louis Cardinals. Someone mentioned to me once that I should read "The Cardinals Way" by Howard Megdal, and in this book, Howard Megdal describes how the Cardinals achieved monumental success, culminating in the 2004 and 2006 World Series Championships. Their success came by way of brilliant management, insightful analytics, and a cohesive team culture. They call it, the

Cardinal way. I'm not sure if you've read this book, but I do believe the Cardinals may have modeled their success after you. It really has been a blessing to be mentored by you, learning how to precisely conceptualize major questions and execute experiments carefully and consistently. Coming into graduate school, I had basic lab skills, but I knew next-to-nothing about developing hypotheses, conducting experiments, or interpreting data. You taught me the nuances of rigorous scientific research by asking me to interpret data (data that were often counterintuitive and negative – that only reinforced the learning). Dan you are absolutely brilliant. Thank you for letting me be a part of the lab and well preparing me for the next stage of my career.

Finally, I am so thankful for the support and invaluable guidance of my committee members, Tim Ley, Laura Schuettpelz, Gran Challen, and Hani Zaher. Without your support, I would not be ready to step into the Medical Scientist Training Program, and I would not be well equipped to navigate science and medicine. I am grateful to the many members of the Link lab who have helped train me and prepared me to undertake this PhD thesis work. Lastly, I would like to acknowledge the support I received from the graduate school of arts and sciences, the Chancellor's Graduate Fellowship Program, the Initiative for Maximizing Student Development, and the National Cancer Institute of the National Institutes of Health F31 Ruth L. Kirschstein Predoctoral Individual National Research Service Award for funding my PhD thesis project.

Joseph Ryan Krambs

*Washington University in St. Louis*

*August 2022*

***In Dedication***
***To those enduring the uncertain outcome of cancer treatment***

Waiting
In anticipation
Like an oak exhausted
By the weight of morning dew
Weary under veil of night
Searching the sky for something new.

Emerge, a long-sought glimmer of hope.

Emotion within me stirring
My resolve not yet returning

From what I've seen of life and love,
This new light shines above
Failed flames I knew of

Still, in this moment I wonder,
Can my nature conjure
Strength enough to wander

To break the sky and get through
So, I might begin anew.

ABSTRACT OF THE DISSERTATION

The Impact of Nucleolar Stress on Thymocyte Development and T Cell Acute Lymphoblastic Leukemia Transformation

by

Joseph Ryan Krambs

Doctor of Philosophy in Biology and Biomedical Sciences

Molecular Genetics and Genomics

Washington University in St. Louis, 2022

Professor Daniel C. Link, Chair

Increased Notch signaling is thought to be central to T-ALL pathogenesis, with activating mutations of NOTCH1 in more than 70% of cases, and Notch pathway activation due to mutations in FBXW7 in an additional 30% of cases. Increased Notch signaling results in markedly increased ribosome biogenesis, inducing a negative feedback loop called the nucleolar stress pathway. This is an evolutionarily conserved homeostatic pathway that is triggered by excessive ribosome biogenesis that serves to limit rRNA synthesis, protein translation, and ultimately cell growth. *CDKN2A*, encoding both *ARF* and *INK4A*, plays a key role in the nucleolar stress pathway. Activation of *ARF* and *INK4A* inhibits ribosome biogenesis and induces a p53-dependent growth arrest. Of note, biallelic deletions of *CDKN2A* are present in the majority (>80%) of T-ALL and universally in cases of T-ALL with NOTCH1 mutations. Also relevant are data showing that deletions of *CDKN2A* are in the founding clone, while mutations in *NOTCH1* are often confined to a subclone, suggesting that loss of *CDKN2A* is an early, potentially driver, event in leukemia transformation, while *NOTCH1* mutations are a later event. Together, these observations suggest

the hypothesis that **increased Notch signaling induces nucleolar stress in T cells and inactivation of the nucleolar stress pathway is essential to the molecular pathogenesis of T-ALL**. This hypothesis supports a model in which *CDKN2A* deletions are an early transformation event that generates a permissive cellular environment for subsequent activating *NOTCH1* mutations.

To test this hypothesis, we first developed a cell culture system to expand murine double positive T cell progenitors. Progenitor T cells are derived from cytokine stimulated CD117+ fetal liver cells grown in co-culture with OP9 cells expressing delta-like ligand 4. These cells differentiate in culture, giving rise to CD4+ CD8a+ (DP) thymocytes. To test how T-ALL relevant *NOTCH1* mutations alter DP thymocytes, we transduced these cells with retrovirus expressing empty vector, wildtype *NOTCH1*, or activating *NOTCH1* mutants (a*NOTCH1*) carrying hotspot mutations *L1594P* or *L1601P*. Increased Notch signaling, as evidence by Hey1 mRNA expression was confirmed in cells expressing a*NOTCH1*. Consistent with our model, expression of a*NOTCH1* induced nucleolar stress, as measured by induction of *ARF* expression, accumulation of 5' external transcribed spacer (ETS) containing pre-rRNA, and NPM translocation from nucleoli to the nucleoplasm. Induction of nucleolar stress in a*NOTCH1* expressing cells was associated with p53 activation, as measured by increased expression of p53 target genes $p21^{CIP1/WAF1}$ and *BAX*. Overall, expression of a*NOTCH1* had a negative impact on cellular proliferation with induction of apoptosis.

We next explored the impact of a*NOTCH1* mutants *in vivo*, using a retroviral transplantation model. In brief, $CD117^{+}$ cells were sorted from adult mice and subjected to two rounds of retroviral transduction for *NOTCH1* variants. These cells were transplanted into lethally irradiated mice and the contribution of NOTCH ($GFP^{+}$) expressing cells to hematopoiesis

examined over time. The contribution of a*NOTCH1* variants to hematopoietic stem cells (HSCs), common lymphoid progenitors (CLPs), and T cells was similar to input percentage and was stable over time. In sharp contrast, there was a near complete loss of a*NOTCH1* expressing myeloid and B cells. We next examined the impact of *CDKN2A* loss on HSC maintenance. In CDKN2A$^{+/-}$ or CDKN2A$^{-/-}$ mice the numbers of phenotypic HSCs were similar to wildtype mice. This is expected since the expression of *CDKN2A* is very low in HSCs under steady state conditions. In contrast, in competitive transplantation assays, both CDKN2A$^{+/-}$ and CDKN2A$^{-/-}$ HSCs consistently outperformed wildtype competitors. We hypothesized that replication stress induced by transplantation may activate *CDKN2A* expression in WT HSCs, suppressing their proliferation. To test this, CDKN2A$^{+/-}$ or CDKN2A$^{-/-}$ bone marrow chimeras were treated with 5-fluorouracil (5-FU) following stable engraftment. Consistent with our model, treatment with 5-FU resulted in significant (~5-fold) increase in CDKN2A$^{+/-}$ or CDKN2A$^{-/-}$ hematopoietic output. Finally, we modeled the impact of *CDKN2A* loss on aNOTCH-induced leukemogenesis by retrovirally transducing NOTCH variants into CDKN2A$^{+/-}$ or CDKN2A$^{-/-}$ HSPCs. Compared with wildtype, expression of a*NOTCH1* in CDKN2A$^{+/-}$ or CDKN2A$^{-/-}$ HSCs resulted in a marked expansion of HSCs (3.70 ± 0.22-fold) and CLPs (6.95 ± 2.28-fold) but did not rescue the aNOTCH-induced block in myeloid of B lymphoid differentiation. A tumor watch confirmed that *CDKN2A* loss strongly cooperated with aNOTCH expression to induce T-ALL in mice (incidence of T-ALL at 200 days of 17/17 (100%) in *NOTCH1 L1601P CDKN2A*$^{-/-}$ cell recipients vs 3/12 (25%) in *NOTCH1 L1601P CDKN2A*$^{+/+}$ cell recipients, P<0.0001).

In summary, these data provide support for a novel model of T-ALL leukemogenesis in which *CDKN2A* loss is an early event that provides a fitness advantage under conditions of replication stress that leads to an expanded pool of CDKN2A$^{+/-}$ (or CDKN2A$^{-/-}$) HSCs and CLPs.

Loss of *CDKN2A* provides a permissive cellular environment for activating *NOTCH* mutations by attenuating nucleolar stress. These data suggest that targeting the nucleolar stress pathway or ribosome biogenesis may have therapeutic activity in T-ALL.

# Chapter 1:

# Introduction to the Genetic Landscape and Molecular Biology of T Cell Acute Lymphoblastic Leukemia

## Preface

This chapter, as well as the summary chapter (Chapter 5) are dedicated to my PhD thesis work, investigating the role of nucleolar stress in T cell acute lymphoblastic leukemia transformation (Chapter 4). Chapters 2 and 3 are first-author works that have been previously peer-reviewed and published and are unrelated to T-ALL or nucleolar stress.

## 1.1. An Overview of T Cell Acute Lymphoblastic Leukemia

T cell acute lymphoblastic leukemia (T-ALL) is an aggressive hematologic malignancy characterized by the transformation and expansion of T cell progenitors. T-ALL comprises 10% to 15% of pediatric and 20% to 25% of adult cases of acute lymphoblastic leukemia.[1,2] A review of Seer-17 data from 2001-2007 shows that there are approximately 2,500 patients in the United States per year with T-cell lymphoblastic leukemia/lymphoma.[3] Approximately 45% of these patients are adults.

Patients typically present to the clinic with elevated white cell counts (as observed by complete blood count (CBC)). These elevated white cell counts are accompanied by a decrease in neutrophils numbers (neutropenia), platelet counts (thrombocytopenia), and red blood cell counts

(anemia). Upon further evaluation, it is often observed that T-ALL patients have mediastinal thymic masses, and in approximately 5% to 15% of cases,[4] neoplastic cells have infiltrated the central nervous system by the time of diagnosis. These clinical observations are similar, yet counter, to T cell lymphoblastic lymphoma in which T cell blasts (tumors) are present as a thymic mass but do not infiltrate the bone marrow to the same extent as T-ALL.

T-ALL is the culmination of acquired genetic aberrations that disrupt cell cycle gate keepers (tumor suppressors), enhance oncogenes, and alter differentiation pathways to exploit proliferation and survival signals that are responsible for thymocyte development. The reliance of T-ALL transformation on T cell developmental pathways is illustrated by the oncogenic signals found in T-ALL, namely the hyperactivation of NOTCH1, a key T cell fate and development signal, whose activating mutations are found in more than 70% of T-ALLs.[5-7] T-ALL tumors with activating *NOTCH1* mutations universally harbor deletions of the cyclin-dependent kinase inhibitor 2A (*CDKN2A*) locus, which encodes the tumor suppressors $p16^{INK4A}$ and $p14^{ARF}$.[8-11] In addition, *CDKN2A* loss is the most common genetic lesion in T-ALL, and its deletion is observed in approximately 80% of cases.[8-11] However, T-ALL genetic lesions are not limited to *NOTCH1* mutations and *CDKN2A* deletion, T-ALL is a heterogenous malignancy with a diverse array of genetic abnormalities.[12,13] T-ALL genetic lesions are broadly represented by chromosomal translocations with distinct gene-expression signatures and mutations and deletions that alter the cellular environment (signaling cascades, protein translation, and cell cycling).

Oncogenes in T-ALL are frequently driven by T cell specific transcription factors and regulatory elements through chromosomal rearrangements, with 50% of blasts from patients with T-ALL harboring chromosomal translocations.[14] Often, these rearrangements involve oncogene overexpression with juxtaposition to the T-cell receptor (TCR) locus, including the basic helix-

loop-helix (bHLH) factors: T cell acute lymphocytic leukemia 1 (*TAL1*),[15] *TAL2*,[16] lymphoblastic leukemia associated hematopoiesis regulator 1 (*LYL1*),[17] and *BHLHB1*;[18] LIM domain only (LMO) genes *LMO1* and *LMO2*;[19-21] the homeobox genes: T cell leukemia homeobox 1 (*TLX1*),[22] *TLX3*,[23] NK2 homeobox 1 (*NKX2-1*),[9] *NKX2-2*,[9] and homeobox A (*HOXA*)[24] and the myelocytomatosis (*MYC*)[25,26] and myeloblastosis (*MYB*) oncogenes.[14,27] However, rearrangements driving T-ALL are quite rare, representing 5% to 10% of cases of T-ALL.[12,13] More common, albeit still uncommon, are rearrangements involving the fusion of transcription factor proteins, including *PCIALM-MLLT10*, *STIL-TAL1*, *TLX3-BCL11B*, and *NUP214-ABL1*, which affects approximately 8%, 20%, 15%, and > 5% of patients, respectively.[28]

In addition to large structural genomic changes, T-ALLs present with a plethora of heterogenous mutations and deletions. The TARGET group recently confirmed the heterogeneity of lesions in T-ALL through extensive genomic analysis of 264 cases of T-ALL, including whole-exome sequencing, copy number analysis, single-cell sequencing, and RNA sequencing. In the TARGET study, more than 170 potential drivers of T-ALL were identified,[29] including mutations of many known genes known to drive T-ALL leukemogenesis, such as *NOTCH1*, *PHF6*, *FBXW7*, *USP7*, *PTEN*, *DNM2*, and *BCL11B*. The most prominent novel driver mutations discovered in this study include the genes *CCND3*, *MYB*, *CTCF*, *MED12*, *SMARCA4*, *CREBBP*, and *USP9X*. Although the tumors were genetically heterogenous, their alterations commonly targeted the NOTCH, PI3K-AKT-mTOR, MAPK, and JAK/STAT signaling pathways.

Unfortunately, unlike genetic aberrations in B-ALL, the vast majority of T-ALL associated genetic lesions are not useful in predicting outcome in T-ALL.[30] Historically, patients with T-ALL have had worse response rates and outcomes compared to B-ALL with early studies showing response rates of 10% in T-ALL compared to 40% in B-ALL.[31] This observation, along with early

clinical trials (the UKALL trials), led to intensified chemotherapy protocols for T-ALL treatment and subsequent improvement in outcomes. Current treatment consists of intense chemotherapy that is associated with acute and chronic life-threatening or debilitating toxicities.[32] Although five-year event-free survival is now 80% to 90% for children,[33-36] this rate deteriorates significantly with age: <40 years = 52.8%, 40-59 years = 37.6%, 60-79 years = 21.7%, and ≥ 80 years = 0%.[37,38]

Despite a steadily increasing event-free survival in pediatric patients, approximately 20% of pediatric and 40% of adult patients will relapse,[39,40] and the prognosis after relapse is dismal with three-year event-free survival of only 10% to 15%.[14,41-43] Additionally, the majority of relapses occur in patients predicted to do well based on favorable MRD response. The only treatment licensed for relapse or refractory T-ALL is an untargeted purine nucleoside analog, nelarabine. The goal of nelarabine treatment is to reduce disease burden so patients may undergo allogeneic hematopoietic cell transplantation (HCT). While HCT may be curative for relapsed T-ALL, in the largest study performed to date overall survival was only 24% after a median follow up of two years.[44] Although the underlying genetic makeup of T-ALL may not predict outcome, understanding the molecular mechanisms underlying T-ALL transformation may help identify novel targets for T-ALL therapy.

## 1.2. T-ALL Risk Assessment and Treatment Strategies

T-ALL treatment involves risk-assessed combination chemotherapy for two to three years. Although slight differences exist between treatment strategies internationally, outcomes are relatively similar with the most significant predictor of outcome being minimal residual disease (MRD) at the end of consolidation with MRD directing treatment strategy. The Children's Oncology Group stratifies risk into three categories:

- Standard risk – day 29 marrow with < 5% blasts; day 29 central flow cytometry-based MRD < 0.01%; <5 WBC/μL and no blasts in the cerebrospinal fluid (CSF); no testicular disease and no steroid pretreatment
- Intermediate risk – day 29 marrow with < 5% to 25% blasts; day 29 central flow cytometry-based MRD ≥ 0.01%; end-of-consolidation MRD < 0.1%; any CNS and testicular disease status and any steroid pretreatment status
- Very high risk - day 29 marrow with > 25% blasts by morphology or end-of-consolidation MRD ≥ 0.1%

Given the dismal prognosis for refractory disease and after relapse, much attention has been given to frontline strategies, including investigating new therapeutic agents, and optimizing conventional agent use, e.g., corticosteroids (dexamethasone versus prednisone).

### 1.2.1. Dexamethasone Reduces Central Nervous System Relapse and Enhances Event-Free Survival in T-ALL

Glucocorticoids (dexamethasone and prednisone) play an essential role in acute lymphoblastic leukemia (ALL) treatment. Several recent clinical trials in B- and T-lineage ALL have compared dexamethasone vs prednisone during the induction phase of treatment.[33,45-48] The advantage to dexamethasone is its longer half-life and superior control of central nervous system leukemia infiltrates relative to prednisone. However, dexamethasone treatment is accompanied by higher rates of infectious toxicity.[49] Despite these higher rates of infection, several trials have supported the use of dexamethasone in T-ALL.[33,36,47]

The recommended use of dexamethasone follows several clinical trials, demonstrating efficacy against CNS leukemia relapse,[50] reduced risk assessment (relative to prednisone),[51] and reduced rates of relapse.[51] Additionally, five-year event-free survival in the UKALL 2003 trial, where patients were given dexamethasone as the sole corticosteroid during therapy, was reported as 81.2% with a 3.5% risk for CNS relapse.[34,36] Further support for dexamethasone was provided in the AEIOP-BFM 2000 trial,[51] where dexamethasone replaced prednisone during induction. Dexamethasone treatment at induction corresponded with relapse rate reductions from 17% to 7% and significant improvements in five-year event-free survival compared to prednisone – dexamethasone five-year event free survival equaled 87.8% ± 2.8% whereas prednisone five-year event free survival equaling 79.2% ± 3.4%.

## 1.2.2. Nelarabine Improves T-ALL Response Rates

Despite a steadily increasing event-free survival in pediatric patients, approximately 20% of pediatric and 40% of adult patients will relapse,[39,40] and the prognosis after relapse is dismal with three-year event-free survival of only 10% to 15%.[14,41-43] Given the dismal event-free survival and overall survival rates of relapse or refractory T-ALL, a large effort has been undertaken to improve induction treatment strategies. Nelarabine is a purine nucleoside analog which is cytotoxic to T-lymphoblasts and is also the only treatment licensed for relapse or refractory T-ALL with a 55% response rate.[52]

In an effort to maximize induction treatment efficacy for high-risk T-ALL patients, clinical trials were established to investigate nelarabine as a frontline therapy. The Children's Oncology Group study, AALL0434, enrolled 1,895 patients, ranging from one to thirty years of age. Patients were randomly assigned to receive nelarabine in combination with a modified Berlin-Frankfurt-

Münster (BFM) regimen. During the safety phase, 94 patients were assigned to this arm of the study with no increased risk of adverse effects.[53] Published results demonstrate that adding nelarabine to standard induction chemotherapy regimens improves survival for both pediatric and young adult patients.[54]

## 1.2.3. Limitations of Immunotherapy in T-ALL

Immunotherapy has revolutionized oncologic treatment over the last decade.[55] Effective immunotherapies – utilizing chimeric antigen receptor modified T cells (CAR-Ts), monoclonal antibodies, and bispecific T-cell-engaging antibodies (BiTEs) – have developed to fight B cell acute lymphoblastic leukemia (B-ALL), however immunotherapeutics have been ineffective against T-ALL for a variety of reasons. One of the greatest challenges facing T-ALL targeting immunotherapies is that lack of target antigens, distinguishing T-ALL from normal T lymphocytes. Additionally, the infectious toxicity that accompanies T cell depletion is life-threatening, as demonstrated by infectious toxicity accompanying dexamethasone treatment.[49] To date, the only immunotherapy therapy studied in clinical trials was the monoclonal antibody alemtuzumab, and this trial was shut down due to infectious toxicity.[55] In addition to the challenge of infectious toxicity, immunotherapies designed for T-ALL treatment undergo unintended fratricide (self-killing), resulting in an inability to harvest sufficient numbers of T cells for therapy. Cooper *et al*. presented the first clinically feasible adoptive T cell gene therapy for T cell malignancies in a preclinical mouse model, developing a third generation CD7-CAR (UCART7) that is resistant to fratricide.[56] UCART7 is currently under clinical investigation.

## 1.2.4. Relapsed T-ALL Outcomes

Despite a steadily increasing event-free survival in pediatric patients, approximately 20% of pediatric and 40% of adult patients will relapse.[39,40] Disease recurrence typically occurs within two years of diagnosis, and survival rates remain less than 25%.[57] The only curative therapy remains allogeneic hematopoietic cell transplantation, and the challenge of successfully getting patients into remission remains a prerequisite. Across studies, remission rates for relapsed or refractory T-ALL are dismal at approximately 30%.[58] In the PETHEMA study, the median survival after relapse was between four and five months with overall one-year survival at 24%. Second remission was achieved in 112 out of 248 patients (45%), following intensive second line treatment. Despite achieving second remission, outcomes were dismal with a median disease-free survival between five and seven months. In total, twenty-eight out of 113 relapsed patients who achieved a second remission lived without further relapse after a median follow-up of six years.

## 1.2.5. Molecular Mechanisms Underlying T-ALL Resistance and Relapse

Historically, patients with T-ALL have had worse response rates and outcomes compared to B-ALL with early studies showing response rates of 10% in T-ALL compared to 40% in B-ALL.[31] The initial observed difference between T cell and B cell acute lymphoblastic leukemias treatment responses[31] is most likely reflective of the different molecular mechanisms and cellular environments underlying T cell and B cell ALL disease progression. T-ALL, specifically, features recurrent mutations and deletions of *PTEN* and activation of the AKT pathway, which has been shown to induce glucocorticoid (dexamethasone and prednisone) resistance in T-ALL.[59]

Clinically, *PTEN* mutations have been associated with poor response to prednisone treatment.[60] AKT1 could lead to glucocorticoid resistance by directly phosphorylating the glucocorticoid receptor, impairing glucocorticoid signaling.[59]

Genomic studies have started to uncover the genetic basis of leukemia relapse and have indicated that clonal evolution and selection of genetic variants that drive chemotherapy resistance are prominent mechanisms driving disease progression in T-ALL. The most prominent variants among samples from relapse T-ALL represent disruption of chemotherapy responsive genes. For example, one of the most common variants (observed in 20% of samples from relapse T-ALL) is the gene *NT5C2*,[61] encoding a nucleotidase that has been shown to inactivate drugs utilized in the treatment of T-ALL (thiopurine nucleoside-analogues).[62,63] It goes without stating, that relapse T-ALL blasts harboring mutations of *NT5C2* acquire increased nucleotidase activity, and *in vitro* assays have demonstrated that *NT5C2* mutations commonly found in T-ALL confer chemoresistance when expressed in T-ALL lymphoblasts.[61] Additionally, relapse T-ALL samples harbor additional mutations which may confer resistance, including in signaling factors, such as *STAT5B* and *NRAS;* the master regulator of apoptosis, *TP53*, and epigenetic factors, including *SUZ12*, *WHSC1*, and *SMARCA4*.[61,64]

## 1.2.6. Clonal Evolution of Relapse/Refractory T-ALL

Deep whole genome sequencing[65,66] and single cell sequencing[67] of relapse T-ALL samples are providing novel insights into the resistivity and sensitivities of the pool of heterogenous T-ALL clones. Similar to T-ALL driver mutations, relapse clones harbor a plethora of mutations that alter signaling pathways, epigenetic regulation, and cell cycle control. Distinct from T-ALL

initiating mutations, relapse clones also acquire mutations that confer resistance to conventional cytotoxic chemotherapies, including *NT5C2*.[68,69]

As is frequently the case in clonal evolution, the dominant clone at relapse is absent or present as a minor clone at diagnosis, suggesting selective pressures of treatment may have conferred a fitness advantage to pre-existing clones or provided the appropriate environment for mutation acquisition.[26,70,71] It has been well established that mutations in relapse T-ALL, once acquired, are selected and driven by chemotherapy. This is exemplified by frequently recurring mutations in *KRAS*, *NRAS*, and *PTPN11* found in relapse clones.[71] Given the dismal outcome of relapse and refractory disease, it is vital to investigate individual treatment tailored to T-ALL clones, e.g., RAS pathway[72] and tyrosine kinase[73] targets. Deep sequencing and data mining of T-ALL relapse samples continues to generate hypotheses on the molecular mechanisms of T-ALL chemoresistance, and sequencing continues to uncover potential clinical targets.

## 1.3. Classification of T-ALL Subgroups

In addition to the heterogeneity of genetic lesions found in T-ALL, T-ALL itself can be divided into two separate clinically relevant disease subtypes – Early T lineage progenitor (ETP) T-ALL and canonical T-ALL (henceforth referred to as T-ALL). Diagnosis of T-ALL or ETP T-ALL is made based on a combination of surface marker immunophenotype and transcriptome features. Each, T-ALL and ETP T-ALL, features unique gene expression patterns and distinct immunophenotypes that correspond with the developmental stage at which leukemogenesis occurs.[8]

### 1.3.1. CD4$^-$ CD8$^-$ Early T-Lineage Progenitor (ETP) T-ALL

Early T-lineage progenitor (ETP) leukemias are similar in immunophenotype to cells at the earliest stages of T cell development in the thymus (CD4$^-$ CD8$^-$ cells), however ETP T-ALL gene expression patterns are similar to less committed hematopoietic progenitors, specifically hematopoietic stem cells and myeloid progenitors.[74,75] In addition to the unique gene expression pattern, relative to canonical T-ALL, ETP T-ALL also have a unique mutation spectrum with lower prevalence of *NOTCH1* hyperactivation or loss of the *CDKN2A* gene locus (commonly found in T-ALL). Instead, activation of other oncogenic transcription factors is commonly derived from their rearrangement to T cell receptor loci. These include the basic helix-loop-helix transcription factor genes *TAL1*,[15] *TAL2*,[16] *LYL1*,[17] and *BHLHB1*;[18] as well as *TLX1*,[22] *TLX3*,[23] *NKX2-1*,[9] *NKX2-2*,[9] and *NKX2-5*; the LIM-only domain genes *LMO1* and *LMO2*[19-21] and the *HOXA* homeobox genes.[24]

Additionally, ETP T-ALL is characterized by mutations commonly seen in myeloid leukemias, including signaling factors such as *NRAS* and fms related tyrosine kinase 3 (*FLT3*)) and epigenetic regulators (e.g., isocitrate dehydrogenase 1 (*IDH1*), *IDH2*, and DNA methyltransferase 3A (*DNMT3A*).[10,68] In addition to alterations in signaling factors and epigenetic regulation, ETP T-ALL has also been shown to mutate transcription factors associated with hematopoietic differentiation and T cell development, including runt related transcription factor 1 (*RUNX1*), GATA binding protein 3 (*GATA3*), and ETS variant 6 (*ETV6*)).[10,68] Although ETP T-ALL accounts for approximately 10% of pediatric T-ALL cases,[74] its incidence increases with age, accounting for approximately 40-50% of adult T-ALLs.[75]

### 1.3.1.1. ETP T-ALL Transcription Factor Tumor Suppressor Mutations

#### 1.3.1.1.1. ETV6

A key regulator of hematopoietic stem cell development is the ETS family transcription repressor ETV6.[76,77] Mutations of the *ETV6* tumor suppressor are present in approximately 25% of cases of ETP T-ALL. ETP T-ALL associated mutations of *ETV6* result in a truncated form of the protein which has been shown to be dominant-negative, abrogating the transcriptional repressor activity of wildtype ETV6.[75]

#### 1.3.1.1.2. RUNX1

Another key tumor suppressor and regulator of hematopoietic differentiation and development commonly mutated in ETP T-ALL is *RUNX1*.[78-80] RUNX1 represents one subunit of the core binding factor heterodimeric transcription factor involved in the development of normal hematopoiesis and associated with several types of leukemia. Somatic mutations in *RUNX1* are found in approximately 5% of T-ALLs.[68,81] However, these mutations are not observed in canonical T-ALL.

#### 1.3.1.1.3. GATA3

Specific to T cell differentiation, GATA3, plays a crucial role in the development of early T lineage progenitors (ETPs).[82] *GATA3* is recurrently mutated in the immature ETP T-ALL,[68] and mutations of *GATA3* typically present as heterozygous point mutations in the zinc finger DNA-binding protein domain, inhibiting GATA3's transcriptional program. The hotspot mutation of *GATA3* is found at residue R276 which is needed for DNA binding.[83]

#### 1.3.1.1.4. BLC11B

BCL11B is a Kruppel-like C2H2-type zinc finger transcription factor important for T cell differentiation. *BCL11B* is mutated in approximately 10% of T-ALLs.[84,85] Loss of *BCL11B* has been shown to arrest T cell differentiation at the DN2-DN3 stage of cortical thymocyte development,[86,87] and the tumor suppressor activity of *BCL11B* was first shown in mouse thymic lymphomas under ionizing radiation.[88]

#### 1.3.1.1.5. LEF1

Monoallelic or biallelic deletions of the *LEF1* locus are found in 10% to 15% of cases of T-ALL.[85] LEF1 is a member of the lymphoid enhancer factor/T cell factor (LEF/TCF) family of transcription factors.[89] LEF1 binds to a functionally important site in the T cell receptor-alpha enhancer and transcription of the WNT signaling pathway. T-ALL clones with *LEF1* mutations arrest at the early cortical thymocyte stage and exhibit elevated *MYC* expression.[85]

#### 1.3.1.1.6. WT1

Deletions and mutations in the tumor suppressor *WT1* are present in approximately 10% of T-ALLs.[90] Mutations of *WT1* in T-ALL typically present as heterozygous frameshift mutations that result in a truncated product. T-ALL associated *WT1* mutations have been shown to enhance oncogenic expression of the *TLX1*, *TLX3*, and *HOXA* oncogenes.[90] *WT1* has been implicated in hematopoietic stem cell quiescence.[91]

### 1.3.1.2. Alterations in Epigenetic Regulators are Prevalent in ETP T-ALL

A distinct feature of ETP T-ALL is its association with recurrent disruption of genes involved epigenetic regulation,[92] including

- **DNA methylation genes**
  - *DNMT3A*, *DNMT3B*, *TET1*, *IDH1*, *IDH2*
- **Histone methylation**
  - *EZH2*, *SUZ12*, *MLL1*, *MLL2*, *DOT1L*, *SETD2*, *EED*, *JARID2*, *UTX*, *JMJD3*, *NSD2*
- **Histone acetylation**
  - *CREBBP*, *EP300*, *HDAC7*, *HDAC5*, *NCOA3*

Significantly, current data suggest that epigenetic dysregulation may correlate with poor prognosis. For instance, global DNA hypomethylation has been associated with increased risk of refractory/relapse disease and poor outcome in T-ALL.[92] In B-ALL, similar alterations in genetic and genomic methylation have been shown to lead to chemoresistance, however preclinical models suggest that these tumors may be sensitized to chemotherapy when treated in combination with epigenetic agents.[92] However, similar observations have yet to be made in relation to T-ALL.

#### 1.3.1.2.1. PHF6

PHF6 is a nucleolar protein which has been shown to be important for ribosome biogenesis and splicing.[93-95] However, PHF6 has also been implicated as an epigenetic modulator with functions in chromatin remodeling through its interaction with the NurD nucleosome repositioning and histone deacetylation complex.[93,96] PHF6 is frequently inactivated in T-ALL with mutations

and deletions of *PHF6* found in approximately 16% of pediatric and 38% of adult cases of T-ALLs.[97] Interestingly, *PHF6* is located on the X chromosome, and *PHF6* mutations are almost exclusively found in male patients with T-ALL.

#### 1.3.1.2.2. EZH2, EED, and SUZ12

One of the primary targets of T-ALL is the disruption of the polycomb repressive complex 2 (PRC2) which is shown to be disrupted in 25% of T-ALLs through mutations and deletions of the genes *EZH2* (enhancer of zeste 2), *EED* (embryonic ectoderm development), and *SUZ12* (suppressor of zeste 12).[68,98] The PRC2 complex plays a key role in epigenetic regulation through its function as a writer of histone H3 lysine 27 trimethylation (H3K27me3), repressing transcription activation at target sites.[99] Mutations of PRC2 is commonly found in T-ALL clones harboring activating mutations of *NOTCH1*, suggesting that loss of the PRC2 complex may augment NOTCH1 hyperactivation, removing transcriptionally repressive marks from NOTCH1 target genes.[98,100]

#### 1.3.1.2.3. KDM6A and KDM6B

In addition to targeting H3K27me3 through PCR2 complex member mutations and deletions, T-ALL frequently features mutations in KDM6A and KDM6B, which serve to demethylate tri- and di-methylated lysine-27 of histone H3.[101] KDM6A mutations are found in 5% to 15% of T-ALLs.[100,102] Interestingly, KDM6A and KDM6B appear to have contrasting roles in T-ALL transformation with KDM6A serving as a tumor suppressor and KDM6B required for NOTCH1-induced leukemogenesis.[100] KDM6 family members underscore the diverse function of

epigenetic regulators, demonstrating the propensity for epigenetic regulators to serve as tumor suppressor or oncogenes.[100]

## 1.3.1.3. ETP T-ALL Transcription Factor Oncogenes

### 1.3.1.3.1. Basic Helix-Loop-Helix Transcription Factor Overexpression

One of the most recurrent, T cell specific, gene patterns observed in T-ALL is the aberrant expression of class II bHLH transcription factors (*TAL1*, *TAL2*, *LYL1*, or *BHLHB1*) with a LIM-only (LMO) protein (LMO1 or LMO2) – found in approximately 60% of cases of T-ALL. Interestingly, overexpression of TAL1 is not driven by a single type of genetic aberration. *TAL1* overexpression can be driven by chromosomal rearrangements, typically placing *TAL1* near T cell receptor alpha (*TCRA*) and delta (*TCRD*) regulatory elements.[15,103,104] Additionally, *TAL1* overexpression has been caused by heterozygous somatic mutations in intergenic sequences upstream of the gene locus in regulatory control elements.[105,106] These intergenic mutations create MYB transcription factor binding sites, serving as a *TAL1* enhancer.[105,106] Mouse models of TAL1 overexpression demonstrate its significance in leukemogenesis by the development of T-ALL in mice engineered to overexpress *TAL1* specifically in developing thymocytes.[107,108] Several studies suggest that mediators of *TAL1* induced T-ALL transformation may include tribbles pseudokinase 2 (*TRIB2*),[109] *NKX3-1*,[110] and microRNA 223 (*MIR223*).[111] However, TAL1 has also been shown to interact with *GATA3* and *RUNX1*, reinforcing *MYB* expression.[109]

#### 1.3.1.3.2. LIM-Only (LMO) Factor Overexpression in T-ALL

LIM-Only 1 (*LMO1*) and *LMO2* are another common overexpressed oncogene observed in approximately 10% to 15% of cases of T-ALL.[19-21] [112,113] The observation that T-ALL relies on the interaction between basic helix-loop-helix transcription factors, MYB, and LMO proteins is strengthened by T-ALL associated *LMO* lesions. LMO proteins rely on TAL1 to form transcription complexes, indirectly facilitating LMO-DNA interactions,[114] and *LMO* mutations frequently co-occur with *TAL1* in T-ALL,[8] suggesting that basic helix-loop-helix factors and LMO oncogenes cooperate in T-ALL transformation. T-ALL associated LMO gene overexpression is resultant of heterogenous lesions, including translocations t(11;14)(p15;q11) and t(11;14)(p13;q11). Additionally, deletions near the *LMO2* gene locus result in its overexpression in an additional 5% of T-ALLs.

#### 1.3.1.3.3. HOX Transcription Factor Oncogenes

HOX factors represent a diverse array of transcription factors capable of activating and repressing hundreds of genes. HOX factors are vital for embryonic development and continued hematopoietic differentiation throughout life.[115,116] Dysregulation of HOX transcription factors is a staple of T-ALL transformation. Of the HOX oncogenic factors, the TLX genes are present in up to 10% of pediatric[8] and 30% of adult[117] cases of T-ALL. The TLX gene, *TLX1*, dysregulation is commonly a result of chromosomal rearrangements, driving *TLX1* overexpression in T-ALL by placing it under control of t cell receptor loci regulatory elements.

*TLX3* is also involved in the pathogenesis of T-ALL, in this case as a result of the t(5;14)(q35;q32) translocation[23] present in 20-25% of pediatric T-ALLs and 5% of adult T-ALLs.[8,23,117-119] Instead of rearranging to the T cell receptor locus, T-ALL-associated *TLX3* is

often rearranged to regulatory elements controlling the *BCL11B* locus (a potent driver of T cell differentiation).[23]

Two master epigenetic regulators of *HOX* gene expression are *HOXA9* and *HOXA10*. *HOXA9* and *HOXA10* have also been shown to play a key role in T-ALL leukemogenesis, although they are the least prominent *HOXA* members dysregulated in T-ALL, representing approximately 3% of T-ALLs.[24,120] *HOXA9* and *HOXA10* dysregulation is common in clones with chromosomal rearrangement that drive oncogenic fusion *KMT2A-MLLT1* (*MLL-ENL*),[121-123] *PICALM-MLLT10*[24,124] and *SET-NUP214*.[125] Notably, these oncogenic fusions and *HOXA9* overexpression are prominent lesions more commonly observed in acute myeloid leukemias.

## 1.3.2. $CD4^+$ $CD8^+$ Cortical T-ALL (T-ALL)

The majority of T-ALL cases have an RNA expression profile and immunophenotype similar to cortical CD4+ CD8+ thymocytes.[126] Mutations leading to increased Notch signaling are thought to be central to the pathogenesis of T-ALL. Activating mutations of *NOTCH1* are present in approximately 60% of cases of T-ALL.[5-7] Moreover, mutations of *FBXW7*, which also lead to Notch activation, are present in an additional 30% of T-ALL cases.[127-130] Hyperactivation of oncogenic transcription factors appears to be a hallmark of T-ALL. In addition to NOTCH1 activating mutations, T-ALL routinely mutates other oncogenic transcription factors, including *MYC*[25,26] and *MYB*.[27] T-ALL is an efficient silencer of tumor suppressors, providing the appropriate cellular environment for oncogenic driver mutation acquisition and positive selection.

The most common genetic lesion of T-ALL is the deletion of the *CDKN2A* tumor suppressor locus, found in more than 80% of cases of T-ALL.[8-11] The *CDKN2A* locus encodes for two tumor suppressors, $P16^{INK4A}$ (*INK4A*) and $P19^{ARF}$ (*ARF*). INK4A directly inhibits cyclin-D-

dependent kinases (CDK4 and CDK6), preventing phosphorylation of retinoblastoma protein (RB) and progression to S phase.[131-134] Functional disruption of *INK4A* or overexpression of CDK4 occur in many cancer types, and the disruption of the RB pathway is thought to be a cornerstone in transformation of cancer cells.[135]

ARF is the second classic tumor suppressor encoded by the *CDKN2A* locus, and *ARF* may be the target of inactivation due to its role in nucleolar stress mediated cell cycle arrest and apoptosis. *ARF* is the alternate reading frame (its namesake) of the $P16^{INK4A}$ gene.[133] The tumor suppressor function of ARF involves its interaction with the transcription factor p53 and p53-independent arrest of ribosome biogenesis. In addition to ARF, other nucleolar components such as the ribosome large proteins (RpL5, RpL11, and RpL22), 5S rRNA, and nucleostemin interact with MDM2, preventing the degradation of p53.[61,136-138] Loss-of-function mutations of *RPL5*, *RPL11*, or *RPL22* are present in up to 20% of cases of T-ALL.[61,136,139]

Other notable deletions observed in T-ALL include genes encoding the cell cycle regulators RB1[10,140] and CDKN1B[141] which are found in approximately 15% and 12% of cases of T-ALL, respectively.

### 1.3.2.1. Cell Cycle Deregulation

The cell cycle – growth, DNA replication, and cell division – are well regulated and monitored for order and integrity. Unsurprisingly, the mechanisms governing cycle activation and inhibition are exploited during leukemogenesis, and the loss of cell cycle control is a hallmark of T-ALL pathogenesis. As mentioned previously, the tumor suppressor $p16^{INK4A}$ and $p14^{ARF}$ encoded by the *CDKN2A* locus are lost via chromosomal deletions in most (>80%) T-ALLs.[8,11] The INK4A tumor suppressor inhibits $G_1$ to S phase cell cycle progression by two means, one)

directly binding to and inactivating cyclin D-CDK4 and cyclinD-CDKN6 complexes,[142] and two) preventing phosphorylation of retinoblastoma protein (RB).[143] ARF, similarly, has multiple tumor suppressor functions, both of which facilitate cell cycle arrest and apoptosis. ARF is stabilized in response to cellular stress and activates p53-depenendent and -independent pathways.[144]

In addition to the loss of INK4A in the *CDKN2A* gene locus deletion of T-ALL, the retinoblastoma gene (*RB1*) itself is deleted in approximately 15% of T-ALLs via chromosomal deletions 13q14.2.[10,140] Another cell cycle master regulator that is commonly lost in T-ALL is the *CDKN1B* gene (deleted in approximately 12% of cases via 12p13.2 deletions). *CDKN1B* encodes $p27^{KIP1}$, an inhibitor of cyclin E-CDK2 and cyclin D-CDK4 complexes.[141] Cell cycle progression has also been shown to be disrupted in T-ALL through aberrant overexpression of cyclin D2 (*CCND2*).

Cyclin D2 is a member of the D-type cyclins which are important in hematopoiesis and leukemogenesis.[145] D-type cyclins bind to and activate cyclin-dependent kinases 4 and 6, forming cyclin D-CDK complexes. These complexes promote cell cycle progression through phosphorylation of the retinoblastoma protein[145] and are inhibited by the *CDKN2A* gene product INK4A.[142,143] Although *CCND2* expression is elevated in only approximately 3% of T-ALLs,[146] together mutations, deletions, and translocation of cell cycle regulators found in T-ALL underscore the prominent role of cell cycle deregulation in T-ALL transformation.

More specifically, Cyclin D3 has been shown to be a key regulator of normal thymocyte development and expansion. In T-ALL, Cyclin D3 is commonly overexpressed and has been shown to be essential for disease initiation and progression.[147] Preliminary data show that drugs targeting cyclins D1, D2, and D3 are potent in preclinical models of T-ALL.[147]

## 1.3.2.2. T-ALL Transcription Factor Oncogenes

### 1.3.2.2.1. MYB

*MYB* encodes an oncogene with three HTH DNA-binding domains that functions as a transcription regulator. MYB is an essential regulator of hematopoiesis, and its dysregulation is a common feature of T-ALL, represented by a diverse array of genetic lesions. The MYB transcription factor is activated in rare cases of T-ALL via translocation between chromosomes 6 and 7 – t(6;7)(q23;q34),[27] typically observed in children under two years of age.[27] Although translocations involving *MYB* are rare in T-ALL, 10% of cases of T-ALL (representing pediatric and adult T-ALL) harbor duplications of the *MYB* locus, driving overexpression.[148,149] The most common alteration leading to increased *MYB* expression is indirect and related to transcriptional activation of *TAL1*.[109] MYB overexpression has also been shown to result from lesions involving the TAL1-miR-223-FBXW7 regulatory axis[111] and downregulation of MYB-targeting microRNAs.[150,151]

### 1.3.2.2.5. MYC

MYC is a basic helix-loop-helix transcription factor that plays a vital role in cell cycle progression and apoptosis that is implicated in tumorigenesis across multiple cancer types.[152,153] In T cell development, the prominent pathways activating MYC are NOTCH1 (vital for T cell fate decision and differentiation) and signaling that primes the T cell receptor loci for rearrangement.[154] Although the direct overexpression of *MYC* is rare in T-ALL, accounting for only 1% of T-ALLs,[25,155] activating mutations of *NOTCH1* are thought to induce leukemic transformation, in part, by activating *MYC*.[156-158] Additionally, MYC is targeted for degradation in the same manner

as NOTCH1, via FBXW7 mediated proteasomal degradation,[159,160] and mutations of *FBXW7* are present in approximately 30% of cases of T-ALL, leading to increased levels of both NOTCH1 and MYC.[161,162]

## 1.3.2.3. Oncogenic Signaling Pathways in T-ALL

### 1.3.2.3.1. A Subset of T-ALL is Driven by PI3K-AKT-mTOR Activation

One recurrently dysregulated signaling pathway in T-ALL is the aberrant activation of the PI3K-AKT-mTOR signaling axis, representing 10% to 15% of T-ALLs.[163-165] This is typically a result of the loss of the tumor suppressor *PTEN* through deletions or inactivating mutations, which stabilizes AKT expression.[166] Additionally, although PTEN loss is the most prominent activator of PI3K-AKT-mTOR signaling in T-ALL, PI3K-AKT-mTOR is also recurrently activated as a result of mutations in *PI3KCA*, *PI3KR1*, *IL7R*, and *AKT1*.[167]

The tumor suppressor role of *PTEN*, specifically in the T cell compartment, has been well established in transgenic mouse models. For example, heterozygous loss of *Pten* results in a diverse tumor spectrum that includes solid tumors and T-ALLs. Interestingly, tumors that develop from these mice exhibit loss of heterozygosity upon tumorigenesis.[168] Additionally, ectopic expression of AKT in developing thymocytes results in increased PI3K signaling, similar to observations made with patient samples, suggesting AKT may drive leukemogenesis in the context of *PTEN* loss.[169]

A number of strategies have been devised in the preclinical and clinical setting to target the PI3K pathway in leukemia.[165,170,171] These studies have utilized small molecule inhibitors of the mTOR protein, such as sirolimus and its rapalogs, demonstrating the efficacy of mTOR

inhibitors and their synergy with conventional frontline therapy.[172,173] Like most signaling pathway disruptions, mTOR inhibitors induced compensatory signaling pathways that restored PI3K-AKT-mTOR signaling, reducing long-term efficacy.[167] Given the promising response of T-ALL to PI3K inhibition, multiple additional drugs targeting the PI3K-AKT-mTOR signaling pathway were developed, including dual inhibitors for mTOR1 and mTOR2,[174] and inhibitors specific to PI3K or AKT.[175]

Lastly, there are a few instances of PTEN degradation in T-ALL as an indirect result of other dysregulated signaling pathways, including JAK-STAT, MAPK, and NOTCH.[167]

#### 1.3.2.3.2. Hyperactivation of NOTCH1 Drives the Majority of Cases of T-ALL

Increased NOTCH signaling is thought to be central to the pathogenesis of T-ALL, with activating mutations of *NOTCH1* present in approximately 60% to 70% of cases of T-ALL[5-7] and NOTCH activation due to mutations in *FBXW7* in an additional 15% to 30% of cases.[161,162] NOTCH1 is a class I transmembrane receptor whose intracellular domain functions as a ligand-activated transcription factor.[26,176] In the context of hematopoiesis and T cell development, NOTCH1 is the key regulator for early T cell fate specification in the bone marrow, and NOTCH1 stimulation in the thymus ensures thymocyte development.[177]

Interestingly, NOTCH1 hyperactivating mutations in T-ALL were first described in a relatively rare T-ALL subset, involving chromosomal translocation t(7;9)(q34;q34.3), which produced a truncated constitutively active NOTCH1 peptide.[178] This translocation is observed in less than 1% of cases of T-ALL, and the vast majority of NOTCH1 hyperactivation observed in T-ALL result from mutations in the HD and PEST domains of NOTCH1, leading to ligand-free

NOTCH1 signaling.[179] Moreover, mutations of *FBXW7*, which also lead to Notch activation, are present in an additional 30% of T-ALL cases.[127-130,161,162]

Initial studies[180] investigating the oncogenic role of NOTCH1 hyperactivation overstated its ability to drive leukemogenesis. The initial model of T-ALL relied on high levels of NOTCH1 stimulation not observed in patients with T-ALL.[181] Specifically, the model relied on expression of a truncated NOTCH1, reducing expression to its intracellular domain (ICN). Although, the ICN shows potent stimulation of NOTCH1 targets, this mutation, and level of NOTCH1 stimulation, have yet to be described in patients with T-ALL. While the NOTCH1 ICN stimulates leukemogenesis in mice, the majority of single NOTCH1 mutations associated with human T-ALL are unable to replicate this finding or initiate T-ALL development.[181] Furthermore, the NOTCH1 activating mutations associated with T-ALL show weak stimulation of hematopoiesis and rely on cooperating oncogenic factors to drive transformation. Lastly, recent genomic analyses of T-ALL have revealed that mutations in *NOTCH1* are often confined to subclones of T-ALL, suggesting *NOTCH1* mutations are a late event.[29,67]

Despite the prevalence of NOTCH1 mutations in T-ALL and the extensive analyses of patient derived mutations, the molecular mechanisms by which NOTCH1 promotes leukemic transformation are still unclear. What appear to be relevant to NOTCH1 mediated T-ALL transformation are its growth-promoting effects[156,182,183] and association with transcriptional upregulation of ribosome biogenesis and protein translation.[156,157] In addition to the pro-growth effects of increased MYC expression associated with NOTCH activation, HES1 (a target of NOTCH1) has been shown to play a vital role in leukemia survival[184] by activating PI3K and NF-κB pathways[185] and negatively regulating glucocorticoid receptor expression.[186,187] Additionally, NOTCH1 activation stimulation of HES1 has been shown to inhibit *BBC3* expression, suppressing

apoptosis.[188] Lastly, NOTCH1 expression in T-ALL has been shown to enhance expression of the long non-coding RNA *LUNAR1* which is associated with enhanced *IGF1R* expression and consequent IGF1 signaling.[189]

### 1.3.2.4. The CDKN2A Locus Tumor Suppressors

The *CDKN2A* locus encodes for two tumor suppressors, $P16^{INK4A}$ (*INK4A*) and $P19^{ARF}$ (*ARF*). *INK4A* and *ARF* share exons two and three of the *CDKN2A* gene locus, but they have independent alpha and beta first exons.[131,190-192] These transcripts encode for wholly unique polypeptides via their different reading frames. INK4A directly inhibits cyclin-D-dependent kinases (CDK4 and CDK6), preventing phosphorylation of retinoblastoma protein (RB) and progression to S phase.[131-134] Functional disruption of *INK4A* or overexpression of CDK4 occur in many cancer types, and the disruption of the RB pathway is thought to be a cornerstone in transformation of cancer cells.[135] It has been reported that CDK4 directly phosphorylates upstream binding factor (UBF), leading to the initiation of ribosome biogenesis,[193,194] however the implications of CDK4 induced ribosome biogenesis in the context of *CDKN2A* biallelic loss have not been examined.

ARF is the second classic tumor suppressor encoded by the *CDKN2A* locus, and *ARF* may be the target of inactivation due to its role in nucleolar stress mediated cell cycle arrest and apoptosis. *ARF* is the alternate reading frame (its namesake) of the $P16^{INK4A}$ gene.[133] The tumor suppressor function of ARF involves its interaction with the transcription factor p53 and p53-independent arrest of ribosome biogenesis. ARF stabilizes and activates p53,[144] initiating a transcriptional program that arrests the cell cycle or leads to apoptosis through genes such as *BAX*, *CD95-FAS*, *DR5*, *NOXA*, *P53DINP1*, *PUMA*, *RGC*, and *CDKN1*.[195-202] The transcription factor

p53 also initiates transcription of its negative feedback regulator – *MDM2*.[203] The stabilization of p53 by ARF involves a complex mechanism induced under nucleolar stress. Under baseline conditions, ARF – a nucleolar protein – cannot interact with p53 which is localized to the nucleus.[204-206] The nucleolus is an organelle formed within, but kept separate from, the nucleus for the purpose of generating ribosomes. Disruptions in ribosome biogenesis disrupt nucleolar structure and cause the release of nucleolar components into the nucleus.[207] Once in the nucleus, ARF interacts with MDM2, inhibiting its activity and stabilizing p53.[144] In addition to ARF, other nucleolar components such as the ribosome large proteins (RpL5, RpL11, and RpL22), 5S rRNA, and nucleostemin interact with MDM2, preventing the degradation of p53.[61,136-138] Mutations of *RPL5*, *RPL11*, or *RPL22* are present in up to 20% of cases of T-ALL.[61,136,139]

#### 1.3.2.4.1. Regulating the Arf locus

Under basal conditions ARF is kept sequestered in the nucleolus by nucleophosmin and its transcription is minimized by epigenetic modification via the polycomb repressive complexes 1 and 2 (PRC1 and PRC2)[208,209] and protein blocks to *ARF* regulatory elements.[210]

PRC2 blocks ARF transcription in tandem with PRC1 by first adding tri- and di-methyl groups to nearby histones, utilizing the EZH2 complex member to methylate lysine-27 on histone H3 (H3K27me$^3$).[211] H3K27me$^3$ marks are then recognized by PRC1 to stabilize the repressive mark.[208] Another polycomb gene important for silencing the *CDKN2A* locus is BMI-1.[212-214] The direct relationship between BMI-1 and *CDKN2A* gene expression was demonstrated in *Bmi-1*-null murine embryonic fibroblasts (MEFs). BMI-1 loss resulted in marked upregulation of both ARF and INK4A, leading to slowed growth and increased apoptosis relative to wildtype MEFs.[215]

Independent of BMI-1, CBX7 and CBX8, members of the polycomb repressive group, have been shown to silence the *CDKN2A* gene locus.[216]

An additional layer of regulatory control, via transcription repression, is provided by E2F-repressive complexes. Depletion of E2F-repressive complexes in MEFs was shown to increase the expression levels of ARF.[217] E2F3b is primarily responsible for *ARF* repression with loss of E2F3b sufficient to induce ARF expression and ARF mediated expression of p53 and p21.[210] Specifically, E2F3b binds the *Arf* promoter, blocking transcription.[210] Other transcriptional repressors of *ARF* include Pokemon, Tbx2, and Tbx3.[218-220] However, it is unclear how these transcriptional repressors specifically block *ARF* expression.

#### 1.3.2.4.2. Arf Transcription and Translation

Oncogenic signals are necessary hallmarks of cancer whose activating mutations are selected due to their enhancement of cell growth and proliferation. Balance out the proliferation signals of oncogenes are the tumor suppressors, acting to extinguish any unorderly or insatiable oncogenic signals. In the context of lymphopoiesis, whereby rampant proliferation is necessary to keep up with immunologic demand, the tumor suppressor ARF is a key to maintaining normal proliferation. Although *ARF* is unmeasurable in most hematopoietic cells, including the most primitive and mature populations, *ARF* is readily transcribed in the context of thymocyte development and responsive to c-Myc, Ras, E2F-1, E1A, and v-Abl.[221-223]

Interestingly, Ras-induced ARF-mediated cell cycle arrest is not immediate. Wild-type MEFs transduced with oncogenic $Ras^{V12}$ accumulate ARF protein over time and do not succumb to ARF-mediated cell cycle arrest for approximately 5 days.[224] While increases in both ARF transcription and translation can be quickly detected upon $Ras^{V12}$ overexpression in wildtype

MEFs, this data suggests that a threshold level of ARF protein must accumulate before cell cycle arrest,[133,223,224] this makes sense as it allows the cell to achieve growth and proliferation before immediately blocking it with cell cycle arrest. While proliferation is necessary, ARF can accumulate over a prolonged growth cycle to prevent unchecked cellular growth.

#### 1.3.2.4.3. Arf structure, cellular localization, and stabilization

The structure of ARF is important to understanding the protein's localization, stabilization, and binding partners. ARF is in a class of proteins known as intrinsically disordered proteins. ARF is between 132 (human) and 169 (mouse) amino acids with 20% of its residues consisting of arginine – a highly basic amino acid. This high alkalinity is consistent with nucleoli affinity and the composition of other nucleolar proteins.[225]

In addition to the chemistry dictating ARF's localization, ARF contains a nucleolar localization signal.[226] The intrinsically disordered nature of ARF also makes it a promiscuous binding partner with a high affinity for acidic domains, such as the central acidic domain of the p53 inhibitor, MDM2. In the nucleolus, ARF can be found bound in high molecular weight complexes.[226] Additionally, ARF carries out its functions in complex with other oppositely charged proteins, binding nucleophosmin, nucleostemin, 5.8S rRNA, and MDM2, inhibiting their function or sequestering these proteins in the nucleolus.[131,227,228]

### 1.3.2.5. Ribosomal Protein Mutations

There is an essential fundamental relationship that exists between cell growth and ribosome biogenesis. In order to keep up with demand for protein synthesis, cancer cells must ramp up

ribosome production. Indeed, many oncogenes and tumor suppressors directly regulate ribosome biogenesis.[193,194,229,230] In particular, NOTCH1, MYC, and PI3K-AKT pathway are positive regulators of ribosome biogenesis and translation, recurrently mutated in T-ALL.[156,231,232] MYC, which is activated in most cases of T-ALL through increased Notch signaling, stimulates ribosomal RNA synthesis and the production of ribosomal proteins.[156] However, increased ribosome biogenesis induces a negative feedback loop known as the nucleolar stress pathway that inhibits ribosome production and cell growth. Two major components of the nucleolar stress pathway are ARF and specific ribosome proteins.[233]

Nucleolar stress induces increased ARF expression, which in turn, inhibits ribosome expression, in part, by binding to nucleophosmin.[207,233] Nucleolar stress also results in the translocation of RpL5, RpL11, and RpL22 to the nucleoplasm, where they bind and inactivate MDM2.[61,136-138] MDM2 is an E3 ubiquitin ligase that binds and targets p53 for ubiquitination and protein degradation. Thus, nucleolar stress, by inhibiting MDM2 function, results in a p53-dependent growth suppression.

Since the discover of RpL5 and RpL11's role in MDM2 inactivation, many other RPs, including RpL3, RpL6, RpL23, RpL26, RpL37, RpS7, RpS14, RpS15, RpS19, RpS20, RpS25, RpS26, and RpS27, have been shown to bind to MDM2, thus stabilizing p53 after induction of ribosomal stress.[234] Loss-of-function mutations are common in T-ALL; sequencing data confirm 10% to 15% of cases of T-ALL harbor ribosomal protein mutations.[61,136,139]

## 1.4. Ribosome Biogenesis

Ribosomes are ribonucleoproteins, comprised of catalytically active RNA species in complex with proteins. Mature, fully assembly, ribosomes are located in the cytoplasm where,

either free or membrane bound, are engaged in protein synthesis. In a single ribosome, there are four classes of rRNA molecules and approximately 80 different ribosomal proteins. Ribosome biogenesis occurs in the nucleolus, a subnuclear organelle, where ribosomal genes are transcribed by Pol I to generate the 47S immature rRNA precursor. 47S rRNA molecules undergo site-specific methylation, pseudo uridylation, and processing to give rise to the mature 18S, 5.8S, and 28S rRNAs (three of the four rRNA species).[235-238] The fourth type of rRNA, the 5S rRNA, is synthesized in the nucleoplasm by RNA polymerase III (Pol III) and then imported in the nucleolus together with the ribosomal protein (RPs), whose mRNA is transcribed by RNA polymerase II (Pol II). The large 60S subunit is comprised of 28S, 5.8S, and 5S RNA molecules, together with 47 "large" ribosomal proteins (RpLs). The small 40S subunit contains only one 18S RNA molecule and 33 "small" ribosomal proteins (RpSs).[239,240]

The transcription of immature 47S pre-rRNA involves factors that are recurrently dysregulated in T-ALL transformation. These factors include the transcription initiation factor I (TIF-I) A, selectivity factor 1 (SL1), and upstream binding factor (UBF).[241] Additionally, the transcription factors responsible for 5S rRNA expression are also dysregulated in T-ALL, specifically the transcription factors TFIIIC and TFIIIB.[242-244]

In proliferating cells, the rate of ribosome biogenesis is enhanced in order to assure an adequate ribosome complement upon cell division and inhibition of ribosome biogenesis arrests cell cycle progression.[245] Furthermore, the rate of ribosome biogenesis influences the length of the cell cycle: higher the level of ribosome biogenesis, more rapid the cell cycle progression.[246] In hematologic malignancies, such as T-ALL, oncogenic cooperation between the *MYC* oncogene (perhaps through stimulation by *NOTCH1* activating mutations) and the phosphatidyl-inositol-3-

kinase (PI3K) signaling pathways,[247] synergistically interact to stimulate rRNA synthesis and ribosome biogenesis.[248]

### 1.4.1. The Nucleolus: A Multifunctional Organelle and its Role in Cellular Stress

Since my birth, over 4,500 nucleolar proteins have been identified through massive advancements in proteomics.[249] Surprisingly, only 30% of known nucleolar proteins have a clear role in ribosome biogenesis. Perhaps more intriguing is the discovery that nucleolar proteins, and the nucleolus, is a key mediator of cellular assaults and stresses, responding to a diverse array of events, including cell cycle regulation, DNA replication and repair, telomere maintenance, aging, telomerase activity, viral infection response, and hyperproliferation.[250,251]

In an effort to define these newfound nucleolar proteins, many researchers noticed that nucleolus-associated proteins frequently shuttled between the nucleolus and nucleoplasm. Nucleoplasmic translocation of nucleolar proteins is often context dependent, occurring under stress conditions.[252-258] Stress induced nucleolar translocations were first described using actinomycin D [259] but has since been described in cells exposed to cytotoxic agents,[254,260] viral proteins,[261] ultraviolet radiation,[255,262] heat shock,[260] and agents inducing DNA damage,[263,264] apoptosis, or senescence.[265-267] The links between the nucleolus and cellular stress were eventually canonized with the finding that the nucleolus plays a key role in regulating the abundance of p53.[252,268-273]

## 1.4.2. The Rate of Ribosome Biogenesis of the Cell

While stabilizing p53 is known to drive cell cycle arrest and apoptosis, p53 stabilization does not automatically induce programmed cell death.[274-276] Recent studies have indicated that apoptosis induced by inhibiting ribosome biogenesis is not binary, and it greatly depends on the degree of p53 stabilization. Interestingly, there is a direct correlation between the rate of ribosome biogenesis and degree of p53 stabilization, suggesting more aggressive forms of T-ALL may have increased sensitivity to p53-induction by ribosome biogenesis inhibitors.[276] Scala *et al*. demonstrated that higher proportions of cells underwent apoptosis as rates of ribosomal RNA synthesis increased, whereas low rates of rRNA synthesis result in cell cycle arrest. These findings were a direct result of secondary functions of ribosomal proteins, binding MDM2 to stabilize p53. Higher rates of rRNA synthesis result in more free ribosomal proteins upon nucleolar stress induction and greater stabilization of p53.[276] These data demonstrate that ribosome biogenesis inhibitors may be effective in T-ALL, where *TP53* lesions are rare.

## 1.4.3. Ribosome Biogenesis and Nucleolar Stress

The nucleolus is a subnuclear compartment, which is primarily known for its role in ribosome biogenesis. Nucleoli encompass ribosomal RNA (rDNA) genes, transcribing ribosomal RNA (rRNA) precursors akin to mRNA transcription in the nucleus. rRNA maturation proceeds stepwise through several cleavage steps, resulting in mature 18S, 5.8S, and 28S transcripts before ribosomal proteins are incorporated and ribosomal subunits assembled. It has become apparent over the last two decades that the nucleolus function is multifaceted and serves as a key mediator of oncogenic assault and cell stress responses.

## 1.4.4. Nucleolar Stress

Although nucleolar stress was first described nearly thirty years ago,[277] the criteria used to define nucleolar stress is not held within one "gold-standard" assay. The variability in approaches is highly context dependent; however, central to all aspects of nucleolar stress is dysregulation of ribosome biogenesis.[277-280] Nucleolar stress may manifest as alterations in nucleoli morphology and number,[281] atypical translocation of ribosome biogenesis related proteins,[282] expression of the *CDKN2A* gene products,[226] and/or p53 stabilization.[283]

Rubbi and Milner were the first to propose that impaired nucleolar function may contribute to p53 stabilization.[206] Their comparative meta-analysis of p53 stimuli revealed that each p53 stabilizing event results in disrupted nucleolar architecture, and subsequent studies have demonstrated that the various assaults which stabilize p53 also induce nucleolar stress.[284,285] Additionally, Rubbi and Milner demonstrated, a now well study phenomenon in nucleolar stress, that nucleophosmin translocates from nucleoli to the nucleoplasm and cytoplasm.

### 1.4.4.1. Hallmarks of Nucleolar Stress

#### 1.4.4.1.1. Nucleoplasmic Translocation of Nucleolar Proteins

Unlike membrane-limited organelles, there is no structural barrier between the nucleolus and the surrounding nucleoplasm. Nucleoli integrity is thought to be maintained by the phase separation induced by intrinsically disordered proteins comprising nucleoli. The nucleolar microenvironment provides the best setting for ribosome biogenesis. Nucleolar disruption during cellular stress events causes the translocation of nucleolar proteins into the nucleoplasm, resulting

in secondary functions. Due to the propensity for nucleolar proteins to be greatly positively charged and contain intrinsic domains, nucleolar proteins "stick" to nuclear proteins, inhibiting their function.

#### 1.4.4.1.2. Ribosomal Proteins

Under nucleolar stress, several ribosomal proteins are known to bind MDM2, stabilizing p53.[137,138] These include RpS3,[286] RpS7,[287,288] RpL5,[289-291] RpL11,[292-295] and RpL23.[296] Since the discover of RpL5 and RpL11, many other RPs, including RpL3, RpL6, RpL23, RpL26, RpL37, RpS7, RpS14, RpS15, RpS19, RpS20, RpS25, RpS26, and RpS27, have been shown to bind to MDM2.[234] Like ARF, these ribosomal proteins bind the acidic central domain of MDM2 due to the chemical interaction between the negatively charged acidic domain and basic ribosomal proteins.

#### 1.4.4.1.3. Nucleoplasmic Translocation of Nucleophosmin (NPM1)

Nucleophosmin (NPM1) is the most abundant protein in the nucleolus,[297,298] residing in the nucleolus under basal conditions,[298,299] stabilizing nucleoli by preventing "sticky" protein aggregation.[300,301] NPM1 is also the principal nuclear chaperone, shuttling between the nucleolus and nucleoplasm and cytoplasm.[302-305] Being the primary nucleolar and nuclear chaperone, NPM1 is partly responsible for ribosome biogenesis[300,306-308] with roles in rRNA maturation[309] and ribosome assembly.[301] NPM1 translocation during nucleolar stress has been well established, and is perhaps the most well characterized nucleolar stress mediated event.[206,302,310-313] NPM1 is integral to the overall health of the cell, as demonstrated by its interaction with tumor suppressors (e.g., RB and CDKN2A)[314] and apoptotic factors (e.g., BAX).[315] The amount of NPM1 is directly

related to the rRNA transcription rate of the cell[316] and correlates with the number and morphology of nucleoli as well as cell proliferation.[317]

#### 1.4.4.1.4. Impaired rRNA Transcription and Processing

Ribosome biogenesis occurs in the nucleolus, a subnuclear organelle, where ribosomal genes are transcribed by Pol I to generate the 47S immature rRNA precursor which are then cleaved to generate 45S, 41S, 36S, and 32S rRNA intermediate precursors and finally matured 18S, 5.8S, and 28S rRNA.[318] Inhibition of rRNA processing can occur at early or late stages of processing,[14,270,319] depending on the trigger (for example, processing arrests vary based on reactive oxygen species or nucleoli disruption). If a late stage is impaired, as in the case of excess ARF, there is an accumulation of immature 5' external transcribed spacer (ETS) containing rRNA relative to mature 18S rRNA.[270,319-321]

## 1.4.5. Role of Ribosomal Proteins in p53-Independent Nucleolar Stress

### 1.4.5.1. RpL11

Beyond RpL11's well-studied interaction with MDM2, RpL11 inhibits ribosome biogenesis by binding c-Myc (a master transcription regulator of all three mammalian RNA polymerases)[231,322] and c-Myc's mRNA.[323] These observations were made in the context of wildtype p53 and p53-null cells, demonstrating RpL11's propensity to arrest cell growth independent of p53.

### 1.4.5.2. RpL3

RpL3 is a second ribosomal protein shown to exhibit p53-independent cell cycle arrest. RpL3 positively regulates p21 expression, inducing cell cycle arrest at the G1/S transition by inhibiting cyclin dependent kinases.[324] Similar to the RpL11 study, RpL3 was overexpressed to simulate nucleolar stress. These *in vitro* experiments were carried out in p53-null cells and resulted in dose-dependent increases in p21 expression.[324]

## 1.4.6. T-ALL Treatments that Mimic Nucleolar Stress

The vast majority of T-ALLs retain wildtype p53 and can theoretically mount p53-mediated apoptotic responses to nucleolar stress. However, exogenous input to induce ribosome biogenesis inhibition are needed, as T-ALL efficiently destroys the cell's innate nucleolar stress pathway. Inhibitors with potential efficacy can be categorized into two groups – those targeting p53 stabilization and activation to induce apoptosis or drugs that mimic ARF mediated disrupt of ribosome biogenesis, starving T-ALL blasts.

Nucleolar stress can be induced at multiple steps within the nucleolus, from Pol I transcription initiation and elongation to early and late pre-rRNA processing (ribosome assembly), through to ribosome maturation and eventual release from the granular component of the nucleolus (GC). Small molecule inhibitors of ribosome biogenesis may disrupt cancer proliferation and indirectly cause disruptions in nucleolar integrity, resulting in the release of nucleolar and ribosomal proteins to the nucleoplasm where they can bind and inhibit MDM2.[206] Evidence of

nucleolar disruption with drugs designed to inhibit RNA polymerase I (Pol I) has been well document.[282,325]

Additionally, several drugs are currently available that have been shown to disrupt ribosome biogenesis and nucleolar integrity,[282,325] including intercalating agents (actinomycin D,[326] mitomycin C, mitoxantrone, and doxorubicin)[282,325] and pre-rRNA processing (camptothecin, flavopiridol, and roscovitin). In response to treatment with these inhibitors, nucleoli fragment, shown using fibrillarin immunostaining.[282] New drugs currently in Phase I and II clinical trials include ellipticine which blocks Pol I transcription initiation,[327] CX-3543 which blocks Pol I elongation by disrupting nucleolin interactions with rDNA,[328] and CX-5461 which blocks Selectivity Factor-1 (SL-1) from binding rDNA promoters, preventing pre-initiation complex assembly.[329]

# Chapter 2: Canonical signaling by TGF family members in mesenchymal stromal cells is dispensable for hematopoietic niche maintenance under basal and stress conditions

## 2.1. Preface

The bone marrow contains a complex population of stromal and hematopoietic cells that together generate a unique microenvironment, or nice, to support hematopoiesis. There is evidence that adaptive changes in bone marrow stromal cells contributes to recovery from myelosuppressive therapy and the development of certain hematopoietic malignancies. However, the signals that contribute to the development, maintenance, and stress response of bone marrow mesenchymal stromal cells are poorly understood.

The TGF-β superfamily consists of approximately 45 members divided into four subgroups: bone morphogenetic proteins (BMPs)/growth differentiation factors (GDFs), TGF-βs, activins/inhibins, and other distant TGF-β members. BMPs play a critical role in development and have been strongly implicated in osteogenesis. TGF-β subgroup members have complex stage-specific effects on mesenchymal bone marrow stromal cells. TGF-βs stimulate osteoprogenitor proliferation and induce MSC migration, while inhibiting terminal osteoblast differentiation. Additionally, our group identified TGF-β signaling as a crucial player in lineage specification of mesenchymal stem and progenitor cells (MSPCs) in fetal bone marrow. Here, I

test the hypothesis that the cytokines of the transforming growth factor superfamily provide signals to mesenchymal stromal cells that contribute to basal and stress hematopoiesis responses.

To test this hypothesis, I abrogated canonical TGF family signaling in mesenchymal stem/progenitor cells by generating a *Smad4*-null protein using a doxycycline-repressible *Osterix-Cre* transgene (*Osx-Cre*), which targets all mesenchymal stromal cells in the bone marrow. We first performed lineage-tracing studies, using *Osx-Cre Smad4*$^{fl/fl}$ *Ai9* mice to show that activation of *Osx-Cre* at birth (by removal of doxycycline) results in the efficient targeting of bone marrow mesenchymal stromal cells. Moreover, we show that *Smad4* mRNA expression is essentially undetectable in sorted mesenchymal stromal cells sorted from the bone marrow of these mice. Basal hematopoiesis and bone marrow stromal cells were analyzed in 6–8-week-old *Osx-Cre Smad4*$^{fl/fl}$ mice. No alterations in the number or spatial organization of CAR cells, osteoblast, or adipocytes were observed, and expression of key niche factors, including *Scf*, *Cxcl12*, and *Spp1* was normal. Basal hematopoiesis, including the number of phenotypic HSCs in bone marrow and spleen also was normal.

Recent studies have shown that inhibition of activin signaling by treating with an activin receptor 2 alpha (ACVR2a) ligand trap stimulates erythropoiesis. Although ACVR2a signaling in erythroid progenitors contributes to this effect, two groups have shown that inhibition of activin signaling in bone marrow stromal cells also stimulates erythropoiesis. Thus, we next characterized basal and stress erythropoiesis in *Osx-Cre Smad4*$^{fl/fl}$ mice. The frequency of phenotypic erythroid progenitors in bone marrow and spleen was similar to control mice. The stress erythropoiesis response was assessed after induction of acute hemolytic anemia by phenylhydrazine treatment. Both the magnitude of anemia and kinetics of erythroid recovery were similar to control mice.

Myelosuppressive therapy induces marked alterations in the bone marrow microenvironment that includes an expansion of osteolineage cells and adipocytes, which have been linked to hematopoietic recovery. Thus, we next characterized stress hematopoiesis in *Osx-Cre Smad4*$^{fl/fl}$ mice in response to 5-fluorouracil (5-FU) treatment. Compared to control mice, the magnitude and duration of neutropenia following 5-FU were similar. Moreover, mouse survival after repeated weekly doses of 5-FU was comparable to control mice.

HSPC mobilization by G-CSF is due, in large part, by downregulation of *Cxcl12* expression in bone marrow mesenchymal stromal cells. A prior study suggested that Smad signaling negatively regulates *Cxcl12* expression in stromal cells. Consistent with this finding, we show that treatment of cultured bone marrow derived MSCs with TGF-β1 for 48 hours results in a significant (3.3-fold, $P < 0.0001$) decrease in *Cxcl12* expression in stromal cells. Thus, in the final experiments, we characterized G-CSF induced HSPC mobilization in *Osx-Cre Smad4*$^{fl/fl}$ or *Osx-Cre Tgfbr2*$^{fl/fl}$ mice. HSPC mobilization, as quantified by CFU-C and lineage$^-$ Sca1$^+$ cKit$^+$ (LSK) cell number in blood or spleen after 5 days of G-CSF treatment was comparable to control mice.

Through careful experimentation and thorough characterization of transgenic mouse models, it was revealed that canonical TGF family signaling is dispensable for bone marrow hematopoietic niche maintenance and hematopoietic stress response. These findings came after I developed a novel mouse model, using an inducible tetracycline-off transgene to drive expression of a bone marrow mesenchymal lineage specific Cre-recombinase to ablate canonical TGF family signaling. This mouse model enabled us to study the developing bone marrow niche and the effects of signal loss in adult mice. I helped develop the research strategy, and I conducted all experiments, including bone histology, *in vitro* differentiation assays, and phenotypic characterization of basal hematopoiesis and hematopoietic responses to stressors including,

granulocyte colony stimulating factor, 5-fluorouracil, irradiation, and phenylhydrazine. In addition, I wrote and revised the manuscript. The findings of this project helped me earn an outstanding abstract achievement award from the American Society of Hematology at the 61st annual meeting and exposition.

## 2.2. Introduction

The bone marrow contains a complex dynamic population of stromal and hematopoietic cells that together generate a unique microenvironment, or niche, to support hematopoiesis. Mesenchymal stromal cells (MSCs) are an important component of the bone marrow hematopoietic niche and include CXCL12-abundant reticular (CAR) cells, adipocytes, osteolineage cells, arteriolar pericytes, and mesenchymal stem cells, all of which have been implicated in hematopoietic stem/progenitor cell (HSPC) maintenance. [1-7] The signals that regulate MSCs and their impact on hematopoiesis are not well characterized.

There is evidence that TGF-β signaling regulates MSCs in the bone marrow. TGF-β has complex stage-specific effects on bone marrow MSCs. It stimulates osteoprogenitor proliferation and induces mesenchymal stem cell migration, while inhibiting terminal osteoblast differentiation.[8] *In vitro* modeling of the interaction between TGF-β and bone marrow MSCs reveal its potential to negatively regulate adipocyte and osteoblast differentiation while promoting osteoblast progenitor proliferation.[9–11] In addition, genetic abrogation of TGF-β signaling in mesenchymal progenitor cells during development results in impaired osteoblast differentiation and a marked expansion of CAR cells and bone marrow adiposity.[12,13] These stromal alterations are associated with a shift in hematopoiesis from lymphopoiesis to myelopoiesis.[12]

In contrast, abrogation of TGF-β signaling in mesenchymal progenitor cells at birth (using a doxycycline-inducible *Osx-Cre* transgene) resulted in no discernable alterations in the niche or basal hematopoiesis. Thus, TGF-β signaling in mesenchymal cells during development is required for the establishment of a normal hematopoietic niche but is dispensable for niche maintenance in adults under steady-state conditions.

There also is evidence that other members of the TGF family of cytokines may contribute to the development, maintenance, and/or function of MSCs in the bone marrow. The TGF superfamily consists of approximately 45 ligands divided into four subgroups: TGF-βs, decapentaplegic-Vg-related (DVR), activins/inhibins, and other distant TGF members.[14,15] The DVR subgroup consists of bone morphogenetic proteins (BMPs) and growth differentiation factors (GDFs) which play a critical role in skeletal patterning and soft and hard tissue development.[8,16–20] Deletion of *Bmpr1a* (Alk3) in hematopoietic and stromal cells using *Mx1-Cre*, which targets osteoblast lineage cells, is associated with an increase in N-cadherin positive osteoblasts and a modest increase in HSCs, suggesting that BMP signaling in stromal cells may negatively regulate the stem cell niche.[21] Multiple groups have also shown that inhibition of activin signaling by treating with an activin receptor 2 alpha (ACVR2a) ligand trap stimulates erythropoiesis *in vivo*.[22–25] Indeed, clinical trials have demonstrated improvements in anemia in patients with myelodysplastic syndrome treated with sotatercept, a ACVR2a antagonist.[23,26] Although ACVR2a signaling in erythroid progenitors contributes to this effect,[22,24] two groups showed that inhibition of ACVR2a signaling in bone marrow stromal cells also stimulates erythropoiesis.[23,27]

Myelosuppressive therapy induces marked alterations in the bone marrow microenvironment that includes an expansion of osteolineage cells and adipocytes, which have

been linked to hematopoietic recovery.[28,29] Relevant to this study, myelosuppressive chemotherapy activates TGF-β in the bone marrow, and inhibition of TGF-β signaling enhances recovery from chemotherapy.[30] Whether TGF-β or other TGF family member signaling in mesenchymal cells contributes to stromal and hematopoietic responses to myeloablative therapy or other stressors is an open and clinically relevant question. Of note, recent single cell RNA sequencing of bone marrow stromal cells shows that *Tgfbr1*, *Tfgbr2*, *Tgfbr3*, and *Smad4* are expressed in osteolineage cells and perivascular stromal cells.[31]

TGF family ligands bind to their cognate type I and type II serine/threonine kinase receptors to phosphorylate and active pathway-restricted SMADs (R-SMADs), which in turn complex with SMAD4 to active target genes. Thus, SMAD4 is required for all canonical TGF family signaling. Here, we show that deletion of *Smad4* in bone marrow MSCs at birth results in no discernible alteration in the bone marrow hematopoietic niche. Indeed, basal and stress hematopoiesis are normal. These data suggest that canonical TGF-β family signaling is not required for hematopoietic niche maintenance or niche response to certain hematopoietic stressors.

# 2.3. Material and Methods

## 2.3.1. Mice and animal housing

*Osx1-GFP*::*Cre*[57], *Ai9*[58], *Smad4* $^{fl/fl}$ [59], and *Tgfbr2*$^{fl/fl}$ [60] mice were obtained from The Jackson Laboratory (Bar Harbor, ME). Mice were crossed to generate *Osx-Cre Tgfbr2*$^{fl/fl}$, *Osx-Cre Ai9 Tgfbr2*$^{fl/fl}$, *Osx-Cre Smad4*$^{fl/fl}$, and *Osx-Cre Ai9 Smad4*$^{fl/fl}$ mice on a C57Bl/6 background. To suppress the *Osx-Cre* transgene throughout embryonic development,

mice were maintained on doxycycline chow (200 mg/serving) until post-natal day 0. All experiments were done using 6-8-week-old mice. An equal number of male and female mice were used. Mice were maintained under standard pathogen-free conditions, and all of the procedures performed in this study were approved by the Washington University Animal Studies Committee (approval number 20180018). Mice were anesthetized using isoflurane for all procedures, and they were euthanized using $CO_2$ asphyxiation followed by cervical dislocation.

### 2.3.2. Flow cytometry

Peripheral blood, bone marrow, and spleen mononuclear cell (MNC) preparations were suspended in Tris-buffered ammonium chloride (pH 7.2) buffer for 15 minutes at room temperature (RT) to lyse red blood cells. MNCs were then incubated with target antibodies at 4°C for 30 minutes in phosphate buffered saline (PBS) containing 1mM ethylenediaminetetraacetic acid (EDTA) and 0.2% (weight/volume) bovine serum albumin (BSA). The HSPC panel included Pe-Cy7-conjugated CD117 (2B8); BV711-conjugated Ly-6A/E; BV605-conjugated CD150 (TC15-12F12.2) BV421-conjugated CD48 (HM48-1); APC-conjugated CD16/32 (2.4G2); FITC-conjugated CD34 (RAM34); and PE-conjugated CD135 (A2F10.1) and the following APC-Cy7-conjugated antibodies recognizing lineage markers: CD3e (145-2C11), B220 (RA3-6B2), Gr1 (RB6-8C5), Ter119 (TER-119), and CD11b (M1/70). The mesenchymal cell panel included PerCP-Cy5.5-conjugated Ly-6A/E (D7), BV421-conjugated CD31 (390), biotin-conjugated PDGFRβ (APB5), PE-conjugated streptavidin, APC-Cy7-conjugated CD45 (30-F11) and Ter119 (TER-119) antibodies. The lineage cell panel included PE-conjugated CD115 (CSF-1R), FITC-conjugated Ly-6G/Ly-6C (RB6-8C5), BV421-conjugated CD45R/B220 (RA3-6B2), and APC-Cy7-conjugated CD3ε (145-2C11). The erythroid panel included FITC-conjugated Ter119 (TER-

119), PE-conjugated CD44 (IM7) and the following APC-Cy7-conjugated antibodies: Ly-6G/Ly-6C (RB6-8C5), CD45R/B220 (RA3-6B2), and CD3ε (145-2C11). All antibodies were obtained from BioLegend (San Diego, CA), unless otherwise indicated. Data were acquired using a FACS Aria III flow cytometer (BD biosciences, San Jose, CA) and analyzed using FlowJoTM v10.6.1 software (BD biosciences).

### 2.3.3. Cell sorting

Mouse femurs, tibias, and pelvises were homogenized in PBS using a mortar and pestle. The cell suspension was then incubated in PBS containing 1.7 mg/ml collagenase type 1 (#17100017, ThermoFisher), 1.7 mg/ml collagenase type 2 (#LS004174, Worthington, Lakewood, NJ), and 1.7 mg/ml collagenase type 4 (#LS004188, Worthington) at 37°C while shaking for 15 minutes. The resulting cell suspension was filtered through CellTrics 50μm filters (Sysmex, Goerlitz, Germany) to remove debris, creating a single-cell suspension. The samples were then incubated at 4°C for 30 minutes in PBS containing 1mM EDTA and 0.2% BSA with the following panel of BV421-conjugated lineage antibodies: CD45, Gr1, CD11b, and B220. Ai9+ lineage- cells were sorted using a Sony iCyt Synergy SY3200 (Synergy) cell sorter (Sony, San Jose, CA).

### 2.3.4. Immunostaining of bone sections

Mouse femurs were fixed in PBS containing 4% paraformaldehyde, pH 7.4, for 24 hours at 4°C. Bones were then decalcified in PBS containing 14% EDTA, pH 7.4, for 14 days at 4°C, changing buffer every 24 hours. Following incubation in PBS containing 30% sucrose for 1 hour at room temperature, bones were embedded in optimal cutting temperature compound (OCT)

(Sakura Finetek, Torrance, CA). The tissue blocks were cut into 12μm sections using a Leica Cryo-Jane system (Leica Biosystems, Wetzlar, Germany). For immunostaining, the slides were first incubated in 0.1M Tris-Cl pH 7.5, 150mM NaCl, and 0.1% Tween 20 (TNT) buffer containing 10% donkey serum for 1 hour at room temperature. Sections were then incubated for 15 minutes at room temperature using the Avidin/Biotin Blocking Kit (SP-2001; Vector Laboratories, Burlingame, CA). Sections were incubated with the primary antibody overnight at 4°C and, where applicable, then incubated with the secondary antibody at a 1 to 100 dilution for 1 hour at room temperature. The following antibodies were used: rabbit anti-osteocalcin (FL-95) at a 1:50 dilution (Santa Cruz Biotechnology Dallas, TX) and goat anti-VE-cadherin (AF1002) at a 1:25 dilution (R&D Systems Minneapolis, MN). Finally, slides were mounted with ProLong Gold antifade reagent with DAPI (Life Technologies, Inc., Grand Island, NY). Images were acquired using an LSM 700 confocal microscope (Carl Zeiss Microscopy, Peabody, MA) and processed using Volocity® v6.5.1 software (PerkinElmer, Waltham, MA). Oil red staining was performed using the Sigma Oil Red O kit per manufacturer's recommendations (Millipore Sigma Darmstadt, Germany). Sections were mounted with Organo/Limonene Mount™ (Millipore Sigma), and images were acquired using a Hamamatsu Nanozoomer (Hamamatsu Photonics, Hamamatsu City, Japan).

### 2.3.5. Quantitative reverse-transcription PCR

Total bone marrow RNA was obtained by flushing femurs with 1 ml of Trizol (Invitrogen). RNA was prepared according to the manufacturer's specification. One-step quantitative reverse-transcription PCR was performed using 50 ng of total RNA and the iTaqTM Universal Probes One-Step Kit (Bio Rad, Hercules, CA) with no template and no reverse transcriptase controls.

mRNA expression is normalized to *β-actin* mRNA expression. Data was collected on a StepOnePlusTM Real-Time PCR System (Thermo Fisher). The following quantitative PCR primer/probe sets were used:

TaqMan® Assays and Arrays:

Actb, Mus_musculus VIC–spanning exons 1–2 Mm04394036_g1

Kit ligand, Mus_musculus FAM–spanning exons 2–3 Mm00442972_m1

Cxcl12, Mus_musculus FAM–spanning exons 2–3 Mm00445553_m1

Spp1, Mus_musculus FAM–spanning exons 3–4 Mm00436767_m1

IDT PrimeTime Std® qPCR Assay:

Smad4, Mus_musculus FAM–spanning exons 8–9 Mm.PT.58.31543505

### 2.3.6. Mesenchymal stromal cell culture

C57BL/6 mice were sacrificed at 3-to-4-weeks-old, and hindlimb bones were harvested and mechanically disrupted in complete Dulbecco's modified eagle medium (DMEM) containing 20% fetal bovine serum (FBS) and penicillin-streptomycin using a mortar and pestle. The resulting cell suspension was cultured overnight at 37°C with 5% CO2, and the following day non-adherent cells removed by gentle aspiration. Adherent cells were cultured until reaching approximately 40% confluence (generally, 5–6 days). 100,000–200,000 cells were plated in 6 well plates 24 hours prior to treatment. TGFβ1 (14-8342-80, Life Technologies) was added every 24 hours for 72 hours at a dose of 10ng/mL.

### 2.3.7. Colony-forming unit assay

25μL of peripheral blood, or 50,000 bone marrow MNCs, or 50,000 spleen MNCs were suspended in DMEM containing 2% FBS and 1% penicillin-streptomycin. The cell suspensions were mixed with 2 mL of methocult (M3434, Stemcell Technologies, Vancouver, Canada) prior to plating 1.1 mL of the methocult-cell mix in one 35 mm dish, repeating with the remaining mix for two technical replicates. The dishes were placed in a 100 mm petri dish with a third 35 mm dish containing 3 mL of sterile water. The samples were incubated at 37°C, 5% CO2 in air and ≥ 95% humidity for 7–10 days prior to colony counting.

### 2.3.8. Phenylhydrazine, 5-FU, and G-CSF treatments

Phenylhydrazine (30 mg/kg, Sigma) was given daily for 2 days by intraperitoneal injection. A single injection of 5-FU (150 mg/kg, F6627-5G, Sigma) was given by intraperitoneal injection. For the HSC exhaustion experiments, mice were treated with weekly 150mg/kg doses of 5-FU. Human G-CSF (125 mg/kg, Amgen, Thousand Oaks, CA) was given twice daily for 7 days via intraperitoneal injection. Complete blood counts were obtained using the HV950 hemavet (Drew Scientific, Miami Lakes, FL).

### 2.3.9. Quantification and statistical analysis

Significance was determined using Prism v8.1.2 (GraphPad, San Diego, CA, USA). For single parameter analysis, unpaired t-test were used to assess statistical significance. For multiple parameter data, statistical significance was calculated using one-way or two-way analysis of

variance (ANOVA). P values less than 0.05 were considered significant. Expression data are log transformed prior to statistical analysis.

# 2.4. Results

## 2.4.1. Post-Natal Loss of *Smad4* in MSCs Does Not Alter the Bone Marrow Stromal Microenvironment

To investigate the role of canonical TGF family member signaling in bone marrow MSCs to hematopoietic niche maintenance, we deleted *Smad4* in mesenchymal cells using a doxycycline-repressible *Sp7* (osterix)-*Cre* transgene (*Osx-Cre*). Prior studies have shown that *Osx-Cre* targets the majority of MSCs in the bone marrow, including osteoblasts, adipocytes, pericytes, and CXCL12-abundant reticular (CAR) cells, but not endothelial cells or hematopoietic cells.[5,32,33] We previously reported that constitutive activation of *Osx-Cre*, by maintaining *Osx-Cre, Smad4*$^{fl/fl}$ mice off of doxycycline throughout embryonic development, results in a loss of osteoblasts, a marked increase in adiposity, and severe runting.[12] Thus, in this study, we activated the *Osx-Cre* transgene post-natally by removing doxycycline 1–2 days after birth. To confirm targeting, we performed lineage mapping studies on 6-to-8-week-old *Osx-Cre, ROSA26*$^{Ai9/+}$ (*Ai9*), *Smad4*$^{fl/fl}$ mice, in which tdTomato expression is induced in cells that have undergone *Cre*-mediated recombination. As expected, in control *Osx-Cre, Ai9* mice tdTomato+ perivascular CAR cells and osteocalcin+ endosteal osteoblasts were observed; a similar pattern was observed in *Osx-Cre, Ai9, Smad4*$^{fl/fl}$ mice (Fig 3.1.A and Fig 3.6.A). To assess *Smad4* deletion, we sorted tdTomato+ stromal cells from the bone marrow of *Osx-Cre, Ai9, Smad4*$^{fl/fl}$ mice. Expression of full length *Smad4*

mRNA was essentially absent, confirming efficient deletion of *Smad4* in bone marrow MSCs (Fig 2.1.B).

Immunostaining of bone sections from *Osx-Cre, Ai9, Smad4$^{fl/fl}$* mice suggested that the number and organization of bone marrow MSCs was comparable to control mice (Fig 3.1.A and Fig 3.6.). To further characterize the hematopoietic niche, we quantified the number of PDGFRβ$^{+}$ Sca1$^{+}$ CD31$^{-}$ lineage$^{-}$ cells (mesenchymal stem/progenitor cells) and PDGFRβ$^{+}$ Sca1$^{-}$ CD31$^{-}$ lineage$^{-}$ cells (a mixture of CAR cells and osteoblasts) by flow cytometry (Fig 3.1.C). We also quantified CD31$^{+}$ Sca1$^{-}$ lineage$^{-}$ venous sinusoidal cells and CD31$^{+}$ Sca1$^{+}$ lineage$^{-}$ arteriolar endothelial cells. In each case, the number of stromal cells was similar to control mice (Fig 3.1.D). We previously reported that loss of TGF-β signaling in MSCs during development results in a marked increase in bone marrow adiposity. However, no increase in bone marrow adipocytes was observed in *Osx-Cre, Smad4$^{fl/fl}$* mice (Fig 3.6.B). Finally, total bone marrow expression of key niche factors, including *Spp1*, *Scf*, and *Cxcl12*, was comparable in *Osx-Cre, Smad4$^{fl/fl}$* and control mice (Fig 3.1.E). Together, these data suggest SMAD4 signaling in bone marrow MSCs is not required for their maintenance under steady-state conditions.

### 2.4.2. Post-Natal Loss of Smad4 in MSCs Does Not Alter Basal Hematopoiesis

We next examined basal hematopoiesis in *Osx-Cre*, *Smad4$^{fl/fl}$* mice. Peripheral blood counts and the level of circulating T cells, B cells, and neutrophils were normal (Fig 3.2.A and 3.2.B). Likewise, the number of myeloid, B-cell, and T-cell lineage cells in the bone marrow was comparable to control mice (Fig 3.2.C and 3.2.D). The number of phenotypic hematopoietic stem cells (HSCs), common myeloid progenitors (CMPs), granulocyte-macrophage progenitors (GMPs), megakaryocyte-erythrocyte progenitors (MEPs), and LSK cells in the bone marrow of

*Osx-Cre*, *Smad4*$^{fl/fl}$ also was similar to control mice (Fig 3.2.E–3.2.G). Finally, no perturbation in the number of mature hematopoietic cells or HSPCs in the spleen of *Osx-Cre*, *Smad4*$^{fl/fl}$ mice was observed (Fig 3.2.H–3.2.L). Collectively, these data show that SMAD4 signaling in bone marrow mesenchymal cells is not required to maintain basal hematopoiesis.

### 2.4.3. Post-Natal Loss of Smad4 in MSCs Does Not Alter Basal or Stress Erythropoiesis

There is evidence that activin signaling in bone marrow stromal cells may contribute to the regulation of erythropoiesis.[23] Flow cytometry was used to identify and quantify phenotypic erythroid progenitors in bone marrow and spleen (Fig 3.3.A). The number of stage I proerythroblasts (CD44$^{high}$ Ter119$^{int}$ cells), stage II basophilic erythroblasts (CD44$^{high}$, Ter119$^{high}$ forward scatter$^{high}$ cells), stage III (polychromatic erythroblasts, (CD44$^{high}$, Ter119$^{high}$ forward scatter$^{int}$ cells), and stage 4 orthochromatic erythroblasts (CD44$^{high}$, Ter119$^{high}$ forward scatter$^{low}$ cells) in the bone marrow or spleen was similar in control and *Osx-Cre*, *Smad4*$^{fl/fl}$ mice (Fig 3.3.B–3.3.D).

To assess stress erythropoiesis, we characterized the response of mice to the induction of acute hemolytic anemia after phenylhydrazine treatment. As expected, in control mice, treatment with phenylhydrazine induced an acute fall in the hematocrit followed by recovery over a 10-day period (Fig 3.3.E). The magnitude of anemia and kinetics of recovery were similar in *Osx-Cre*, *Smad4*$^{fl/fl}$ mice. These data show that SMAD4-dependent signaling in mesenchymal stromal cells is not required for the suppressive effect of activins on erythropoiesis.

### 2.4.4. Post-Natal Loss of Smad4 in Mesenchymal Stromal Cells Does Not Alter Hematopoietic Recovery Following Myeloablative Chemotherapy

A prior study suggested that TGF-β contributes to hematopoietic recovery following myeloablative therapy. However, the contribution of TGF-β signaling in MSCs to hematopoietic recovery is unknown. To address this question, we characterized the hematopoietic response to 5-fluorouracil (5-FU) in *Osx-Cre*, *Tgfbr2*$^{fl/fl}$ mice, in which both canonical and non-canonical TGF-β signaling is abrogated in MSCs. Of note, we previously reported that basal hematopoiesis was normal in these mice when *Osx-Cre* was activated on day 1–2 after birth.[12] In control mice, treatment with a single dose of 5-FU induced neutropenia with a nadir on day 7 and complete recovery by day 9 (Fig 3.4.A). Both the magnitude of neutropenia induced by 5-FU and kinetics of neutrophil recovery were similar in *Osx-Cre*, *Tgfbr2*$^{fl/fl}$ mice. Repeated doses of 5-FU induce HSC exhaustion and death in mice due to hematopoietic failure. Similar median survival after weekly 5-FU was observed in *Osx-Cre*, *Tgfbr2*$^{fl/fl}$ and control mice (Fig 3.4.B). These data show that TGF-β signaling in bone marrow MSCs does not contribute to hematopoietic recovery following myeloablative therapy. Of note, survival following repeated treatment with 5-FU in *Osx-Cre*, *Smad4*$^{fl/fl}$ mice was comparable to control mice, suggesting that canonical signaling by other TGF-β family members in MSCs also does not contribute to hematopoietic stress responses to myeloablative therapy (Fig 3.4.C).

### 2.4.5. Loss of Smad4 in Mesenchymal Stromal Cells Does Not Affect HSPC Mobilization by Granulocyte-Colony Stimulating Factor

There is strong evidence that G-CSF induced HSPC mobilization is mediated, at least in part, by the downregulation of CXCL12 expression in bone marrow MSCs.[34–39] Treatment of bone marrow stromal cell lines with TGF downregulates CXCL12 expression in a SMAD4-dependent fashion.[40,41] There also is evidence that G-CSF treatment is associated with increased circulating TGF-β1 levels.[42] Together, these observations suggest the hypothesis that canonical TGF-β family signaling in bone marrow MSCs, by downregulating CXCL12 expression, may contribute to G-CSF induced HSC mobilization. To test this hypothesis, we first asked whether TGF-β1 regulates CXCL12 in primary murine bone marrow MSCs. Indeed, treatment of cultures of primary bone marrow MSC with TGF-β1 for 3 days resulted in a significant decrease in CXCL12 mRNA expression (Fig 3.5.A). We next characterized G-CSF induced HSPC mobilization in *Osx-Cre*, *Smad4*$^{fl/fl}$ mice. Treatment of control mice with G-CSF for 5 days induced robust mobilization of colony-forming cells (CFU-C) and Lineage$^{-}$ Sca$^{+}$ Kit$^{+}$ (LSK) cells into the blood and spleen (Fig 3.5.B–3.5.F). A similar level of HSPC mobilization was observed in *Osx-Cre*, *Smad4*$^{fl/fl}$ mice. Consistent with prior studies, G-CSF induced a marked decrease in total bone marrow CXCL12 mRNA expression, with a similar decrease observed in *Osx-Cre*, *Smad4*$^{fl/fl}$ mice (Fig 3.5.G). We also analyzed G-CSF induced HSPC mobilization in *Osx-Cre*, *Tgfbr2*$^{fl/fl}$ mice, where all TGF-β1 signaling in MSCs is abrogated. Again, HPSC mobilization by G-CSF, as measured by CFU-C levels in blood and spleen, was comparable to control mice (Fig 3.7.). Collectively, these data show that neither TGF-β1 signaling nor canonical TGF family signaling in bone marrow MSCs is required for efficient HSPC mobilization by G-CSF.

## 2.5. Discussion

Recent single cell RNA sequencing studies of murine bone marrow stromal cells show that most of the receptors for TGF family members are expressed at low levels on mesenchymal stromal cells, including osteolineage cells, isolated from adult mice under steady state conditions. Prior studies have established that TGF family members play an important role during development in the generation of the hematopoietic niche in the bone marrow. In particular, we recently showed that TGF-β signaling plays a key role in the specification of fetal mesenchymal progenitor cells to a non-adipocyte fate. There also is evidence, mainly from cell culture systems, that TGF family members can regulate the function of mesenchymal stromal cells. In contrast, our data suggest that canonical SMAD4-dependent TGF family member signaling in mesenchymal stromal cells is dispensable for their maintenance in the bone marrow hematopoietic niche once the niche is established. Of note, since *Osx-Cre* only targets mesenchymal stromal cells in the bone marrow, the contribution of TGF family member signaling in other stromal cells, such as endothelial cells, to basal and stress hematopoiesis remains uncertain.

There is evidence that alterations in mesenchymal stromal cells contribute to stress hematopoiesis responses. G-CSF induced HSPC mobilization is associated with a loss of active osteoblasts and decreased CXCL12 expression in bone marrow MSCs. Myeloablation due to chemotherapy or radiation therapy is associated with an expansion of bone marrow adipocytes, which support hematopoietic recovery through secretion of stem cell factor.[29] Myeloablative radiation also induces a loss of osteoblasts, which is followed by an expansion of osteolineage cells.[28] Our data suggest that SMAD-dependent signaling by TGF family members in bone marrow MSCs is not a major contributor to hematopoiesis responses to certain stressors, including myeloablation therapy with 5-FU, acute anemia, and G-CSF treatment. Whether TGF family

member signaling contributes to hematopoiesis responses after other stressors, such as irradiation needs further study.

TGF family members activate multiple intracellular signaling pathways besides SMADs, including Erk [43–45], Rho-like GTPases [46–51], JNK/p38[52,53], and PI3K/Akt [54–56]. Our prior and current data suggest that both SMAD-dependent and -independent TGF-β signaling in bone marrow MSCs is dispensable for hematopoietic niche maintenance and response to certain stressors. However, for the other TGF family members, there is a possibility that non-SMAD dependent signaling may regulate bone marrow MSCs. Indeed, a prior study showed that loss of BMP receptor type 1A (Bmpr1a) in bone marrow MSCs results in an expansion of N-cadherin+ osteoblastic cells and an increase in HSCs.[21] Our data suggests that non-SMAD4 dependent BMP signaling likely mediates this response. Further studies are needed to test this hypothesis and characterize the contribution of non-canonical signaling by TGF family members in bone marrow MSCs to the regulation of basal or stress hematopoiesis.

## 2.6. Acknowledgement

We thank the Alvin J. Siteman Cancer Center at Washington University School of Medicine and Barnes-Jewish Hospital in St. Louis, MO., for the use of the Siteman Flow Cytometry, which provided cell sorting services.

## 2.7. Author Contributions

Joseph R. Krambs and Daniel C. Link conceived and designed the experiments, analyzed the data, and wrote the manuscript. Joseph R. Krambs performed all of the experiments. Joseph R. Krambs generated the *Osx-Cre; Smad4*$^{fl/fl}$ mice. Grazia Abou Ezzi contributed Figure 2.4.A. Juo-Chin Yao contributed Figure 2.5.A. Daniel C. Link supervised the research.

# 2.8. Figures

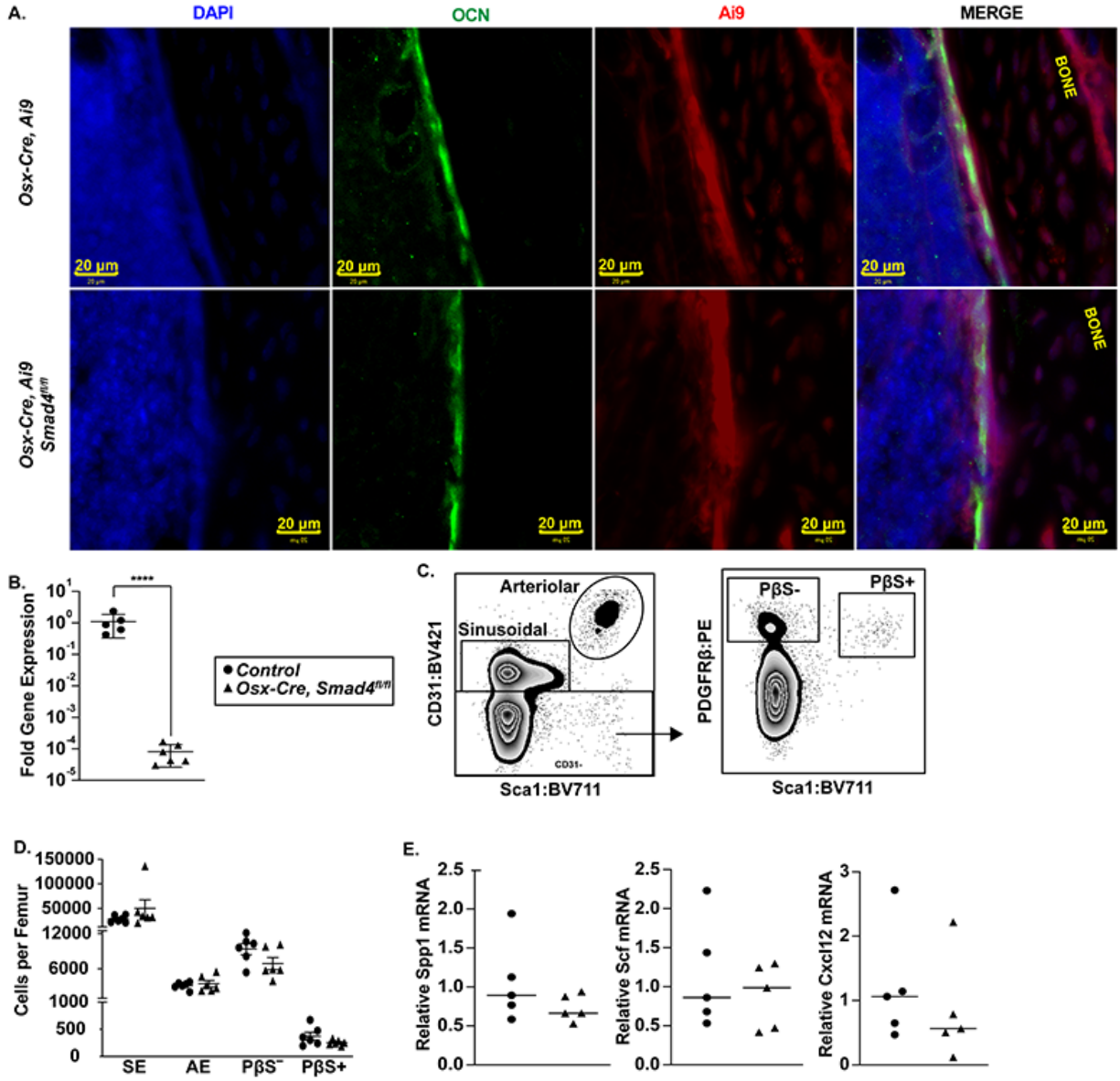
A.
DAPI
OCN
Ai9
MERGE
Osx-Cre, Ai9
Osx-Cre, Ai9 Smad4f/f
BONE
20 μm
B.
Fold Gene Expression
****
Control
Osx-Cre, Smad4f/f
C.
Arteriolar
Sinusoidal
CD31:BV421
Sca1:BV711
PDGFRβ:PE
PβS-
PβS+
D.
Cells per Femur
SE
AE
PβS⁻
PβS+
E.
Relative Spp1 mRNA
Relative Scf mRNA
Relative Cxcl12 mRNA

**Fig 2.1. Mesenchymal stromal cell number and organization are normal in *Osx-Cre*, *Smad4*$^{fl/fl}$ mice.** (A) Representative photomicrographs of femur sections from *Osx-Cre Ai9* or *Osx-Cre*, *Ai9*, *Smad4*$^{fl/fl}$ mice showing DAPI stained nuclei (blue), osteocalcin (OCN) expressing mature osteoblasts (green), and tdTomato$^{+}$ mesenchymal stromal cells (red). (B) Relative Smad4 mRNA expression of sorted tdTomato$^{+}$ CD45$^{-}$ Ter119$^{-}$ stromal cells normalized to β-actin mRNA. (C) Representative flow plots showing the gating strategy used to identify CD31$^{+}$ Sca1$^{-}$ sinusoidal endothelial cells (SE) and CD31$^{+}$ Sca1$^{+}$ arteriolar endothelial cells (AE, left panel); data are gated on CD45$^{-}$ Ter119$^{-}$ cells. The right panel shows PDGFRβ$^{+}$ Sca1$^{-}$ CD31$^{-}$ mesenchymal stromal (PβS$^{-}$) cells and PDGFRβ$^{+}$ Sca1$^{+}$ (PβS$^{+}$) mesenchymal stem cells. (D) Number of SE, AE, PβS$^{-}$ and PβS$^{+}$ cells per femur is shown for *Osx-Cre* (control) or *Osx-Cre*, *Smad4*$^{fl/fl}$ mice. (E) Relative mRNA expression in whole bone marrow compared to β-actin mRNA of the indicated gene. Data represent the mean ± SEM. ****P < 0.0001 by unpaired student t-test.

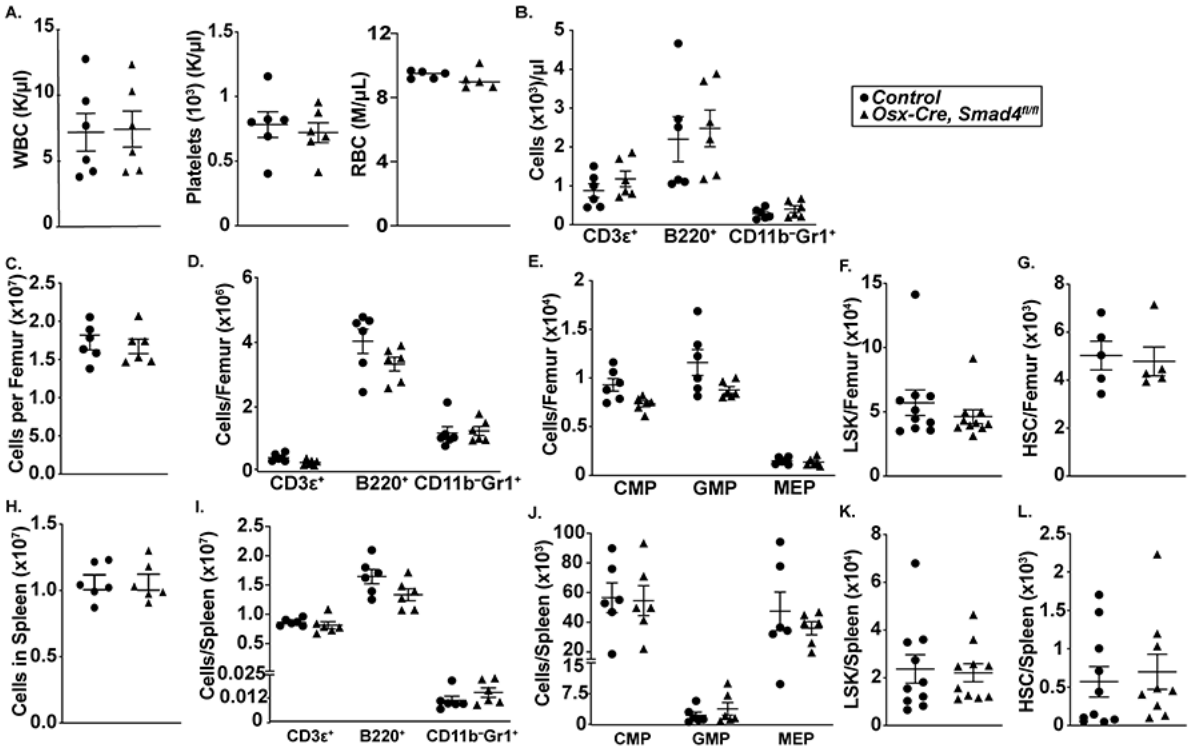
A.
WBC (K/μl)
Platelets ($10^3$) (K/μl)
RBC (M/μL)
B.
Cells ($x10^3$)/μl
CD3ε+
B220+
CD11b-Gr1+
Control
Osx-Cre, Smad4fl/fl
C.
Cells per Femur ($x10^7$)
D.
Cells/Femur ($x10^6$)
CD3ε+
B220+
CD11b-Gr1+
E.
Cells/Femur ($x10^4$)
CMP
GMP
MEP
F.
LSK/Femur ($x10^4$)
G.
HSC/Femur ($x10^3$)
H.
Cells in Spleen ($x10^7$)
I.
Cells/Spleen ($x10^7$)
CD3ε+
B220+
CD11b-Gr1+
J.
Cells/Spleen ($x10^3$)
CMP
GMP
MEP
K.
LSK/Spleen ($x10^4$)
L.
HSC/Spleen ($x10^3$)

**Fig 2.2. Basal hematopoiesis is normal in *Osx-Cre*, *Smad4*$^{fl/fl}$ mice.** (A) Peripheral counts in *Osx-Cre* (control) or *Osx-Cre*, *Smad4*$^{fl/fl}$ mice. (B) Number of circulating CD3ε$^{+}$ (T-lineage), B220$^{+}$ (B-lineage), and CD11b$^{+}$ Gr1$^{+}$ (Granulocytes). (C) Bone marrow cellularity. (D) Number of CD3ε$^{+}$, B220$^{+}$, and CD11b$^{-}$ Gr1$^{+}$ cells per femur. (E) Number of common myeloid progenitors (CMP, lineage$^{-}$ Sca1$^{-}$ Kit$^{+}$ CD34$^{+}$ cells), granulocyte-macrophage progenitors (GMP, lineage$^{-}$ Sca1$^{-}$ Kit$^{+}$ CD34$^{+}$ CD16/32$^{+}$ cells), and megakaryocyte-erythrocyte progenitors (MEP, lineage$^{-}$ Sca1$^{-}$ Kit$^{+}$ CD34$^{-}$ CD16/32$^{-}$ cells) per femur. (F) Number of phenotypic hematopoietic stem/progenitor cells (lineage$^{-}$ Sca1$^{+}$ Kit$^{+}$, LSK cells) per femur. (G) Number of phenotypic hematopoietic stem cells (LSK CD48$^{-}$ CD41$^{-}$ CD150$^{+}$ cells) per femur. (H) Spleen cellularity. (I) Number of CD3ε$^{+}$, B220$^{+}$, and CD11b$^{+}$ Gr1$^{+}$ per spleen. (J) Number of CMP, GMP, and MEP per spleen. (K) Number of LSK cells per spleen. (L) Number of phenotypic HSCs per spleen. Data represent the mean ± SEM.

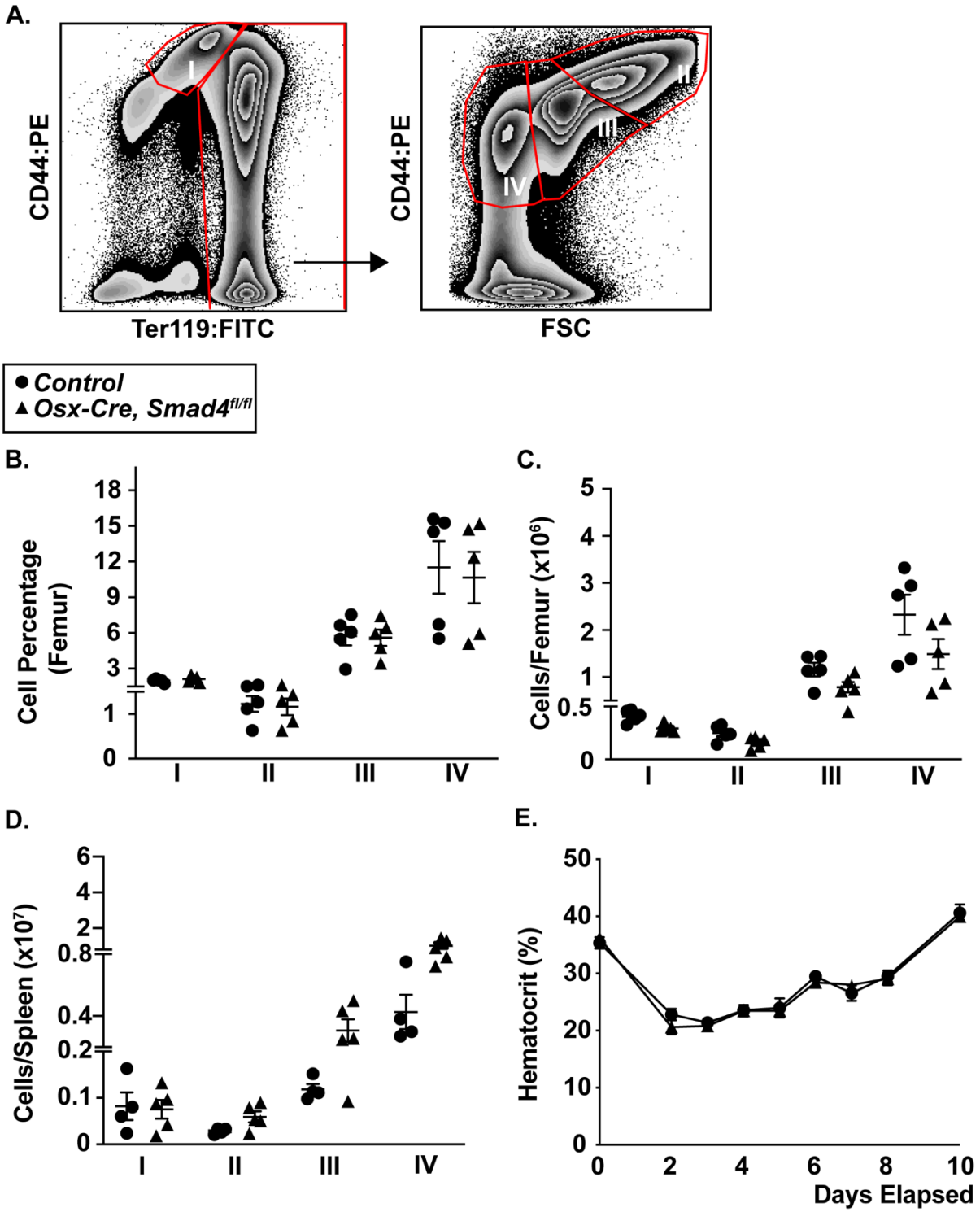
A.
CD44:PE
Ter119:FITC
I
CD44:PE
FSC
II
III
IV
Control
Osx-Cre, Smad4fl/fl
B.
Cell Percentage (Femur)
18
15
12
9
6
3
1
0
I
II
III
IV
C.
Cells/Femur (x10⁶)
5
4
3
2
1
0.5
0
I
II
III
IV
D.
Cells/Spleen (x10⁷)
6
4
2
0.8
0.4
0.2
0.1
0
I
II
III
IV
E.
Hematocrit (%)
50
40
30
20
10
0
0
2
4
6
8
10
Days Elapsed

**Figure 2.3. Erythropoiesis is normal in *Osx-Cre Smad$^{fl/fl}$* mice.** (A) Representative flow plots showing the gating strategy to identify different stages of erythroid development: stage I proerythroblasts (CD44$^{high}$ Ter119$^{int}$ cells); stage II basophilic erythroblasts (CD44$^{high}$, Ter119$^{high}$, forward scatter$^{high}$ cells); stage III polychromatic erythroblasts (CD44$^{high}$, Ter119$^{high}$, forward scatter$^{int}$ cells); stage IV orthochromatic erythroblasts (CD44$^{high}$, Ter119$^{high}$, forward scatter$^{low}$ cells). (B) Percentage of erythroid progenitors in the bone marrow. (C) Absolute number of erythroid progenitors per femur. (D) Absolute number of erythroid progenitors per spleen. (E) Mice were treated with a single 30 mg/kg dose of phenylhydrazine to induce hemolysis on day 0. Shown is the hematocrit at the indicated time after phenylhydrazine. Data represent the mean ± SEM. Significance determined by one-way ANOVA.

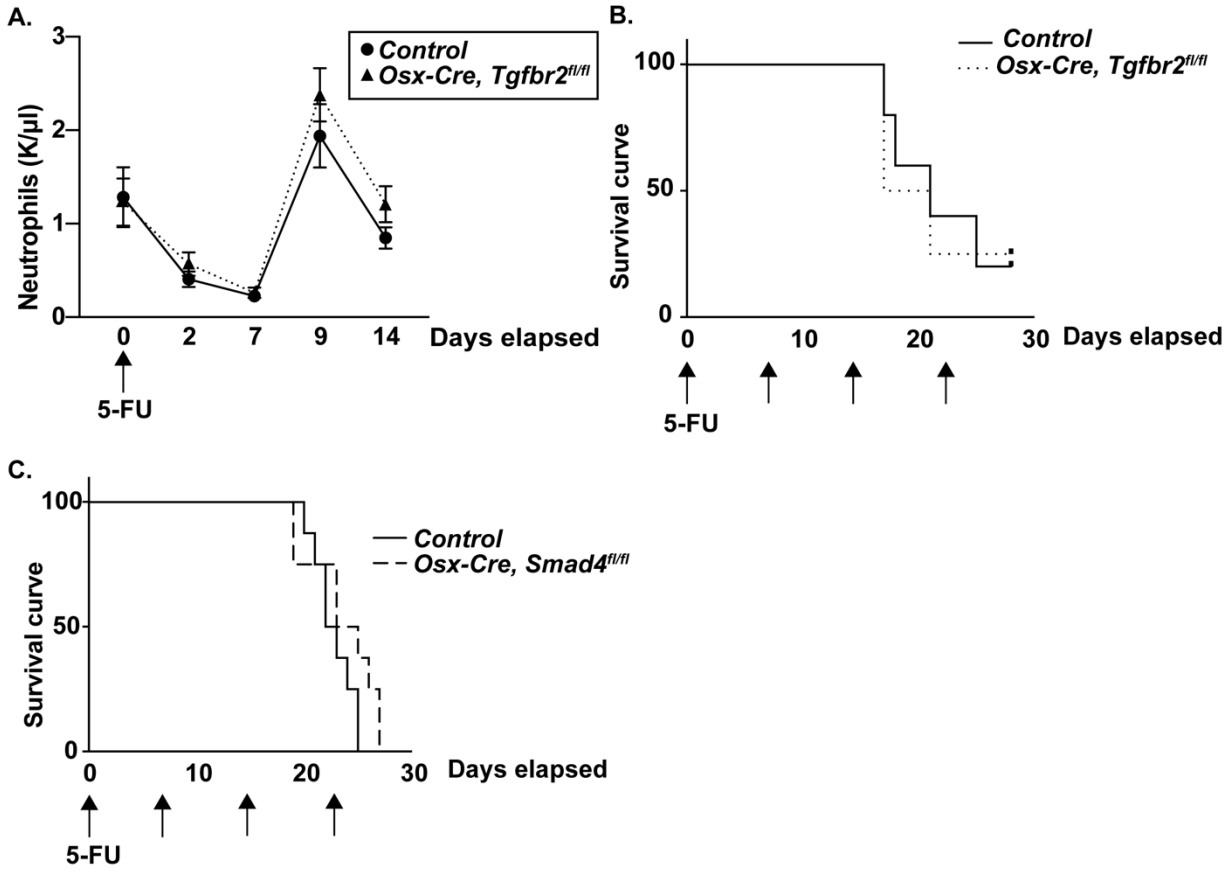
A.
Neutrophils (K/μl)
3
2
1
0
Control
Osx-Cre, Tgfbr2fl/fl
0
2
7
9
14
Days elapsed
5-FU
B.
Survival curve
100
50
0
Control
Osx-Cre, Tgfbr2fl/fl
0
10
20
30
Days elapsed
5-FU
C.
Survival curve
100
50
0
Control
Osx-Cre, Smad4fl/fl
0
10
20
30
Days elapsed
5-FU

**Figure 2.4. TGF-β signaling in mesenchymal stromal cells is not required for hematopoietic recovery following myeloablation with 5-FU.** (A) *Osx-Cre Tgfbr2*$^{fl/fl}$ or *Osx-Cre* (control) mice were treated with a single 150 mg/kg dose of 5-fluorouracil (5-FU) and hematopoietic recovery assessed by serial blood counts (n = 5 per cohort). (B) *Osx-Cre Tgfbr2*$^{fl/fl}$ or control mice were treated weekly with 150 mg/kg of 5-FU for 4 weeks to induce HSC exhaustion. Shown is mouse survival (n = 5 per cohort). (C) *Osx-Cre Smad4*$^{fl/fl}$ or control mice were treated weekly with 150 mg/kg of 5-FU for 4 weeks to induce HSC exhaustion. Shown is mouse survival (n = 8 per cohort). Data represent the mean ± SEM. Significance determined by Log-rank Mantel-Cox test with Gehan-Breslow-Wilcoxon test.

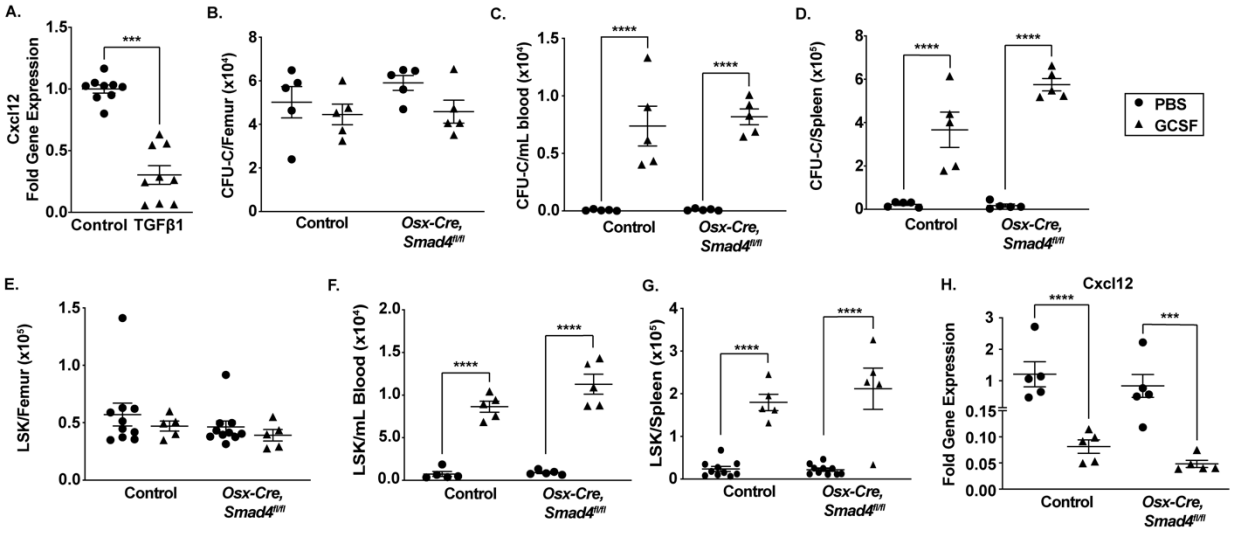
A.
Cxcl12 Fold Gene Expression
***
Control TGFβ1
B.
CFU-C/Femur (x10⁴)
Control
Osx-Cre, Smad4fl/fl
C.
CFU-C/mL blood (x10⁴)
****
Control
Osx-Cre, Smad4fl/fl
D.
CFU-C/Spleen (x10⁵)
****
Control
Osx-Cre, Smad4fl/fl
PBS
GCSF
E.
LSK/Femur (x10⁵)
Control
Osx-Cre, Smad4fl/fl
F.
LSK/mL Blood (x10⁴)
****
Control
Osx-Cre, Smad4fl/fl
G.
LSK/Spleen (x10⁵)
****
Control
Osx-Cre, Smad4fl/fl
H.
Cxcl12
Fold Gene Expression
****
***
Control
Osx-Cre, Smad4fl/fl

**Figure 2.5. TGF-β signaling in mesenchymal stromal cells is not required for G-CSF induced HSPC mobilization.** (A) Bone marrow mesenchymal stromal cell cultures were established from wildtype mice. Cells were treated with TGFβ1 ligand (10 ng/mL) for 72 hours and then RNA harvested. Shown is *Cxcl12* mRNA expression relative to *β–actin* mRNA. (B-D) *Osx-Cre Smad4*$^{fl/fl}$ or control mice were treated with 125 mg/kg of granulocyte-colony stimulating factor (G-CSF) or saline alone twice daily for 7 days. Shown are the number of colony forming cells (CFU-C) in bone marrow (B), blood (C), or spleen (D). (E-G) Shown are the number of LSK cells in bone marrow (E), blood (F), or Spleen (G) after 7 days of G-CSF or saline treatment. Data represent the mean ± SEM. Significance determined by two-way ANOVA with alpha of 0.05 and Sidak's multiple comparisons test. ***P<0.001 ****P<0.0001.

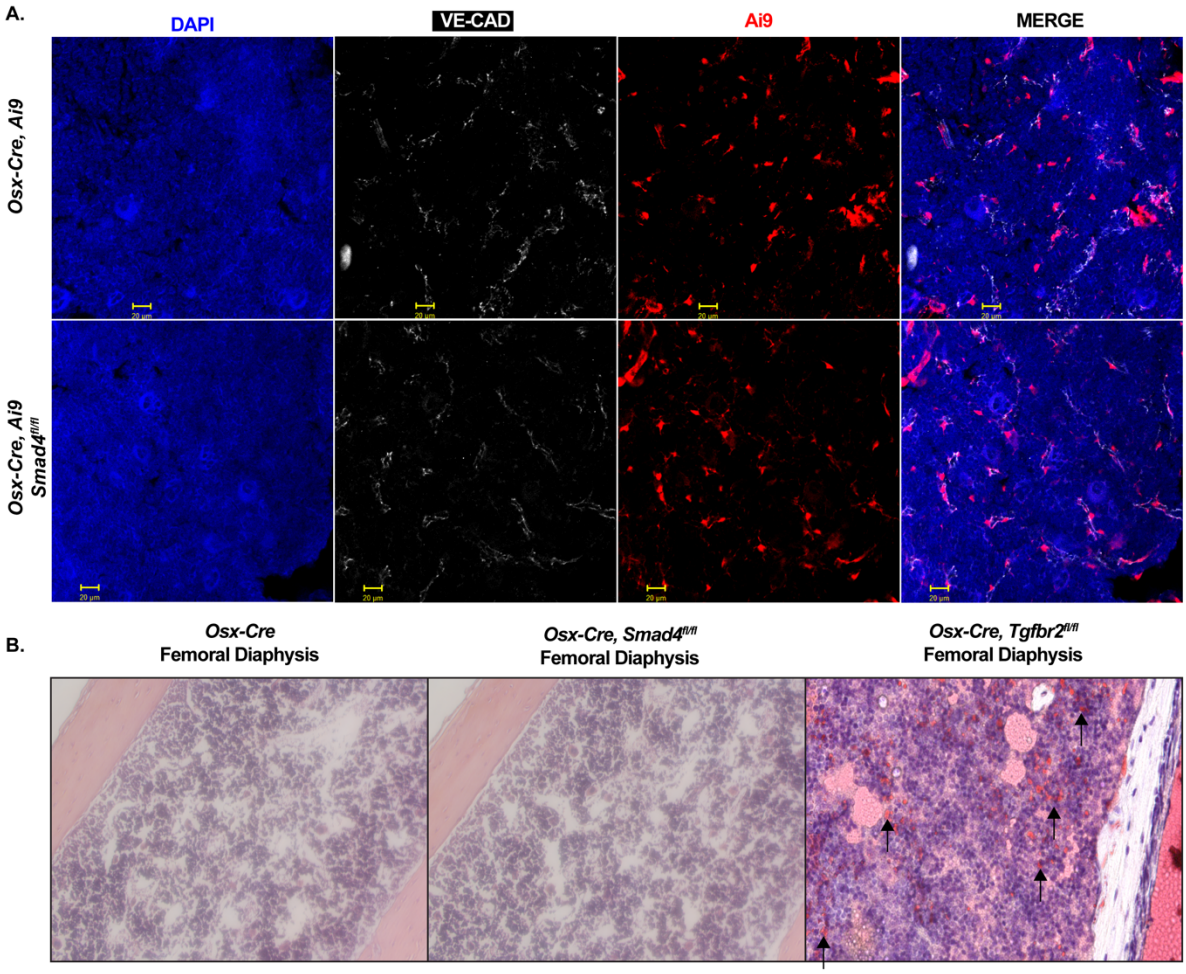
A.
DAPI
VE-CAD
Ai9
MERGE
Osx-Cre, Ai9
Osx-Cre, Ai9 Smad4fl/fl
B.
Osx-Cre
Femoral Diaphysis
Osx-Cre, Smad4fl/fl
Femoral Diaphysis
Osx-Cre, Tgfbr2fl/fl
Femoral Diaphysis

**Figure 2.6. Characterization of mesenchymal stromal cells in *Osx-Cre, Ai9, Smad4$^{fl/fl}$* mice.** (A) Representative photomicrographs of femur sections from *Osx-Cre Ai9* (control) or *Osx-Cre*, *Ai9*, *Smad4$^{fl/fl}$* (*Smad$^{fl/fl}$*) mice showing DAPI stained nuclei and tdTomato (Ai9) mesenchymal stromal cells with morphologic similarities to CAR cells. (B) Representative images of femurs stained with oil red o (purple/red staining) to identify adipocytes (black arrowheads). Femur sections from *Osx-Cre Tgfbr2$^{fl/fl}$* mice are included as a positive control, since we previously showed that constitutively deletion of *Tgfbr2* in mesenchymal stromal cells is associated with a marked increase in bone marrow adiposity. [Abou Ezzi]

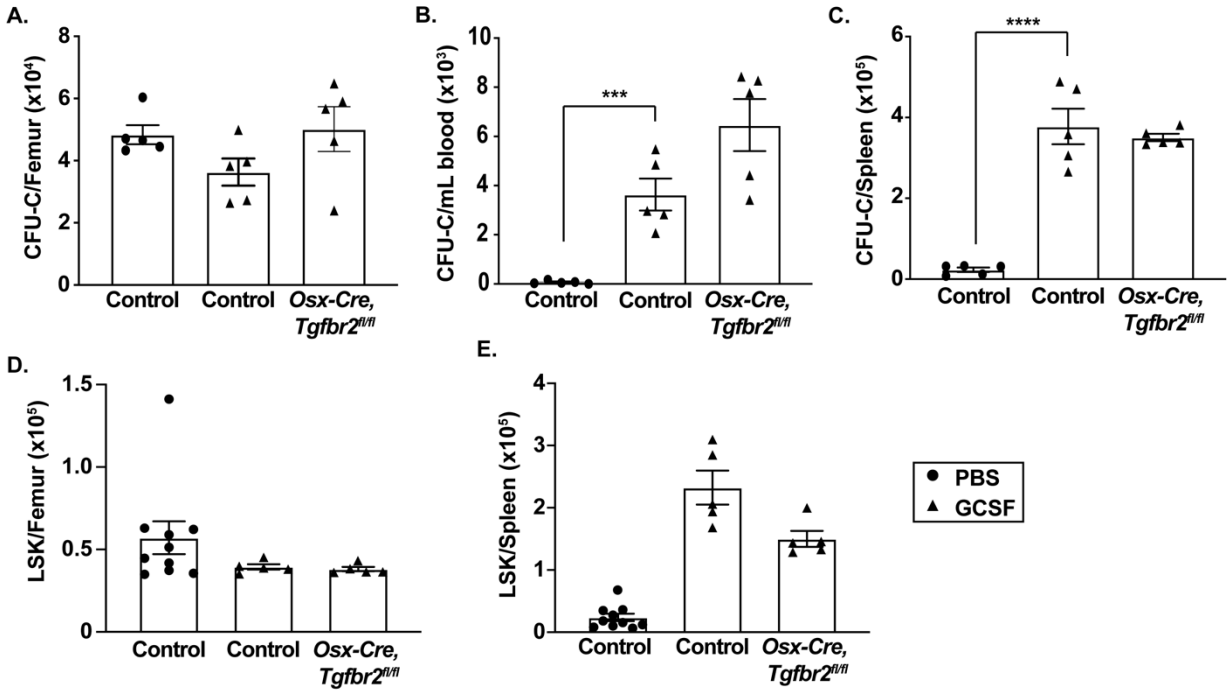
A.
CFU-C/Femur (x10⁴)
8
6
4
2
0
Control
Control
Osx-Cre, Tgfbr2fl/fl
B.
CFU-C/mL blood (x10³)
10
8
6
4
2
0
***
Control
Control
Osx-Cre, Tgfbr2fl/fl
C.
CFU-C/Spleen (x10⁵)
6
4
2
0
****
Control
Control
Osx-Cre, Tgfbr2fl/fl
D.
LSK/Femur (x10⁵)
1.5
1.0
0.5
0
Control
Control
Osx-Cre, Tgfbr2fl/fl
E.
LSK/Spleen (x10⁵)
4
3
2
1
0
Control
Control
Osx-Cre, Tgfbr2fl/fl
PBS
GCSF

**Figure 2.7. G-CSF induced HSPC mobilization is normal in *Osx-Cre Tgfbr2$^{fl/fl}$* mice.** (A-C) *Osx-Cre Tgfbr2$^{fl/fl}$* or *Osx-Cre* (control) mice were treated with 125 mg/kg of granulocyte-colony stimulating factor (G-CSF) twice daily for 7 days. Shown are the number of colony forming cells (CFU-C) in bone marrow (A), blood (B), or spleen (C). (D-E) Shown are the number of LSK cells in bone marrow (D) and spleen (E) after 7 days of G-CSF. Data represent the mean ± SEM. ***P<0.001 and ****P<0.0001 by two-way ANOVA with an alpha of 0.05 and Sidak's multiple comparisons test. The saline treated cohort is the same as in Figure 2.5.

# Chapter 3: Microbiota Signals Suppress B Lymphopoiesis with Aging in Mice

## 3.1. Preface

Aging is associated with an expansion of phenotypic hematopoietic stem cells (HSCs) with reduced self-renewal capacity and myeloid-skewing lineage differentiation. An intricate network of dynamic intrinsic and extrinsic signals is responsible for hematopoietic homeostasis, directing HSC lineage commitment, enhancing, or suppressing myelopoiesis, lymphopoiesis, and erythropoiesis. Inflammation is one factor implicated in driving hematopoietic dynamics. Proinflammatory cytokines of the hematopoietic system – including interleukins, colony-stimulating factors, and interferons – have been shown to instruct hematopoietic stem and progenitor cell (HSPC) proliferation and lineage commitment. Previous reports have demonstrated the accumulation of these signals with age and the proximate association with reduced function of aged HSCs – increased HSC frequency, decreased engraftment, reduced repopulating potential, and myeloid skewing. Although increased inflammatory signaling is observed with chronologic aging, the relationship between inflammation and HSC aging is not well understood.

Accumulating evidence suggests that the microbiota and microbiota-derived compounds may contribute to age-related phenotypes, especially in the context of hematopoiesis. Previous reports have demonstrated that microbiota influence multipotent progenitors to initiate emergency myelopoiesis, however the effect of microbiota-derived compounds, especially those derived from commensal flora, on the regulation of hematopoietic output has not been well characterized.

Signals from commensal flora support basal myelopoiesis in young mice; however, their contribution to hematopoietic aging is largely unknown. Here we characterize hematopoiesis in young and middle-aged mice housed under specific pathogen free (SPF) and germ-free (GF) conditions. We did not analyze older mice due to the difficulty in maintaining mice in a gnotobiotic facility for more than one year. Consistent with prior studies, there is a shift in hematopoiesis in aged SPF mice towards granulopoiesis, with a significant increase in the percentage of granulocytic cells and a decrease in B lineage cells in the bone marrow. The marked shift from lymphopoiesis to myelopoiesis that develops during aging of SPF mice is mostly abrogated in GF mice. Compared with aged SPF mice, there is a marked expansion of B lymphopoiesis in aged GF mice, which is evident at the earliest stages of B cell development.

To investigate the impact of microbiota signals on multipotent HSPCs, we first quantified HSPCs by flow cytometry. In aged SPF mice, the number of lineage$^-$ Sca1$^+$ cKit$^+$ CD150$^+$ CD48$^-$ (LSK-SLAM) cells and CD34$^-$ LT-HSCs is increased 6.4 ± 1.7-fold and 3.4 ± 1.2-fold, respectively. Similar increases were observed in aged GF mice, with LSK-SLAM increasing 5.3 ± 1.6-fold ($P$ = NS compared to SPF mice) and CD34$^-$ LT-HSCs increasing 2.8 ± 0.31-fold ($P$ = NS). To quantify functional HSCs, limiting dilution transplantation experiments using unsorted bone marrow cells was performed. Although on a per cell basis the repopulating activity of aged HSCs is reduced, due to the large increase in phenotypic HSCs, the number of functional HSCs actually increases with aging with similar increases in functional HSCs in aged SPF and GF mice. Finally, to assess lineage-bias, we transplanted a limited number of sorted HSCs and assessed lineage output. As expected, in young SPF mice, the majority of HSCs displayed a balanced myeloid/lymphoid lineage output with a significant increase in myeloid-biased HSCs observed with aging. In young GF mice, the majority of HSCs are lymphoid-biased. Moreover, although

the myeloid output increased modestly with aging, the majority of HSCs in aged GF remained lymphoid-biased or balanced. Consistent with these data, RNA expression profiling of phenotypic HSCs from aged GF mice show enrichment for non-myeloid biased HSCs. Surprisingly, the RNA expression profiling data also suggest that inflammatory signaling is increased in aged GF HSCs compared with aged SPF HSCs. Collectively, these data suggest that microbiota-related signals suppress the lymphoid potential of HSCs, contributing to the expansion of myeloid-biased HSCs that occurs with aging.

The characterization of the effect of microbiota on age related hematopoietic dynamics was a major scientific undertaking between the Schuettpelz and Link labs, spanning more than four years. For my part, I characterized phenotypic hematopoietic populations by flow cytometry, measured the frequency of HSCs through limiting dilution transplantation, assessed intrinsic HSC properties by sorted HSC transplantation, quantified cytokine serum levels, and analyzed differentially expressed gene signatures. Together, our data demonstrate that the expansion of hematopoietic stem and progenitor cells with age is not dependent on microbiota. In addition, microbiota induce cell autonomous changes in HSCs, suppressing lymphopoiesis in young mice and reducing aged-HSC capacity for B lymphopoiesis. These data support the hypothesis that microbiota prime HSCs for myeloid lineage production early in development, resulting in intrinsic alterations. In addition to experimentation, I statistically assessed data, generated figures, and wrote and revised the manuscript.

## 3.2. Introduction

Aging is associated with significant changes in hematopoiesis which includes a shift from lymphopoiesis to myelopoiesis [1-4]. A decline in lymphopoiesis is evident early in adulthood and progressively declines with aging [5]. Prior studies show that there is a loss of the earliest lymphoid-restricted progenitors in aged mice, including decreases in lymphoid-primed multipotent progenitors (LMPPs) and common lymphoid progenitors (CLPs) [6-9]. Decreased proliferation and cytokine responsiveness of pre-pro-B and pro-B cells also has been reported [6,7,10]. Finally, there is evidence that impaired lineage-specification of hematopoietic stem cells (HSCs) may contribute to the decrease in lymphopoiesis. Specifically, phenotypic HSCs expand with age, but they have reduced self-renewal capacity and display myeloid-lineage skewing [1,11,12].

There is evidence suggesting that inflammation may contribute to age-related changes in hematopoiesis [13-18]. Expression of certain inflammatory cytokines increases with aging, including tumor necrosis factor-alpha (TNF-α) and interleukin-1β (IL1-β) [19,20]. This is relevant to aging, since chronic stimulation with IL1-β results in reduced HSC self-renewal and enhanced myeloid differentiation [21], and TNF-α signaling has been implicated in the reduced proliferation of aged pro-B cells and myeloid skewing of HSCs [22,23]. Increased toll-like receptor signaling also has been implicated in hematopoietic aging. Prolonged (4-6 weeks) treatment with the TLR4 ligand, lipopolysaccharide (LPS), is associated with an expansion of phenotypic HSCs with reduced repopulating and enhanced myeloid differentiation, reproducing some of the most prominent features of hematopoietic aging [24]. Likewise, prolonged treatment with a TLR2 agonist results in an expansion of phenotypic HSCs but a loss of HSC self-renewal capacity [25].

One source of inflammatory signaling is the microbiota. Prior studies have established through the study of germ-free mice or antibiotic treated mice that signals from microbiota play an important role in the regulation of hematopoiesis [26,27]. A consistent finding from multiple groups is modestly reduced myelopoiesis in germ-free or antibiotic treated young mice, with decreases in mature neutrophils, monocytes, and myeloid progenitors [27-29]. The impact of microbiota on multipotent hematopoietic progenitors is less clear with two groups showing a modest reduction in phenotypic HSCs and multipotent progenitors in germ-free or antibiotic treated mice [26,30], while our data using young germ-free mice showed no difference in HSC number or quiescence [31]. In the present study, we examined the impact of microbiota on basal hematopoiesis in young adult or middle-aged mice. Our data suggest that microbiota signals play an important role in the age-dependent shift from lymphopoiesis to myelopoiesis.

# 3.3. Material and Methods

## 3.3.1. Mice and Mouse Housing

All mouse experiments were approved by Washington University Animal Studies Committee. Germ-free C57BL/6J mice were housed in a sterile environment of plastic flexible film isolators (Class Biologically Clean Ltd., Madison, WI), as described previously [32]. Manipulations are carried out within the sterile workspace using neoprene gloves directly attached to the bag by metal compression rings. A double-door port is located in the wall of the isolator opposite the gloves. This port is used to bring supplies into the isolator. Air is supplied to each isolator by a dedicated blower attached to a filter by a flexible vinyl hose. Air exits the isolator

through an identical filter assembly. Air pressure within the isolator is kept slightly above atmospheric, so that the isolator remains inflated and immediate entrance of airborne contaminants is prevented in the case of accidental puncture. Sterile supplies, such as autoclaved food, water, and bedding, are brought into the isolator through the side port. Since germ-free mice lack nutrients synthesized by gut microbes (e.g., vitamin K), mice were maintained on an enriched rodent diet (BeeKay autoclavable rodent diet; B&K Universal).

Routine monitoring of isolators for the presence of bacteria and fungi is imperative when maintaining a germ-free colony. Animal feces were monitored on a weekly basis for microbial contamination. In addition, the inside surfaces of the isolator were swabbed and cultured weekly. All samples were cultured aerobically and anaerobically in three different media: nutrient broth (a general-purpose medium for cultivating microorganisms with non-exacting nutritional requirements), brain/heart infusion broth (allows cultivation of a wide variety of fastidious microorganisms), and Sabouraud Dextrose Broth (supports growth of yeasts, molds, and aciduric microorganisms). All three media are available from BD Difco. Anaerobic incubations are done at 37°C in GasPak jars (Fisher) with activated GasPak Hydrogen + $CO_2$ envelopes (Fisher). Aerobic incubations are done at 37°C and 42°C.

Specific pathogen-free mice were maintained under specific pathogen-free conditions and include C57BL/6 (*Ly45.2* wildtype) and B6.SJL-*Ptprc*$^{a}$ *Pepc*$^{b}$/BoyJ (*Ly45.1* wildtype) mice which were obtained from The Jackson Laboratory (Bar Harbor, ME). Mice were crossed in-house to generate *Ly5.2*/*Ly5.1* expressing mice on a C57BL/6 background. All experiments were done using young 6-8-week-old mice and middle-aged 10-12-month-old mice. Transplant donor and support/competitor mice were age and sex matched.

### 3.3.2. Flow cytometry and cell sorting

Peripheral blood, bone marrow, and spleen mononuclear cell (MNC) preparations were red blood cell lysed. The resulting cell suspension was filtered through CellTrics 70 μm nylon filters (Sysmex, Goerlitz, Germany) to generate single cell suspensions. MNCs were counted using trypan blue (Thermo Fisher, Waltham, MA) and a Cellometer Auto T4 Bright Field Cell Counter (Nexcelom, Lawrence, MA). Complete blood counts were obtained using the HV950 hemavet (Drew Scientific, Miami Lakes, FL). MNCs were incubated with target antibodies at 4°C for 30-90 minutes (or overnight for HSC CD45.2/CD45.1 staining) in phosphate buffered saline (PBS) containing 1mM ethylenediaminetetraacetic acid (EDTA) and 0.2% (weight/volume) bovine serum albumin (BSA). Data were acquired using a FACS Aria III flow cytometer (BD biosciences, San Jose, CA) and analyzed using FlowJo™ v10.6.1 software (BD biosciences). LSK-SLAM cells were sorted using a Sony iCyt Synergy SY3200 (Synergy cell sorter (Sony, San Jose, CA).

The hematopoietic stem/progenitor cell (HSPC) panel included PE-Cy7-conjugated anti-CD117 (2B8); PerCP-Cy5.5-conjugated anti-Ly-6A/E; PE-conjugated anti-CD150 (TC15-12F12.2); BV421-conjugated anti-CD48 (HM48-1); APC-conjugated anti-CD16/32 (2.4G2); FITC-conjugated anti-CD34 (RAM34); and BV711-conjugated anti-CD135 (A2F10.1) and the following APC-Cy7-conjufated antibodies: anti-CD3ε (145-2C11), anti-B220 (RA3-6B2), anti-Gr1 (RB6-8C5), anti-Ter119 (TER-119), anti-CD11b (M1/70), and anti-NK1.1 (PK136). The B progenitor panel included FITC-conjugated anti-Ly6D (49-H4), PE-conjugated anti-CD43 (S11), PE-Cy7-conjugated anti-CD19 (6D5), APC-conjugated anti-IgM (RMM1), BV421-conjugated anti-B220 (RA3-6B2), PerCP-Cy5.5-conjugated anti-IgD (11-26c.2a), and the following APC-

Cy7-conjufated antibodies: anti-CD11c (N418), anti-CD3ε (145-2C11), and anti-NK1.1 (PK136). The common lymphoid progenitor panel included BV421-conjugated anti-IL7Rα (A7R34), PerCP-Cy5.5-conjugated anti-CD27 (LG.3A10), APC-conjugated anti-CD135 (A2F10), FITC-conjugated anti-Ly6D (49-H4), and the following APC-Cy7-conjufated antibodies: anti-CD3ε (145-2C11), anti-B220 (RA3-6B2), anti-Gr1 (RB6-8C5), anti-Ter119 (TER-119), anti-CD11b (M1/70), anti-CD11c (N418), and anti-NK1.1 (PK136). Antibodies were obtained from BioLegend of BD Biosciences.

### 3.3.3. Transplantation

Six-to-eight-week-old wildtype *Ly5.1*/*Ly5.2* recipient mice were irradiated twice with 600 cGy six hours apart. Donor (*Ly5.2*) bone marrow cells were then injected retro-orbitally and placed on prophylactic antibiotics (trimethoprim-sulfamethoxazole) for two weeks. Peripheral blood chimerism was analyzed every four weeks until mice were sacrificed twenty-four weeks post-transplantation when donor chimerism in bone marrow and blood were analyzed. For the sorted HSPC transplantation experiments, 50 lineage$^-$ Sca1$^+$ cKit$^+$ CD150$^+$ CD48$^-$ (LSK-SLAM) cells were double sorted into single wells of a 96 well plate containing 250,000 support (*Ly5.1*) whole bone marrow cells and then injected into recipient mice. HSC purity of the double sort was greater than 90%. Only mice with at least 1% trilineage donor chimerism were used to assess lineage output.

### 3.3.4. RNA expression profiling

RNA was purified from sorted LSK-SLAM cells using the Qiagen RNeasy Micro Kit (74004, Qiagen). Following amplification of RNA using the WTA2 kit (Sigma Aldrich, St. Louis, MO), libraries were generated using the Kreatech ULS RNA labeling kit (Leica Biosystems, Wetzlar, Germany) and hybridized to the Agilent SurePrint G3 Mouse GE microarray (Santa Clara, CA), containing 62,976 probes for 24,241 annotated genes. Raw images were first passed-through quality control tools from the Bioconductor package of R [2]. Array intensity data were then background adjusted, and quantile normalized [3]. To test for differential expression, the linear models for Microarray data (limma) package was used [4]. Features were filtered based on normalized expression > 100 within all groups and coefficient of variation ≤75 within all groups. Gene set enrichment analysis was performed using the GSEA v4.0.3 software. Enrichment score (ES) and false discovery rate (FDR) value were applied to filter pathways enriched after gene set permutations were performed 1000 times for the analysis.

### 3.3.5. Serum Inflammatory Mediator Measurement

The level of 40 different cytokines, chemokines, or acute phase proteins in the serum of mice was quantified using the Mouse Cytokine Antibody Array, Panel A, as per manufacturer's recommendations (R&D systems, Minneapolis, MN).

### 3.3.6. Statistical analysis

For single parameter analysis, unpaired t-test were used to assess statistical signficance. For multiple parameter data, statistical signficance was calculated using one-way ANOVA. For

the limiting dilution analysis, a log-fraction plot of the limiting dilution model was fit to data from limiting dilution transplantation of 25k, 50k, or 100k cells from whole bone marrow preparations. P values less than 0.05 were considered significant. The log-fraction plots and statistical analysis were generated using the Extreme Limiting Dilution Analysis software [34].

# 3.4. Results

## 3.4.1. Microbiota Signals Contribute to the Suppression of B Lymphopoiesis with Aging

To investigate the impact of the microbiome on hematopoiesis during aging, we analyzed young (6-to-8-week-old) and middle-aged (10-to-12-month-old) mice (hereafter referred to as aged mice) housed under specific pathogen free (SPF) or germ-free (GF) conditions. We did not analyze older mice due to the difficulty in maintaining mice in a gnotobiotic facility for more than one year. However, age-associated changes in hematopoiesis , including myeloid skewing, lymphoid progenitor reduction, and reduced self-renewal capacity are evident in C57BL/6 mice by 12 months [6,9,35]. Complete blood counts were similar between SPF and GF mice in both young and aged mice, except for a mild anemia in aged SPF mice (Figure 4.7.A). As reported previously [27-29], the percentage and absolute number of circulating neutrophils ($Gr1^{high}$ $CD115^{-}$ $SSC^{high}$ cells) and monocytes ($CD115^{+}$ $Gr1^{low/neg}$ cells) are reduced in young GF mice (Figure 4.1.A and Figure 4.7.B-C). Interestingly, this difference is lost in aged GF mice. In the bone marrow of young GF mice, the percentage and absolute number of neutrophils, Gr1-intermediate granulocytic precursors ($CD115^{+}$ $Gr1^{Int}$ cells), and myeloid progenitors are normal, suggesting that granulopoiesis is intact (Figures 4.1.A, C, and 4.8.B-D).

Consistent with prior studies, there is a shift in hematopoiesis in aged SPF mice towards granulopoiesis with a significant increase in the percentage of granulocytic cells and a decrease in B lineage cells in the bone marrow (Figure 4.1.A) [6,36,37]. Due to the increase in BM cellularity in aged mice (Figure 4.8.A), on an absolute basis, there is a marked increase in granulocytic cells, while B lineage cell number is unchanged (Figure 4.8.B). This shift from B-lymphopoiesis to granulopoiesis with aging is mostly abrogated in GF mice. Compared with aged SPF mice, a significant increase in the percentage of B lineage cells was observed in the bone marrow and blood of aged GF mice, with a modestly attenuated increase in granulocytic cells (Figures 4.1A, B, and 4.8.B). Indeed, whereas the ratio of granulocytic cells to B lineages cells in the bone marrow of SPF mice increased nearly 4-fold with aging, no increase was observed in GF mice (Figure 4.1.B).

### 3.4.2. Microbiota Signals Regulate B Lymphopoiesis at Multiple Stages of Development

We next examined B lymphopoiesis, quantifying different stages of B cell development starting with lymphoid-primed multipotent progenitors (LMPP/MPP4, lineage$^-$ Sca1$^+$ cKit$^+$ CD34$^+$ FLT3$^+$ CD48$^+$ CD150$^-$), lymphoid-committed common lymphoid progenitors (CLPS, lineage$^-$ CD27$^+$ FLT3$^+$ IL7R$\alpha^+$ cells), and the following B cell precursors: pre-pro-B cells (lineage$^-$ B220$^+$ IgM$^-$ CD19$^-$ CD43$^+$ Ly6D$^+$ cells), pro-B cells (lineage$^-$ B220$^+$ IgM$^-$ CD19$^+$ CD43$^+$ cells), and pre-B cells (lineage$^-$ B220$^+$ IgM$^-$ CD43$^-$ cells). Representative flow plots showing the gating strategy to identify each cell population are shown in Figures 4.2.A-C; gating was based on young SPF mice. Consistent with a recent study, a decrease in the percentage of MPP4s, but not MPP2s or myeloid-primed MPP3s was observed in middle aged SPF mice (Figure

4.2D) [9]. A similar trend was observed in middle aged GF mice. Although no change in the percentage of CLPs was observed, a significant decrease in most B cell precursor populations was observed in middle aged SPF mice (Figures 4.2.E, F). This trend was reversed in GF mice, with significant increases in the percentage and absolute number of CLPs and B cell precursors induced with aging (Figure 4.9). These data suggest the microbiota signals contribute to the suppression of B lymphopoiesis during aging primarily at the CLP stage.

### 3.4.3. Microbiota Signals Are Not Required for the Aging-Dependent Increase in HSPCs

The impact of microbiota signals on HSCs, especially with aging, is not well characterized. To address this issue, we first quantified HSCs by flow cytometry (Figures 4.3.A-C). On a percentage basis, a non-significant trend to increased phenotypic HSCs was observed in SPF mice with aging (Figure 4.3.B). On an absolute basis, the increase in phenotypic HSCs is highly significant (Figure 4.3.C). In particular, the number of lineage$^-$ Sca1$^+$ cKit$^+$ CD150$^+$ CD48$^-$ (LSK-SLAM) cells and FLT3$^-$ CD34$^-$ LT-HSCs increased 6.4 ± 1.7-fold and 3.4 ± 1.2-fold, respectively. Similar increases were observed in aged GF mice, with LSK-SLAM increasing 5.3 ± 1.6-fold ($p$ = NS compared to SPF mice) and LT-HSCs increasing 2.8 ± 0.3-fold ($p$ = NS). Aging is associated with an increase in myeloid biased HSCs [38]. Prior studies have shown that high CD150 expression marks myeloid biased HSCs [9]. Thus, we next assessed CD150 expression on phenotypic HSCs (LSK, CD34$^-$ cells). As expected, a significant increase in the percentage of CD150-high HSCs and a corresponding decrease in CD150-low HSCs was observed in aged SPF mice (Figures 4.3.D, E). This shift was largely attenuated in GF mice. Indeed, a significant

increase in CD150-low lymphoid biased HSCs is present in both young and aged GF mice compared with aged-matched SPF mice. Of note, no significant difference in the cell cycle status of lineage$^-$ cKit$^+$ committed progenitors or LSK-SLAM cells was observed with aging in either SPF or GF mice (Figures 4.3.F, G, and 4.10).

Prior studies have shown that phenotypic HSCs from aged mice have reduced repopulating activity on a per cell basis [2,39,40]. Thus, we performed limiting dilution transplantation using unsorted bone marrow cells as an unbiased approach to assess functional HSC frequency. As reported previously [4], the number of functional HSCs increases in the bone marrow of SPF with age (Figures 4.4.A, B). A similar expansion of functional HSCs is present in GF mice. Together, these data suggest that signals from the microbiota are dispensable for the expansion of phenotypic and functional HSCs that occurs with chronologic aging.

### 3.4.4. Microbiota Signals Contribute to the Lineage Bias of HSCs

To assess the impact of microbiota on HSC lineage commitment, we transplanted a limiting number of sorted HSCs and assessed lineage output (Figure 4.5). Stable overall donor engraftment was observed over time, with reduced engraftment of aged HSCs from both SPF and GF mice (Figure 4.5.B, C, E). A significant decrease in donor granulocytic cell chimerism was seen in both young and aged GF HSC recipients (Figures 4.5.B-D). Conversely, donor B cell chimerism in the blood was increased in aged GF HSC recipients, with a similar trend observed in the bone marrow 24 weeks after transplantation. We next analyzed individual mice with at least 1% trilineage engraftment 24 weeks after transplantation to assess HSC lineage bias. As expected, in young SPF mice, the majority of HSCs displayed a balanced myeloid/lymphoid lineage output, with a

significant increase in myeloid-biased HSCs observed with aging (Figure 4.5.F, G). In young GF mice, the majority of HSCs are lymphoid-biased. Moreover, although the myeloid output, as measured by granulocytic cell chimerism, increased modestly with aging, the majority of HSCs in aged GF remained lymphoid-biased or balanced. In young GF HSCs, an increase in the output of both B- and T-lineage cells was observed (Figure 4.5H, I). In contrast in aged GF HSCs, the increase in lymphoid output was mainly due to an increased production of B cells. Collectively, these data show that microbiota-related signals play a key role in determining the lineage potential of bone marrow resident HSCs, promoting myeloid lineage development at the expense of lymphoid cells.

To begin to explore mechanisms by which microbiota signals regulate HSC lineage bias, gene expression profiling was performed on sorted LSK-SLAM cells from aged SPF and aged GF mice. A list of differentially expressed genes is provided in Table 4.1. Consistent with our lineage-output transplantation data, aged GF HSCs had a gene expression signature enriched for non-myeloid biased HSCS (Figure 4.6.A and 4.11) [41]. Surprisingly, gene set enrichment analysis showed that GF HSCs were enriched for expression signatures related to inflammatory signaling, including tumor necrosis factor (TNF) and interferon (IFN) signaling (Figure 4.6.B). This prompted us to measure the circulating level of 40 different inflammatory cytokines, chemokines, or acute phase proteins, including TNF$\alpha$, interleukin-1$\beta$, and IFN gamma. Only five of these inflammatory mediators were detected above background (Figure 4.6.C). Increased expression of C5, CXCL13, soluble ICAM, and M-CSF was observed in the serum of SPF mice with aging, with a similar increase seen in aged GF mice. Together, these data suggest the microbiota signals are not major drivers of increased systemic inflammatory cytokine/chemokine expression or inflammatory signaling in HSCs.

## 3.5. Discussion

Prior studies suggest that aging impacts B lymphopoiesis at multiple stages of development. First, HSCs become myeloid-biased with aging [1,3,4,12]. Second, Young *et al*. provided evidence that the lymphoid potential of MPP4/LMPP decreases with aging [9]. Finally, several studies have shown that there is a loss of early B-cell committed progenitors [6-9]. Our data are consistent with these observations, although most prior studies have reported a decrease in CLPs in aged (18-to-24-month-old) mice. This discrepancy may be due to the younger age (10-to-12-month) of SPF mice analyzed in our study. Indeed, Young *et al*. showed that CLPs progressively decline with age and are within normal limits in 12-month-old mice [9]. Our data suggest the microbiota signals contribute to the suppression of B lymphopoiesis with aging primarily by regulating the production and/or maintenance of committed B cell progenitors, although molecular mechanisms are unclear. Of note, prior studies suggest that reduced interleukin-7 responsiveness [6], or increased senescence [7] or TNFα-induced apoptosis [22] may contribute to the loss of B cell precursors with aging. Whether any of these mechanisms are dependent on microbiota will require further study.

Our data suggest that microbiota signals play an important role in determining the lineage bias of HSCs.

Consistent with prior studies [1-4], we show that aging is associated with an expansion of phenotypic HSCs with reduced repopulating activity in mice. Despite the decrease in repopulating activity on a per cell basis, the large increase in phenotypic HSCs with aging compensates for this loss. Indeed, limiting dilution studies using total bone marrow cells show that the number of long-

term repopulating HSCs is actually increased in aged mice [4]. This is consistent with recent single cell RNA sequencing studies suggesting that there is marked expansion of myeloid-restricted HSCs, along with a moderate expansion of multipotent HSCs [41,42]. Interestingly, the number of phenotypic and functional HSCs increases to a similar degree with aging in GF mice, suggesting that microbiome signals do not contribute to this phenotype. A consistent finding in many studies, including our own, is an increase in myeloid-biased HSCs with aging [1,3,4,10-12]. Our transplantation studies show that the lymphoid lineage output of young GF HSCs is increased compared with SPF HSCs. With aging, although there is some shift toward increased myeloid cell production, lymphoid cell production, particularly B lineage cell production, remains high in GF HSCs. Consistent with this conclusion, a recent paper showed that aged GF mice maintain HSCs with balanced lympho-myeloid lineage output upon transplantation [43]. There are some caveats to the transplantation studies, including the use of irradiation in recipient mice which induces transient systemic inflammation [44,45] and the short-term treatment of recipients with antibiotics, which may alter the microbiota. Although these factors were controlled for in our experimental approach, the data suggest that microbiota result in, as yet undefined, epigenetic changes in HSCs that contribute to lineage specification.

The mechanisms regulating lineage bias of HSCs is not well understood. Numerous prior studies comparing young to aged HSCs have identified alterations in the epigenome, metabolism, cell polarity, and proteostasis (reviewed in Mejia-Ramirez *et al*.) [46]. Reactive oxygen species (ROS) levels increase in aged HSCs and correlate with myeloid lineage skewing and reduced long-term repopulating activity [47]. Although we did not measure ROS, our RNA expression profiling suggest that aged GF HSCs are more metabolically active, with increased oxidative phosphorylation compared to aged SPF HSCs. There is considerable interest in the role of

inflammation in HSC aging. Chronic stimulation with certain inflammatory cytokines or TLR ligands results in an HSC aging phenotype, with a loss of HSC repopulating and enhanced myeloid differentiation [21,24,25]. Moreover, He *et al*. recently provided evidence that elevated TNFα signaling, by increasing IL27RA expression in HSCs, contributes to their biased myeloid differentiation [23]. Most recently, Kovtonyuk *et al*. provided compelling data suggesting that interleukin-1 contributes to the increase in myeloid biased HSC with aging. Of note, they showed that blocking interleukin-a signaling or suppression of gut microbiota with oral antibiotics was able to partially revert the myeloid-biased HSC aging phenotype. Surprisingly, our RNA expression profiling data suggest that inflammatory signaling (including TNFα and interferon) is increased in aged GF HSCs compared to SPF HSCs. However, the relationship between the microbiota and inflammation is likely to be complex and further study of the mechanisms by which microbiota and inflammatory signaling regulate HSC lineage output is needed.

In summary, these data show that microbiota signals contribute to hematopoietic aging and HSC lineage specification. The nature of the signals remains an open and important question, whose answer will provide important new insights into the regulation of hematopoiesis.

## 3.6. Acknowledgement

We thank Dr. Jeffrey I. Gordon for gifting GF mice. We also thank the Alvin J. Siteman Cancer Center at Washington University Flow Cytometry core facility, which provided cell sorting services. The Siteman Cancer Center is supported in part by NCI Cancer Center Support Grant #P30 CA091842. This study was supported by the National Institutes of Health grants R01HL131655 (Daniel C. Link, MD), R01HL134896 (Laura G. Schuettpelz, MD, PhD), and

F31CA247136 (Joseph R. Krambs), and the Children's Discovery Institute of Washington University and St. Louis Children's Hospital (Laura G. Schuettpelz, MD, PhD).

## 3.7. Author Contributions

Daniel C. Link, MD and Laura G. Schuettpelz, MD, PhD conceived and jointly supervised the study. Joseph R. Krambs, Laura G. Schuettpelz, MD, PhD, and Darlene A. Monlish, PhD designed the experiments. Joseph R. Krambs, Laura G. Schuettpelz, MD, PhD, and Darlene A. Monlish, PhD performed the experiments. Joseph R. Krambs and Daniel C. Link, MD wrote the manuscript. Joseph R. Krambs and Feng Gao, PhD performed statistical analysis. All authors contributed to the article and approved the submitted version.

# 3.8. Figures

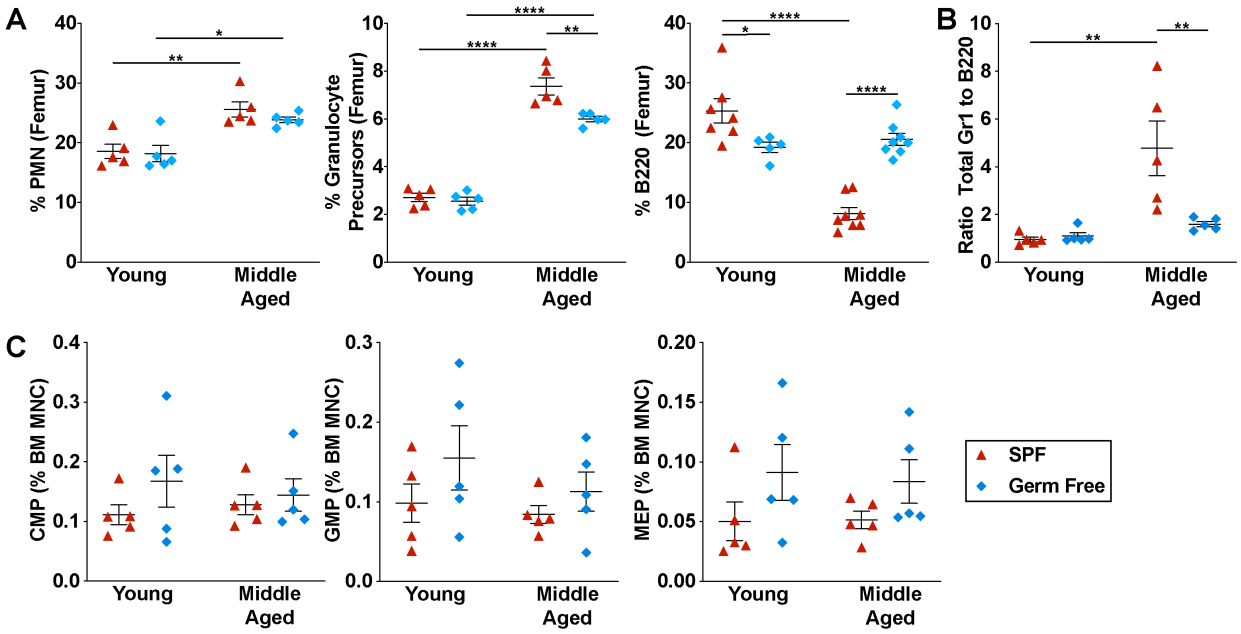
A
% PMN (Femur)
% Granulocyte Precursors (Femur)
% B220 (Femur)
B
Ratio Total Gr1 to B220
Young
Middle Aged
C
CMP (% BM MNC)
GMP (% BM MNC)
MEP (% BM MNC)
SPF
Germ Free

**Figure 3.1. Microbiota signals contribute to the suppression of B lymphopoiesis.** (A) Percentage of mature neutrophils ($Gr1^{high}$ $SSC^{high}$ cells), granulocyte precursors ($CD115^{+}$ $Gr1^{Int}$ cells), and $B220^{+}$ cells in the bone marrow. (B) Ratio of $Gr1^{+}$ cells to $B220^{+}$ cells in the bone marrow. (C) Percentage of common myeloid progenitors (CMP, $lineage^{-}$ $Sca1^{-}$ $cKit^{+}$ $CD34^{+}$ $CD16/32^{-}$ cells), granulocyte-macrophage progenitors (GMP, $lineage^{-}$ $Sca1^{-}$ $cKit^{+}$ $CD34^{+}$ $Cd16/32^{+}$ cells), and megakaryocyte-erythrocyte progenitors (MEP, $lineage^{-}$ $Sca1^{-}$ $cKit^{+}$ $CD34^{-}$ $CD16/32^{-}$ cells) in the bone marrow. Middle aged is defined as 10-12 months. Data represent the mean ± SEM. *P < 0.05, **P < 0.01, and ****P < 0.0001 by one-way ANOVA with alpha = 0.05 and Sidak's multiple comparisons test. Technical replicates were completed at least three times over the span of four years due to availability of gem-free mice.

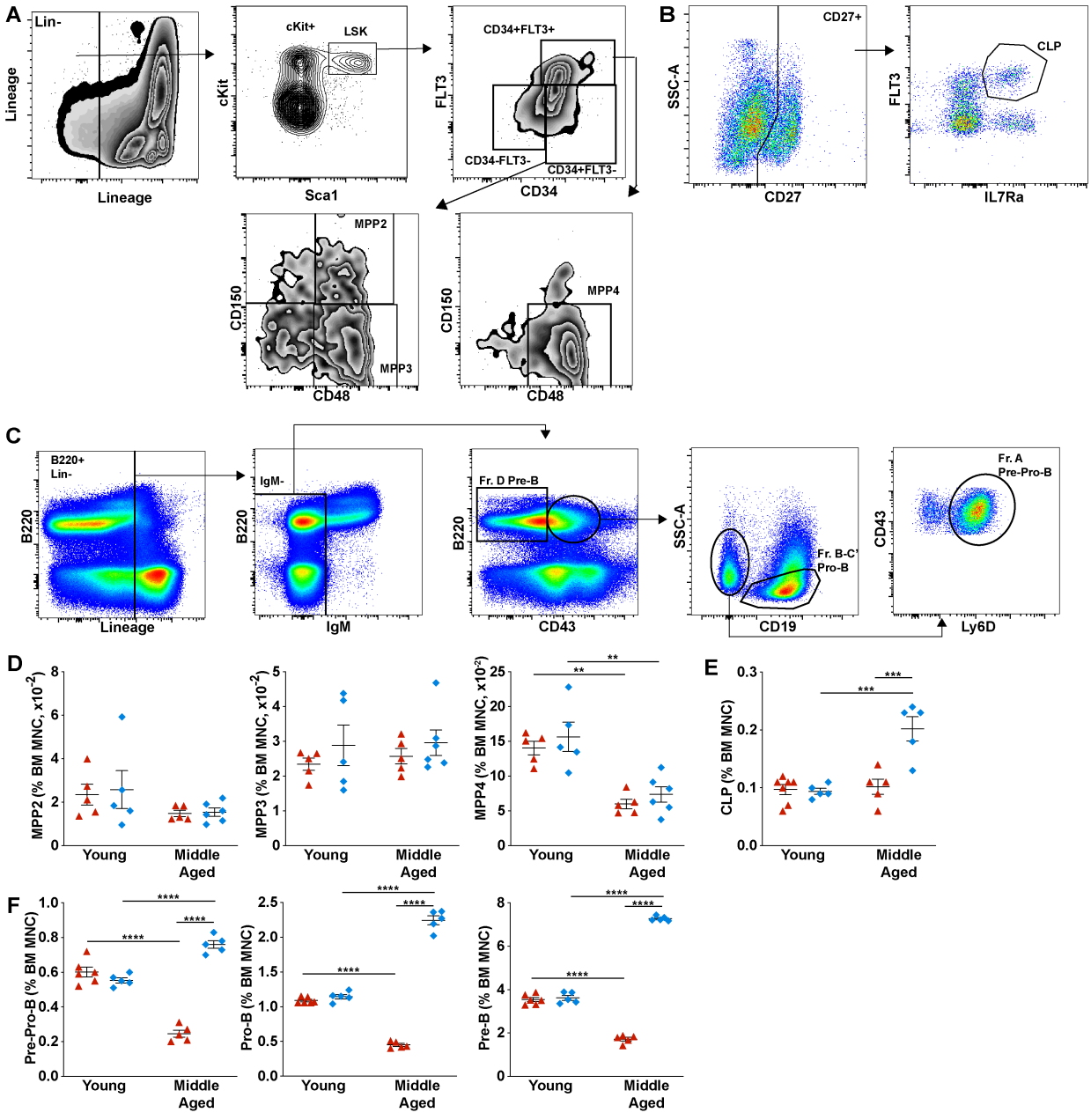
A
Lin-
Lineage
Lineage
cKit+
LSK
cKit
Sca1
CD34+FLT3+
FLT3
CD34-FLT3-
CD34+FLT3-
CD34
MPP2
CD150
MPP3
CD48
MPP4
CD150
CD48
B
CD27+
SSC-A
CD27
CLP
FLT3
IL7Ra
C
B220+
Lin-
B220
Lineage
IgM-
B220
IgM
Fr. D Pre-B
B220
CD43
SSC-A
Fr. B-C'
Pro-B
CD19
Fr. A
Pre-Pro-B
CD43
Ly6D
D
MPP2 (% BM MNC, x10-2)
MPP3 (% BM MNC, x10-2)
MPP4 (% BM MNC, x10-2)
Young
Middle Aged
E
CLP (% BM MNC)
Young
Middle Aged
F
Pre-Pro-B (% BM MNC)
Pro-B (% BM MNC)
Pre-B (% BM MNC)
Young
Middle Aged

**Figure 3.2. Microbiota signals suppress B lymphopoiesis through down-regulating common lymphoid progenitors in aged mice.** (A) Representative flow plots of young SPF mouse BM showing the gating strategy used to identify multipotent progenitor (MPP) populations MPP2 (lineage$^-$ Sca1$^+$ cKit$^+$ CD34$^+$ FLT3$^-$ CD48$^+$ CD150$^+$), MPP3 (lineage$^-$ Sca1$^+$ cKit$^+$ CD34$^+$ FLT3$^-$ CD48$^+$ CD150$^-$), MPP4 (lineage$^-$ Sca1$^+$ cKit$^+$ CD34$^+$ FLT3$^+$ CD48$^+$ CD150$^-$). (B) Common lymphoid progenitors (lineage$^-$ CD27$^+$ FLT3$^+$ IL7R$\alpha^+$ cells). (C) B cell progenitors Pre-Pro-B (lineage$^-$ B220$^+$ IgM$^-$ CD19$^-$ CD43$^+$ Ly6D$^+$ cells), Pro-B (lineage$^-$ CD27$^+$ B220$^+$ IgM$^-$ CD19$^+$ CD43$^+$ cells), and Pre-B (lineage$^-$ B220$^+$ IgM$^-$ CD43$^-$ cells). (D) Percent of multipotent MPP2, MPP3, and MPP4 per femur. (E) Percentage of common lymphoid progenitors. (F) Percentage of Pre-Pro-B cells, Pro-B cells, Pre-B cells, and immature B cells (lineage$^-$ B220$^+$ IgD$^-$ IgM$^+$ cells) in the bone marrow. Data represent the mean ± SEM. **P < 0.01, ***P < 0.001, and ****P < 0.0001 by one-way ANOVA with alpha = 0.05 and Sidak's multiple comparisons test.

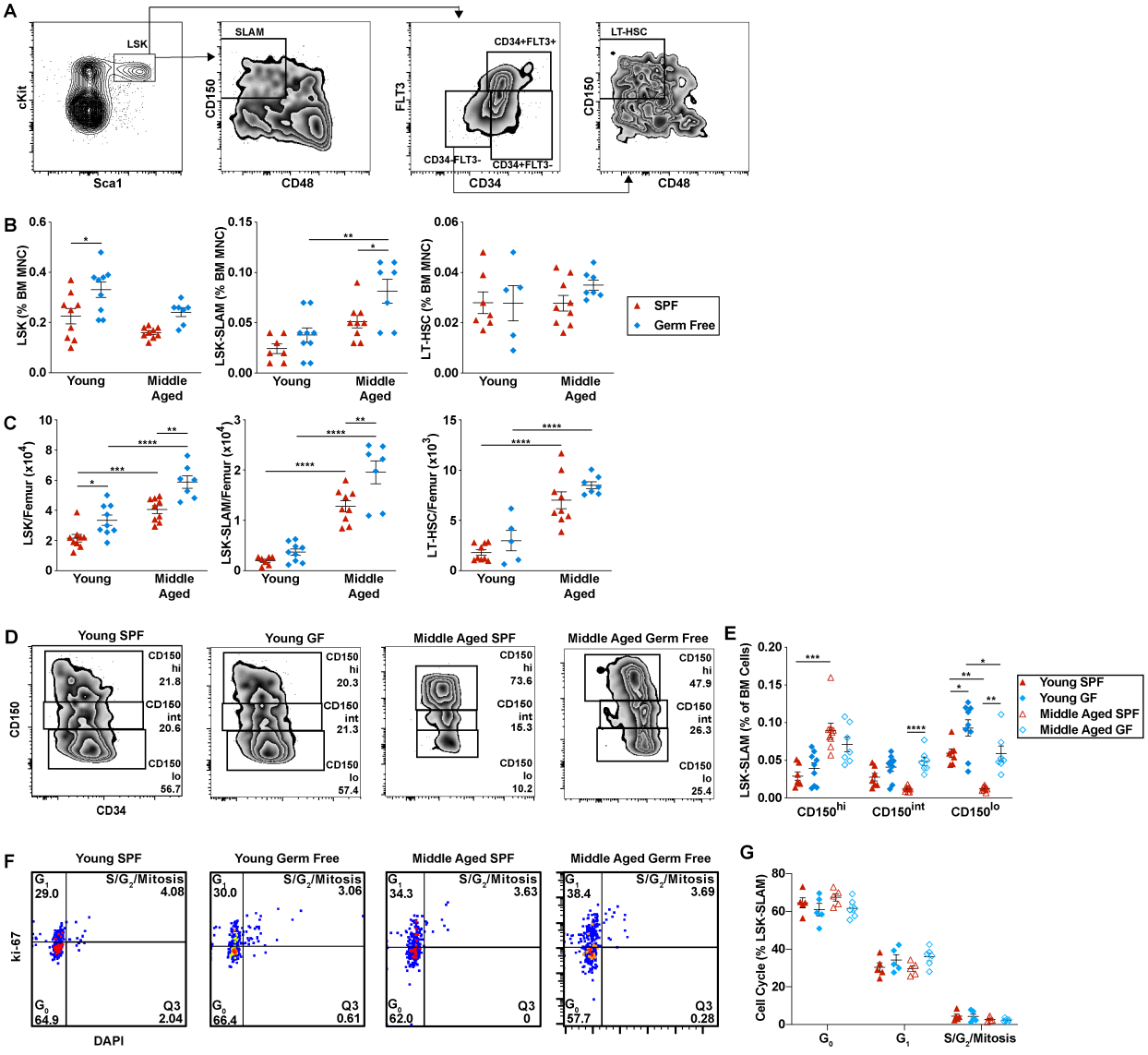
A
LSK
cKit
Sca1
SLAM
CD150
CD48
CD34+FLT3+
FLT3
CD34-FLT3-
CD34+FLT3-
CD34
LT-HSC
CD150
CD48
B
LSK (% BM MNC)
LSK-SLAM (% BM MNC)
LT-HSC (% BM MNC)
Young
Middle Aged
SPF
Germ Free
C
LSK/Femur (x10^4)
LSK-SLAM/Femur (x10^4)
LT-HSC/Femur (x10^3)
Young
Middle Aged
D
Young SPF
Young GF
Middle Aged SPF
Middle Aged Germ Free
CD150
CD34
CD150 hi 21.8
CD150 int 20.6
CD150 lo 56.7
CD150 hi 20.3
CD150 int 21.3
CD150 lo 57.4
CD150 hi 73.6
CD150 int 15.3
CD150 lo 10.2
CD150 hi 47.9
CD150 int 26.3
CD150 lo 25.4
E
LSK-SLAM (% of BM Cells)
CD150hi
CD150int
CD150lo
Young SPF
Young GF
Middle Aged SPF
Middle Aged GF
F
Young SPF
Young Germ Free
Middle Aged SPF
Middle Aged Germ Free
ki-67
DAPI
G1 29.0
S/G2/Mitosis 4.08
G0 64.9
Q3 2.04
G1 30.0
S/G2/Mitosis 3.06
G0 66.4
Q3 0.61
G1 34.3
S/G2/Mitosis 3.63
G0 62.0
Q3 0
G1 38.4
S/G2/Mitosis 3.69
G0 57.7
Q3 0.28
G
Cell Cycle (% LSK-SLAM)
G0
G1
S/G2/Mitosis

**Figure 3.3. Microbiota signals are not required for the expansion of HSCs with aging.** (A) representative flow plots of young SPF mouse BM showing the gating strategy used to identify LSK, LSK-SLAM, and LT-HSC cells. (B) Percent and (C) number of LSK, LSK-SLAM, and LT-HSCs per femur. (D) Representative flow plots showing the frequency of $CD150^{high}$, $CD150^{Int}$, and $CD150^{low}$ HSCs; data are gated on $CD34^{-}$ LSK cells. CD150 gating for each experiment was adjusted based on FMO controls. (E) Frequency of $CD150^{high}$, $CD150^{Int}$, and $CD150^{low}$ HSCs. (F) Representative flow plots showing the gating strategy used to identify cell cycle status of LSK-SLAM cells. (G) Cell cycle distribution of LSK-SLAM cells. Data represent the mean ± SEM. *P < 0.05, **P < 0.01, ***P < 0.001, and ****P < 0.0001 by one-way ANOVA with alpha = 0.05 and Sidak's multiple comparisons test.

A

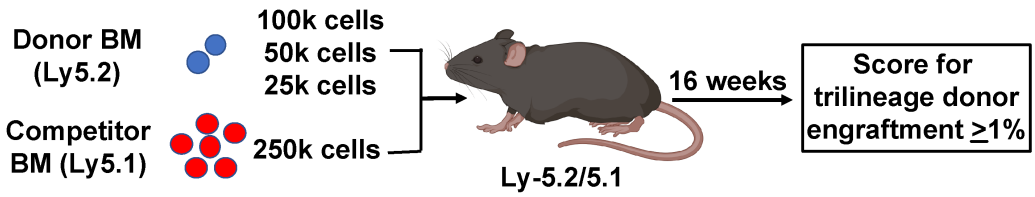


B

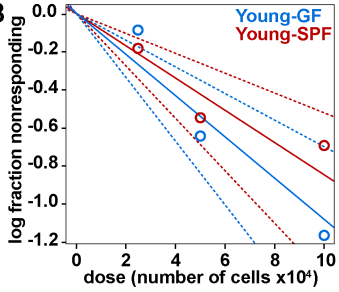


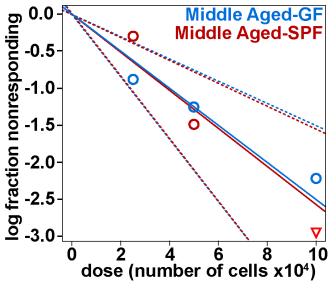


| Group | Lower | Estimate | Upper |
|---|---|---|---|
| Young-SPF | 192375 | 118315 | 72767 |
| Young-GF | 143294 | 92604 | 59846 |

| Group | Lower | Estimate | Upper |
|---|---|---|---|
| Middle Aged-SPF | 64569 | 39110 | 23689 |
| Middle Aged-GF | 66728 | 39849 | 23797 |

**Figure 3.4. Microbiota signals do not alter age related expansion of HSCs.** (A) Limiting dilution transplantation strategy to measure frequency of functional HSCs. (B) Limiting dilution analysis of repopulating activity. Shown is the fraction of mince showing long-term multilineage engraftment versus dose of total bone marrow cells transplanted. The dotted lines give the 95% confidence interval. The table represents exact one-sided 95% confidence interval estimates of HSC frequency.

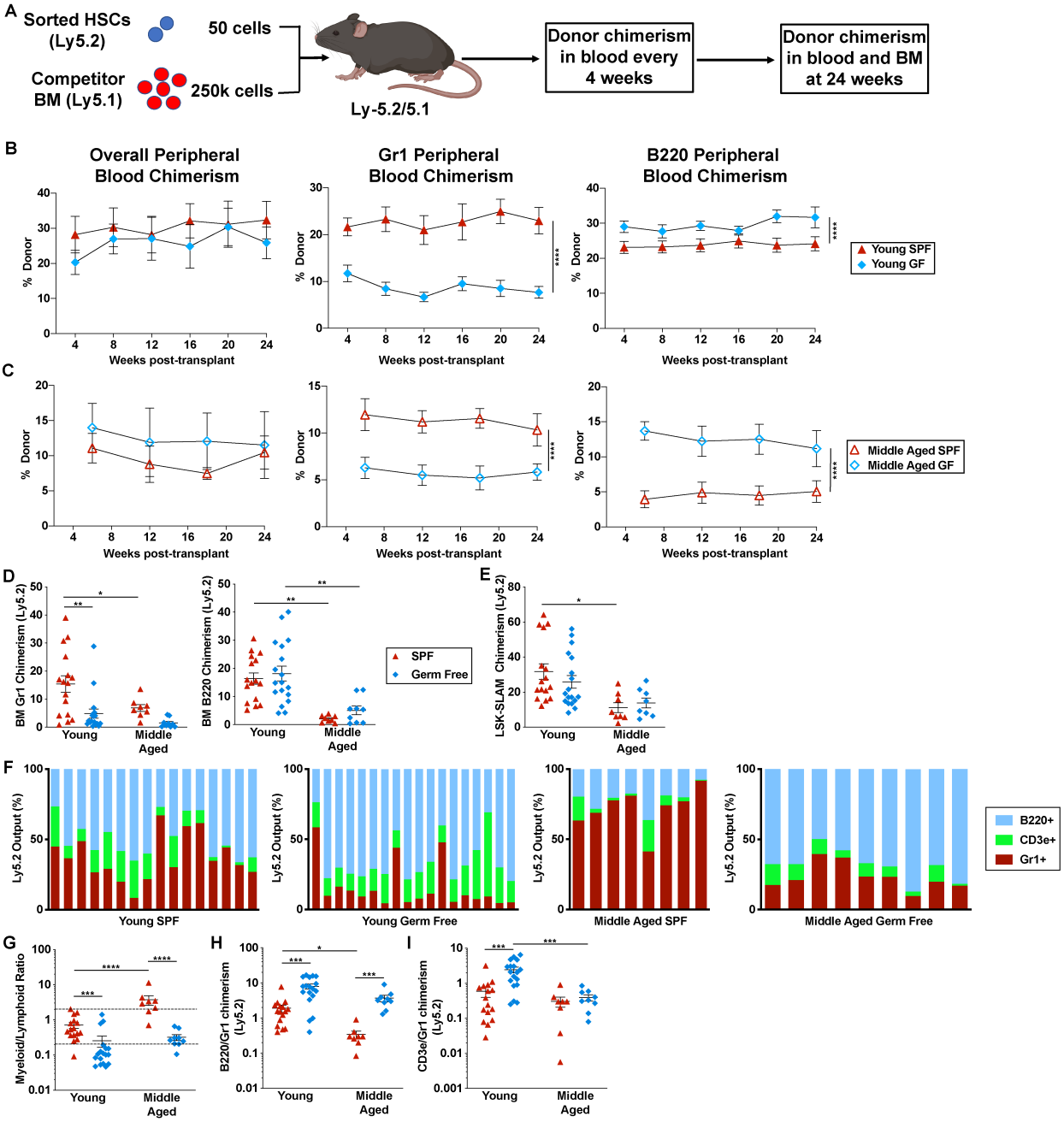
A
Sorted HSCs (Ly5.2)
50 cells
Competitor BM (Ly5.1)
250k cells
Ly-5.2/5.1
Donor chimerism in blood every 4 weeks
Donor chimerism in blood and BM at 24 weeks
B
Overall Peripheral Blood Chimerism
Gr1 Peripheral Blood Chimerism
B220 Peripheral Blood Chimerism
% Donor
Weeks post-transplant
Young SPF
Young GF
C
Middle Aged SPF
Middle Aged GF
D
BM Gr1 Chimerism (Ly5.2)
BM B220 Chimerism (Ly5.2)
Young
Middle Aged
SPF
Germ Free
E
LSK-SLAM Chimerism (Ly5.2)
F
Ly5.2 Output (%)
Young SPF
Young Germ Free
Middle Aged SPF
Middle Aged Germ Free
B220+
CD3e+
Gr1+
G
Myeloid/Lymphoid Ratio
H
B220/Gr1 chimerism (Ly5.2)
I
CD3e/Gr1 chimerism (Ly5.2)

**Figure 3.5. Microbiota signals suppress the lymphoid potential of aged HSCs.** (A) Experimental schema. (B) Fifty sorted LSK-SLAM cells from the indicated donors were transplanted into irradiated wildtype SPF mice and donor peripheral blood chimerism assessed every four to six weeks. Shown is donor (*Ly5.2*) contribution to total leukocytes, granulocytes, and B cells in recipients of transplanted young HSCs (B) or aged HSCs (C). (D, E) Donor chimerism in bone marrow $Gr1^+$ cells and $B220^+$ cells (D) or LSK-SLAM cells (E) harvested 24 weeks after transplantation. (G) Quotient of donor bone marrow myeloid cells ($Gr1^+$) cells to lymphoid ($CD3\varepsilon^+$ plus $B220^+$) cells for each recipient. Myeloid-biased mice had a ratio > 2, lineage balanced were between 0.25 and 2, and lymphoid-biased mice had a ratio < 0.25. (H, I) Ratio of donor bone marrow $B220^+$ to $Gr1^+$ chimerism (H) or donor bone marrow $CD3\varepsilon^+$ to $Gr1^+$ chimerism (I). Data represent the mean ± SEM. *P < 0.05, **P < 0.01, ***P < 0.001, and ****P < 0.0001 by one-way ANOVA with alpha = 0.05 and Sidak's multiple comparisons test.

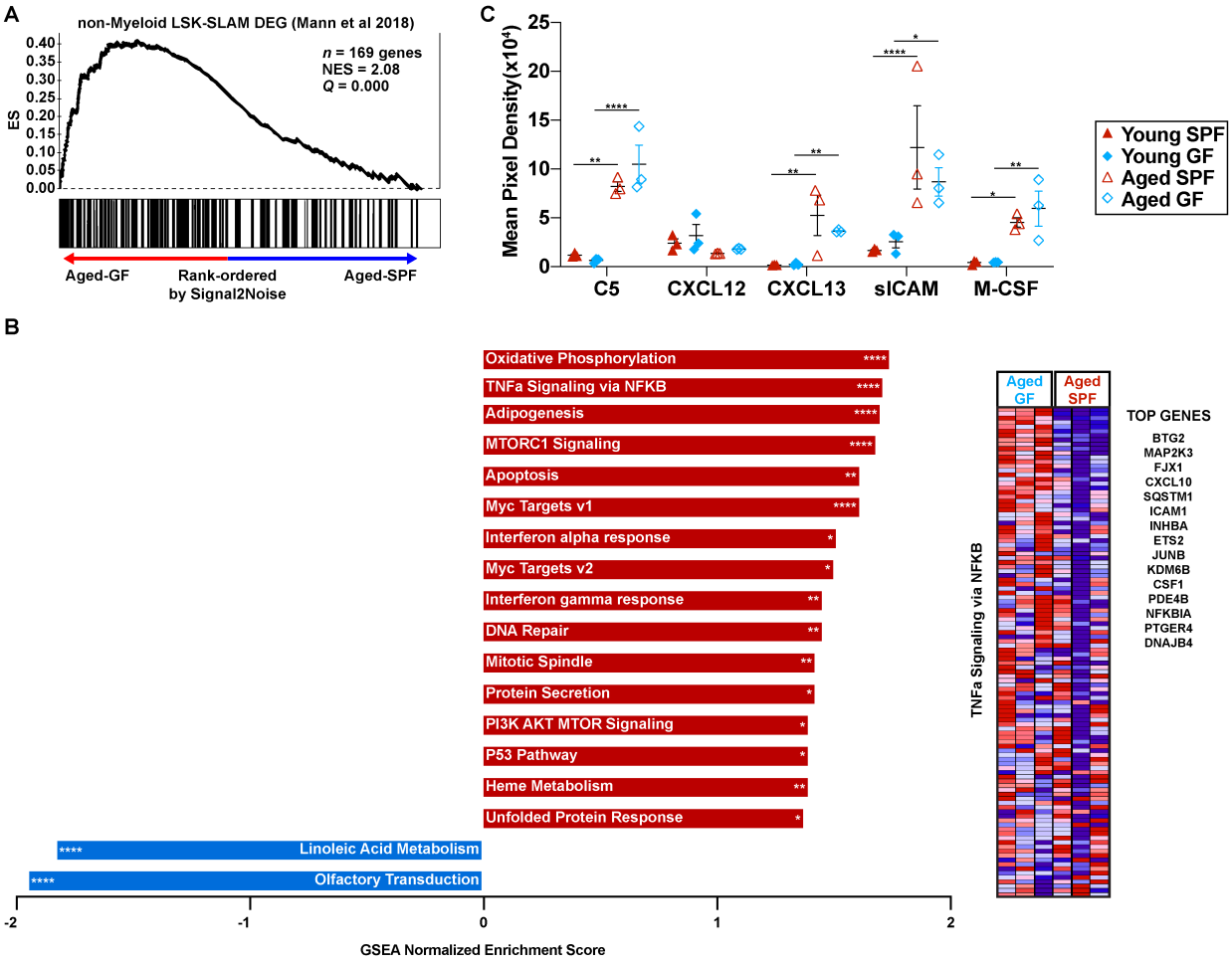
A
non-Myeloid LSK-SLAM DEG (Mann et al 2018)
n = 169 genes
NES = 2.08
Q = 0.000
ES
Aged-GF
Rank-ordered by Signal2Noise
Aged-SPF
C
Mean Pixel Density(x10⁴)
C5
CXCL12
CXCL13
sICAM
M-CSF
Young SPF
Young GF
Aged SPF
Aged GF
B
Oxidative Phosphorylation
TNFa Signaling via NFKB
Adipogenesis
MTORC1 Signaling
Apoptosis
Myc Targets v1
Interferon alpha response
Myc Targets v2
Interferon gamma response
DNA Repair
Mitotic Spindle
Protein Secretion
PI3K AKT MTOR Signaling
P53 Pathway
Heme Metabolism
Unfolded Protein Response
Linoleic Acid Metabolism
Olfactory Transduction
GSEA Normalized Enrichment Score
Aged GF
Aged SPF
TNFa Signaling via NFKB
TOP GENES
BTG2
MAP2K3
FJX1
CXCL10
SQSTM1
ICAM1
INHBA
ETS2
JUNB
KDM6B
CSF1
PDE4B
NFKBIA
PTGER4
DNAJB4

**Figure 3.6. Microbiota signals enhance the myeloid gene signature of HSCs with age but are not required for expression of inflammatory mediators in the blood.** (A) Gene set enrichment analysis for genes consistent with non-myeloid biased LSK-SLAM cells. (B) Significantly enriched gene sets from the Hallmark, KEGG, and Reactome gene sets (adjusted FDR < 0.1, nominal p-value <0.05). Red bars represent gene sets upregulated in aged GF HSCs and blue bars gene sets upregulated in aged SPF HSCs. *P < 0.05, **P < 0.01, ***P < 0.001, and ****P < 0.0001 by GSEA. Heatmap of the TNFα signaling via NFκB gene set with a list of the top 15 differentially expressed genes between aged GF and aged SPF HSCs. (C) Quantification of arrays that interrogate inflammatory cytokines/chemokines hybridized with serum. Data represent the mean ± SEM. *P < 0.05, **P < 0.01, and ****P < 0.0001 by two-way ANOVA with alpha = 0.05 and Sidak's multiple comparisons test.

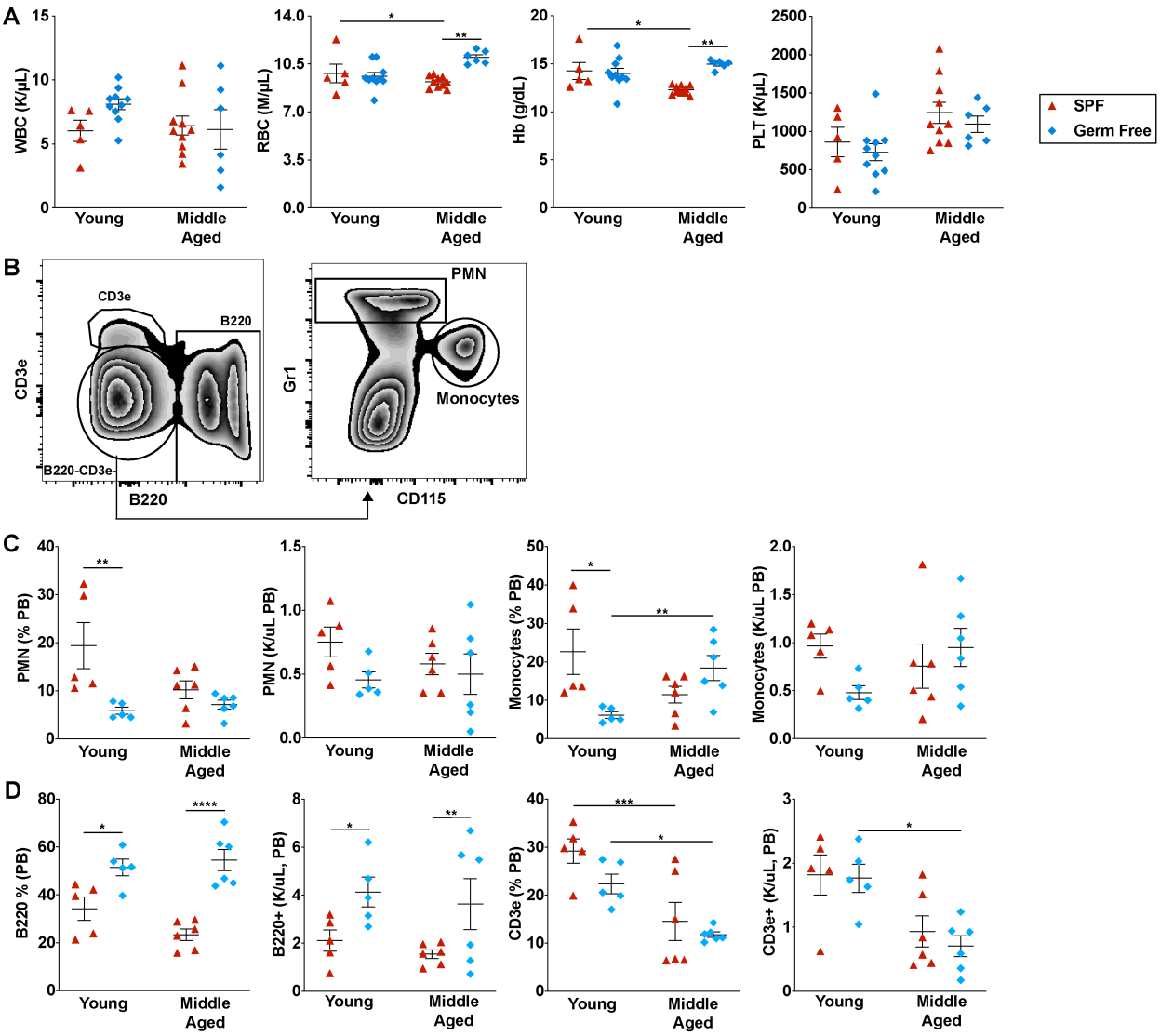
A
WBC (K/μL)
RBC (M/μL)
Hb (g/dL)
PLT (K/μL)
Young
Middle Aged
SPF
Germ Free
B
CD3e
B220
B220-CD3e-
Gr1
PMN
Monocytes
CD115
C
PMN (% PB)
PMN (K/uL PB)
Monocytes (% PB)
Monocytes (K/uL PB)
D
B220 % (PB)
B220+ (K/uL, PB)
CD3e (% PB)
CD3e+ (K/uL, PB)

**Figure 3.7. Basal hematopoiesis in young and aged SPF and GF mice.** (A) Peripheral blood counts. (B) Representative flow plots showing the gating strategy to identify $B220^{+}$ (B cells), $CD3\varepsilon^{+}$ (T cells), $Gr1^{high}$ $SSC^{high}$ $CD115^{-}$ (neutrophils), and $Gr1^{Int}$ $CD115^{+}$ (monocytes) in the blood. (C) Number and percent of circulating neutrophils (PMNs, $Gr1^{high}$ $CD115^{-}$ $SSC^{high}$ cells) and monocytes ($CD115^{+}$ $Gr1^{low/neg}$ cells). (D) Number and percent of circulating T cells and B cells. Data represent the mean ± SEM. *P < 0.05, **P < 0.01, ***P < 0.001, and ****P < 0.0001 by one-way ANOVA with alpha = 0.05 and Sidak's multiple comparisons test.

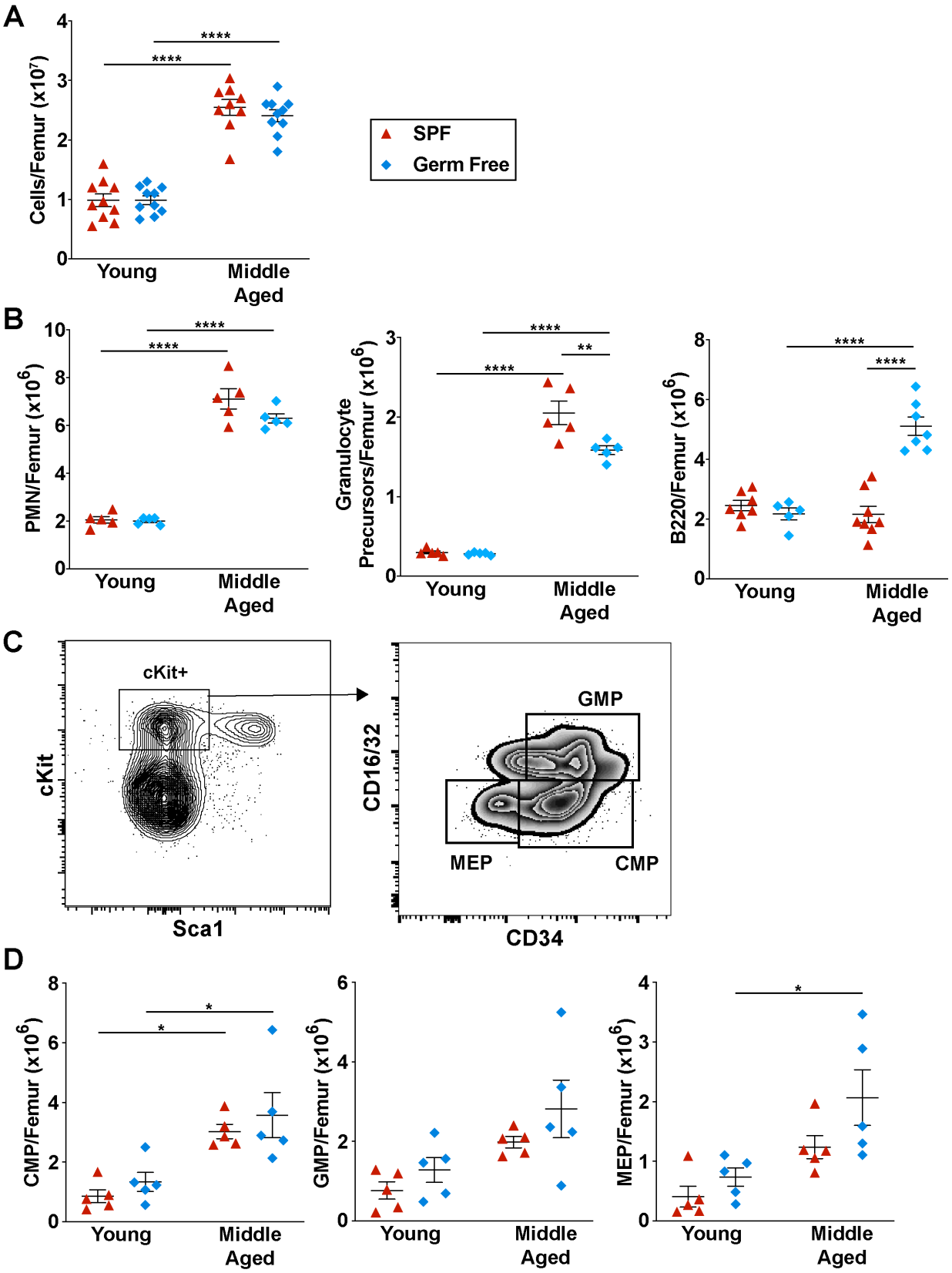
A
Cells/Femur (x10^7)
SPF
Germ Free
Young
Middle Aged
B
PMN/Femur (x10^6)
Granulocyte Precursors/Femur (x10^6)
B220/Femur (x10^6)
C
cKit+
cKit
Sca1
CD16/32
CD34
GMP
MEP
CMP
D
CMP/Femur (x10^6)
GMP/Femur (x10^6)
MEP/Femur (x10^6)

**Figure 3.8. Basal hematopoiesis in young and aged GF and SPF mice.** (A) Bone marrow cellularity. (B) Number of $B220^{+}$, $CD115^{+}$ $Gr1^{Int}$ cells, and mature neutrophils ($Gr1^{high}$ $SSC^{high}$ cells) in the bone marrow. (C) Representative flow plot gating of common myeloid progenitors (CMP, $lineage^{-}$ $Sca1^{-}$ $cKit^{+}$ $CD34^{+}$ $CD16/32^{-}$ cells), granulocyte-macrophage progenitors (GMP, $lineage^{-}$ $Sca1^{-}$ $cKit^{+}$ $CD34^{+}$ $CD16/32^{+}$ cells), and megakaryocyte-erythrocyte progenitors (MEP, $lineage^{-}$ $Sca1^{-}$ $cKit^{+}$ $CD34^{-}$ $CD16/32^{-}$ cells) in the bone marrow. (D) Number of CMP, GMP, and MEP per femur. Data represent the mean ± SEM. *P < 0.05, **P < 0.01, ***P < 0.001, and ****P < 0.0001 by one-way ANOVA with alpha = 0.05 and Sidak's multiple comparisons test.

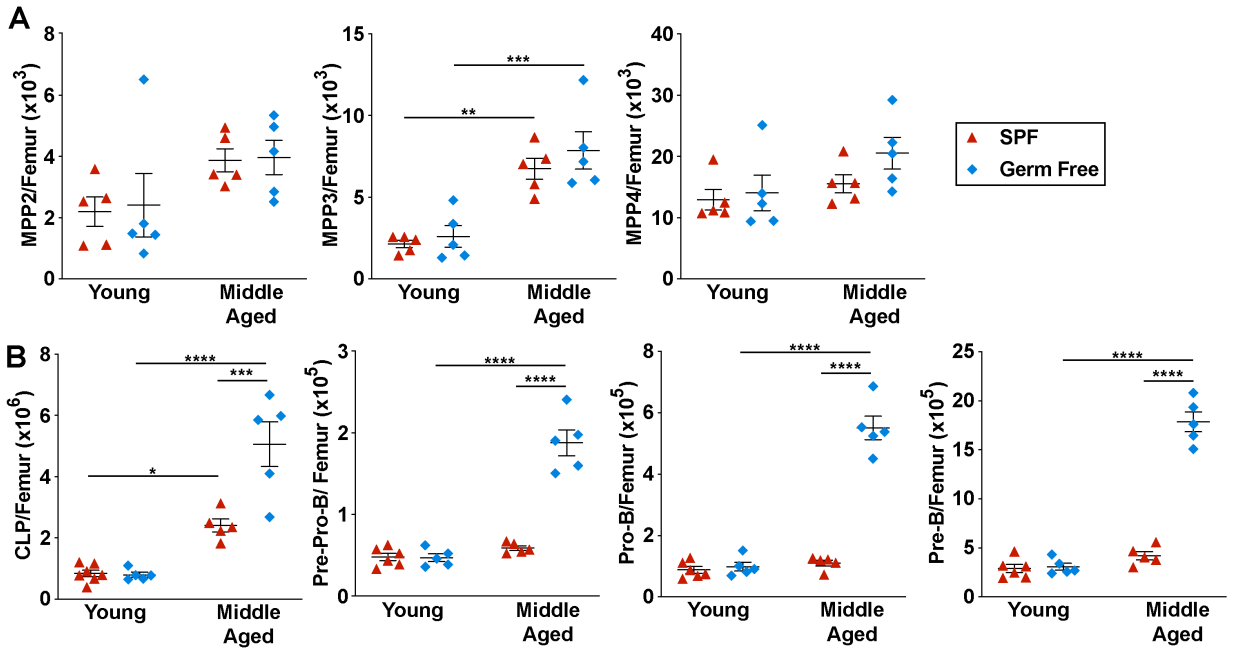
A
MPP2/Femur (x10^3)
MPP3/Femur (x10^3)
MPP4/Femur (x10^3)
Young
Middle Aged
SPF
Germ Free
B
CLP/Femur (x10^6)
Pre-Pro-B/ Femur (x10^5)
Pro-B/Femur (x10^5)
Pre-B/Femur (x10^5)

**Figure 3.9. Early committed progenitor populations in young and aged GF and SPF mice.** (A) Number of multipotent progenitor 2 (MPP2, lineage$^-$ Sca1$^+$ cKit$^+$ CD34$^+$ FLT3$^-$ CD48$^+$ CD150$^+$), MPP3 (lineage$^-$ Sca1$^+$ cKit$^+$ CD34$^+$ FLT3$^-$ CD48$^+$ CD150$^-$), and MPP4 (lineage$^-$ Sca1$^+$ cKit$^+$ CD34$^+$ FLT3$^+$ CD48$^+$ CD150$^-$) per femur. (B) Number of common lymphoid progenitors (CLP, lineage$^-$ CD27$^+$ FLT3$^+$ IL7R$\alpha^+$ cells), Pre-Pro-B cells (lineage$^-$ B220$^+$ IgD$^-$ IgM$^-$ CD19$^-$ CD43$^+$ Ly6D$^+$), Pro-B cells (lineage$^-$ B220$^+$ IgD$^-$ IgM$^-$ CD19$^+$ CD43$^+$), and Pre-B cells (lineage$^-$ B220$^+$ IgD$^-$ IgM$^-$ CD19$^+$ CD43$^-$) in the bone marrow. Data represent the mean ± SEM. *P < 0.05, **P < 0.01, ***P < 0.001, and ****P < 0.0001 by one-way ANOVA with alpha = 0.05 and Sidak's multiple comparisons test.

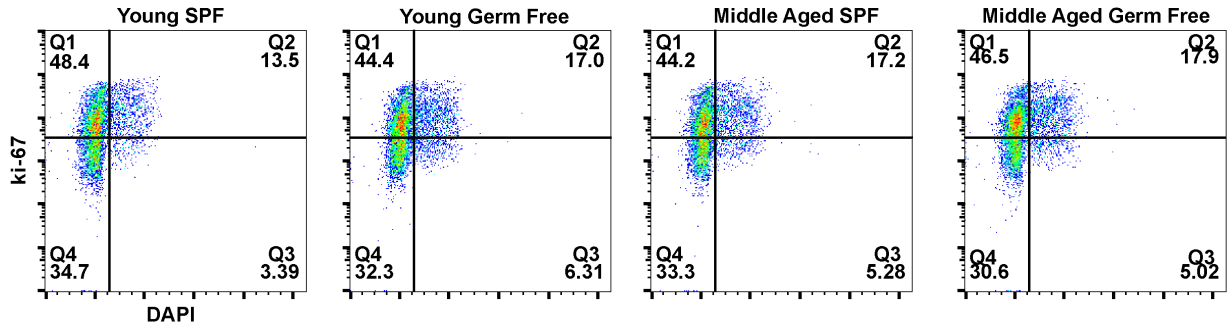
Young SPF
Q1
48.4
Q2
13.5
Q4
34.7
Q3
3.39
Young Germ Free
Q1
44.4
Q2
17.0
Q4
32.3
Q3
6.31
Middle Aged SPF
Q1
44.2
Q2
17.2
Q4
33.3
Q3
5.28
Middle Aged Germ Free
Q1
46.5
Q2
17.9
Q4
30.6
Q3
5.02
ki-67
DAPI

**Figure 3.10. Cell cycle status of cKit$^+$ lineage$^-$ hematopoietic progenitors.** (A) Representative flow plots showing DAPI and Ki-67 staining of cKit$^+$ lineage$^-$ cells harvested from the bone marrow of the indicated mice. Cells in the $G_0$, $G_1$, $G_2$/S/M phase of the cell cycle are located in Q4, Q1, and Q2, respectively.

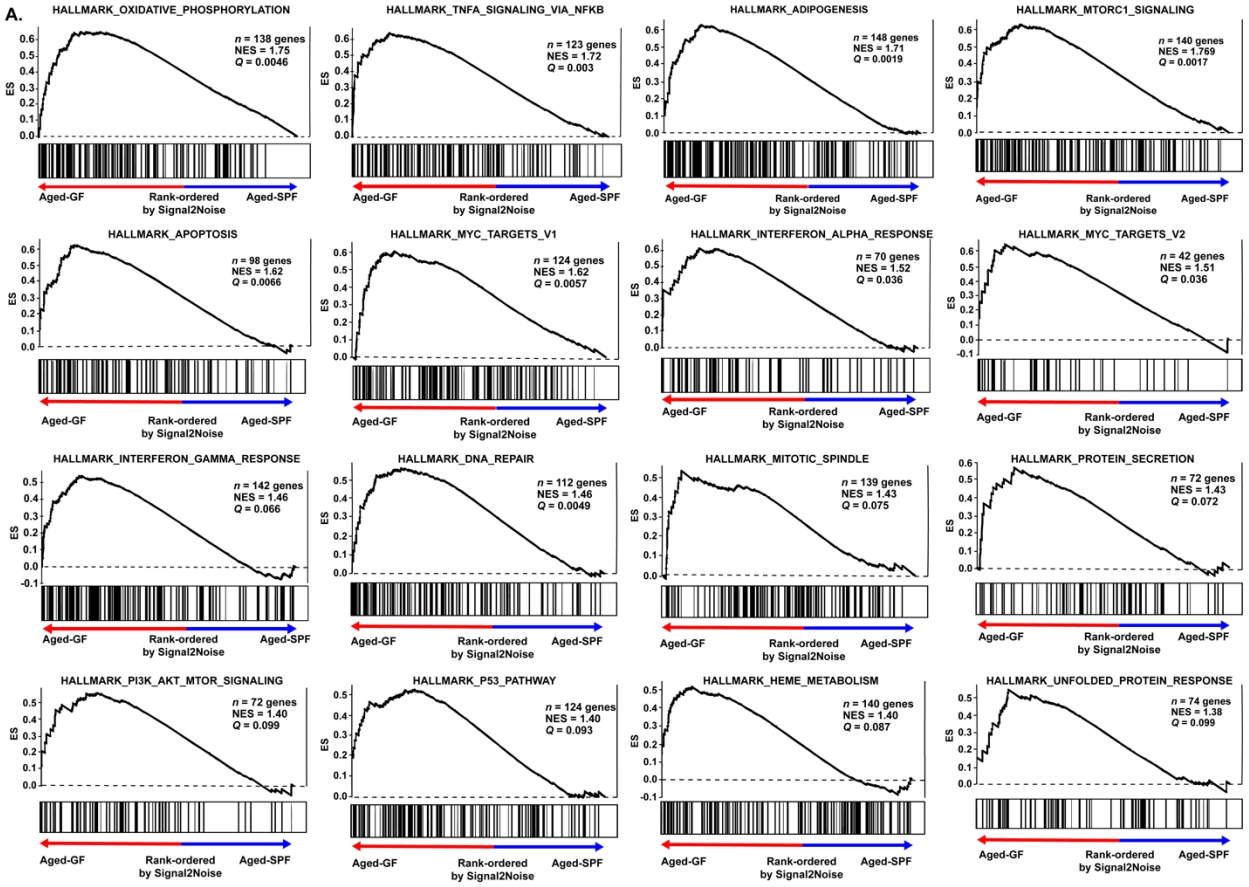
A.
HALLMARK_OXIDATIVE_PHOSPHORYLATION
n = 138 genes
NES = 1.75
Q = 0.0046
HALLMARK_TNFA_SIGNALING_VIA_NFKB
n = 123 genes
NES = 1.72
Q = 0.003
HALLMARK_ADIPOGENESIS
n = 148 genes
NES = 1.71
Q = 0.0019
HALLMARK_MTORC1_SIGNALING
n = 140 genes
NES = 1.769
Q = 0.0017
HALLMARK_APOPTOSIS
n = 98 genes
NES = 1.62
Q = 0.0066
HALLMARK_MYC_TARGETS_V1
n = 124 genes
NES = 1.62
Q = 0.0057
HALLMARK_INTERFERON_ALPHA_RESPONSE
n = 70 genes
NES = 1.52
Q = 0.036
HALLMARK_MYC_TARGETS_V2
n = 42 genes
NES = 1.51
Q = 0.036
HALLMARK_INTERFERON_GAMMA_RESPONSE
n = 142 genes
NES = 1.46
Q = 0.066
HALLMARK_DNA_REPAIR
n = 112 genes
NES = 1.46
Q = 0.0049
HALLMARK_MITOTIC_SPINDLE
n = 139 genes
NES = 1.43
Q = 0.075
HALLMARK_PROTEIN_SECRETION
n = 72 genes
NES = 1.43
Q = 0.072
HALLMARK_PI3K_AKT_MTOR_SIGNALING
n = 72 genes
NES = 1.40
Q = 0.099
HALLMARK_P53_PATHWAY
n = 124 genes
NES = 1.40
Q = 0.093
HALLMARK_HEME_METABOLISM
n = 140 genes
NES = 1.40
Q = 0.087
HALLMARK_UNFOLDED_PROTEIN_RESPONSE
n = 74 genes
NES = 1.38
Q = 0.099
ES
Aged-GF
Rank-ordered by Signal2Noise
Aged-SPF

**Figure 3.11. Gene set enrichment analysis of aged GF and SPF HSCs RNA expression data.**

(A) Significantly enriched gene sets from the Hallmark, KEGG, and Reactome gene sets (adjusted FDR < .1, nominal p-value < 0.05, and have ≥ 25 genes).

# 3.8. Tables

**Table 3.1. Differentially expressed genes in hematopoietic stem cells of aged GF compared to aged SPF mice.**

| Gene Symbol | Aged SPF1 | Aged SPF2 | Aged SPF3 | Aged GF1 | Aged GF2 | Aged GF3 | Aged SPF Average | Aged GF Average | Fold change (Aged GF vs. Aged SPF) | FDR |
|---|---|---|---|---|---|---|---|---|---|---|
| HIF1AN | 167 | 194 | 24 | 182 | 654 | 1059 | 128.33 | 631.67 | 4.92 | 3.25E-03 |
| CANT1 | 451 | 182 | 299 | 1252 | 651 | 2639 | 310.67 | 1514 | 4.87 | 5.49E-04 |
| RASD1 | 141 | 103 | 80 | 614 | 252 | 607 | 108 | 491 | 4.55 | 6.13E-04 |
| IGF2 | 154 | 159 | 153 | 933 | 660 | 522 | 155.33 | 705 | 4.54 | 1.50E-04 |
| TTYH2 | 402 | 460 | 456 | 2081 | 763 | 2520 | 439.33 | 1788 | 4.07 | 2.46E-04 |
| ISLR | 261 | 280 | 49 | 824 | 613 | 891 | 196.67 | 776 | 3.95 | 7.27E-04 |
| INHBA | 257 | 180 | 58 | 946 | 414 | 579 | 165 | 646.33 | 3.92 | 1.15E-03 |
| TMEM132A | 345 | 59 | 176 | 474 | 401 | 1245 | 193.33 | 706.67 | 3.66 | 3.88E-03 |
| CXCL10 | 539 | 166 | 272 | 980 | 1534 | 825 | 325.67 | 1113 | 3.42 | 1.17E-03 |
| VMA21 | 214 | 115 | 168 | 403 | 636 | 643 | 165.67 | 560.67 | 3.38 | 5.87E-04 |
| 2010107G12RIK | 169 | 81 | 57 | 480 | 252 | 269 | 102.33 | 333.67 | 3.26 | 5.13E-03 |
| GM10560 | 192 | 232 | 97 | 343 | 418 | 927 | 173.67 | 562.67 | 3.24 | 6.61E-03 |
| AK048000 | 336 | 404 | 261 | 822 | 771 | 1634 | 333.67 | 1075.67 | 3.22 | 1.12E-03 |
| NOL10 | 371 | 438 | 93 | 1587 | 623 | 627 | 300.67 | 945.67 | 3.15 | 4.09E-03 |
| HTRA1 | 134 | 71 | 197 | 313 | 371 | 574 | 134 | 419.33 | 3.13 | 6.55E-03 |
| MYO1H | 159 | 361 | 118 | 647 | 378 | 956 | 212.67 | 660.33 | 3.11 | 4.42E-03 |
| GM21057 | 140 | 95 | 91 | 329 | 369 | 313 | 108.67 | 337 | 3.1 | 2.60E-03 |
| F630042J09RIK | 173 | 192 | 91 | 410 | 379 | 624 | 152 | 471 | 3.1 | 8.82E-03 |
| BTG2 | 191 | 187 | 261 | 524 | 561 | 873 | 213 | 652.67 | 3.06 | 3.00E-03 |

| | | | | | | | | | | |
|---|---|---|---|---|---|---|---|---|---|---|
| AW045869 | 212 | 401 | 269 | 1387 | 646 | 624 | 294 | 885.67 | 3.01 | 3.00E-03 |
| TSPAN1 | 218 | 236 | 48 | 548 | 381 | 563 | 167.33 | 497.33 | 2.97 | 5.88E-03 |
| ZFP689 | 338 | 413 | 603 | 1614 | 713 | 1587 | 451.33 | 1304.67 | 2.89 | 1.91E-03 |
| H2-AA | 11564 | 14066 | 6915 | 29263 | 36490 | 27910 | 10848.33 | 31221 | 2.88 | 8.84E-04 |
| AK187431 | 295 | 196 | 390 | 569 | 655 | 1293 | 293.67 | 839 | 2.86 | 2.39E-03 |
| SAMM50 | 1457 | 1564 | 1107 | 4399 | 3069 | 3955 | 1376 | 3807.67 | 2.77 | 8.65E-05 |
| GM32819 | 208 | 384 | 93 | 428 | 501 | 970 | 228.33 | 633 | 2.77 | 7.53E-03 |
| HRAS | 1209 | 875 | 917 | 2023 | 1380 | 4890 | 1000.33 | 2764.33 | 2.76 | 3.61E-03 |
| DHRS3 | 9239 | 7616 | 15451 | 31406 | 35081 | 19306 | 10768.67 | 28597.67 | 2.66 | 1.96E-04 |
| TLR12 | 900 | 681 | 399 | 1251 | 1241 | 2780 | 660 | 1757.33 | 2.66 | 6.90E-03 |
| B3GNT8 | 658 | 644 | 272 | 1083 | 1015 | 2050 | 524.67 | 1382.67 | 2.64 | 3.74E-03 |
| PKLR | 221 | 154 | 197 | 401 | 394 | 673 | 190.67 | 489.33 | 2.57 | 9.71E-03 |
| BF536591 | 573 | 303 | 546 | 569 | 1369 | 1655 | 474 | 1197.67 | 2.53 | 9.12E-03 |
| LDLRAD1 | 101 | 211 | 49 | 377 | 288 | 250 | 120.33 | 305 | 2.53 | 9.41E-03 |
| UCK1 | 1297 | 837 | 1176 | 3507 | 1646 | 3127 | 1103.33 | 2760 | 2.5 | 1.52E-03 |
| LTB | 7995 | 2706 | 3314 | 7329 | 7580 | 20138 | 4671.67 | 11682.33 | 2.5 | 4.27E-03 |
| CSL | 479 | 159 | 330 | 871 | 553 | 984 | 322.67 | 802.67 | 2.49 | 4.93E-03 |
| PPP4C | 2356 | 2009 | 1438 | 2329 | 3900 | 8193 | 1934.33 | 4807.33 | 2.49 | 6.93E-03 |
| B3GNT7 | 139 | 207 | 77 | 384 | 316 | 352 | 141 | 350.67 | 2.49 | 8.02E-03 |
| COQ5 | 425 | 233 | 210 | 689 | 569 | 858 | 289.33 | 705.33 | 2.44 | 4.05E-03 |
| ZFP873 | 258 | 142 | 236 | 541 | 340 | 667 | 212 | 516 | 2.43 | 8.20E-03 |
| GGA1 | 933 | 658 | 532 | 2048 | 830 | 2231 | 707.67 | 1703 | 2.41 | 9.23E-03 |
| SLC25A10 | 741 | 416 | 864 | 2148 | 1447 | 1220 | 673.67 | 1605 | 2.38 | 2.03E-03 |
| KCNA3 | 366 | 550 | 701 | 1475 | 1012 | 1296 | 539 | 1261 | 2.34 | 1.42E-03 |
| TBC1D22BOS | 737 | 1582 | 2416 | 5132 | 2861 | 3030 | 1578.33 | 3674.33 | 2.33 | 3.78E-03 |
| CLNS1A | 1186 | 614 | 939 | 2825 | 1138 | 2381 | 913 | 2114.67 | 2.32 | 4.85E-03 |

| | | | | | | | | | | |
|---|---|---|---|---|---|---|---|---|---|---|
| CD74 | 57489 | 29744 | 25031 | 86962 | 84070 | 87755 | 37421.33 | 86262.33 | 2.31 | 1.77E-04 |
| PPIE | 2381 | 3015 | 1899 | 4437 | 5067 | 7274 | 2431.67 | 5592.67 | 2.3 | 4.85E-04 |
| MED22 | 2672 | 1773 | 2252 | 4266 | 3749 | 7385 | 2232.33 | 5133.33 | 2.3 | 1.05E-03 |
| PIGH | 329 | 450 | 698 | 1473 | 708 | 1221 | 492.33 | 1134 | 2.3 | 4.57E-03 |
| ADRB2 | 503 | 864 | 542 | 1881 | 1651 | 838 | 636.33 | 1456.67 | 2.29 | 5.88E-03 |
| D86604 | 473 | 884 | 783 | 1615 | 1346 | 1900 | 713.33 | 1620.33 | 2.27 | 2.50E-03 |
| TRAF3IP2 | 571 | 1045 | 983 | 2779 | 1546 | 1529 | 866.33 | 1951.33 | 2.25 | 3.72E-03 |
| KCNK5 | 416 | 502 | 309 | 953 | 667 | 1138 | 409 | 919.33 | 2.25 | 6.79E-03 |
| NENF | 808 | 803 | 1320 | 2604 | 1383 | 2548 | 977 | 2178.33 | 2.23 | 5.60E-03 |
| ARPC4 | 20094 | 20785 | 15067 | 55573 | 30585 | 38160 | 18648.67 | 41439.33 | 2.22 | 5.29E-04 |
| CLEC7A | 1214 | 1337 | 1622 | 3818 | 2130 | 3302 | 1391 | 3083.33 | 2.22 | 1.81E-03 |
| NAPSA | 14218 | 10883 | 7868 | 27652 | 17546 | 27537 | 10989.67 | 24245 | 2.21 | 1.31E-03 |
| RABGGTB | 375 | 678 | 371 | 1003 | 1463 | 675 | 474.67 | 1047 | 2.21 | 6.41E-03 |
| PIM3 | 1366 | 714 | 718 | 1519 | 1482 | 3135 | 932.67 | 2045.33 | 2.19 | 6.05E-03 |
| RPRL2 | 77591 | 41797 | 54770 | 154110 | 90812 | 135610 | 58052.67 | 126844 | 2.18 | 3.16E-03 |
| 1700122E12RIK | 6075 | 9383 | 9852 | 19179 | 17350 | 18303 | 8436.67 | 18277.33 | 2.17 | 2.03E-04 |
| GEMIN4 | 2335 | 1493 | 1493 | 4635 | 3157 | 3708 | 1773.67 | 3833.33 | 2.16 | 8.71E-04 |
| IER5 | 890 | 376 | 801 | 1151 | 1526 | 1778 | 689 | 1485 | 2.16 | 4.10E-03 |
| CGRRF1 | 461 | 736 | 656 | 1491 | 1160 | 1338 | 617.67 | 1329.67 | 2.15 | 2.96E-03 |
| CLDN10 | 489 | 822 | 1233 | 2594 | 1604 | 1271 | 848 | 1823 | 2.15 | 5.72E-03 |
| RPRL3 | 57853 | 42122 | 44186 | 126423 | 69369 | 111362 | 48053.67 | 102384.67 | 2.13 | 3.87E-03 |
| TNFRSF12A | 939 | 957 | 971 | 1923 | 1547 | 2574 | 955.67 | 2014.67 | 2.11 | 2.15E-03 |
| H2-DMB2 | 1352 | 793 | 806 | 1908 | 2320 | 1978 | 983.67 | 2068.67 | 2.1 | 4.69E-03 |
| GBP9 | 4110 | 4470 | 2432 | 8814 | 8660 | 5466 | 3670.67 | 7646.67 | 2.08 | 2.35E-03 |

| | | | | | | | | | | |
|---|---|---|---|---|---|---|---|---|---|---|
| CSF1 | 3335 | 1185 | 1564 | 4433 | 3014 | 5189 | 2028 | 4212 | 2.08 | 5.15E-03 |
| MBLAC1 | 603 | 574 | 1138 | 1620 | 1115 | 2028 | 771.67 | 1587.67 | 2.06 | 7.40E-03 |
| SHMT1 | 1330 | 833 | 1296 | 3115 | 1426 | 2597 | 1153 | 2379.33 | 2.06 | 9.41E-03 |
| GM5779 | 21035 | 35576 | 31188 | 59228 | 53717 | 66603 | 29266.33 | 59849.33 | 2.04 | 2.24E-04 |
| PSMB5 | 21167 | 15617 | 15651 | 27639 | 27091 | 52086 | 17478.33 | 35605.33 | 2.04 | 3.66E-03 |
| RPP30 | 593 | 866 | 1420 | 2131 | 2009 | 1727 | 959.67 | 1955.67 | 2.04 | 4.01E-03 |
| COA5 | 817 | 543 | 715 | 1267 | 1563 | 1392 | 691.67 | 1407.33 | 2.03 | 3.11E-03 |
| CLP1 | 1564 | 2280 | 3301 | 5845 | 3231 | 5395 | 2381.67 | 4823.67 | 2.03 | 5.95E-03 |
| PYGB | 4915 | 3529 | 3483 | 6538 | 6439 | 11082 | 3975.67 | 8019.67 | 2.02 | 4.39E-03 |
| OAZ1 | 23122 | 20230 | 14003 | 21333 | 39504 | 54911 | 19118.33 | 38582.67 | 2.02 | 5.47E-03 |
| BANF1 | 7875 | 6899 | 9301 | 10100 | 12573 | 25865 | 8025 | 16179.33 | 2.02 | 9.08E-03 |
| NAB2 | 5749 | 4674 | 4335 | 8827 | 7409 | 13477 | 4919.33 | 9904.33 | 2.01 | 2.52E-03 |
| H2-AB1 | 28364 | 24920 | 24009 | 52123 | 52674 | 50509 | 25764.33 | 51768.67 | 2.01 | 5.03E-03 |
| ORAOV1 | 18181 | 12230 | 7065 | 21806 | 22718 | 30892 | 12492 | 25138.67 | 2.01 | 5.89E-03 |
| SPATS2L | 2941 | 2781 | 1798 | 1296 | 1450 | 1011 | 2506.67 | 1252.33 | -2 | 3.55E-03 |
| IL2RB | 1019 | 915 | 964 | 396 | 747 | 289 | 966 | 477.33 | -2.02 | 7.39E-03 |
| COL15A1 | 1112 | 1225 | 2119 | 531 | 927 | 742 | 1485.33 | 733.33 | -2.03 | 9.68E-03 |
| AK084079 | 1243 | 1184 | 913 | 540 | 706 | 375 | 1113.33 | 540.33 | -2.06 | 8.79E-03 |
| OLFR537-PS1 | 1322 | 1741 | 1703 | 510 | 886 | 902 | 1588.67 | 766 | -2.07 | 2.91E-03 |
| BQ416348 | 2412 | 4874 | 2947 | 1355 | 1855 | 1679 | 3411 | 1629.67 | -2.09 | 5.44E-03 |
| 4930511M06RIK | 61169 | 135367 | 106587 | 32142 | 73827 | 39196 | 101041 | 48388.33 | -2.09 | 7.01E-03 |
| FDXACB1 | 23188 | 37430 | 23196 | 11871 | 16799 | 11426 | 27938 | 13365.33 | -2.09 | 7.14E-03 |

| | | | | | | | | | | |
|---|---|---|---|---|---|---|---|---|---|---|
| TULP2 | 1901 | 1136 | 1057 | 503 | 793 | 649 | 1364.67 | 648.33 | -2.1 | 5.75E-03 |
| 4921518K17RIK | 713 | 1093 | 730 | 498 | 366 | 336 | 845.33 | 400 | -2.11 | 7.79E-03 |
| 4930509J09RIK | 1007 | 971 | 1148 | 384 | 646 | 443 | 1042 | 491 | -2.12 | 6.35E-03 |
| ELF5 | 1010 | 893 | 687 | 501 | 225 | 498 | 863.33 | 408 | -2.12 | 7.22E-03 |
| VAX2 | 23031 | 59989 | 35074 | 17309 | 24341 | 13705 | 39364.67 | 18451.67 | -2.13 | 8.41E-03 |
| 4933409G03RIK | 822 | 915 | 724 | 329 | 527 | 287 | 820.33 | 381 | -2.15 | 4.83E-03 |
| BRWD3 | 75584 | 124053 | 80942 | 26043 | 69134 | 35480 | 93526.33 | 43552.33 | -2.15 | 6.02E-03 |
| GM11213 | 1705 | 1054 | 970 | 396 | 686 | 650 | 1243 | 577.33 | -2.15 | 6.35E-03 |
| FPR2 | 1051 | 2374 | 1854 | 956 | 1061 | 433 | 1759.67 | 816.67 | -2.15 | 7.95E-03 |
| 4930512M02RIK | 177825 | 255879 | 262471 | 99748 | 162502 | 60498 | 232058.3 | 107582.67 | -2.16 | 5.30E-03 |
| AK037291 | 558 | 621 | 509 | 329 | 279 | 173 | 562.67 | 260.33 | -2.16 | 9.11E-03 |
| AK031035 | 806 | 792 | 1082 | 422 | 501 | 307 | 893.33 | 410 | -2.18 | 6.29E-03 |
| PHOX2A | 940 | 2034 | 1622 | 748 | 738 | 627 | 1532 | 704.33 | -2.18 | 7.35E-03 |
| GM11944 | 1159 | 1182 | 1269 | 354 | 638 | 657 | 1203.33 | 549.67 | -2.19 | 3.80E-03 |
| AK029233 | 3641 | 1575 | 2219 | 671 | 792 | 1913 | 2478.33 | 1125.33 | -2.2 | 8.25E-03 |
| ADRA2B | 115617 | 271897 | 141447 | 65850 | 123615 | 50378 | 176320.3 | 79947.67 | -2.21 | 2.85E-03 |
| ADAM25 | 660 | 1469 | 1445 | 377 | 711 | 524 | 1191.33 | 537.33 | -2.22 | 9.64E-03 |
| GM5953 | 1053 | 953 | 1280 | 495 | 534 | 440 | 1095.33 | 489.67 | -2.24 | 2.20E-03 |
| GM2090 | 3005 | 2849 | 2617 | 1473 | 1189 | 1090 | 2823.67 | 1250.67 | -2.26 | 3.02E-03 |
| KIRREL3 | 2065 | 4240 | 1863 | 1528 | 1229 | 864 | 2722.67 | 1207 | -2.26 | 5.89E-03 |
| OLFR1360 | 1080 | 826 | 696 | 310 | 388 | 441 | 867.33 | 379.67 | -2.28 | 5.13E-03 |
| HHLA1 | 1635 | 3377 | 1650 | 740 | 1304 | 867 | 2220.67 | 970.33 | -2.29 | 3.58E-03 |
| GM26911 | 465 | 813 | 550 | 338 | 345 | 116 | 609.33 | 266.33 | -2.29 | 9.46E-03 |
| 9630013D21RIK | 5995 | 5001 | 6937 | 2467 | 3154 | 2169 | 5977.67 | 2596.67 | -2.3 | 1.26E-03 |

| | | | | | | | | | | |
|---|---|---|---|---|---|---|---|---|---|---|
| GM12128 | 1219 | 959 | 1067 | 389 | 825 | 194 | 1081.67 | 469.33 | -2.3 | 4.46E-03 |
| GM5833 | 26122 | 8388 | 10628 | 4842 | 5742 | 9033 | 15046 | 6539 | -2.3 | 9.40E-03 |
| GM4787 | 1745 | 1925 | 908 | 860 | 689 | 398 | 1526 | 649 | -2.35 | 6.70E-03 |
| BM934693 | 1014 | 1905 | 647 | 368 | 820 | 320 | 1188.67 | 502.67 | -2.36 | 9.83E-03 |
| GM11482 | 884 | 2417 | 1161 | 464 | 886 | 526 | 1487.33 | 625.33 | -2.38 | 8.24E-03 |
| GM36551 | 1268 | 3538 | 1513 | 719 | 1120 | 821 | 2106.33 | 886.67 | -2.38 | 8.32E-03 |
| OLFR103 | 744 | 623 | 897 | 423 | 406 | 120 | 754.67 | 316.33 | -2.39 | 9.41E-03 |
| HCN4 | 395 | 477 | 407 | 94 | 301 | 137 | 426.33 | 177.33 | -2.4 | 7.30E-03 |
| RAB9B | 1330 | 786 | 808 | 309 | 476 | 429 | 974.67 | 404.67 | -2.41 | 3.64E-03 |
| ANKLE1 | 8860 | 25055 | 12244 | 5774 | 7318 | 5880 | 15386.33 | 6324 | -2.43 | 4.59E-03 |
| GM6042 | 527 | 725 | 896 | 267 | 321 | 293 | 716 | 293.67 | -2.44 | 9.09E-03 |
| GM32093 | 2898 | 1949 | 1425 | 900 | 1014 | 635 | 2090.67 | 849.67 | -2.46 | 1.43E-03 |
| GM15482 | 1162 | 892 | 653 | 199 | 641 | 259 | 902.33 | 366.33 | -2.46 | 6.56E-03 |
| 2210407C18RIK | 605 | 477 | 408 | 181 | 228 | 191 | 496.67 | 200 | -2.48 | 5.86E-03 |
| DLX6 | 2454 | 1086 | 1214 | 514 | 735 | 658 | 1584.67 | 635.67 | -2.49 | 7.93E-03 |
| OLFR554 | 410 | 812 | 779 | 251 | 225 | 320 | 667 | 265.33 | -2.51 | 4.60E-03 |
| TNXB | 589 | 625 | 473 | 180 | 256 | 231 | 562.33 | 222.33 | -2.53 | 3.04E-03 |
| FSTL4 | 451 | 479 | 403 | 179 | 234 | 113 | 444.33 | 175.33 | -2.53 | 9.21E-03 |
| OLFR722 | 1248 | 459 | 766 | 389 | 260 | 318 | 824.33 | 322.33 | -2.56 | 8.21E-03 |
| CNGA3 | 560 | 1333 | 1013 | 377 | 598 | 156 | 968.67 | 377 | -2.57 | 4.59E-03 |
| B230303O12RIK | 651 | 1294 | 1131 | 470 | 571 | 153 | 1025.33 | 398 | -2.58 | 6.32E-03 |
| ZFP366 | 8757 | 6590 | 5504 | 2461 | 3963 | 1542 | 6950.33 | 2655.33 | -2.62 | 2.50E-04 |
| GM6116 | 2990 | 3589 | 1952 | 1044 | 1441 | 774 | 2843.67 | 1086.33 | -2.62 | 3.89E-04 |
| OLFR46 | 1466 | 1599 | 2037 | 502 | 680 | 758 | 1700.67 | 646.67 | -2.63 | 7.70E-04 |
| CES4A | 476 | 500 | 620 | 111 | 281 | 214 | 532 | 202 | -2.63 | 4.30E-03 |
| GM32975 | 604 | 367 | 719 | 124 | 301 | 209 | 563.33 | 211.33 | -2.67 | 3.81E-03 |
| OLFR773 | 1467 | 876 | 1018 | 639 | 556 | 61 | 1120.33 | 418.67 | -2.68 | 9.21E-03 |

| | | | | | | | | | | |
|---|---|---|---|---|---|---|---|---|---|---|
| BY550418 | 406 | 904 | 831 | 275 | 376 | 138 | 713.67 | 263 | -2.71 | 4.00E-03 |
| GM32930 | 797 | 279 | 734 | 166 | 354 | 142 | 603.33 | 220.67 | -2.73 | 8.11E-03 |
| SLC35E3 | 468 | 638 | 320 | 255 | 160 | 105 | 475.33 | 173.33 | -2.74 | 3.30E-03 |
| AK031296 | 1861 | 945 | 623 | 529 | 364 | 318 | 1143 | 403.67 | -2.83 | 3.96E-03 |
| GPR61 | 1033 | 767 | 515 | 135 | 170 | 496 | 771.67 | 267 | -2.89 | 6.68E-03 |
| ARID3C | 548 | 1646 | 1799 | 233 | 374 | 764 | 1331 | 457 | -2.91 | 4.11E-03 |
| ZFP385B | 529 | 418 | 294 | 120 | 195 | 112 | 413.67 | 142.33 | -2.91 | 6.97E-03 |
| APOB | 490 | 474 | 515 | 230 | 202 | 70 | 493 | 167.33 | -2.95 | 6.87E-03 |
| BC052181 | 607 | 598 | 846 | 394 | 119 | 178 | 683.67 | 230.33 | -2.97 | 8.68E-04 |
| ZFP750 | 222 | 529 | 666 | 235 | 203 | 27 | 472.33 | 155 | -3.05 | 7.98E-03 |
| GM6999 | 306 | 399 | 374 | 183 | 137 | 31 | 359.67 | 117 | -3.07 | 4.01E-03 |
| STARD6 | 592 | 306 | 234 | 142 | 196 | 27 | 377.33 | 121.67 | -3.1 | 9.46E-03 |
| OLFR1451 | 461 | 278 | 429 | 88 | 135 | 127 | 389.33 | 116.67 | -3.34 | 2.46E-03 |
| MMP12 | 899 | 598 | 992 | 55 | 374 | 247 | 829.67 | 225.33 | -3.68 | 3.52E-03 |
| PRP2 | 481 | 401 | 347 | 154 | 77 | 97 | 409.67 | 109.33 | -3.75 | 6.86E-04 |
| KCNH7 | 1474 | 673 | 310 | 327 | 67 | 232 | 819 | 208.67 | -3.92 | 6.83E-03 |
| 4930417H01RIK | 586 | 575 | 372 | 133 | 153 | 48 | 511 | 111.33 | -4.59 | 5.16E-04 |
| AK034071 | 1146 | 1534 | 942 | 148 | 441 | 180 | 1207.33 | 256.33 | -4.71 | 2.44E-05 |
| GHRH | 582 | 881 | 641 | 141 | 244 | 37 | 701.33 | 140.67 | -4.99 | 1.97E-04 |
| GM10714 | 1317 | 369 | 597 | 29 | 143 | 159 | 761 | 110.33 | -6.9 | 1.66E-04 |

Shown are normalized expression values from SurePrint G3 Mouse GE 8x60K Microarray calculated with limma. The average expression level of each gene for both conditions are calculated and shown as Aged SPF Average or Aged GF Average. Fold change is calculated as (Aged GF Average/Aged SPF Average). FDR, false discovery rate.

# Chapter 4: The Impact of Nucleolar Stress on T Cell Acute Lymphoblastic Leukemia Transformation

## 4.1. Introduction

T cell acute lymphoblastic leukemia (T-ALL) is an aggressive hematologic malignancy characterized by the transformation and expansion of T cell progenitors. T-ALL comprises 10% to 15% of pediatric and 20% to 25% of adult cases of acute lymphoblastic leukemia.[1,2] Current treatment consists of intense chemotherapy that is associated with acute and chronic life-threatening or debilitating toxicities.[32] Although five-year event-free survival is now 80% to 90% for children,[33-36] this rate deteriorates significantly with age: <40 years = 52.8%, 40-59 years = 37.6%, 60-79 years = 21.7%, and ≥ 80 years = 0%.[37,38] Despite a steadily increasing event-free survival in pediatric patients, approximately 20% of pediatric and 40% of adult patients will relapse,[39,40] and the prognosis after relapse is dismal with three-year event-free survival of only 10% to 15%.[14,41-43] While HCT may be curative for relapsed T-ALL, in the largest study performed to date overall survival was only 24% after a median follow up of two years.[44] Although the underlying genetic makeup of T-ALL may not predict outcome, understanding the molecular mechanisms underlying T-ALL transformation may help identify novel targets for T-ALL therapy.

Increased NOTCH signaling is thought to be central to the pathogenesis of T-ALL, with activating mutations of *NOTCH1* present in approximately 70% of cases of T-ALL[5-7] and NOTCH activation due to mutations in *FBXW7* in an additional 30% of cases.[161,162] In the context of hematopoiesis and T cell development, NOTCH1 is the key regulator for early T cell fate specification in the bone marrow, and NOTCH1 stimulation in the thymus ensures thymocyte

development.[177] Expression of an intracellular cleaved form on *NOTCH1, NOTCH ICN*, strongly induces NOTCH signaling and is sufficient to induce T-ALL in mice. In contrast, expression of hotspot mutations *NOTCH1*, which are typically seen in T-ALL, required cooperating oncogenic factors to drive transformation. Of note, recent genetic studies suggest that *NOTCH1* mutations are often subclonal, suggesting that they are late events in leukemic transformation.[29,67]

The molecular mechanisms by which activating *NOTCH1* mutations promote leukemic transformation are still unclear. What appears to be relevant are its growth-promoting effects[156,182,183] and association with transcriptional upregulation of ribosome biogenesis and protein translation.[156,157] NOTCH signaling results in increased MYC expression, which in turn stimulates ribosomal RNA synthesis and the production of ribosomal proteins.[156-158] However, increased ribosome biogenesis induces a negative feedback loop known as the nucleolar stress pathway that inhibits ribosome production and cell growth. A major component of the nucleolar stress pathway is the tumor suppressor ARF.[233] Nucleolar stress induces increased ARF expression, which in turn, inhibits ribosome expression, in part, by binding to MDM2 in a p53-dependent manner[203] and halting ribosome biogenesis independent of p53.[207,233]

T-ALL tumors with activating *NOTCH1* mutations universally harbor deletions of the cyclin-dependent kinase inhibitor 2A (*CDKN2A*) locus.[8-11] Recurrent monoallelic and biallelic deletions of *CDKN2A* have been described in both pediatric and adult cases of T-ALL, but their prognostic value is unclear. A recent analysis of the Spanish PETHEMA studies showed that monoallelic *CDKN2A* loss is observed in 25% to 30% of cases with *CDKN2A* copy number alterations.[330] Additionally, Sulong *et al*. showed that *CDKN2A* lesions at relapse are a mixture of monoallelic and biallelic deletions.[331] Furthermore, they highlighted that T-ALL clones with monoallelic loss of *CDKN2A* often fall below the resolution of commercial FISH probes. The

*CDKN2A* locus encodes for two tumor suppressors, $P16^{INK4A}$ (*INK4A*) and $P19^{ARF}$ (*ARF*). *INK4A* and *ARF* share exons two and three of the *CDKN2A* gene locus, but they have independent alpha and beta first exons.[131,190-192] These transcripts encode for wholly unique polypeptides via their different reading frames. INK4A directly inhibits cyclin-D-dependent kinases (CDK4 and CDK6), preventing phosphorylation of retinoblastoma protein (RB) and progression to S phase.[131-134] It has been reported that CDK4 directly phosphorylates upstream binding factor (UBF), leading to the initiation of ribosome biogenesis,[193,194] however the implications of CDK4 induced ribosome biogenesis in the context of *CDKN2A* biallelic loss have not been fully characterized.

ARF is the second classic tumor suppressor encoded by the *CDKN2A* locus, the alternate reading frame (its namesake) of the $P16^{INK4A}$ gene.[133] ARF stabilizes and activates p53,[144] initiating a transcriptional program that arrests the cell cycle or leads to apoptosis.[195-202] The transcription factor p53 also initiates transcription of its negative feedback regulator *MDM2*.[203] The stabilization of p53 by ARF involves a complex mechanism induced under nucleolar stress. Under baseline conditions, ARF – a nucleolar protein – cannot interact with p53 which is localized to the nucleus.[204-206] The nucleolus is an organelle formed within, but kept separate from, the nucleus for the purpose of generating ribosomes. Disruptions in ribosome biogenesis disrupt nucleolar structure and cause the release of nucleolar components into the nucleus.[207] Once in the nucleus, ARF interacts with MDM2, inhibiting its activity and stabilizing p53.[144] Additionally, ARF has been shown to interact with rRNA processing complexes to inhibit ribosome biogenesis,[272,321-323] and ARF is known to regulate the nucleolar export of NPM1[Brady 2004 ARF impedes]. Of note, *CDKN2A* loss appears to be a lymphoid-enriched genetic lesion with B- and T-ALL prevalence at 50% and 80%, respectively, but the *CDKN2A* locus is unaltered in myeloid malignancy.[10,68,74,75]

Collectively, these observations suggest the hypothesis that Notch signaling induces nucleolar stress in T-ALL and that inactivation of the nucleolar stress pathway via loss of *CDNK2A* is essential to the molecular pathogenesis of T-ALL. Here, we provide evidence in support for this hypothesis and a novel model of T-ALL leukemogenesis in which *CDKN2A* loss is an early event that provides a fitness advantage under conditions of replicative stress that leads to an expanded pool of hematopoietic stem cells and common lymphoid progenitors. Loss of *CDKN2A* provides a permissive cellular environment for activating NOTCH mutations by attenuating nucleolar stress. These data suggest that targeting nucleolar stress pathway may have therapeutic activity in T-ALL.

# 4.2. Material and Methods

## 4.2.1. Animal Husbandry and Transgenic Mouse Models

Mice were maintained under specific pathogen-free conditions and include C57BL/6 (*Ly45.2* wildtype) and B6.SJL-*Ptprc*$^{a}$ *Pepc*$^{b}$/BoyJ (*Ly45.1* wildtype) which were obtained from The Jackson Laboratory (Bar Harbor, ME). Mice were crossed in-house to generate *Ly5.2*/*Ly5.1* expressing mice on a C57BL/6 background. B6.129-*Cdkn2a*$^{tm1Rdp}$/Nci (Ink4a/Arf null) mice [Serrano 1996 Role of the INK4a 8620534] were obtained from the Frederick National Laboratory (Frederick, MD). All experiments were done using young 6-8-week-old mice . An equal number of male and female mice were used. Transplant donor and support/competitor mice were age and sex matched. All of the procedures performed in this study were approved by the Washington University Animal Studies Committee (approval number 20-0495). Mice were anesthetized using isoflurane for all procedures, and they were euthanized using $CO_2$ followed by cervical dislocation.

### 4.2.2. Flow cytometry

Peripheral blood, bone marrow, and thymus mononuclear cell (MNC) preparations were red blood cell lysed using ACK lysing buffer (Thermo Fisher, Waltham, MA). For bone marrow and spleen, MNC preparations were lysed for five minutes at room temperature. Peripheral blood was resuspended in 4x volume ACK buffer, centrifugated at 400 rcf for five minutes, and the supernatant was aspirated (four to six rounds until pellet is white). The resulting cell suspension (excluding peripheral blood) was filtered through CellTrics 70 μm nylon filters (Sysmex, Goerlitz, Germany) to generate single cell suspensions. MNCs were counted using trypan blue (Thermo Fisher) and a Cellometer Auto T4 Bright Field Cell Counter (Nexcelom, Lawrence, MA). Complete blood counts were obtained using the HV950 hemavet (Drew Scientific, Miami Lakes, FL). MNCs were incubated with target antibodies at 4°C for 30-90 minutes (or overnight for HSC CD45.2/CD45.1 staining) in phosphate buffered saline (PBS) containing 1mM ethylenediaminetetraacetic acid (EDTA) and 0.2% (weight/volume) bovine serum albumin (BSA). Data were acquired using a FACS Aria III flow cytometer (BD biosciences, San Jose, CA) and analyzed using FlowJo™ v10.8.1 software (BD biosciences).

The hematopoietic stem/progenitor cell (HSPC) panel included PE-Cy7-conjugated anti-CD117 (2B8); PerCP-Cy5.5-conjugated anti-Ly-6A/E; PE-conjugated anti-CD150 (TC15-12F12.2); BV421-conjugated anti-CD48 (HM48-1); APC-conjugated anti-CD16/32 (2.4G2); FITC-conjugated anti-CD34 (RAM34); and BV711-conjugated anti-CD135 (A2F10.1) and the following APC-Cy7-conjufated antibodies: anti-CD3ε (145-2C11), anti-B220 (RA3-6B2), anti-Gr1 (RB6-8C5), anti-Ter119 (TER-119), anti-CD11b (M1/70), and anti-NK1.1 (PK136).

The B progenitor panel included FITC-conjugated anti-Ly6D (49-H4), PE-conjugated anti-CD43 (S11), PE-Cy7-conjugated anti-CD19 (6D5), APC-conjugated anti-IgM (RMM1), BV421-conjugated anti-B220 (RA3-6B2), PerCP-Cy5.5-conjugated anti-IgD (11-26c.2a), and the following APC-Cy7-conjufated antibodies: anti-CD11c (N418), anti-CD3ε (145-2C11), and anti-NK1.1 (PK136).

The common lymphoid progenitor panel included BV421-conjugated anti-IL7Rα (A7R34), PerCP-Cy5.5-conjugated anti-CD27 (LG.3A10), APC-conjugated anti-CD135 (A2F10), FITC-conjugated anti-Ly6D (49-H4), and the following APC-Cy7-conjufated antibodies: anti-CD3ε (145-2C11), anti-B220 (RA3-6B2), anti-Gr1 (RB6-8C5), anti-Ter119 (TER-119), anti-CD11b (M1/70), anti-CD11c (N418), and anti-NK1.1 (PK136).

The thymocyte progenitor panel included BV421-conjugated anti-CD44 (clone), PE-conjugated anti-CD25 (clone), PE-Cy7-conjugated anti-CD8a (clone), APC-conjugated anti-CD4 (clone), BV605-conjugated anti-CD117 (clone), and the following APC-Cy7-conjugated antibodies: anti-B220 (RA3-6B2), anti-Gr1 (RB6-8C5), anti-Ter119 (TER-119), and anti-CD11b (M1/70).

The mature cell panel included BV421-conjugated anti-B220 (RA3-6B2), APC-Cy7-conjugated CD3ε (145-2C11), FITC-conjugated anti-Gr1 (RB6-8C5), and PE-conjugated anti-CD115 (clone). Antibodies were obtained from BioLegend or BD Biosciences.

### 4.2.3. Transplantation and Cell sorting

Six-to-eight-week-old wildtype *Ly5.1*/*Ly5.2* recipient mice were irradiated twice with 600 cGy six hours apart. Donor (*Ly5.2*) bone marrow cells were then injected retro-orbitally and placed on prophylactic antibiotics (trimethoprim-sulfamethoxazole) for two weeks. Peripheral blood chimerism was analyzed every four weeks until mice were sacrificed 16-to-twenty-four weeks post-transplantation when donor chimerism in bone marrow, blood, and thymus were analyzed. For whole bone marrow competitive transplantations, the indicated ratio of *Ly5.2* to *Ly5.1* whole bone marrow cells were used for a total of two million cells. For transplants involving the retroviral transduction of *NOTCH1* constructs, five hundred thousand CD117-selected cells were transplanted with varying transduction efficiency (~80% for empty vector controls and 20% or less for *NOTCH1* constructs).

### 4.2.4. Immunofluorescent Confocal Microscopy

Fixed sample images were acquired using an LSM 700 laser scanning confocal microscope with a 63x 1.4 NA Plan-Apochromat oil-immersion objective (CarlZeiss). Acquisition parameters were established using the brightest control specimen such that just a few pixels reached saturation in order to achieve the greatest dynamic range in our experiments. For quantitative measurements, parameters including gain, laser power, scan speed, dwell time, resolution, and zoom were kept consistent between comparisons.

### 4.2.5. Quantitative reverse-transcription PCR

Two-step quantitative reverse-transcription PCR was performed using total RNA and the SuperScript VILO cDNA synthesis kit (Thermo Fisher) and the TaqMan Fast Advanced Master Mix kit (Thermo Fisher) with no template and no reverse transcriptase controls. mRNA expression is normalized to *β-actin* mRNA expression. Data was collected on a StepOnePlus Real-Time PCR System (Thermo Fisher). The following quantitative PCR primer/probe sets were used:

TaqMan® Assays and Arrays:

*Actb*, Mus_musculus VIC–spanning exons 1–2 Mm04394036_g1

IDT PrimeTime Std® qPCR Assay:

*Bax*, Mus_musculus
FAM/ZEN/IBFQ
Sequence 1
GCC ATC AGC AAA CAT GTC AG
Sequence 2
GGA GAT GAA CTG GAC AGC AAT
Sequence 3
/56-FAM/CG TCA GCA A/Zen/T CAT CCT CTG CAG CT/3IABkFQ/

*Bbc3*, Mus_musculus
FAM/ZEN/IBFQ
Sequence 1
AGA GAT TGT ACA TGA CCC TCC A
Sequence 2
GAC CTC AAC GCG CAG TA
Sequence 3
/56-FAM/CG GAG ACA A/Zen/G AAG AGC AGC ATC GA/3IABkFQ/

*Fas*, Mus_musculus
FAM/ZEN/IBFQ
Sequence 1
CTC GGA GAT GCT ATT ACC TTG
Sequence 2
AGA CATGCT GTG GAT CTG G
Sequence 3

/56-FAM/TC CTG CCT C/Zen/T GGT GCT TGC TG/3IABkFQ/

*Cdkn1a*, Mus_musculus
FAM/ZEN/IBFQ
Sequence 1
AAT CTG CGC TTG GAG TGA TAG
Sequence 2
CTT GTC GCT GTC TTG CAC T
Sequence 3
/56-FAM/TG TCT GAG C/Zen/G GCC TGA AGA TTC C/3IABkFQ/

*Mdm2*, Mus_musculus
FAM/ZEN/IBFQ
Sequence 1
TCT GAT AGA CTG TGA CCC GAT
Sequence 2
GCG TGG AAT TTG AAG TTG AGT C
Sequence 3
/56-FAM/AG CTC GTG C/Zen/C CTT CGT CAC TC/3IABkFQ/

*Pmaip1*, Mus_musculus
FAM/ZEN/IBFQ
Sequence 1
GCA CAC TCG TCC TTC AAG T
Sequence 2
CCG GAC ATA ACT GTG GTT CT
Sequence 3
/56-FAM/TC ATC CTG C/Zen/T CTT TTG CGA CTT CCC/3IABkFQ/

*Notch1*, Mus_musculus 6-FAM/ZEN/IBFQ Mm.PT.58.28794468

*Hes1*, Mus_musculus 6-FAM/ZEN/IBFQ Mm.PT.58.41697865

*Hey1*, Mus_musculus 6-FAM/ZEN/IBFQ Mm.PT.58.31332652

*Cdkn2a*, Mus_musculus
FAM/ZEN/IBFQ
Sequence 1
TGG GTG CTC TTT GTG TTC C
Sequence 2
GAG GCC GGA TTT AGC TCT G
Sequence 3
/56-FAM/TG GTC TTT/Zen/T GTA CCG CTG GGA AC/3IABkFQ/

*Arf*, Mus_musculus
FAM/ZEN/IBFQ

Sequence 1
CTC TGG CTT TCG TGA ACA TG
Sequence 2
TCG AAT CTG CAC CGT AGT TG
Sequence 3
/56-FAM/TG CGG CCC/Zen/C TTC TCA AGA TCC/3IABkFQ/

*Ink4a*, Mus_musculus
FAM/ZEN/IBFQ
Sequence 1
AAC GCC CCG AAC TCT TTC
Sequence 2
AGA AGA GCT GCT ACG TGA AC
Sequence 3
/56-FAM/CG GTC GTA C/Zen/C CCG ATT CAG GTG/3IABkFQ/

### 4.2.6. Progenitor T cell culture and *Notch1* construct transduction

Murine embryonic hematopoietic stem cells (eHSC) were collected as previously described.[332,333] Briefly, CD117-selected eHSCs were cultured in α-MEM with 15% FCS, 100 U/mL penicillin, 100 μg/mL streptomycin, 5 ng/mL recombinant human FLT3-L, 1 ng/mL recombinant mouse IL-7, and 25 ng/mL recombinant mouse SCF on 50-60% confluence OP9-DL4 stromal cells in 24 wells plates at a density of 0.8 x $10^5$ cells/mL.

The control GFP-expressing MSCV-IRES-GFP construct (MigR1) and the *NOTCH1* mutant constructs found in human T-ALL were gifted by Warren Pear's group and described previously.[7,334]

For ProT transduction, CD117-selected eHSCs were cultured in Opti-MEM GlutaMAX supplement with 15% FCS, 55 μM beta-mercaptoethanol (Gibco), 100 U/mL penicillin, 100

μg/mL streptomycin, 5 ng/mL recombinant human FLT3-L, 1 ng/mL recombinant mouse IL-7, and 25 ng/mL recombinant mouse SCF on 50-60% confluence OP9-DL4 stromal cells in 24 wells plates at a density of 0.8 x $10^5$ cells/mL. Retrovirus was produced by transfecting HEK-293T cells with MSCV vectors and collecting supernatant 48 hours and 72 hours later. Viral supernatant was passed through a 0.45 μm syringe filter (Corning) and concentrated with Amicon 100 kDa centrifugal filters (Millipore). Primary HSCs were infected by addition of concentrated virus in the presence of 4 μg/mL polybrene and centifuged at 1100 x g for 90 minutes at 28°C.

For adult murine HSCs, CD117-selected bone marrow MNCs were cultured in Opti-MEM GlutaMAX supplement with 10% FCS, 55 μM beta-mercaptoethanol (Gibco), 100 U/mL penicillin, 100 μg/mL streptomycin, 10 ng/mL recombinant mouse IL-3, 10 ng/mL recombinant IL-6, 25 ng/mL recombinant mouse IL-7, 50 ng/mL recombinant mouse Flt3-L, 50 ng/mL recombinant mouse SCF, and 25 ng/mL recombinant mouse TPO in 24-well plates at a density of 0.5 x $10^6$ cell/mL. Retrovirus was produced by transfecting HEK-293T cells with MSCV vectors and collecting supernatant 48 hours and 72 hours later. Viral supernatant was passed through a 0.45 μm syringe filter (Corning) and concentrated with Amicon 100 kDa centrifugal filters (Millipore). Primary HSCs were infected by addition of concentrated virus in the presence of 4 μg/mL polybrene and centifuged at 1100 x g for 90 minutes at 28°C.

### 4.2.7. 5-fluorouracil treatment

All doses of 5-fluorouracil (5-FU) were given at 150 mg/kg (F6627-5G, Sigma) by intraperitoneal injection. For the replication stress transplantation experiments, recipient mice were treated at 6 and 8 weeks post-transplant with 150mg/kg doses of 5-FU. For cell cycle analysis, wildtype mice

were treated with 5-FU and sacrificed 24 hours post-treatment for assessment.

### 4.2.8. Live-Cell Image Analysis

Cells were seeded in 24 well plates as described in 2.2.6. Cells were imaged using phase contrast and red-fluorescence in the IncuCyte S3 platform (Sartorius, Göttingen, Germany) in conjunction with Cytotox-Red stain, as per the manufacturer's instructions. The live cell imaging experiments was performed in quintuplet. Sixteen sets of images from distinct regions within each well were taken at four-hour intervals for ninety-six hours, using a 10x objective. IncuCyte S3 image analysis software was set to detect the edges of the cells, to determine their confluence, their absolute number, and the number of red-fluorescent cells per image.

### 4.2.9. Whole Genome Sequencing and Analysis

Mouse data were aligned to mm10 using BWA-MEM.[335] The aligned reads were sorted, deduplicated, and run through base quality score recalibration (BQSR). Structural variants (SVs) and large indels were detected using Manta.[336] SNVs and small indels were detected using VarScan2,[337] Strelka2,[338] and MuTect2.[339] Transcript annotation was performed using VEP version 95 for both mouse and human.[340] Variants in regions of low-quality mapping and low coverage (< 20X) were removed. Copy number variants were inferred and visualized using CNVkit.[341] The entire somatic pipeline is available as a CWL workflow at https://github.com/genome/analysis-workflows/commit/3e653e78fea91cf9c487534ceca1db328b6b68e0.

### 4.2.10. Quantification and statistical analysis

Significance was determined using Prism v8.1.2 (GraphPad, San Diego, CA, USA). For single parameter analysis, unpaired t-test were used to assess statistical significance. For multiple parameter data, statistical significance was calculated using one-way or two-way analysis of variance (ANOVA). P values less than 0.05 were considered significant. Expression data are log transformed prior to statistical analysis.

## 4.3. Results

### 4.3.1. Notch1 expression in primary murine thymocytes induces nucleolar stress and inhibits cell growth

To test our hypothesis that activating *NOTCH1* mutants induce nucleolar stress, we first modified protocols established by the Zuñiga-Pfluecker group[332,333] to generate progenitor T cells in culture (Figure 4.1.A). Our progenitor T cell cultures are derived from cKit selected fetal liver cells. Phenotypically, greater than 90% of these cells resembled $CD4^+$ $CD8^+$ double positive thymocytes (Figure 4.1.B). To test how T-ALL relevant *NOTCH1* mutations alter DP thymocytes, we transduced these cells with retrovirus expressing empty vector, wildtype *NOTCH1*, or activating *NOTCH1* mutants (a*NOTCH1*) carrying hotspot mutations *L1594P* or *L1601P*. After sorting on GFP, we assessed Notch activation via its target *Hey1* and observed a nearly 4-fold increase in Notch activity in cells expressing a*NOTCH1* (Figure 4.1.C). Having enhanced Notch activation, we investigated to what extent nucleolar stress was induced by measuring hallmarks of nucleolar stress. First, we measured expression of the *Cdkn2a* genes ($p16^{Ink4a}$ and $p19^{Arf}$, Figure 4.1.D). We observed a hundreds-fold increase in both *Cdkn2a* genes in cells expressing a*NOTCH1*.

Additionally, a*NOTCH1* induced expression of key p53 target genes, *p21* and *Bax* (Figure 4.1.E), which suggest p53 stabilization through Arf. Cells expressing a*NOTCH1* also exhibited stalled ribosome biogenesis, as observed by the accumulation of immature 5'-external transcribed spacer (ETS) containing rRNA to mature 18S rRNA (Figure 4.1.F). Finally, a*NOTCH1* was shown to induce the canonical sign of nucleolar stress – translocation of nucleophosmin from nucleoli to the nucleoplasm (data not shown). Consistent with data from Warren Pear's group,[181] live-cell imaging over 96 hours revealed that a*NOTCH1* mutations have a negative impact on cellular proliferation. Collectively, these data show that expression of a*NOTCH1* mutants is sufficient to induce nucleolar stress, resulting in p53 activation and impaired cell proliferation.

### 4.3.2. *Cdkn2a* expression is induced during early lymphoid differentiation

To investigate *Cdkn2a* expression and nucleolar stress induction during normal hematopoiesis, we first measured the basal level of *Arf* and *Ink4a* across hematopoietic populations (Figure 4.2.A). Hematopoietic stem cells (HSCs), common lymphoid progenitors (CLPs), granulocyte-monocyte progenitors (GMPs), Pre-Pro-B cells, Pro-B cells, Pre-B cells, Early T lineage progenitors (ETPs), $CD4^-$ $CD8^-$ double negative 2/3 (DN2/3) T lineage progenitors, DN4, $CD4^+$ $CD8^+$ double positive (DP) T lineage progenitors, and circulating B cells, T cells, neutrophils, and monocytes were sorted to assess mRNA transcript expression by qRT-PCR. Low-level or absent expression of *Ink4a* and *Arf* was observed in the most immature hematopoietic progenitors, HSCs, CLPs and GMPs. Similarly, expression of *Ink4a* and *Arf* was minimal in myeloid cells, including GMPs and mature circulating neutrophils and monocytes. In contrast, expression of both *Ink4a* and *Arf* was elevated throughout both B lymphopoiesis and T

lymphopoiesis. *Cdkn2a* expression in T cell development is elevated in the earliest thymic T lineage progenitors, ETPs, and remains elevated to the DP thymocyte stage, returning to baseline levels thereafter.

We next examined basal levels of nucleolar stress in hematopoiesis by measuring the accumulation of immature 5' external transcribed spacer (ETS) containing rRNA relative to mature 18S rRNA (Figure 4.2.B). Congruent with expression of *Cdkn2a* genes and data on excess ARF,[270,319-321] immature rRNA accumulation relative to mature 18S rRNA is highest in developing thymocytes, elevated above the baseline ETS/18S ratios of early hematopoietic progenitors and myeloid cells.

### 4.3.3. Loss of *Cdkn2a* has minimal impact on basal hematopoiesis or HSC function

The impact of *CDKN2A* loss on HSC maintenance or hematopoietic differentiation has not been fully characterized. To address this issue, we first quantified phenotypic HSCs by flow cytometry (Figure 4.3.A). By percentage and absolute number, the frequency and number of HSCs in *Cdkn2a*$^{+/-}$ and *Cdkn2a*$^{-/-}$ mice is similar to wildtype mice. This is expected since the expression of *Cdkn2a* is very low in HSCs under steady state conditions. Despite the relative high expression of Arf and Ink4a during lymphopoiesis, B- and T-lymphopoiesis are normal in *Cdkn2a*$^{-/-}$ mice (data not shown). Similarly, granulopoiesis was similar between *Cdkn2a* deficient mice and wildtype controls. Peripheral blood counts; the level of circulating T cells, B cells, neutrophils, and monocytes; and the number of myeloid, B-cell, and T-cell lineage cells in the bone marrow and thymus were also comparable to control mice.

We hypothesized that replication stress induced by transplantation may activate *CDKN2A* expression in WT HSCs, suppressing their proliferation. To assess the impact of *Cdkn2a* loss on HSC response to replication stress, we first transplanted whole bone marrow from *Cdkn2a*$^{+/-}$ or *Cdkn2a*$^{-/-}$ mice (*Ly5.2*) against whole bone marrow from wildtype mice (*Ly5.1*) in a 50:50 competitive manner and measured chimerism (Figure 4.3.B). Stable overall donor engraftment was observed over time with enhanced engraftment of both *Cdkn2a*$^{+/-}$ and *Cdkn2a*$^{-/-}$ HSCs. Contrary to what is observed at baseline in *Cdkn2a*$^{+/-}$ and *Cdkn2a*$^{-/-}$ transgenic mice, both *Cdkn2a*$^{+/-}$ and *Cdkn2a*$^{-/-}$ HSCs consistently outperformed wildtype competitors in transplantation assays with HSC chimerism reflected across all hematopoietic lineages. Strikingly, both *Cdkn2a*$^{+/-}$ and *Cdkn2a*$^{-/-}$ cells completely eclipsed any remaining wildtype cells upon secondary transplant (Figure 4.3.C).

To begin to explore mechanisms by which *Cdkn2a* deficiency confers fitness to HSCs, we assessed the expression of *Cdkn2a* genes, *Ink4a* and *Arf*, by qRT-PCR in response to 5-fluorouracil treatment (5-FU, 150 mg/kg intraperitoneal injection), sorting HSCs from wildtype mice treated with 5-FU twenty-four-hours post-treatment (Figure 4.3.D). Interestingly, we observed a several-hundred-fold induction of *Arf* expression in HSCs after 5-FU treatment, however *Ink4a* transcripts were not detected. We next characterized the response of *Cdkn2a*$^{+/-}$ and *Cdkn2a*$^{-/-}$ cells to serial replication stress *in vivo*. Briefly, *Cdkn2a*$^{+/-}$ or *Cdkn2a*$^{-/-}$ whole bone marrow was transplanted at one-to-ten against wildtype whole bone marrow, and recipients were treated with 5-fluorouracil (5-FU) following stable engraftment at six weeks and eight weeks post-transplantation. Consistent with our model, treatment with 5-FU resulted in significant (~5-fold) expansion of *Cdkn2a*$^{+/-}$ and *Cdkn2a*$^{-/-}$ HSCs with concomitant hematopoietic output (Figure 4.3.F).

### 4.3.4. *Cdkn2a* loss supports mutant Notch-driven expansion of lymphoid progenitors

We next explored the impact of a*NOTCH1* mutants *in vivo*, using a retroviral transplantation model. In brief, $CD117^{+}$ cells were sorted from adult mice and subjected to two rounds of retroviral transduction for *NOTCH1* variants. These cells were transplanted into lethally irradiated mice and the contribution of a*NOTCH* ($GFP^{+}$) expressing cells to hematopoiesis examined over time (Figure 4.4.A). The contribution of a*NOTCH1* variants to hematopoietic stem cells (HSCs), common lymphoid progenitors (CLPs), and T cells was similar to input percentage and was stable over time (Figure 4.4.B). However, a*NOTCH* variants were selected against throughout both myelopoiesis and B lymphopoiesis, with a near complete loss of a*NOTCH1* expressing myeloid and B cells.

Finally, to get at our hypothesis that CDKN2A loss is an early transformation event that provides a permissive environment for secondary driver mutations, we modeled the impact of CDKN2A loss on activating notch-induced leukemogenesis by retrovirally transducing a*NOTCH* variants into $CDKN2A^{+/-}$ HSPCs and transplanting these cells into lethally irradiated wildtype recipients (Figure 4.4.C). At 16 weeks post-transplant, we found that compared to HSCs expressing a*NOTCH* in a CDKN2A wildtype background, expression of a*NOTCH* in the context of CDKN2A loss resulted in a significant expansion of hematopoietic stem cells and common lymphoid progenitors (Figure 4.4.D). However, CDKN2A loss did not rescue the activating notch induced block in the myeloid or B lymphoid lineages.

### 4.3.5. *Cdkn2a* loss cooperates with activated *Notch* mutants to induce T-ALL in mice

Consistent with the oncogenic cooperativity of a*NOTCH1* variants demonstrated by Chiang *et al*., a tumor watch confirmed that *Cdkn2a* loss strongly cooperates with activating notch expression to induce T-ALL in mice (Figure 4.5). All 17 mice in the *NOTCH1 L1601P CDKN2A*$^{-/-}$ group developed a double positive T cell leukemia by 200 days compared to 3 out of 12 mice in the *NOTCH1 L1601P CDKN2A*$^{+/+}$ group.

Finally, we were interested in whether tumors that develop from *Cdkn2a*$^{+/-}$ a*NOTCH1* cells lose the second copy of *Cdkn2a*. To this end, we performed matched-pair whole genome sequencing on these tumors at 30X coverage. Briefly, cKit-selected *Cdkn2a*$^{+/-}$ cells from pooled donors were split amongst four wells in tissue culture to generate *Cdkn2a*$^{+/-}$ empty vector controls, *Cdkn2a*$^{+/-}$ expressing wildtype *NOTCH1*, *Cdkn2a*$^{+/-}$ expressing *NOTCH1*$^{L1594P}$, and *Cdkn2a*$^{+/-}$ expressing *NOTCH1*$^{L1601P}$. DNA from *Cdkn2a*$^{+/-}$ empty vector control cells was used as paired-normal, enabling acquired genetic lesion calling. Tumors generated from all mice were immunophenotypically CD4+ CD8+ with significant bone marrow infiltration, significant thrombocytopenia and anemia, and leukocytosis. Consistent with these observation, all of our *Cdkn2a*$^{+/-}$ a*NOTCH1* induced mouse T-ALL samples retained the wildtype allele of *Cdkn2a*.

We identified 2,398 nonsynonymous single-nucleotide variant (SNV), insertion/deletion (indel), or internal tandem duplication sequence mutations in 1,332 genes by whole genome sequencing in a cohort of five *Cdkn2a*$^{+/-}$ a*NOTCH1* tumors. Interestingly, we identified driver mutations similar to what has been reported in patient T-ALL, including ASXL2, DDX3X, FAT1, IKZF1, KMT2A, KMT2C, PTEN, and SETD2. We observed mutations that alter transcription factors genes (*Hoxa7*, *Bcl11b*, *Ccnd3*, *Runx1*, *Etv6*, and *Wt1*), mutations that activate signaling

pathways (*Pten* and *Flt3*), ribosomal proteins (*Rpl10-ps4*, *Rpl37*, *Rpl21-ps12*, *Rpl19-ps10*, and *Rpl31-ps18*), and epigenetic regulators (*Usp7* and *Crebbp*) commonly recurrent in pediatric and adult cases of T-ALL. All of these mutations have been described previously and highlight the heterogeneity of mutations leading to leukemogenesis.

## 4.4. Discussion

Given the prevalence of *NOTCH1* mutations in T-ALL and its role in T cell lineage specification, mutations in *NOTCH1* are thought to be central to T cell acute lymphoblastic leukemia pathogenesis. However, recent T-ALL whole genome sequencing[65,66] and single cell sequencing[67] data show that activating *NOTCH1* mutations are secondary, or subclonal events. Recent evidence suggests that the most recurrent *NOTCH1* mutations, *NOTCH1 L1594P* and *L1601P* are not sufficient to induce leukemogenesis in mice, but these *NOTCH1* mutations cooperate with additional oncogenic drivers to drive T-ALL. In line with these observation, our data show that activating mutations of the oncogene *NOTCH1* paradoxically slow cell growth by triggering the evolutionarily conserved nucleolar stress homeostatic pathway as a result of the excess demand on ribosome biogenesis. A key component of nucleolar stress pathway, *Arf*, is encoded by the *CDKN2A* gene locus, which is deleted in the vast majority of cases of T-ALL. Similar to observations made by Chiang *et al*., our study shows that *NOTCH1* hyperactivation cooperates with additional T-ALL drivers to induce leukemogenesis. Specifically, a*NOTCH1* mutations cooperate with *Cdkn2a* loss, and our data shows that activating *NOTCH1* mutations are not effective T-ALL initiators. Of note, although a*NOTCH1* mutations do not confer an advantage to hematopoietic stem cells, a*NOTCH1* mutations are maintained in both HSCs and T-lineage cells.

However, a*NOTCH1* mutations are selected against in both myelopoiesis and B lymphopoiesis. Furthermore, there is a paucity of a*NOTCH1* mutations in myeloid and B lymphoid malignancies,[10,68,74,75] suggesting a level of tolerance for a*NOTCH1* mutations that is specific to the cellular environment of T lymphopoiesis. However, the molecular mechanisms governing hyperactive *NOTCH1* maintenance in T lymphopoiesis despite clear stimulation of nucleolar stress and slowed growth *in vitro* remains unclear.

*CDKN2A* is a master regulator of ribosome biogenesis, p53 stabilization, and cell cycle regulation through cyclin-dependent kinases.[131-134] The prevalent deletion of *Cdkn2a*, and/or mutation of ribosomal proteins, specifically in acute lymphoblastic leukemia suggest that ablating nucleolar stress is central to ALL pathogenesis. Given the degree of *Cdkn2a* activation in both T and B lymphopoiesis, we hypothesized that loss of *Cdkn2a* would result in increased B and T lineage relative abundance compared to control mice. Surprisingly, transgenic $Cdkn2a^{+/-}$ and $Cdkn2a^{-/-}$ mice do not have altered hematopoiesis. Our data show that, while *Cdkn2a* loss does not alter basal hematopoiesis, *Cdkn2a* deficient hematopoietic stem cells do expand under replication stress conditions, suggesting that somatic loss of *CDKN2A* may result in an expanded pool of hematopoietic stem and progenitor cells as a result of hematopoietic insult or replication stress. Given the heterogeneity of T-ALL and prevalence of multiclonal mutations,[29] our data suggest that an expanded pool of $Cdkn2a^{+/-}$ or $Cdkn2a^{-/-}$ provide a permissive cellular environment to these acquired secondary mutations, including *NOTCH1*.

Early studies of *CDKN2A* loss,[342] demonstrated a strong selective pressure in favor of loss-of-heterozygosity. Reports of the prevalence of biallelic *CDKN2A* loss may have been limited by the resolution of bulk sequencing. The advent of single cell sequencing enabled higher resolution *CDKN2A* locus analysis. Naturally, the hallmark subclonal evolution of T-ALL has since been

extended to *CDKN2A* loss.[330,331] High resolution next-generation sequencing and cytogenetic studies have revealed that T-ALL is often subclonal in regard to *CDKN2A* loss. Interestingly, monoallelic and biallelic loss of *CDKN2A* has not been associated with differential disease prognoses.[330] Our data suggest that the loss of one or both copies of *CDKN2A* may effect predisposition to ALL and disease latency. This is supported by the increased incidence and decreased latency of *Cdkn2a*$^{-/-}$ tumors compared to *Cdkn2a*$^{+/-}$ tumors despite a lack of discernable difference between *Cdkn2a*$^{+/-}$ and *Cdkn2a*$^{-/-}$ hematopoietic cells in response to replication stress.

In summary, these data provide support for a novel model of T-ALL leukemogenesis in which *CDKN2A* loss is an early transformation event that provides a fitness advantage under conditions of replication stress, leading to an expanded pool of *CDKN2A*$^{+/-}$ or *CDKN2A*$^{-/-}$ HSCs and CLPs. Loss of CDKN2A provides a permissive cellular environment for activating *NOTCH1* mutations by attenuating nucleolar stress, setting up T-ALL transformation with secondary driver mutations. Furthermore, these data suggest that targeting the nucleolar stress pathway or ribosome biogenesis may have therapeutic activity in T-ALL.

# 4.5. Acknowledgement

We thank the Alvin J. Siteman Cancer Center at Washington University School of Medicine and Barnes-Jewish Hospital in St. Louis, MO., for the use of the Siteman Flow Cytometry, which provided cell sorting services. The Siteman Cancer Center is supported in part by NCI Cancer Center Support Grant #P30 CA091842. This study was supported by the National Institutes of Health grants R01HL131655 (Daniel C. Link, MD) and F31CA247136 (Joseph R. Krambs).

## 4.6. Author Contributions

Joseph R. Krambs and Daniel C. Link, MD conceived and jointly supervised the study. Joseph R. Krambs and Daniel C. Link, M.D. designed the experiments. Joseph R. Krambs and Isabelle Genter performed the experiments. Joseph R. Krambs and Daniel C. Link, MD wrote the manuscript. Christopher Miller, Ph.D., and Sai Ramakrishnan performed whole genome sequencing analysis. All authors contributed to the article.

# 4.7. Figures

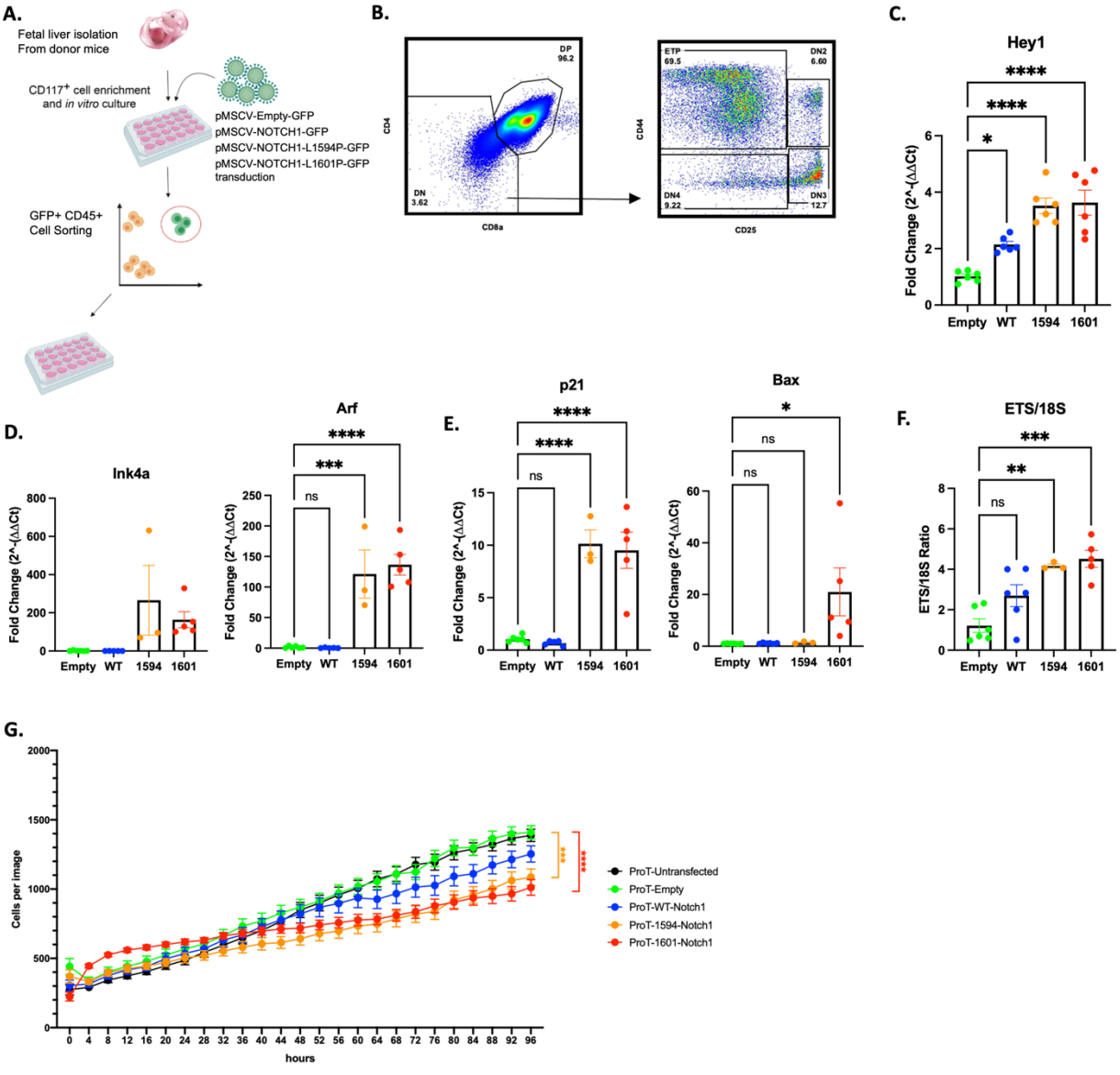
A.
Fetal liver isolation
From donor mice
CD117+ cell enrichment
and in vitro culture
pMSCV-Empty-GFP
pMSCV-NOTCH1-GFP
pMSCV-NOTCH1-L1594P-GFP
pMSCV-NOTCH1-L1601P-GFP
transduction
GFP+ CD45+
Cell Sorting
B.
DP
96.2
CD4
DN
3.62
CD8a
ETP
69.5
DN2
6.60
CD44
DN4
9.22
DN3
12.7
CD25
C.
Hey1
Fold Change (2^-(ΔΔCt))
Empty
WT
1594
1601
D.
Ink4a
Arf
E.
p21
Bax
F.
ETS/18S
ETS/18S Ratio
ns
G.
Cells per image
hours
ProT-Untransfected
ProT-Empty
ProT-WT-Notch1
ProT-1594-Notch1
ProT-1601-Notch1

**Fig 4.1. *Notch1* expression in primary murine thymocytes induces nucleolar stress and inhibits cell growth.**

(A) Strategy for generating CD4+ CD8+ double positive (DP) thymocytes *in vitro*. (B) Representative flow plot of cells in culture, showing the gating strategy to identify phenotypic DP thymocytes. (C-F) Relative mRNA expression of NOTCH1 targets (C), *Cdkn2a* locus genes (*Ink4a* and *Arf,* D), p53 targets (E), and rRNA processing (F) in thymocyte cultures, expressing GFP-alone (empty vector control), full-length wildtype NOTCH1, or an activating NOTCH1 variant *L1594P* or *L1601P* compared to *B-actin* mRNA. (G) Growth rate of DP thymocytes expressing NOTCH1 constructs over 96 hours. (H) Nucleophosmin localization in DP thymocytes expressing NOTCH1 constructs. Data represent the mean ± SEM. *P < 0.05, **P < 0.01, ***P < 0.001, and ****P < 0.0001 by one-way ANOVA with alpha = 0.05 and Sidak's multiple comparisons test.

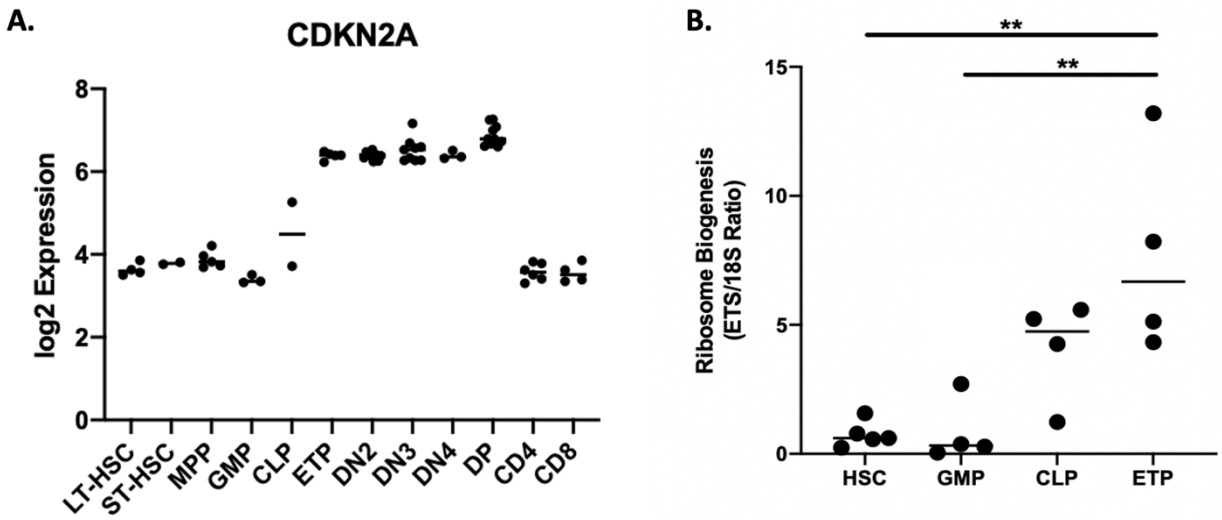
A.
CDKN2A
log2 Expression
8
6
4
2
0
LT-HSC
ST-HSC
MPP
GMP
CLP
ETP
DN2
DN3
DN4
DP
CD4
CD8
B.
**
**
Ribosome Biogenesis
(ETS/18S Ratio)
15
10
5
0
HSC
GMP
CLP
ETP

**Figure 4.2. *Cdkn2a* expression is induced during early lymphoid differentiation.**

(A-D) Relative mRNA expression of *Cdkn2a* (A) and rRNA processing (B) in sorted hematopoietic populations: lineage$^-$ cKit$^+$ Sca1$^+$ CD150$^+$ CD48$^-$ cells (hematopoietic stem and progenitor cells); lineage$^-$ CD27$^+$ IL7R$\alpha^+$ cells (common lymphoid progenitors); lineage$^-$ cKit$^+$ Sca1$^-$ CD16/32$^+$ CD34$^+$ cells (granulocyte-monocyte progenitors); lineage$^-$ CD4$^-$ CD8$\alpha^-$ CD44$^+$ CD25$^-$ cKit$^+$ cells (early T lineage progenitors); lineage$^-$ CD4$^-$ CD8$\alpha^-$ CD44$^+$ CD25$^+$ cells (DN2 thymocytes); lineage$^-$ CD4$^-$ CD8$\alpha^-$ CD44$^-$ CD25$^+$ cells (DN3 thymocytes); lineage$^-$ CD4$^-$ CD8$\alpha^-$ CD44$^-$ CD25$^-$ cells (DN4 thymocytes); lineage$^-$ B220$^+$ IgM$^-$ CD43$^+$ CD19$^-$ Ly6D$^+$ cells (Pre-Pro-B cell progenitors); lineage$^-$ B220$^+$ IgM$^-$ CD43$^+$ CD19$^+$ cells (Pro-B cells); lineage$^-$ B220$^+$ IgM$^-$ CD43$^-$ cells (Pre-B cells) and circulating B220$^+$ (B cells), CD3$\varepsilon^+$ (T cells), Gr1$^+$ CD115$^-$ (neutrophils), and CD115$^+$ Gr1$^{low/int}$ (monocytes). Data represent the mean ± SEM. *P < 0.05 and **P < 0.01 by one-way ANOVA with alpha = 0.05 and Sidak's multiple comparisons test.

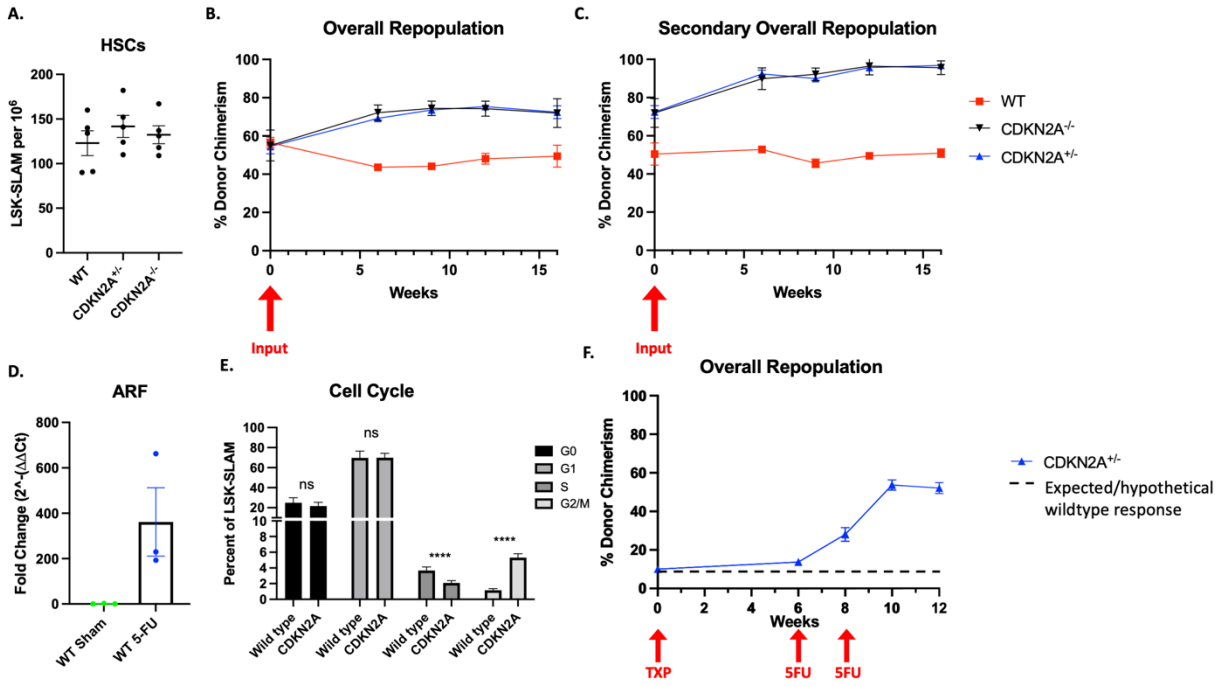
A.
HSCs
LSK-SLAM per 10^6
WT
CDKN2A+/-
CDKN2A-/-
B.
Overall Repopulation
% Donor Chimerism
Weeks
Input
C.
Secondary Overall Repopulation
% Donor Chimerism
Weeks
Input
WT
CDKN2A-/-
CDKN2A+/-
D.
ARF
Fold Change (2^-(ΔΔCt))
WT Sham
WT 5-FU
E.
Cell Cycle
Percent of LSK-SLAM
ns
ns
****
****
G0
G1
S
G2/M
Wild type
CDKN2A
F.
Overall Repopulation
% Donor Chimerism
Weeks
TXP
5FU
5FU
CDKN2A+/-
Expected/hypothetical wildtype response

**Figure 4.3. Loss of *Cdkn2a* has minimal impact on basal hematopoiesis of HSC function.**

(A) Number of LSK-SLAM cells per femur. (B-C) Two million bone marrow mononuclear cells from *Cdkn2a* transgenic (*Ly5.2*, 50%) and wildtype (*Ly5.1*, 50%) were transplanted into irradiated wildtype mice and donor chimerism assessed every four to six weeks. Shown is donor (*Ly5.2*) contribution to total leukocytes for primary transplant (B) and secondary transplant (C). (D) Relative mRNA expression of the *Cdkn2a* gene *Arf* in sorted HSCs of wildtype mice treated with 5-fluorouracil 24-hours post-treatment compared to *B-actin* mRNA. (E) Cell cycle distribution of LSK-SLAM cells 24-hours post-5-FU treatment. (F) $Cdkn2a^{+/-}$ chimerism after transplant and serial 5-FU treatment. Data represent the mean ± SEM. *P < 0.05, **P < 0.01, ***P < 0.001, and ****P < 0.0001 by one-way ANOVA with alpha = 0.05 and Sidak's multiple comparisons test.

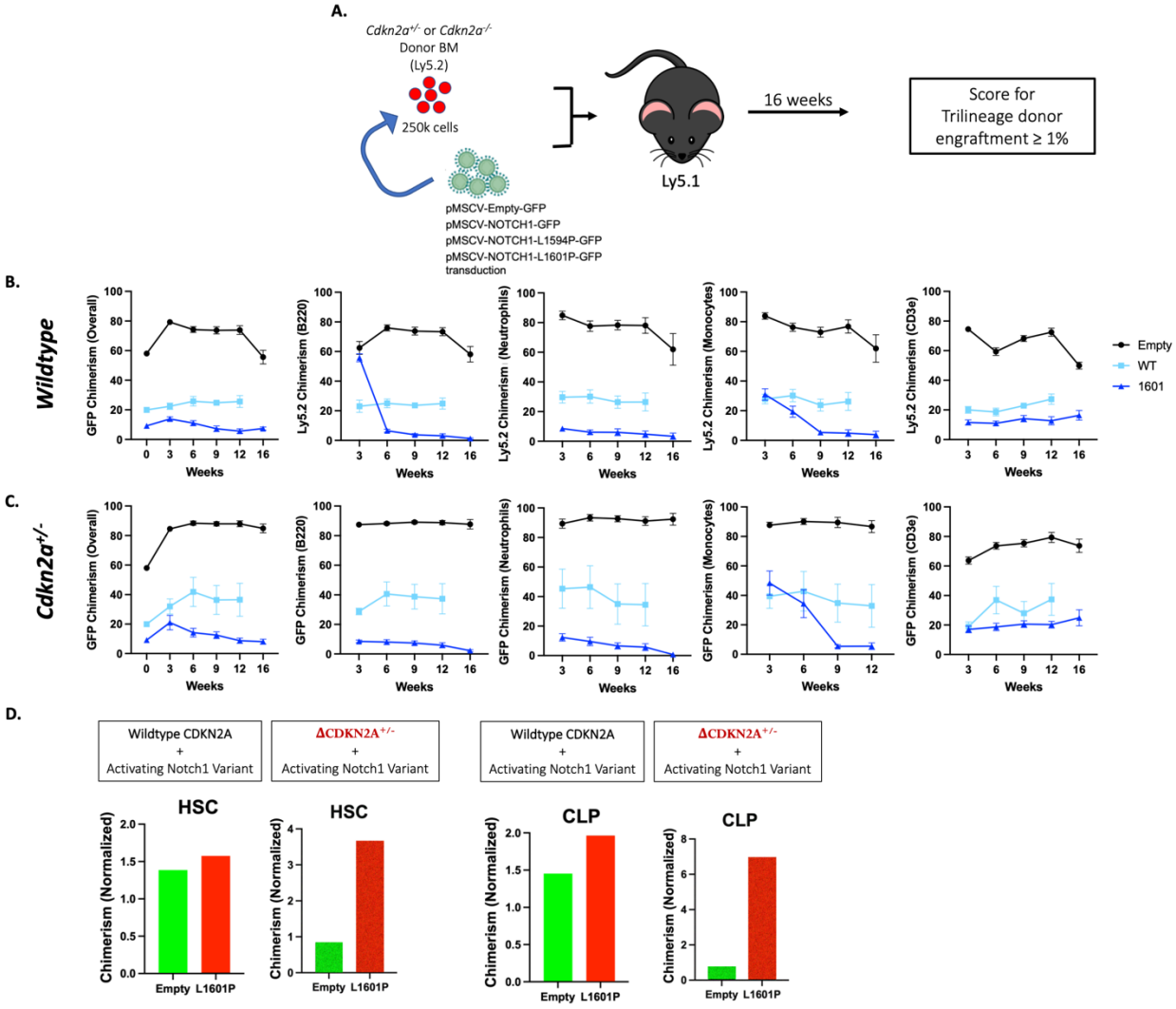
A.
Cdkn2a+/- or Cdkn2a-/-
Donor BM
(Ly5.2)
250k cells
pMSCV-Empty-GFP
pMSCV-NOTCH1-GFP
pMSCV-NOTCH1-L1594P-GFP
pMSCV-NOTCH1-L1601P-GFP
transduction
Ly5.1
16 weeks
Score for
Trilineage donor
engraftment ≥ 1%
B.
Wildtype
GFP Chimerism (Overall)
Ly5.2 Chimerism (B220)
Ly5.2 Chimerism (Neutrophils)
Ly5.2 Chimerism (Monocytes)
Ly5.2 Chimerism (CD3e)
Weeks
Empty
WT
1601
C.
Cdkn2a+/-
GFP Chimerism (Overall)
GFP Chimerism (B220)
GFP Chimerism (Neutrophils)
GFP Chimerism (Monocytes)
GFP Chimerism (CD3e)
Weeks
D.
Wildtype CDKN2A
+
Activating Notch1 Variant
ΔCDKN2A+/-
+
Activating Notch1 Variant
Wildtype CDKN2A
+
Activating Notch1 Variant
ΔCDKN2A+/-
+
Activating Notch1 Variant
HSC
HSC
CLP
CLP
Chimerism (Normalized)
Empty L1601P

**Figure 4.4. *Cdkn2a* loss supports mutant Notch-driven expansion of lymphoid progenitors.**

(A) Experimental schema. (B) Total leukocyte contribution of *Cdkn2a* wildtype cells expressing a *NOTCH1* construct normalized to input GFP chimerism. (C) Total leukocyte contribution of *Cdkn2a*$^{+/-}$ cells expressing a *NOTCH1* construct normalized to input GFP chimerism. (D) HSC and CLP expansion post-transplant in wildtype cells and *Cdkn2a*$^{+/-}$ cells expressing a*NOTCH1 L1601P* mutants or empty vector control. Data represent the mean ± SEM. *P < 0.05, **P < 0.01, ***P < 0.001, and ****P < 0.0001 by one-way ANOVA with alpha = 0.05 and Sidak's multiple comparisons test.

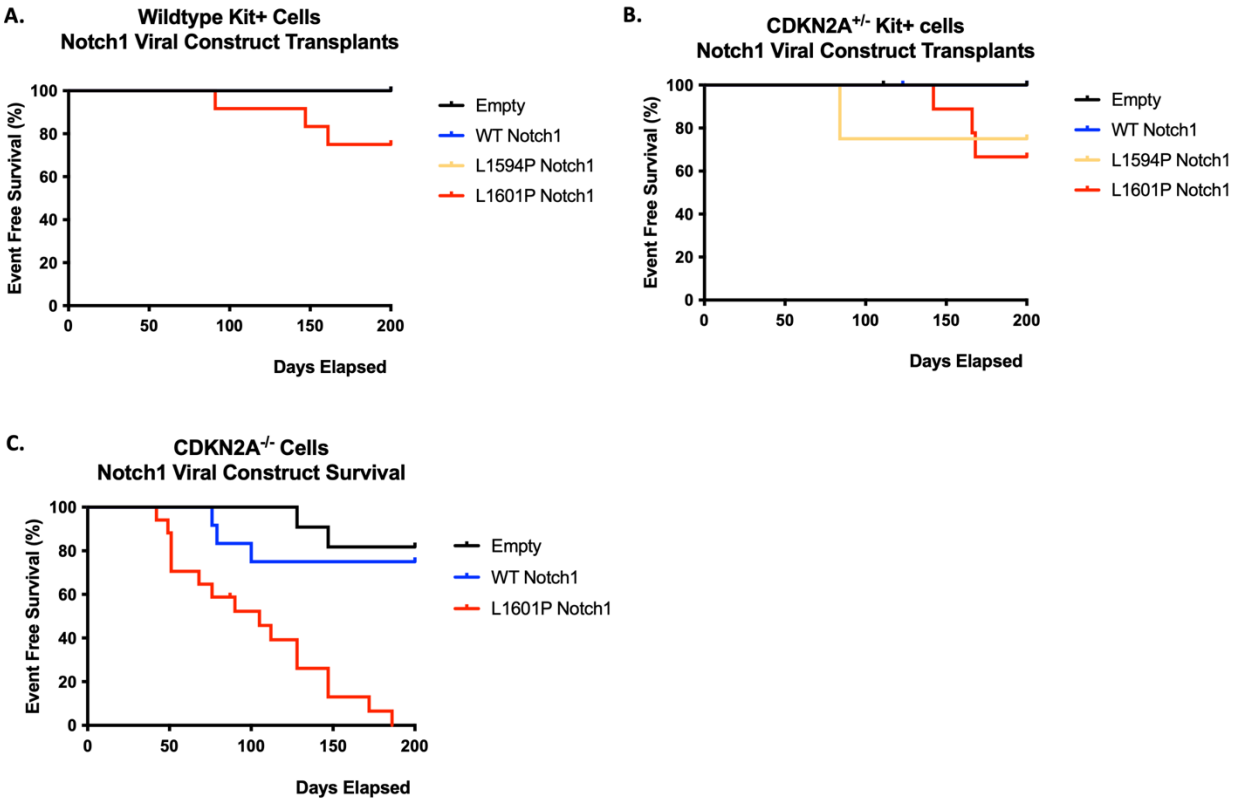
A.
Wildtype Kit+ Cells
Notch1 Viral Construct Transplants
Event Free Survival (%)
Days Elapsed
Empty
WT Notch1
L1594P Notch1
L1601P Notch1
B.
CDKN2A+/- Kit+ cells
Notch1 Viral Construct Transplants
Event Free Survival (%)
Days Elapsed
Empty
WT Notch1
L1594P Notch1
L1601P Notch1
C.
CDKN2A-/- Cells
Notch1 Viral Construct Survival
Event Free Survival (%)
Days Elapsed
Empty
WT Notch1
L1601P Notch1

**Figure 4.5. *Cdkn2a* loss cooperates with activated Notch mutants to induce T-ALL in mice.**

(A-C) Kaplan-Meier graphs show the fraction of mice without T-ALL as a function of time for wildtype (A), *Cdkn2a*$^{+/-}$ (B), or *Cdkn2a*$^{-/-}$ (C) cells expressing a*NOTCH1* mutants.

# Chapter 5: Summary and Future Directions

My PhD training has encompassed a wide range of hematopoietic subjects, including bone marrow mesenchymal stromal cell signaling on hematopoietic stress responses, bone marrow hematopoietic niche development, hematopoietic stem cell clonal evolution, age-related shifts in hematopoiesis, microbial signal influences on hematopoiesis, and the malignant transformation of developing thymocytes. My initials studies focused on the hematopoietic bone marrow niche and the contribution of stromal cells on hematopoiesis (Chapter 2). Specifically, I studied the role of SMAD4, a downstream mediator of TGF-β superfamily signaling, in bone marrow stromal cells in establishing and maintaining the bone marrow hematopoietic stem cell (HSC) niche. We developed a mouse model of SMAD4 abrogation, specifically in bone marrow mesenchymal stromal cells. We showed that the post-natal loss of SMAD4 results in minimal perturbations in basal and stress hematopoiesis, suggesting that TGF-β family signaling is largely dispensable for the maintenance of hematopoietic niches in the bone marrow. I also contributed to five other studies, characterizing hematopoietic niches in the bone marrow, involving myeloproliferative neoplasms and myelofibrosis, bone marrow resident dendritic cell effects on HSC trafficking and function, bone marrow mesenchymal stromal cell lineage specification, and the effects of radiation on hematopoiesis.

Subsequently, I have completed a project in the Link and Schuettpelz labs, contributing to our understanding of the dynamic relationship between commensal flora and hematopoiesis (Chapter 3). Specifically, I helped investigate whether the microbiome assists in establishing myeloid potential in early development and how myeloid potential is maintained with age. We showed, through functional and phenotyping assays, that the commensal flora does not influence

the age-associated expansion of hematopoietic stem and progenitor cells, but commensal flora do influence the maintenance of B lymphopoiesis, enhancing myelopoiesis and simultaneously downregulating B lymphopoiesis.

In addition to these projects, my PhD thesis project focused on the contribution of nucleolar stress to the development of T cell acute lymphoblastic leukemia (T-ALL, Chapter 4). In brief, our data provide support for a novel model of T-ALL leukemogenesis in which *CDKN2A* loss is an early event that provides a fitness advantage under conditions of replication stress that leads to an expanded pool of CDKN2A deficient hematopoietic stem cells and common lymphoid progenitors. Loss of *CDKN2A* provides a permissive cellular environment for activating *NOTCH1* mutations by attenuating nucleolar stress, and our data suggest that targeting the nucleolar stress pathway or ribosome biogenesis may have therapeutic activity in T-ALL.

Zhang J, Supakorndej T, **Krambs JR**, Rao M, Abou-Ezzi G, Ye RY, Li S, Trinkaus K, Link DC. Bone marrow dendritic cells regulate hematopoietic stem/progenitor cell trafficking. J Clin Invest. 2019 Apr 30;129(7):2920-2931. doi: 10.1172/JCI124829. PMID: 31039135

Abou-Ezzi, Supakorndej T, Zhang J, Anthony B, **Krambs JR**, Celik H, Karpova D, Carft CS, Link DC. TGF-β signaling plays an essential role in the lineage specification of mesenchymal stem/progenitor cells in fetal bone marrow. Stem Cell Reports. 2019 Jul 9;13(1):48-60. doi: 10.1016/j.stemcr.2019.05.017. Epub 2019 Jun 13. PMID: 31204302; PMCID: PMC6626889.

Kapoor V, Collins A, Griffith K, Wong N, Wang X, Challen G, **Krambs JR**, Link DC, Hallahan DE, Thotala D. Radiation induces iatrogenic immunosuppression by indirectly affecting hematopoiesis in bone marrow. Oncotarget. 2020 May 12;11(19):1681-1690. doi: 10.18632/Oncotarget.27564. PMID: 32477458; PMCID: PMC7233802.

**Krambs JR**, Abou-Ezzi G, Yao J, Link DC. Canonical signaling by TGF family members in mesenchymal stromal cells is dispensable for hematopoietic niche maintenance under basal and stress conditions. PLoS One. 2020 May 29;15(5):e0233751. doi: 10.1371/journal.pone.0233751. PMID: 32470079; PMCID: PMC7259882.

**Krambs JR**, Monlish DA, Gao F, Schuettpelz LG, Link DC. Microbiota signals suppress B lymphopoiesis with aging in mice. Front Immunol. 2021 Oct 19;12:767267. PMID:34737755; PMCID: PMC8560790.

Yao JC, Oetjen KA, Wang T, Xu H, Abou-Ezzi G, **Krambs JR**, Uttarwar S, Duncavage EJ, Link DC. TGF-β signaling in myeloproliferative neoplasms contributes to myelofibrosis without disrupting the hematopoietic niche. J Clin Invest. 2022 Jun 1;132(11):e154092. doi: 10.1172/JCI154092. PMID: 35439167; PMCID: PMC9151699.

Li S, Yao JC, Oetjen KA, **Krambs JR**, Xia J, Zhang J, Schmidt AP, Helton NM, Fulton RS, Heath SE, Turnbull IR, Mbalaviele G, Ley TJ, Walter MJ, Link DC. IL-1b expression in bone marrow dendritic cells is induced by TLR2 agonists and regulates HSC function. Blood. 2022 Jun 8:blood.2022016084. doi: 10.1182/blood.2022016084. Epub ahead of print. PMID:35675516.

# 5.1. Future Directions: Molecular Mechanisms of *CDKN2A* Permissibility

In chapter 4, we demonstrated that, despite the prevalence of *NOTCH1* mutations in T-ALL and its role in driving T cell lineage specification, activating *NOTCH1* mutations are secondary, or subclonal, events in T-ALL pathogenesis and must cooperate with additional oncogenic mutations to initiate T-ALL. In line with this observation, our data show that activating *NOTCH1* mutations result in cell growth inhibition by triggering nucleolar stress. Previous reports demonstrate that a threshold level of ARF protein exists, whereby a sufficient amount of ARF must accumulate before cell cycle arrest, and ARF has been shown to accumulate over prolonged growth cell cycles to prevent unchecked proliferation.[133,223,224] Perhaps, ARF, a key mediator of the nucleolar stress response, accumulates in the context of *NOTCH1* hyperactivation, slowing cell cycle progression at first until ARF is sufficiently abundant to stabilize p53[133,223,224] (in the context of p53 wildtype cells) or inhibit rRNA processing[343] and NPM1 shuttling.[309,344] This question can be addressed, in part, by our progenitor T cell culture *in vitro*. We are currently collecting data to address whether loss of *Cdkn2a* relieves ribosome biogenesis stress and increases *NOTCH1*-dependent proliferation. The ongoing experiments include, investigating proliferation, apoptosis, p53 target gene expression, cell growth, and nucleolar stress in *Cdkn2a*$^{+/-}$ and *Cdkn2a*$^{-/-}$ progenitor T cells expressing a*NOTCH1* mutants in culture.

To understand the role of *CDKN2A* in basal hematopoiesis, we first characterized *Cdkn2a* expression across hematopoietic lineages. We observed that *Cdkn2a* expression is minimal in HSPCs and throughout myelopoiesis but activated in response to B and T lymphopoiesis. Given this observation and the role of *Cdkn2a* in regulating ribosome biogenesis and cell cycle

progression, we hypothesized that loss of *Cdkn2a* would result in enhanced B and T lymphopoiesis. Surprisingly, transgenic *Cdkn2a*$^{+/-}$ and *Cdkn2a*$^{-/-}$ mice do not have altered hematopoiesis, however *CDKN2A* deficiency does confer a competitive advantage in the context of replication stress. Both *Cdkn2a*$^{+/-}$ and *Cdkn2a*$^{-/-}$ HSCs consistently outperformed wildtype competitors in transplantation assays and in response to 5-FU treatment. We are currently investigating whether the relative abundance of T, B, and myeloid lineages shift in response to replication stress in the context of *Cdkn2a* loss.

We next tested whether *Cdkn2a* loss is an early transformation event permissive to a*NOTCH1* variants by retrovirally transducing a*NOTCH1* variants in *Cdkn2a* deficient (*Cdkn2a*$^{+/-}$ and *Cdkn2a*$^{-/-}$) cells and transplanting these cells into wildtype recipients. *NOTCH1* hyperactivation in the context of *Cdkn2a* loss resulted in enhanced expansion of HSPCs, specifically the expansion of HSC and CLP. However, *Cdkn2a* loss did not rescue the activating *NOTCH1* induced loss of myeloid and B lymphoid lineages. Additionally, a tumor watch of mice transplanted with *Cdkn2a* deficient cells harboring activating *NOTCH1* mutations confirmed that *Cdkn2a* loss strongly cooperates with a*NOTCH1* expression to induce T-ALL in mice. Our data suggest that loss of *CDKN2A* provides a permissive cellular environment, promoting acquisition of secondary mutations like activating *NOTCH1*.

In summary, these data provide support for a novel model of T-ALL leukemogenesis in which *CDKN2A* loss is an early transformation event that provides a fitness advantage under conditions of replication stress, leading to an expanded pool of *CDKN2A*$^{+/-}$ or *CDKN2A*$^{-/-}$ HSCs and CLPs. Loss of CDKN2A provides a permissive cellular environment for activating *NOTCH1* mutations by attenuating nucleolar stress, setting up T-ALL transformation with secondary driver mutations.

Given the recurrent role of *CDKN2A* loss in cell line immortalization, conferring stem-like properties to astrocytes,[345] macrophages,[346] and v-abl transduced lymphocytes,[347] we hypothesized that *Cdkn2a* loss may support a*NOTCH1* driven leukemogenesis of common lymphoid progenitors (CLPs). To test this hypothesis, we transplanted wildtype mice with retrovirally transduced *Cdkn2a*$^{+/-}$ cells harboring a*NOTCH1 L1601P*. *Cdkn2a*$^{+/-}$ a*NOTCH1 L1601P* CLPs (*Ly5.2*) from these recipients were sorted 6-weeks post-transplant and transplanted into a new cohort of wildtype recipients along with 250,000 support cells (*Ly5.1*). A tumor watch on these mice is ongoing to address whether *Cdkn2a*$^{+/-}$ a*NOTCH1 L1601P* CLPs have stable engraftment over time and promote leukemogenesis.

Early studies of *CDKN2A* loss,[342] demonstrated a strong selective pressure in favor of loss-of-heterozygosity. Reports of the prevalence of biallelic *CDKN2A* loss may have been limited by the resolution of bulk sequencing, and the advent of single cell sequencing has enabled higher resolution *CDKN2A* locus analysis. Naturally, the subclonal evolution of T-ALL has since been extended to *CDKN2A* loss.[330,331] Recurrent monoallelic and biallelic deletions of *CDKN2A* have been described in both pediatric and adult cases of T-ALL. A recent analysis of the Spanish PETHEMA studies showed that monoallelic *CDKN2A* loss is observed in 25% to 30% of cases with *CDKN2A* copy number alterations.[330] Of note, Sulong *et al*. found that biallelic *CDKN2A* deletions were more prevalent among children ten-years or older and those with a white cell count above 50 x $10^9$/L.[331] Additionally, their analysis showed that *CDKN2A* lesions at relapse are a mixture of monoallelic and biallelic deletions,[331] and T-ALL clones with monoallelic loss of *CDKN2A* often fall below the resolution of commercial FISH probes.

High resolution next-generation sequencing and cytogenetic studies have revealed that T-ALL is often subclonal in regard to *CDKN2A* loss. Unpublished data from our lab, examining the

*CDKN2A* status of patient samples, has revealed that many patients have subclonal biallelic and monoallelic *CDKN2A* loss. Interestingly, monoallelic and biallelic loss of *CDKN2A* has not been associated with differential disease prognoses.[330] Our data suggest that the loss of one or both copies of *CDKN2A* may effect predisposition to ALL and disease latency. This is supported by the increased incidence and decreased latency of *Cdkn2a*$^{-/-}$ tumors compared to *Cdkn2a*$^{+/-}$ tumors despite a lack of discernable difference between *Cdkn2a*$^{+/-}$ and *Cdkn2a*$^{-/-}$ hematopoietic cells in response to replication stress.

Given the unique opportunity presented by *CDKN2A* encoding two tumor suppressors, its prevalence in acute lymphoid leukemia, and the advantage *CDKN2A* loss confers to HSCs, it is a wonder that *CDKN2A* deletions are not prevalent (or have not been noted to date) in clonal hematopoiesis. This may be due to the underlying approach to the study of age-related clonal hematopoiesis (ARCH). ARCH studies have primarily focused on nonsynonymous single nucleotide variants (SNVs) - hotspot mutations, whereas recurrent insertions and deletions in pre-leukemia have been largely overlooked. One challenge in finding recurrent indels associated with ARCH is the sequencing depth need to generate enough power to call indels. Current calculations show that 60X whole genome sequencing coverage is needed to recover 95% of indels.[348] Additionally, detection of heterozygous indels requires higher coverage than homozygous ones, reaffirming the need for a minimum 60X coverage to achieve high accuracy indel detection. However, the high cost of WGS has resulted in most sequencing runs being performed at 30X coverage (sufficient for SNV calling but limited in indel detection). We are currently working in collaboration with the Bolton lab to analyze available data from healthy individuals sequenced under the UK biobank project. We believe we have sufficient power (sample number and sequencing depth) to call somatic copy number alterations in the *CDKN2A* locus.

Lastly, although a*NOTCH1* mutations may not be sufficient to initiate leukemogenesis, our data suggest that activating *NOTCH1* mutations play a vital role in the fate decision of acute lymphoblastic leukemia, steering ALL toward T cell commitment. This hypothesis stems from our model of T-ALL, whereby *CDKN2A* deletions (which are prevalent in both T-ALL and B-ALL) prime HSPCs for other secondary mutations that will ultimately drive T-ALL transformation. Of note, our data show that a*NOTCH1* mutations are neutral non-deleterious mutations in the context of HSC and T cell biology, however they are selected against in B lymphopoiesis. Additionally, a*NOTCH1* mutations have not been described in B-ALL transformation.[10,68,74,75] Given these observations, I hypothesize that *CDKN2A* loss primes HSPCs for ALL transformation, and *aNOTCH1* mutations are a cornerstone for T-ALL transformation.

# References


1 Goldberg, J. M. *et al.* Childhood T-cell acute lymphoblastic leukemia: the Dana-Farber Cancer Institute acute lymphoblastic leukemia consortium experience. *J Clin Oncol* **21**, 3616-3622, doi:10.1200/JCO.2003.10.116 (2003).

2 Pui, C. H. & Evans, W. E. Treatment of acute lymphoblastic leukemia. *N Engl J Med* **354**, 166-178, doi:10.1056/NEJMra052603 (2006).

3 Fielding, A. K. *et al.* Outcome of 609 adults after relapse of acute lymphoblastic leukemia (ALL); an MRC UKALL12/ECOG 2993 study. *Blood* **109**, 944-950, doi:10.1182/blood-2006-05-018192 (2007).

4 Chamberlain, M. C. Carcinomatous meningitis. *Arch Neurol* **54**, 16-17, doi:10.1001/archneur.1997.00550130008003 (1997).

5 Breit, S. *et al.* Activating NOTCH1 mutations predict favorable early treatment response and long-term outcome in childhood precursor T-cell lymphoblastic leukemia. *Blood* **108**, 1151-1157, doi:10.1182/blood-2005-12-4956 (2006).

6 van Grotel, M. *et al.* The outcome of molecular-cytogenetic subgroups in pediatric T-cell acute lymphoblastic leukemia: a retrospective study of patients treated according to DCOG or COALL protocols. *Haematologica* **91**, 1212-1221 (2006).

7 Weng, A. P. *et al.* Activating mutations of NOTCH1 in human T cell acute lymphoblastic leukemia. *Science* **306**, 269-271, doi:10.1126/science.1102160 (2004).

8 Ferrando, A. A. *et al.* Gene expression signatures define novel oncogenic pathways in T cell acute lymphoblastic leukemia. *Cancer Cell* **1**, 75-87, doi:10.1016/s1535-6108(02)00018-1 (2002).

9 Homminga, I. *et al.* Integrated transcript and genome analyses reveal NKX2-1 and MEF2C as potential oncogenes in T cell acute lymphoblastic leukemia. *Cancer Cell* **19**, 484-497, doi:10.1016/j.ccr.2011.02.008 (2011).

10 Van Vlierberghe, P. *et al.* Prognostic relevance of integrated genetic profiling in adult T-cell acute lymphoblastic leukemia. *Blood* **122**, 74-82, doi:10.1182/blood-2013-03-491092 (2013).

11 Hebert, J., Cayuela, J. M., Berkeley, J. & Sigaux, F. Candidate tumor-suppressor genes MTS1 (p16INK4A) and MTS2 (p15INK4B) display frequent homozygous deletions in primary cells from T- but not from B-cell lineage acute lymphoblastic leukemias. *Blood* **84**, 4038-4044 (1994).

12 Durinck, K. *et al.* Novel biological insights in T-cell acute lymphoblastic leukemia. *Exp Hematol* **43**, 625-639, doi:10.1016/j.exphem.2015.05.017 (2015).

13 Patrick, K. & Vora, A. Update on biology and treatment of T-cell acute lymphoblastic leukaemia. *Curr Opin Pediatr* **27**, 44-49, doi:10.1097/MOP.0000000000000171 (2015).

14 Van Vlierberghe, P. & Ferrando, A. The molecular basis of T cell acute lymphoblastic leukemia. *J Clin Invest* **122**, 3398-3406, doi:10.1172/JCI61269 (2012).

15 Begley, C. G. *et al.* Chromosomal translocation in a human leukemic stem-cell line disrupts the T-cell antigen receptor delta-chain diversity region and results in a previously unreported fusion transcript. *Proc Natl Acad Sci U S A* **86**, 2031-2035, doi:10.1073/pnas.86.6.2031 (1989).

16 Xia, Y. *et al.* TAL2, a helix-loop-helix gene activated by the (7;9)(q34;q32) translocation in human T-cell leukemia. *Proc Natl Acad Sci U S A* **88**, 11416-11420, doi:10.1073/pnas.88.24.11416 (1991).

17 Mellentin, J. D., Smith, S. D. & Cleary, M. L. lyl-1, a novel gene altered by chromosomal translocation in T cell leukemia, codes for a protein with a helix-loop-helix DNA binding motif. *Cell* **58**, 77-83, doi:10.1016/0092-8674(89)90404-2 (1989).
18 Wang, J. *et al.* The t(14;21)(q11.2;q22) chromosomal translocation associated with T-cell acute lymphoblastic leukemia activates the BHLHB1 gene. *Proc Natl Acad Sci U S A* **97**, 3497-3502, doi:10.1073/pnas.97.7.3497 (2000).
19 Royer-Pokora, B., Loos, U. & Ludwig, W. D. TTG-2, a new gene encoding a cysteine-rich protein with the LIM motif, is overexpressed in acute T-cell leukaemia with the t(11;14)(p13;q11). *Oncogene* **6**, 1887-1893 (1991).
20 McGuire, E. A. *et al.* The t(11;14)(p15;q11) in a T-cell acute lymphoblastic leukemia cell line activates multiple transcripts, including Ttg-1, a gene encoding a potential zinc finger protein. *Mol Cell Biol* **9**, 2124-2132, doi:10.1128/mcb.9.5.2124-2132.1989 (1989).
21 Kennedy, M. A. *et al.* HOX11, a homeobox-containing T-cell oncogene on human chromosome 10q24. *Proc Natl Acad Sci U S A* **88**, 8900-8904, doi:10.1073/pnas.88.20.8900 (1991).
22 Hatano, M., Roberts, C. W., Minden, M., Crist, W. M. & Korsmeyer, S. J. Deregulation of a homeobox gene, HOX11, by the t(10;14) in T cell leukemia. *Science* **253**, 79-82, doi:10.1126/science.1676542 (1991).
23 Bernard, O. A. *et al.* A new recurrent and specific cryptic translocation, t(5;14)(q35;q32), is associated with expression of the Hox11L2 gene in T acute lymphoblastic leukemia. *Leukemia* **15**, 1495-1504, doi:10.1038/sj.leu.2402249 (2001).
24 Soulier, J. *et al.* HOXA genes are included in genetic and biologic networks defining human acute T-cell leukemia (T-ALL). *Blood* **106**, 274-286, doi:10.1182/blood-2004-10-3900 (2005).
25 Erikson, J. *et al.* Deregulation of c-myc by translocation of the alpha-locus of the T-cell receptor in T-cell leukemias. *Science* **232**, 884-886, doi:10.1126/science.3486470 (1986).
26 Ma, X. *et al.* Rise and fall of subclones from diagnosis to relapse in pediatric B-acute lymphoblastic leukaemia. *Nat Commun* **6**, 6604, doi:10.1038/ncomms7604 (2015).
27 Clappier, E. *et al.* The C-MYB locus is involved in chromosomal translocation and genomic duplications in human T-cell acute leukemia (T-ALL), the translocation defining a new T-ALL subtype in very young children. *Blood* **110**, 1251-1261, doi:10.1182/blood-2006-12-064683 (2007).
28 Kraszewska, M. D., Dawidowska, M., Szczepanski, T. & Witt, M. T-cell acute lymphoblastic leukaemia: recent molecular biology findings. *Br J Haematol* **156**, 303-315, doi:10.1111/j.1365-2141.2011.08957.x (2012).
29 Liu, Y. *et al.* The genomic landscape of pediatric and young adult T-lineage acute lymphoblastic leukemia. *Nat Genet* **49**, 1211-1218, doi:10.1038/ng.3909 (2017).
30 Teachey, D. T. & Hunger, S. P. Predicting relapse risk in childhood acute lymphoblastic leukaemia. *Br J Haematol* **162**, 606-620, doi:10.1111/bjh.12442 (2013).
31 Greaves, M. F., Janossy, G., Peto, J. & Kay, H. Immunologically defined subclasses of acute lymphoblastic leukaemia in children: their relationship to presentation features and prognosis. *Br J Haematol* **48**, 179-197 (1981).
32 Gaynon, P. S. *et al.* Bone marrow transplantation versus prolonged intensive chemotherapy for children with acute lymphoblastic leukemia and an initial bone marrow relapse within 12 months of the completion of primary therapy: Children's Oncology

Group study CCG-1941. *J Clin Oncol* **24**, 3150-3156, doi:10.1200/JCO.2005.04.5856 (2006).
33 Moricke, A. *et al.* Dexamethasone vs prednisone in induction treatment of pediatric ALL: results of the randomized trial AIEOP-BFM ALL 2000. *Blood* **127**, 2101-2112, doi:10.1182/blood-2015-09-670729 (2016).
34 Patrick, K. *et al.* Outcome for children and young people with Early T-cell precursor acute lymphoblastic leukaemia treated on a contemporary protocol, UKALL 2003. *Br J Haematol* **166**, 421-424, doi:10.1111/bjh.12882 (2014).
35 Place, A. E. *et al.* Intravenous pegylated asparaginase versus intramuscular native Escherichia coli L-asparaginase in newly diagnosed childhood acute lymphoblastic leukaemia (DFCI 05-001): a randomised, open-label phase 3 trial. *Lancet Oncol* **16**, 1677-1690, doi:10.1016/S1470-2045(15)00363-0 (2015).
36 Vora, A. *et al.* Treatment reduction for children and young adults with low-risk acute lymphoblastic leukaemia defined by minimal residual disease (UKALL 2003): a randomised controlled trial. *Lancet Oncol* **14**, 199-209, doi:10.1016/S1470-2045(12)70600-9 (2013).
37 Gokbuget, N. *et al.* High single-drug activity of nelarabine in relapsed T-lymphoblastic leukemia/lymphoma offers curative option with subsequent stem cell transplantation. *Blood* **118**, 3504-3511, doi:10.1182/blood-2011-01-329441 (2011).
38 Guru Murthy, G. S., Pondaiah, S. K., Abedin, S. & Atallah, E. Incidence and survival of T-cell acute lymphoblastic leukemia in the United States. *Leuk Lymphoma* **60**, 1171-1178, doi:10.1080/10428194.2018.1522442 (2019).
39 Goldstone, A. H. *et al.* In adults with standard-risk acute lymphoblastic leukemia, the greatest benefit is achieved from a matched sibling allogeneic transplantation in first complete remission, and an autologous transplantation is less effective than conventional consolidation/maintenance chemotherapy in all patients: final results of the International ALL Trial (MRC UKALL XII/ECOG E2993). *Blood* **111**, 1827-1833, doi:10.1182/blood-2007-10-116582 (2008).
40 Kozlowski, P. *et al.* High relapse rate of T cell acute lymphoblastic leukemia in adults treated with Hyper-CVAD chemotherapy in Sweden. *Eur J Haematol* **92**, 377-381, doi:10.1111/ejh.12269 (2014).
41 Dores, G. M., Devesa, S. S., Curtis, R. E., Linet, M. S. & Morton, L. M. Acute leukemia incidence and patient survival among children and adults in the United States, 2001-2007. *Blood* **119**, 34-43, doi:10.1182/blood-2011-04-347872 (2012).
42 Raetz, E. A. *et al.* Reinduction platform for children with first marrow relapse of acute lymphoblastic Leukemia: A Children's Oncology Group Study[corrected]. *J Clin Oncol* **26**, 3971-3978, doi:10.1200/JCO.2008.16.1414 (2008).
43 You, M. J., Medeiros, L. J. & Hsi, E. D. T-lymphoblastic leukemia/lymphoma. *Am J Clin Pathol* **144**, 411-422, doi:10.1309/AJCPMF03LVSBLHPJ (2015).
44 Brammer, J. E. *et al.* Multi-center analysis of the effect of T-cell acute lymphoblastic leukemia subtype and minimal residual disease on allogeneic stem cell transplantation outcomes. *Bone Marrow Transplant* **52**, 20-27, doi:10.1038/bmt.2016.194 (2017).
45 Bostrom, B. C. *et al.* Dexamethasone versus prednisone and daily oral versus weekly intravenous mercaptopurine for patients with standard-risk acute lymphoblastic leukemia: a report from the Children's Cancer Group. *Blood* **101**, 3809-3817, doi:10.1182/blood-2002-08-2454 (2003).

46 Larsen, E. C. *et al.* Dexamethasone and High-Dose Methotrexate Improve Outcome for Children and Young Adults With High-Risk B-Acute Lymphoblastic Leukemia: A Report From Children's Oncology Group Study AALL0232. *J Clin Oncol* **34**, 2380-2388, doi:10.1200/JCO.2015.62.4544 (2016).
47 Mitchell, C. D. *et al.* Benefit of dexamethasone compared with prednisolone for childhood acute lymphoblastic leukaemia: results of the UK Medical Research Council ALL97 randomized trial. *Br J Haematol* **129**, 734-745, doi:10.1111/j.1365-2141.2005.05509.x (2005).
48 Teuffel, O. *et al.* Dexamethasone versus prednisone for induction therapy in childhood acute lymphoblastic leukemia: a systematic review and meta-analysis. *Leukemia* **25**, 1232-1238, doi:10.1038/leu.2011.84 (2011).
49 Hurwitz, C. A. *et al.* Substituting dexamethasone for prednisone complicates remission induction in children with acute lymphoblastic leukemia. *Cancer* **88**, 1964-1969 (2000).
50 Mitchell, C., Richards, S., Harrison, C. J. & Eden, T. Long-term follow-up of the United Kingdom medical research council protocols for childhood acute lymphoblastic leukaemia, 1980-2001. *Leukemia* **24**, 406-418, doi:10.1038/leu.2009.256 (2010).
51 Schrappe, M. *et al.* Late MRD response determines relapse risk overall and in subsets of childhood T-cell ALL: results of the AIEOP-BFM-ALL 2000 study. *Blood* **118**, 2077-2084, doi:10.1182/blood-2011-03-338707 (2011).
52 Berg, S. L. *et al.* Phase II study of nelarabine (compound 506U78) in children and young adults with refractory T-cell malignancies: a report from the Children's Oncology Group. *J Clin Oncol* **23**, 3376-3382, doi:10.1200/JCO.2005.03.426 (2005).
53 Winter, S. S. *et al.* Safe integration of nelarabine into intensive chemotherapy in newly diagnosed T-cell acute lymphoblastic leukemia: Children's Oncology Group Study AALL0434. *Pediatr Blood Cancer* **62**, 1176-1183, doi:10.1002/pbc.25470 (2015).
54 Abaza, Y. *et al.* Hyper-CVAD plus nelarabine in newly diagnosed adult T-cell acute lymphoblastic leukemia and T-lymphoblastic lymphoma. *Am J Hematol* **93**, 91-99, doi:10.1002/ajh.24947 (2018).
55 Portell, C. A. & Advani, A. S. Novel targeted therapies in acute lymphoblastic leukemia. *Leuk Lymphoma* **55**, 737-748, doi:10.3109/10428194.2013.823493 (2014).
56 Cooper, M. L. *et al.* An "off-the-shelf" fratricide-resistant CAR-T for the treatment of T cell hematologic malignancies. *Leukemia* **32**, 1970-1983, doi:10.1038/s41375-018-0065-5 (2018).
57 Reismuller, B. *et al.* Long-term outcome of initially homogenously treated and relapsed childhood acute lymphoblastic leukaemia in Austria--a population-based report of the Austrian Berlin-Frankfurt-Munster (BFM) Study Group. *Br J Haematol* **144**, 559-570, doi:10.1111/j.1365-2141.2008.07499.x (2009).
58 Oriol, A. *et al.* Outcome after relapse of acute lymphoblastic leukemia in adult patients included in four consecutive risk-adapted trials by the PETHEMA Study Group. *Haematologica* **95**, 589-596, doi:10.3324/haematol.2009.014274 (2010).
59 Piovan, E. *et al.* Direct reversal of glucocorticoid resistance by AKT inhibition in acute lymphoblastic leukemia. *Cancer Cell* **24**, 766-776, doi:10.1016/j.ccr.2013.10.022 (2013).
60 Bandapalli, O. R. *et al.* NOTCH1 activation clinically antagonizes the unfavorable effect of PTEN inactivation in BFM-treated children with precursor T-cell acute lymphoblastic leukemia. *Haematologica* **98**, 928-936, doi:10.3324/haematol.2012.073585 (2013).

61 Tzoneva, G. *et al.* Activating mutations in the NT5C2 nucleotidase gene drive chemotherapy resistance in relapsed ALL. *Nat Med* **19**, 368-371, doi:10.1038/nm.3078 (2013).
62 Brouwer, C. *et al.* Role of 5'-nucleotidase in thiopurine metabolism: enzyme kinetic profile and association with thio-GMP levels in patients with acute lymphoblastic leukemia during 6-mercaptopurine treatment. *Clin Chim Acta* **361**, 95-103, doi:10.1016/j.cccn.2005.05.006 (2005).
63 Hunsucker, S. A., Mitchell, B. S. & Spychala, J. The 5'-nucleotidases as regulators of nucleotide and drug metabolism. *Pharmacol Ther* **107**, 1-30, doi:10.1016/j.pharmthera.2005.01.003 (2005).
64 Kunz, J. B. *et al.* Pediatric T-cell lymphoblastic leukemia evolves into relapse by clonal selection, acquisition of mutations and promoter hypomethylation. *Haematologica* **100**, 1442-1450, doi:10.3324/haematol.2015.129692 (2015).
65 Sentis, I. *et al.* The evolution of relapse of adult T cell acute lymphoblastic leukemia. *Genome Biol* **21**, 284, doi:10.1186/s13059-020-02192-z (2020).
66 Richter-Pechanska, P. *et al.* Pediatric T-ALL type-1 and type-2 relapses develop along distinct pathways of clonal evolution. *Leukemia* **36**, 1759-1768, doi:10.1038/s41375-022-01587-0 (2022).
67 De Bie, J. *et al.* Single-cell sequencing reveals the origin and the order of mutation acquisition in T-cell acute lymphoblastic leukemia. *Leukemia* **32**, 1358-1369, doi:10.1038/s41375-018-0127-8 (2018).
68 Zhang, J. *et al.* The genetic basis of early T-cell precursor acute lymphoblastic leukaemia. *Nature* **481**, 157-163, doi:10.1038/nature10725 (2012).
69 Hogan, L. E. *et al.* Integrated genomic analysis of relapsed childhood acute lymphoblastic leukemia reveals therapeutic strategies. *Blood* **118**, 5218-5226, doi:10.1182/blood-2011-04-345595 (2011).
70 Mullighan, C. G. *et al.* Genomic analysis of the clonal origins of relapsed acute lymphoblastic leukemia. *Science* **322**, 1377-1380, doi:10.1126/science.1164266 (2008).
71 Oshima, K. *et al.* Mutational landscape, clonal evolution patterns, and role of RAS mutations in relapsed acute lymphoblastic leukemia. *Proc Natl Acad Sci U S A* **113**, 11306-11311, doi:10.1073/pnas.1608420113 (2016).
72 Holmfeldt, L. *et al.* The genomic landscape of hypodiploid acute lymphoblastic leukemia. *Nat Genet* **45**, 242-252, doi:10.1038/ng.2532 (2013).
73 Roberts, K. G. *et al.* Targetable kinase-activating lesions in Ph-like acute lymphoblastic leukemia. *N Engl J Med* **371**, 1005-1015, doi:10.1056/NEJMoa1403088 (2014).
74 Coustan-Smith, E. *et al.* Early T-cell precursor leukaemia: a subtype of very high-risk acute lymphoblastic leukaemia. *Lancet Oncol* **10**, 147-156, doi:10.1016/S1470-2045(08)70314-0 (2009).
75 Van Vlierberghe, P. *et al.* ETV6 mutations in early immature human T cell leukemias. *J Exp Med* **208**, 2571-2579, doi:10.1084/jem.20112239 (2011).
76 Wang, L. C. *et al.* The TEL/ETV6 gene is required specifically for hematopoiesis in the bone marrow. *Genes Dev* **12**, 2392-2402, doi:10.1101/gad.12.15.2392 (1998).
77 Hock, H. *et al.* Tel/Etv6 is an essential and selective regulator of adult hematopoietic stem cell survival. *Genes Dev* **18**, 2336-2341, doi:10.1101/gad.1239604 (2004).

78 Okuda, T., van Deursen, J., Hiebert, S. W., Grosveld, G. & Downing, J. R. AML1, the target of multiple chromosomal translocations in human leukemia, is essential for normal fetal liver hematopoiesis. *Cell* **84**, 321-330, doi:10.1016/s0092-8674(00)80986-1 (1996).
79 Cai, Z. *et al.* Haploinsufficiency of AML1 affects the temporal and spatial generation of hematopoietic stem cells in the mouse embryo. *Immunity* **13**, 423-431, doi:10.1016/s1074-7613(00)00042-x (2000).
80 Growney, J. D. *et al.* Loss of Runx1 perturbs adult hematopoiesis and is associated with a myeloproliferative phenotype. *Blood* **106**, 494-504, doi:10.1182/blood-2004-08-3280 (2005).
81 Della Gatta, G. *et al.* Reverse engineering of TLX oncogenic transcriptional networks identifies RUNX1 as tumor suppressor in T-ALL. *Nat Med* **18**, 436-440, doi:10.1038/nm.2610 (2012).
82 Ting, C. N., Olson, M. C., Barton, K. P. & Leiden, J. M. Transcription factor GATA-3 is required for development of the T-cell lineage. *Nature* **384**, 474-478, doi:10.1038/384474a0 (1996).
83 Zahirieh, A. *et al.* Functional analysis of a novel GATA3 mutation in a family with the hypoparathyroidism, deafness, and renal dysplasia syndrome. *J Clin Endocrinol Metab* **90**, 2445-2450, doi:10.1210/jc.2004-1969 (2005).
84 De Keersmaecker, K. *et al.* The TLX1 oncogene drives aneuploidy in T cell transformation. *Nat Med* **16**, 1321-1327, doi:10.1038/nm.2246 (2010).
85 Gutierrez, A. *et al.* Inactivation of LEF1 in T-cell acute lymphoblastic leukemia. *Blood* **115**, 2845-2851, doi:10.1182/blood-2009-07-234377 (2010).
86 Li, L., Leid, M. & Rothenberg, E. V. An early T cell lineage commitment checkpoint dependent on the transcription factor Bcl11b. *Science* **329**, 89-93, doi:10.1126/science.1188989 (2010).
87 Wakabayashi, Y. *et al.* Bcl11b is required for differentiation and survival of alphabeta T lymphocytes. *Nat Immunol* **4**, 533-539, doi:10.1038/ni927 (2003).
88 Wakabayashi, Y. *et al.* Homozygous deletions and point mutations of the Rit1/Bcl11b gene in gamma-ray induced mouse thymic lymphomas. *Biochem Biophys Res Commun* **301**, 598-603, doi:10.1016/s0006-291x(02)03069-3 (2003).
89 Brantjes, H., Roose, J., van De Wetering, M. & Clevers, H. All Tcf HMG box transcription factors interact with Groucho-related co-repressors. *Nucleic Acids Res* **29**, 1410-1419, doi:10.1093/nar/29.7.1410 (2001).
90 Tosello, V. *et al.* WT1 mutations in T-ALL. *Blood* **114**, 1038-1045, doi:10.1182/blood-2008-12-192039 (2009).
91 Ellisen, L. W., Carlesso, N., Cheng, T., Scadden, D. T. & Haber, D. A. The Wilms tumor suppressor WT1 directs stage-specific quiescence and differentiation of human hematopoietic progenitor cells. *EMBO J* **20**, 1897-1909, doi:10.1093/emboj/20.8.1897 (2001).
92 Peirs, S. *et al.* Epigenetics in T-cell acute lymphoblastic leukemia. *Immunol Rev* **263**, 50-67, doi:10.1111/imr.12237 (2015).
93 Todd, M. A. & Picketts, D. J. PHF6 interacts with the nucleosome remodeling and deacetylation (NuRD) complex. *J Proteome Res* **11**, 4326-4337, doi:10.1021/pr3004369 (2012).
94 Wang, J. *et al.* PHF6 regulates cell cycle progression by suppressing ribosomal RNA synthesis. *J Biol Chem* **288**, 3174-3183, doi:10.1074/jbc.M112.414839 (2013).

95 Zhang, C. *et al.* The X-linked intellectual disability protein PHF6 associates with the PAF1 complex and regulates neuronal migration in the mammalian brain. *Neuron* **78**, 986-993, doi:10.1016/j.neuron.2013.04.021 (2013).
96 Liu, Z. *et al.* Structural basis of plant homeodomain finger 6 (PHF6) recognition by the retinoblastoma binding protein 4 (RBBP4) component of the nucleosome remodeling and deacetylase (NuRD) complex. *J Biol Chem* **290**, 6630-6638, doi:10.1074/jbc.M114.610196 (2015).
97 Van Vlierberghe, P. *et al.* PHF6 mutations in adult acute myeloid leukemia. *Leukemia* **25**, 130-134, doi:10.1038/leu.2010.247 (2011).
98 Ntziachristos, P. *et al.* Genetic inactivation of the polycomb repressive complex 2 in T cell acute lymphoblastic leukemia. *Nat Med* **18**, 298-301, doi:10.1038/nm.2651 (2012).
99 Cao, R. *et al.* Role of histone H3 lysine 27 methylation in Polycomb-group silencing. *Science* **298**, 1039-1043, doi:10.1126/science.1076997 (2002).
100 Ntziachristos, P. *et al.* Contrasting roles of histone 3 lysine 27 demethylases in acute lymphoblastic leukaemia. *Nature* **514**, 513-517, doi:10.1038/nature13605 (2014).
101 Lan, F. *et al.* A histone H3 lysine 27 demethylase regulates animal posterior development. *Nature* **449**, 689-694, doi:10.1038/nature06192 (2007).
102 Van der Meulen, J. *et al.* The H3K27me3 demethylase UTX is a gender-specific tumor suppressor in T-cell acute lymphoblastic leukemia. *Blood* **125**, 13-21, doi:10.1182/blood-2014-05-577270 (2015).
103 Chen, Q. *et al.* Coding sequences of the tal-1 gene are disrupted by chromosome translocation in human T cell leukemia. *J Exp Med* **172**, 1403-1408, doi:10.1084/jem.172.5.1403 (1990).
104 Bernard, O. *et al.* Two distinct mechanisms for the SCL gene activation in the t(1;14) translocation of T-cell leukemias. *Genes Chromosomes Cancer* **1**, 194-208, doi:10.1002/gcc.2870010303 (1990).
105 Mansour, M. R. *et al.* Oncogene regulation. An oncogenic super-enhancer formed through somatic mutation of a noncoding intergenic element. *Science* **346**, 1373-1377, doi:10.1126/science.1259037 (2014).
106 Navarro, J. M. *et al.* Site- and allele-specific polycomb dysregulation in T-cell leukaemia. *Nat Commun* **6**, 6094, doi:10.1038/ncomms7094 (2015).
107 Kelliher, M. A., Seldin, D. C. & Leder, P. Tal-1 induces T cell acute lymphoblastic leukemia accelerated by casein kinase IIalpha. *EMBO J* **15**, 5160-5166 (1996).
108 Condorelli, G. L. *et al.* T-cell-directed TAL-1 expression induces T-cell malignancies in transgenic mice. *Cancer Res* **56**, 5113-5119 (1996).
109 Sanda, T. *et al.* Core transcriptional regulatory circuit controlled by the TAL1 complex in human T cell acute lymphoblastic leukemia. *Cancer Cell* **22**, 209-221, doi:10.1016/j.ccr.2012.06.007 (2012).
110 Kusy, S. *et al.* NKX3.1 is a direct TAL1 target gene that mediates proliferation of TAL1-expressing human T cell acute lymphoblastic leukemia. *J Exp Med* **207**, 2141-2156, doi:10.1084/jem.20100745 (2010).
111 Mansour, M. R. *et al.* The TAL1 complex targets the FBXW7 tumor suppressor by activating miR-223 in human T cell acute lymphoblastic leukemia. *J Exp Med* **210**, 1545-1557, doi:10.1084/jem.20122516 (2013).

112 Van Vlierberghe, P. *et al.* The cryptic chromosomal deletion del(11)(p12p13) as a new activation mechanism of LMO2 in pediatric T-cell acute lymphoblastic leukemia. *Blood* **108**, 3520-3529, doi:10.1182/blood-2006-04-019927 (2006).
113 Van Vlierberghe, P. *et al.* Monoallelic or biallelic LMO2 expression in relation to the LMO2 rearrangement status in pediatric T-cell acute lymphoblastic leukemia. *Leukemia* **22**, 1434-1437, doi:10.1038/sj.leu.2405063 (2008).
114 Larson, R. C. *et al.* Protein dimerization between Lmo2 (Rbtn2) and Tal1 alters thymocyte development and potentiates T cell tumorigenesis in transgenic mice. *EMBO J* **15**, 1021-1027 (1996).
115 Pearson, J. C., Lemons, D. & McGinnis, W. Modulating Hox gene functions during animal body patterning. *Nat Rev Genet* **6**, 893-904, doi:10.1038/nrg1726 (2005).
116 Garcia-Fernandez, J. The genesis and evolution of homeobox gene clusters. *Nat Rev Genet* **6**, 881-892, doi:10.1038/nrg1723 (2005).
117 Ferrando, A. A. *et al.* Prognostic importance of TLX1 (HOX11) oncogene expression in adults with T-cell acute lymphoblastic leukaemia. *Lancet* **363**, 535-536, doi:10.1016/S0140-6736(04)15542-6 (2004).
118 Ballerini, P. *et al.* HOX11L2 expression defines a clinical subtype of pediatric T-ALL associated with poor prognosis. *Blood* **100**, 991-997, doi:10.1182/blood-2001-11-0093 (2002).
119 Asnafi, V. *et al.* Impact of TCR status and genotype on outcome in adult T-cell acute lymphoblastic leukemia: a LALA-94 study. *Blood* **105**, 3072-3078, doi:10.1182/blood-2004-09-3666 (2005).
120 Speleman, F. *et al.* A new recurrent inversion, inv(7)(p15q34), leads to transcriptional activation of HOXA10 and HOXA11 in a subset of T-cell acute lymphoblastic leukemias. *Leukemia* **19**, 358-366, doi:10.1038/sj.leu.2403657 (2005).
121 Chervinsky, D. S., Sait, S. N., Nowak, N. J., Shows, T. B. & Aplan, P. D. Complex MLL rearrangement in a patient with T-cell acute lymphoblastic leukemia. *Genes Chromosomes Cancer* **14**, 76-84, doi:10.1002/gcc.2870140114 (1995).
122 Rubnitz, J. E. *et al.* Molecular analysis of t(11;19) breakpoints in childhood acute leukemias. *Blood* **87**, 4804-4808 (1996).
123 Tkachuk, D. C., Kohler, S. & Cleary, M. L. Involvement of a homolog of Drosophila trithorax by 11q23 chromosomal translocations in acute leukemias. *Cell* **71**, 691-700, doi:10.1016/0092-8674(92)90602-9 (1992).
124 Asnafi, V. *et al.* CALM-AF10 is a common fusion transcript in T-ALL and is specific to the TCRgammadelta lineage. *Blood* **102**, 1000-1006, doi:10.1182/blood-2002-09-2913 (2003).
125 Van Vlierberghe, P. *et al.* The recurrent SET-NUP214 fusion as a new HOXA activation mechanism in pediatric T-cell acute lymphoblastic leukemia. *Blood* **111**, 4668-4680, doi:10.1182/blood-2007-09-111872 (2008).
126 Niehues, T. *et al.* A classification based on T cell selection-related phenotypes identifies a subgroup of childhood T-ALL with favorable outcome in the COALL studies. *Leukemia* **13**, 614-617, doi:10.1038/sj.leu.2401382 (1999).
127 Asnafi, V. *et al.* NOTCH1/FBXW7 mutation identifies a large subgroup with favorable outcome in adult T-cell acute lymphoblastic leukemia (T-ALL): a Group for Research on Adult Acute Lymphoblastic Leukemia (GRAALL) study. *Blood* **113**, 3918-3924, doi:10.1182/blood-2008-10-184069 (2009).

128 Larson Gedman, A. *et al.* The impact of NOTCH1, FBW7 and PTEN mutations on prognosis and downstream signaling in pediatric T-cell acute lymphoblastic leukemia: a report from the Children's Oncology Group. *Leukemia* **23**, 1417-1425, doi:10.1038/leu.2009.64 (2009).
129 Mansour, M. R. *et al.* Prognostic implications of NOTCH1 and FBXW7 mutations in adults with T-cell acute lymphoblastic leukemia treated on the MRC UKALLXII/ECOG E2993 protocol. *J Clin Oncol* **27**, 4352-4356, doi:10.1200/JCO.2009.22.0996 (2009).
130 Park, M. J. *et al.* FBXW7 and NOTCH1 mutations in childhood T cell acute lymphoblastic leukaemia and T cell non-Hodgkin lymphoma. *Br J Haematol* **145**, 198-206, doi:10.1111/j.1365-2141.2009.07607.x (2009).
131 Quelle, D. E., Zindy, F., Ashmun, R. A. & Sherr, C. J. Alternative reading frames of the INK4a tumor suppressor gene encode two unrelated proteins capable of inducing cell cycle arrest. *Cell* **83**, 993-1000, doi:10.1016/0092-8674(95)90214-7 (1995).
132 Serrano, M., Hannon, G. J. & Beach, D. A new regulatory motif in cell-cycle control causing specific inhibition of cyclin D/CDK4. *Nature* **366**, 704-707, doi:10.1038/366704a0 (1993).
133 Kamijo, T. *et al.* Tumor suppression at the mouse INK4a locus mediated by the alternative reading frame product p19ARF. *Cell* **91**, 649-659, doi:10.1016/s0092-8674(00)80452-3 (1997).
134 Zhang, Y., Xiong, Y. & Yarbrough, W. G. ARF promotes MDM2 degradation and stabilizes p53: ARF-INK4a locus deletion impairs both the Rb and p53 tumor suppression pathways. *Cell* **92**, 725-734, doi:10.1016/s0092-8674(00)81401-4 (1998).
135 Sherr, C. J. Cancer cell cycles. *Science* **274**, 1672-1677, doi:10.1126/science.274.5293.1672 (1996).
136 De Keersmaecker, K. *et al.* Exome sequencing identifies mutation in CNOT3 and ribosomal genes RPL5 and RPL10 in T-cell acute lymphoblastic leukemia. *Nat Genet* **45**, 186-190, doi:10.1038/ng.2508 (2013).
137 Warner, J. R. & McIntosh, K. B. How common are extraribosomal functions of ribosomal proteins? *Mol Cell* **34**, 3-11, doi:10.1016/j.molcel.2009.03.006 (2009).
138 Zhang, Y. & Lu, H. Signaling to p53: ribosomal proteins find their way. *Cancer Cell* **16**, 369-377, doi:10.1016/j.ccr.2009.09.024 (2009).
139 Rao, S. *et al.* Inactivation of ribosomal protein L22 promotes transformation by induction of the stemness factor, Lin28B. *Blood* **120**, 3764-3773, doi:10.1182/blood-2012-03-415349 (2012).
140 Mullighan, C. G. *et al.* Genome-wide analysis of genetic alterations in acute lymphoblastic leukaemia. *Nature* **446**, 758-764, doi:10.1038/nature05690 (2007).
141 Remke, M. *et al.* High-resolution genomic profiling of childhood T-ALL reveals frequent copy-number alterations affecting the TGF-beta and PI3K-AKT pathways and deletions at 6q15-16.1 as a genomic marker for unfavorable early treatment response. *Blood* **114**, 1053-1062, doi:10.1182/blood-2008-10-186536 (2009).
142 McConnell, B. B., Gregory, F. J., Stott, F. J., Hara, E. & Peters, G. Induced expression of p16(INK4a) inhibits both CDK4- and CDK2-associated kinase activity by reassortment of cyclin-CDK-inhibitor complexes. *Mol Cell Biol* **19**, 1981-1989, doi:10.1128/MCB.19.3.1981 (1999).

143 Fahraeus, R., Paramio, J. M., Ball, K. L., Lain, S. & Lane, D. P. Inhibition of pRb phosphorylation and cell-cycle progression by a 20-residue peptide derived from p16CDKN2/INK4A. *Curr Biol* **6**, 84-91, doi:10.1016/s0960-9822(02)00425-6 (1996).
144 Kamijo, T. *et al.* Functional and physical interactions of the ARF tumor suppressor with p53 and Mdm2. *Proc Natl Acad Sci U S A* **95**, 8292-8297, doi:10.1073/pnas.95.14.8292 (1998).
145 Roti, G. & Stegmaier, K. New Approaches to Target T-ALL. *Front Oncol* **4**, 170, doi:10.3389/fonc.2014.00170 (2014).
146 Clappier, E. *et al.* Cyclin D2 dysregulation by chromosomal translocations to TCR loci in T-cell acute lymphoblastic leukemias. *Leukemia* **20**, 82-86, doi:10.1038/sj.leu.2404008 (2006).
147 Sawai, C. M. *et al.* Therapeutic targeting of the cyclin D3:CDK4/6 complex in T cell leukemia. *Cancer Cell* **22**, 452-465, doi:10.1016/j.ccr.2012.09.016 (2012).
148 Lahortiga, I. *et al.* Duplication of the MYB oncogene in T cell acute lymphoblastic leukemia. *Nat Genet* **39**, 593-595, doi:10.1038/ng2025 (2007).
149 O'Neil, J. *et al.* Alu elements mediate MYB gene tandem duplication in human T-ALL. *J Exp Med* **204**, 3059-3066, doi:10.1084/jem.20071637 (2007).
150 Mets, E. *et al.* MicroRNA-193b-3p acts as a tumor suppressor by targeting the MYB oncogene in T-cell acute lymphoblastic leukemia. *Leukemia* **29**, 798-806, doi:10.1038/leu.2014.276 (2015).
151 Sanghvi, V. R. *et al.* Characterization of a set of tumor suppressor microRNAs in T cell acute lymphoblastic leukemia. *Sci Signal* **7**, ra111, doi:10.1126/scisignal.2005500 (2014).
152 Stine, Z. E., Walton, Z. E., Altman, B. J., Hsieh, A. L. & Dang, C. V. MYC, Metabolism, and Cancer. *Cancer Discov* **5**, 1024-1039, doi:10.1158/2159-8290.CD-15-0507 (2015).
153 Dang, C. V. MYC on the path to cancer. *Cell* **149**, 22-35, doi:10.1016/j.cell.2012.03.003 (2012).
154 Dose, M. *et al.* c-Myc mediates pre-TCR-induced proliferation but not developmental progression. *Blood* **108**, 2669-2677, doi:10.1182/blood-2006-02-005900 (2006).
155 Mathieu-Mahul, D. *et al.* A t(8;14)(q24;q11) translocation in a T-cell leukemia (L1-ALL) with c-myc and TcR-alpha chain locus rearrangements. *Int J Cancer* **38**, 835-840, doi:10.1002/ijc.2910380609 (1986).
156 Palomero, T. *et al.* NOTCH1 directly regulates c-MYC and activates a feed-forward-loop transcriptional network promoting leukemic cell growth. *Proc Natl Acad Sci U S A* **103**, 18261-18266, doi:10.1073/pnas.0606108103 (2006).
157 Weng, A. P. *et al.* c-Myc is an important direct target of Notch1 in T-cell acute lymphoblastic leukemia/lymphoma. *Genes Dev* **20**, 2096-2109, doi:10.1101/gad.1450406 (2006).
158 Sharma, V. M. *et al.* Notch1 contributes to mouse T-cell leukemia by directly inducing the expression of c-myc. *Mol Cell Biol* **26**, 8022-8031, doi:10.1128/MCB.01091-06 (2006).
159 Yada, M. *et al.* Phosphorylation-dependent degradation of c-Myc is mediated by the F-box protein Fbw7. *EMBO J* **23**, 2116-2125, doi:10.1038/sj.emboj.7600217 (2004).
160 Welcker, M. *et al.* The Fbw7 tumor suppressor regulates glycogen synthase kinase 3 phosphorylation-dependent c-Myc protein degradation. *Proc Natl Acad Sci U S A* **101**, 9085-9090, doi:10.1073/pnas.0402770101 (2004).

161 O'Neil, J. *et al.* FBW7 mutations in leukemic cells mediate NOTCH pathway activation and resistance to gamma-secretase inhibitors. *J Exp Med* **204**, 1813-1824, doi:10.1084/jem.20070876 (2007).
162 Thompson, B. J. *et al.* The SCFFBW7 ubiquitin ligase complex as a tumor suppressor in T cell leukemia. *J Exp Med* **204**, 1825-1835, doi:10.1084/jem.20070872 (2007).
163 Palomero, T. *et al.* Mutational loss of PTEN induces resistance to NOTCH1 inhibition in T-cell leukemia. *Nat Med* **13**, 1203-1210, doi:10.1038/nm1636 (2007).
164 Mendes, R. D. *et al.* PTEN microdeletions in T-cell acute lymphoblastic leukemia are caused by illegitimate RAG-mediated recombination events. *Blood* **124**, 567-578, doi:10.1182/blood-2014-03-562751 (2014).
165 Barrett, D., Brown, V. I., Grupp, S. A. & Teachey, D. T. Targeting the PI3K/AKT/mTOR signaling axis in children with hematologic malignancies. *Paediatr Drugs* **14**, 299-316, doi:10.2165/11594740-000000000-00000 (2012).
166 Gutierrez, A. *et al.* High frequency of PTEN, PI3K, and AKT abnormalities in T-cell acute lymphoblastic leukemia. *Blood* **114**, 647-650, doi:10.1182/blood-2009-02-206722 (2009).
167 Tasian, S. K., Teachey, D. T. & Rheingold, S. R. Targeting the PI3K/mTOR Pathway in Pediatric Hematologic Malignancies. *Front Oncol* **4**, 108, doi:10.3389/fonc.2014.00108 (2014).
168 Suzuki, A. *et al.* High cancer susceptibility and embryonic lethality associated with mutation of the PTEN tumor suppressor gene in mice. *Curr Biol* **8**, 1169-1178, doi:10.1016/s0960-9822(07)00488-5 (1998).
169 Mao, C. *et al.* Unequal contribution of Akt isoforms in the double-negative to double-positive thymocyte transition. *J Immunol* **178**, 5443-5453, doi:10.4049/jimmunol.178.9.5443 (2007).
170 Teachey, D. T., Grupp, S. A. & Brown, V. I. Mammalian target of rapamycin inhibitors and their potential role in therapy in leukaemia and other haematological malignancies. *Br J Haematol* **145**, 569-580, doi:10.1111/j.1365-2141.2009.07657.x (2009).
171 Janes, M. R. & Fruman, D. A. Targeting TOR dependence in cancer. *Oncotarget* **1**, 69-76, doi:10.18632/oncotarget.110 (2010).
172 Wei, G. *et al.* Gene expression-based chemical genomics identifies rapamycin as a modulator of MCL1 and glucocorticoid resistance. *Cancer Cell* **10**, 331-342, doi:10.1016/j.ccr.2006.09.006 (2006).
173 Schlis, K. *et al.* A Pilot Trial of Rapamycin with Glucocorticoids In Children and Adults with Relapsed ALL. *Blood* **116**, 3244, doi:https://doi.org/10.1182/blood.V116.21.3244.3244 (2010).
174 Chiarini, F. *et al.* Dual inhibition of class IA phosphatidylinositol 3-kinase and mammalian target of rapamycin as a new therapeutic option for T-cell acute lymphoblastic leukemia. *Cancer Res* **69**, 3520-3528, doi:10.1158/0008-5472.CAN-08-4884 (2009).
175 Yang, J. *et al.* Targeting PI3K in cancer: mechanisms and advances in clinical trials. *Mol Cancer* **18**, 26, doi:10.1186/s12943-019-0954-x (2019).
176 Dumortier, A., Wilson, A., MacDonald, H. R. & Radtke, F. Paradigms of notch signaling in mammals. *Int J Hematol* **82**, 277-284, doi:10.1532/IJH97.05099 (2005).
177 Radtke, F. *et al.* Deficient T cell fate specification in mice with an induced inactivation of Notch1. *Immunity* **10**, 547-558, doi:10.1016/s1074-7613(00)80054-0 (1999).

178 Ellisen, L. W. *et al.* TAN-1, the human homolog of the Drosophila notch gene, is broken by chromosomal translocations in T lymphoblastic neoplasms. *Cell* **66**, 649-661, doi:10.1016/0092-8674(91)90111-b (1991).
179 Sulis, M. L. *et al.* NOTCH1 extracellular juxtamembrane expansion mutations in T-ALL. *Blood* **112**, 733-740, doi:10.1182/blood-2007-12-130096 (2008).
180 Pear, W. S. *et al.* Exclusive development of T cell neoplasms in mice transplanted with bone marrow expressing activated Notch alleles. *J Exp Med* **183**, 2283-2291, doi:10.1084/jem.183.5.2283 (1996).
181 Chiang, M. Y. *et al.* Leukemia-associated NOTCH1 alleles are weak tumor initiators but accelerate K-ras-initiated leukemia. *J Clin Invest* **118**, 3181-3194, doi:10.1172/JCI35090 (2008).
182 Herranz, D. *et al.* A NOTCH1-driven MYC enhancer promotes T cell development, transformation and acute lymphoblastic leukemia. *Nat Med* **20**, 1130-1137, doi:10.1038/nm.3665 (2014).
183 Yashiro-Ohtani, Y. *et al.* Long-range enhancer activity determines Myc sensitivity to Notch inhibitors in T cell leukemia. *Proc Natl Acad Sci U S A* **111**, E4946-4953, doi:10.1073/pnas.1407079111 (2014).
184 Wendorff, A. A. *et al.* Hes1 is a critical but context-dependent mediator of canonical Notch signaling in lymphocyte development and transformation. *Immunity* **33**, 671-684, doi:10.1016/j.immuni.2010.11.014 (2010).
185 Palomero, T., Dominguez, M. & Ferrando, A. A. The role of the PTEN/AKT Pathway in NOTCH1-induced leukemia. *Cell Cycle* **7**, 965-970, doi:10.4161/cc.7.8.5753 (2008).
186 Real, P. J. *et al.* Gamma-secretase inhibitors reverse glucocorticoid resistance in T cell acute lymphoblastic leukemia. *Nat Med* **15**, 50-58, doi:10.1038/nm.1900 (2009).
187 Espinosa, L. *et al.* The Notch/Hes1 pathway sustains NF-kappaB activation through CYLD repression in T cell leukemia. *Cancer Cell* **18**, 268-281, doi:10.1016/j.ccr.2010.08.006 (2010).
188 Schnell, S. A. *et al.* Therapeutic targeting of HES1 transcriptional programs in T-ALL. *Blood* **125**, 2806-2814, doi:10.1182/blood-2014-10-608448 (2015).
189 Trimarchi, T. *et al.* Genome-wide mapping and characterization of Notch-regulated long noncoding RNAs in acute leukemia. *Cell* **158**, 593-606, doi:10.1016/j.cell.2014.05.049 (2014).
190 Duro, D., Bernard, O., Della Valle, V., Berger, R. & Larsen, C. J. A new type of p16INK4/MTS1 gene transcript expressed in B-cell malignancies. *Oncogene* **11**, 21-29 (1995).
191 Mao, L. *et al.* A novel p16INK4A transcript. *Cancer Res* **55**, 2995-2997 (1995).
192 Stone, S. *et al.* Complex structure and regulation of the P16 (MTS1) locus. *Cancer Res* **55**, 2988-2994 (1995).
193 Voit, R., Hoffmann, M. & Grummt, I. Phosphorylation by G1-specific cdk-cyclin complexes activates the nucleolar transcription factor UBF. *EMBO J* **18**, 1891-1899, doi:10.1093/emboj/18.7.1891 (1999).
194 Voit, R. & Grummt, I. Phosphorylation of UBF at serine 388 is required for interaction with RNA polymerase I and activation of rDNA transcription. *Proc Natl Acad Sci U S A* **98**, 13631-13636, doi:10.1073/pnas.231071698 (2001).

195 Thornborrow, E. C. & Manfredi, J. J. One mechanism for cell type-specific regulation of the bax promoter by the tumor suppressor p53 is dictated by the p53 response element. *J Biol Chem* **274**, 33747-33756, doi:10.1074/jbc.274.47.33747 (1999).
196 Muller, M. *et al.* p53 activates the CD95 (APO-1/Fas) gene in response to DNA damage by anticancer drugs. *J Exp Med* **188**, 2033-2045, doi:10.1084/jem.188.11.2033 (1998).
197 Takimoto, R. & El-Deiry, W. S. Wild-type p53 transactivates the KILLER/DR5 gene through an intronic sequence-specific DNA-binding site. *Oncogene* **19**, 1735-1743, doi:10.1038/sj.onc.1203489 (2000).
198 Oda, E. *et al.* Noxa, a BH3-only member of the Bcl-2 family and candidate mediator of p53-induced apoptosis. *Science* **288**, 1053-1058, doi:10.1126/science.288.5468.1053 (2000).
199 Okamura, S. *et al.* p53DINP1, a p53-inducible gene, regulates p53-dependent apoptosis. *Mol Cell* **8**, 85-94, doi:10.1016/s1097-2765(01)00284-2 (2001).
200 Yu, J., Zhang, L., Hwang, P. M., Kinzler, K. W. & Vogelstein, B. PUMA induces the rapid apoptosis of colorectal cancer cells. *Mol Cell* **7**, 673-682, doi:10.1016/s1097-2765(01)00213-1 (2001).
201 Kern, S. E. *et al.* Identification of p53 as a sequence-specific DNA-binding protein. *Science* **252**, 1708-1711, doi:10.1126/science.2047879 (1991).
202 el-Deiry, W. S. *et al.* WAF1, a potential mediator of p53 tumor suppression. *Cell* **75**, 817-825, doi:10.1016/0092-8674(93)90500-p (1993).
203 Zauberman, A., Flusberg, D., Haupt, Y., Barak, Y. & Oren, M. A functional p53-responsive intronic promoter is contained within the human mdm2 gene. *Nucleic Acids Res* **23**, 2584-2592, doi:10.1093/nar/23.14.2584 (1995).
204 Zhang, Y. & Xiong, Y. Mutations in human ARF exon 2 disrupt its nucleolar localization and impair its ability to block nuclear export of MDM2 and p53. *Mol Cell* **3**, 579-591, doi:10.1016/s1097-2765(00)80351-2 (1999).
205 Weber, J. D. *et al.* Cooperative signals governing ARF-mdm2 interaction and nucleolar localization of the complex. *Mol Cell Biol* **20**, 2517-2528, doi:10.1128/MCB.20.7.2517-2528.2000 (2000).
206 Rubbi, C. P. & Milner, J. Disruption of the nucleolus mediates stabilization of p53 in response to DNA damage and other stresses. *EMBO J* **22**, 6068-6077, doi:10.1093/emboj/cdg579 (2003).
207 Chan, P. K., Qi, Y., Amley, J. & Koller, C. A. Quantitation of the nucleophosmin/B23-translocation using imaging analysis. *Cancer Lett* **100**, 191-197, doi:10.1016/0304-3835(95)04100-1 (1996).
208 Sparmann, A. & van Lohuizen, M. Polycomb silencers control cell fate, development and cancer. *Nat Rev Cancer* **6**, 846-856, doi:10.1038/nrc1991 (2006).
209 Schwartz, Y. B. & Pirrotta, V. Polycomb silencing mechanisms and the management of genomic programmes. *Nat Rev Genet* **8**, 9-22, doi:10.1038/nrg1981 (2007).
210 Aslanian, A., Iaquinta, P. J., Verona, R. & Lees, J. A. Repression of the Arf tumor suppressor by E2F3 is required for normal cell cycle kinetics. *Genes Dev* **18**, 1413-1422, doi:10.1101/gad.1196704 (2004).
211 Levine, S. S., King, I. F. & Kingston, R. E. Division of labor in polycomb group repression. *Trends Biochem Sci* **29**, 478-485, doi:10.1016/j.tibs.2004.07.007 (2004).

212 Bracken, A. P. *et al.* The Polycomb group proteins bind throughout the INK4A-ARF locus and are disassociated in senescent cells. *Genes Dev* **21**, 525-530, doi:10.1101/gad.415507 (2007).
213 Haupt, Y., Alexander, W. S., Barri, G., Klinken, S. P. & Adams, J. M. Novel zinc finger gene implicated as myc collaborator by retrovirally accelerated lymphomagenesis in E mu-myc transgenic mice. *Cell* **65**, 753-763, doi:10.1016/0092-8674(91)90383-a (1991).
214 van Lohuizen, M. *et al.* Identification of cooperating oncogenes in E mu-myc transgenic mice by provirus tagging. *Cell* **65**, 737-752, doi:10.1016/0092-8674(91)90382-9 (1991).
215 Jacobs, J. J., Kieboom, K., Marino, S., DePinho, R. A. & van Lohuizen, M. The oncogene and Polycomb-group gene bmi-1 regulates cell proliferation and senescence through the ink4a locus. *Nature* **397**, 164-168, doi:10.1038/16476 (1999).
216 Dietrich, N. *et al.* Bypass of senescence by the polycomb group protein CBX8 through direct binding to the INK4A-ARF locus. *EMBO J* **26**, 1637-1648, doi:10.1038/sj.emboj.7601632 (2007).
217 Rowland, B. D. *et al.* E2F transcriptional repressor complexes are critical downstream targets of p19(ARF)/p53-induced proliferative arrest. *Cancer Cell* **2**, 55-65, doi:10.1016/s1535-6108(02)00085-5 (2002).
218 Jacobs, J. J. *et al.* Senescence bypass screen identifies TBX2, which represses Cdkn2a (p19(ARF)) and is amplified in a subset of human breast cancers. *Nat Genet* **26**, 291-299, doi:10.1038/81583 (2000).
219 Maeda, T. *et al.* Role of the proto-oncogene Pokemon in cellular transformation and ARF repression. *Nature* **433**, 278-285, doi:10.1038/nature03203 (2005).
220 Suzuki, A., Sekiya, S., Buscher, D., Izpisua Belmonte, J. C. & Taniguchi, H. Tbx3 controls the fate of hepatic progenitor cells in liver development by suppressing p19ARF expression. *Development* **135**, 1589-1595, doi:10.1242/dev.016634 (2008).
221 Sherr, C. J. The INK4a/ARF network in tumour suppression. *Nat Rev Mol Cell Biol* **2**, 731-737, doi:10.1038/35096061 (2001).
222 Sherr, C. J. An Arf(GFP/GFP) reporter mouse reveals that the Arf tumor suppressor monitors latent oncogenic signals in vivo. *Cell Cycle* **3**, 239-240, doi:10.4161/cc.3.3.674 (2004).
223 Zindy, F. *et al.* Arf tumor suppressor promoter monitors latent oncogenic signals in vivo. *Proc Natl Acad Sci U S A* **100**, 15930-15935, doi:10.1073/pnas.2536808100 (2003).
224 Groth, A., Weber, J. D., Willumsen, B. M., Sherr, C. J. & Roussel, M. F. Oncogenic Ras induces p19ARF and growth arrest in mouse embryo fibroblasts lacking p21Cip1 and p27Kip1 without activating cyclin D-dependent kinases. *J Biol Chem* **275**, 27473-27480, doi:10.1074/jbc.M003417200 (2000).
225 DiGiammarino, E. L., Filippov, I., Weber, J. D., Bothner, B. & Kriwacki, R. W. Solution structure of the p53 regulatory domain of the p19Arf tumor suppressor protein. *Biochemistry* **40**, 2379-2386, doi:10.1021/bi0024005 (2001).
226 Bertwistle, D., Sugimoto, M. & Sherr, C. J. Physical and functional interactions of the Arf tumor suppressor protein with nucleophosmin/B23. *Mol Cell Biol* **24**, 985-996, doi:10.1128/MCB.24.3.985-996.2004 (2004).
227 Ozenne, P., Eymin, B., Brambilla, E. & Gazzeri, S. The ARF tumor suppressor: structure, functions and status in cancer. *Int J Cancer* **127**, 2239-2247, doi:10.1002/ijc.25511 (2010).

228 Sherr, C. J. Divorcing ARF and p53: an unsettled case. *Nat Rev Cancer* **6**, 663-673, doi:10.1038/nrc1954 (2006).
229 Ruggero, D. & Pandolfi, P. P. Does the ribosome translate cancer? *Nat Rev Cancer* **3**, 179-192, doi:10.1038/nrc1015 (2003).
230 Draptchinskaia, N. *et al.* The gene encoding ribosomal protein S19 is mutated in Diamond-Blackfan anaemia. *Nat Genet* **21**, 169-175, doi:10.1038/5951 (1999).
231 van Riggelen, J., Yetil, A. & Felsher, D. W. MYC as a regulator of ribosome biogenesis and protein synthesis. *Nat Rev Cancer* **10**, 301-309, doi:10.1038/nrc2819 (2010).
232 Hsieh, A. C., Truitt, M. L. & Ruggero, D. Oncogenic AKTivation of translation as a therapeutic target. *Br J Cancer* **105**, 329-336, doi:10.1038/bjc.2011.241 (2011).
233 Apicelli, A. J. *et al.* A non-tumor suppressor role for basal p19ARF in maintaining nucleolar structure and function. *Mol Cell Biol* **28**, 1068-1080, doi:10.1128/MCB.00484-07 (2008).
234 Stepinski, D. Nucleolus-derived mediators in oncogenic stress response and activation of p53-dependent pathways. *Histochem Cell Biol* **146**, 119-139, doi:10.1007/s00418-016-1443-6 (2016).
235 Mayer, C. & Grummt, I. Ribosome biogenesis and cell growth: mTOR coordinates transcription by all three classes of nuclear RNA polymerases. *Oncogene* **25**, 6384-6391, doi:10.1038/sj.onc.1209883 (2006).
236 Kopp, K. *et al.* Pol I transcription and pre-rRNA processing are coordinated in a transcription-dependent manner in mammalian cells. *Mol Biol Cell* **18**, 394-403, doi:10.1091/mbc.e06-03-0249 (2007).
237 Lempiainen, H. & Shore, D. Growth control and ribosome biogenesis. *Curr Opin Cell Biol* **21**, 855-863, doi:10.1016/j.ceb.2009.09.002 (2009).
238 Grummt, I. Wisely chosen paths--regulation of rRNA synthesis: delivered on 30 June 2010 at the 35th FEBS Congress in Gothenburg, Sweden. *FEBS J* **277**, 4626-4639, doi:10.1111/j.1742-4658.2010.07892.x (2010).
239 Odintsova, T. I. *et al.* Characterization and analysis of posttranslational modifications of the human large cytoplasmic ribosomal subunit proteins by mass spectrometry and Edman sequencing. *J Protein Chem* **22**, 249-258, doi:10.1023/a:1025068419698 (2003).
240 Vladimirov, S. N. *et al.* Characterization of the human small-ribosomal-subunit proteins by N-terminal and internal sequencing, and mass spectrometry. *Eur J Biochem* **239**, 144-149, doi:10.1111/j.1432-1033.1996.0144u.x (1996).
241 Grummt, I. Life on a planet of its own: regulation of RNA polymerase I transcription in the nucleolus. *Genes Dev* **17**, 1691-1702, doi:10.1101/gad.1098503R (2003).
242 White, R. J. RNA polymerase III transcription and cancer. *Oncogene* **23**, 3208-3216, doi:10.1038/sj.onc.1207547 (2004).
243 White, R. J. RNA polymerases I and III, growth control and cancer. *Nat Rev Mol Cell Biol* **6**, 69-78, doi:10.1038/nrm1551 (2005).
244 Goodfellow, S. J. & White, R. J. Regulation of RNA polymerase III transcription during mammalian cell growth. *Cell Cycle* **6**, 2323-2326, doi:10.4161/cc.6.19.4767 (2007).
245 Volarevic, S. *et al.* Proliferation, but not growth, blocked by conditional deletion of 40S ribosomal protein S6. *Science* **288**, 2045-2047, doi:10.1126/science.288.5473.2045 (2000).

246 Derenzini, M. *et al.* Key role of the achievement of an appropriate ribosomal RNA complement for G1-S phase transition in H4-II-E-C3 rat hepatoma cells. *J Cell Physiol* **202**, 483-491, doi:10.1002/jcp.20144 (2005).
247 Sander, S. *et al.* Synergy between PI3K signaling and MYC in Burkitt lymphomagenesis. *Cancer Cell* **22**, 167-179, doi:10.1016/j.ccr.2012.06.012 (2012).
248 Chan, J. C. *et al.* AKT promotes rRNA synthesis and cooperates with c-MYC to stimulate ribosome biogenesis in cancer. *Sci Signal* **4**, ra56, doi:10.1126/scisignal.2001754 (2011).
249 Ahmad, Y., Boisvert, F. M., Gregor, P., Cobley, A. & Lamond, A. I. NOPdb: Nucleolar Proteome Database--2008 update. *Nucleic Acids Res* **37**, D181-184, doi:10.1093/nar/gkn804 (2009).
250 Boisvert, F. M., van Koningsbruggen, S., Navascues, J. & Lamond, A. I. The multifunctional nucleolus. *Nat Rev Mol Cell Biol* **8**, 574-585, doi:10.1038/nrm2184 (2007).
251 Andersen, J. S. *et al.* Nucleolar proteome dynamics. *Nature* **433**, 77-83, doi:10.1038/nature03207 (2005).
252 David-Pfeuty, T. Potent inhibitors of cyclin-dependent kinase 2 induce nuclear accumulation of wild-type p53 and nucleolar fragmentation in human untransformed and tumor-derived cells. *Oncogene* **18**, 7409-7422, doi:10.1038/sj.onc.1203103 (1999).
253 Chan, P. K., Aldrich, M. B. & Yung, B. Y. Nucleolar protein B23 translocation after doxorubicin treatment in murine tumor cells. *Cancer Res* **47**, 3798-3801 (1987).
254 Desnoyers, S., Kaufmann, S. H. & Poirier, G. G. Alteration of the nucleolar localization of poly(ADP-ribose) polymerase upon treatment with transcription inhibitors. *Exp Cell Res* **227**, 146-153, doi:10.1006/excr.1996.0259 (1996).
255 Thielmann, H. W., Popanda, O. & Staab, H. J. Subnuclear distribution of DNA topoisomerase I and Bax protein in normal and xeroderma pigmentosum fibroblasts after irradiation with UV light and gamma rays or treatment with topotecan. *J Cancer Res Clin Oncol* **125**, 193-208, doi:10.1007/s004320050263 (1999).
256 Mayer, C. & Grummt, I. Cellular stress and nucleolar function. *Cell Cycle* **4**, 1036-1038, doi:10.4161/cc.4.8.1925 (2005).
257 Perlaky, L., Valdez, B. C. & Busch, H. Effects of cytotoxic drugs on translocation of nucleolar RNA helicase RH-II/Gu. *Exp Cell Res* **235**, 413-420, doi:10.1006/excr.1997.3686 (1997).
258 Valdez, B. C., Perlaky, L., Cai, Z. J., Henning, D. & Busch, H. Green fluorescent protein tag for studies of drug-induced translocation of nucleolar protein RH-II/Gu. *Biotechniques* **24**, 1032-1036, doi:10.2144/98246cr03 (1998).
259 Yung, B. Y., Busch, R. K., Busch, H., Mauger, A. B. & Chan, P. K. Effects of actinomycin D analogs on nucleolar phosphoprotein B23 (37,000 daltons/pI 5.1). *Biochem Pharmacol* **34**, 4059-4063, doi:10.1016/0006-2952(85)90387-9 (1985).
260 Chan, P. K., Bloom, D. A. & Hoang, T. T. The N-terminal half of NPM dissociates from nucleoli of HeLa cells after anticancer drug treatments. *Biochem Biophys Res Commun* **264**, 305-309, doi:10.1006/bbrc.1999.1255 (1999).
261 Matthews, D. A. Adenovirus protein V induces redistribution of nucleolin and B23 from nucleolus to cytoplasm. *J Virol* **75**, 1031-1038, doi:10.1128/JVI.75.2.1031-1038.2001 (2001).

262 Colombo, E., Marine, J. C., Danovi, D., Falini, B. & Pelicci, P. G. Nucleophosmin regulates the stability and transcriptional activity of p53. *Nat Cell Biol* **4**, 529-533, doi:10.1038/ncb814 (2002).
263 Kim, J. Y. *et al.* Involvement of GLTSCR2 in the DNA Damage Response. *Am J Pathol* **179**, 1257-1264, doi:10.1016/j.ajpath.2011.05.041 (2011).
264 Yogev, O., Saadon, K., Anzi, S., Inoue, K. & Shaulian, E. DNA damage-dependent translocation of B23 and p19 ARF is regulated by the Jun N-terminal kinase pathway. *Cancer Res* **68**, 1398-1406, doi:10.1158/0008-5472.CAN-07-2865 (2008).
265 Avitabile, D. *et al.* Nucleolar stress is an early response to myocardial damage involving nucleolar proteins nucleostemin and nucleophosmin. *Proc Natl Acad Sci U S A* **108**, 6145-6150, doi:10.1073/pnas.1017935108 (2011).
266 Duangmano, S., Sae-Lim, P., Suksamrarn, A., Domann, F. E. & Patmasiriwat, P. Cucurbitacin B inhibits human breast cancer cell proliferation through disruption of microtubule polymerization and nucleophosmin/B23 translocation. *BMC Complement Altern Med* **12**, 185, doi:10.1186/1472-6882-12-185 (2012).
267 Kar, B., Liu, B., Zhou, Z. & Lam, Y. W. Quantitative nucleolar proteomics reveals nuclear re-organization during stress- induced senescence in mouse fibroblast. *BMC Cell Biol* **12**, 33, doi:10.1186/1471-2121-12-33 (2011).
268 Ljungman, M., Zhang, F., Chen, F., Rainbow, A. J. & McKay, B. C. Inhibition of RNA polymerase II as a trigger for the p53 response. *Oncogene* **18**, 583-592, doi:10.1038/sj.onc.1202356 (1999).
269 Sherr, C. J. & Weber, J. D. The ARF/p53 pathway. *Curr Opin Genet Dev* **10**, 94-99, doi:10.1016/s0959-437x(99)00038-6 (2000).
270 Pestov, D. G., Strezoska, Z. & Lau, L. F. Evidence of p53-dependent cross-talk between ribosome biogenesis and the cell cycle: effects of nucleolar protein Bop1 on G(1)/S transition. *Mol Cell Biol* **21**, 4246-4255, doi:10.1128/MCB.21.13.4246-4255.2001 (2001).
271 Klein, J. & Grummt, I. Cell cycle-dependent regulation of RNA polymerase I transcription: the nucleolar transcription factor UBF is inactive in mitosis and early G1. *Proc Natl Acad Sci U S A* **96**, 6096-6101, doi:10.1073/pnas.96.11.6096 (1999).
272 Budde, A. & Grummt, I. p53 represses ribosomal gene transcription. *Oncogene* **18**, 1119-1124, doi:10.1038/sj.onc.1202402 (1999).
273 David-Pfeuty, T., Nouvian-Dooghe, Y., Sirri, V., Roussel, P. & Hernandez-Verdun, D. Common and reversible regulation of wild-type p53 function and of ribosomal biogenesis by protein kinases in human cells. *Oncogene* **20**, 5951-5963, doi:10.1038/sj.onc.1204741 (2001).
274 Haupt, S., Berger, M., Goldberg, Z. & Haupt, Y. Apoptosis - the p53 network. *J Cell Sci* **116**, 4077-4085, doi:10.1242/jcs.00739 (2003).
275 Jin, S. & Levine, A. J. The p53 functional circuit. *J Cell Sci* **114**, 4139-4140, doi:10.1242/jcs.114.23.4139 (2001).
276 Scala, F. *et al.* Direct relationship between the level of p53 stabilization induced by rRNA synthesis-inhibiting drugs and the cell ribosome biogenesis rate. *Oncogene* **35**, 977-989, doi:10.1038/onc.2015.147 (2016).
277 Iordanov, M. S. *et al.* Ribotoxic stress response: activation of the stress-activated protein kinase JNK1 by inhibitors of the peptidyl transferase reaction and by sequence-specific

RNA damage to the alpha-sarcin/ricin loop in the 28S rRNA. *Mol Cell Biol* **17**, 3373-3381, doi:10.1128/MCB.17.6.3373 (1997).
278 Shifrin, V. I. & Anderson, P. Trichothecene mycotoxins trigger a ribotoxic stress response that activates c-Jun N-terminal kinase and p38 mitogen-activated protein kinase and induces apoptosis. *J Biol Chem* **274**, 13985-13992, doi:10.1074/jbc.274.20.13985 (1999).
279 Iordanov, M. S. & Magun, B. E. Loss of cellular K+ mimics ribotoxic stress. Inhibition of protein synthesis and activation of the stress kinases SEK1/MKK4, stress-activated protein kinase/c-Jun NH2-terminal kinase 1, and p38/HOG1 by palytoxin. *J Biol Chem* **273**, 3528-3534, doi:10.1074/jbc.273.6.3528 (1998).
280 Laskin, J. D., Heck, D. E. & Laskin, D. L. The ribotoxic stress response as a potential mechanism for MAP kinase activation in xenobiotic toxicity. *Toxicol Sci* **69**, 289-291, doi:10.1093/toxsci/69.2.289 (2002).
281 Arcangeletti, M. C. *et al.* Human cytomegalovirus proteins PP65 and IEP72 are targeted to distinct compartments in nuclei and nuclear matrices of infected human embryo fibroblasts. *J Cell Biochem* **90**, 1056-1067, doi:10.1002/jcb.10655 (2003).
282 Burger, K. *et al.* Chemotherapeutic drugs inhibit ribosome biogenesis at various levels. *J Biol Chem* **285**, 12416-12425, doi:10.1074/jbc.M109.074211 (2010).
283 Llanos, S., Clark, P. A., Rowe, J. & Peters, G. Stabilization of p53 by p14ARF without relocation of MDM2 to the nucleolus. *Nat Cell Biol* **3**, 445-452, doi:10.1038/35074506 (2001).
284 Suzuki, A. *et al.* A new PICTure of nucleolar stress. *Cancer Sci* **103**, 632-637, doi:10.1111/j.1349-7006.2012.02219.x (2012).
285 Boulon, S., Westman, B. J., Hutten, S., Boisvert, F. M. & Lamond, A. I. The nucleolus under stress. *Mol Cell* **40**, 216-227, doi:10.1016/j.molcel.2010.09.024 (2010).
286 Yadavilli, S. *et al.* Ribosomal protein S3: A multi-functional protein that interacts with both p53 and MDM2 through its KH domain. *DNA Repair (Amst)* **8**, 1215-1224, doi:10.1016/j.dnarep.2009.07.003 (2009).
287 Chen, D. *et al.* Ribosomal protein S7 as a novel modulator of p53-MDM2 interaction: binding to MDM2, stabilization of p53 protein, and activation of p53 function. *Oncogene* **26**, 5029-5037, doi:10.1038/sj.onc.1210327 (2007).
288 Zhu, Y. H. *et al.* Wip1 regulates the generation of new neural cells in the adult olfactory bulb through p53-dependent cell cycle control. *Stem Cells* **27**, 1433-1442, doi:10.1002/stem.65 (2009).
289 Marechal, V., Elenbaas, B., Piette, J., Nicolas, J. C. & Levine, A. J. The ribosomal L5 protein is associated with mdm-2 and mdm-2-p53 complexes. *Mol Cell Biol* **14**, 7414-7420, doi:10.1128/mcb.14.11.7414-7420.1994 (1994).
290 Dai, M. S. & Lu, H. Inhibition of MDM2-mediated p53 ubiquitination and degradation by ribosomal protein L5. *J Biol Chem* **279**, 44475-44482, doi:10.1074/jbc.M403722200 (2004).
291 Bursac, S. *et al.* Mutual protection of ribosomal proteins L5 and L11 from degradation is essential for p53 activation upon ribosomal biogenesis stress. *Proc Natl Acad Sci U S A* **109**, 20467-20472, doi:10.1073/pnas.1218535109 (2012).
292 Zhang, Y. *et al.* Ribosomal protein L11 negatively regulates oncoprotein MDM2 and mediates a p53-dependent ribosomal-stress checkpoint pathway. *Mol Cell Biol* **23**, 8902-8912, doi:10.1128/MCB.23.23.8902-8912.2003 (2003).

293 Lohrum, M. A., Ludwig, R. L., Kubbutat, M. H., Hanlon, M. & Vousden, K. H. Regulation of HDM2 activity by the ribosomal protein L11. *Cancer Cell* **3**, 577-587, doi:10.1016/s1535-6108(03)00134-x (2003).
294 Bhat, K. P., Itahana, K., Jin, A. & Zhang, Y. Essential role of ribosomal protein L11 in mediating growth inhibition-induced p53 activation. *EMBO J* **23**, 2402-2412, doi:10.1038/sj.emboj.7600247 (2004).
295 Fumagalli, S. *et al.* Absence of nucleolar disruption after impairment of 40S ribosome biogenesis reveals an rpL11-translation-dependent mechanism of p53 induction. *Nat Cell Biol* **11**, 501-508, doi:10.1038/ncb1858 (2009).
296 Dai, M. S. *et al.* Ribosomal protein L23 activates p53 by inhibiting MDM2 function in response to ribosomal perturbation but not to translation inhibition. *Mol Cell Biol* **24**, 7654-7668, doi:10.1128/MCB.24.17.7654-7668.2004 (2004).
297 Yung, B. Y., Hui, E. K. & Chan, P. K. Protein B23 (M.W./pI = 37 kD/5.1) is the only major protein extracted from HeLa nucleoli with 3M urea. *Life Sci* **51**, 915-920, doi:10.1016/0024-3205(92)90399-a (1992).
298 Spector, D. L., Ochs, R. L. & Busch, H. Silver staining, immunofluorescence, and immunoelectron microscopic localization of nucleolar phosphoproteins B23 and C23. *Chromosoma* **90**, 139-148, doi:10.1007/BF00292451 (1984).
299 Biggiogera, M. *et al.* Simultaneous immunoelectron microscopic visualization of protein B23 and C23 distribution in the HeLa cell nucleolus. *J Histochem Cytochem* **37**, 1371-1374, doi:10.1177/37.9.2768807 (1989).
300 Lindstrom, M. S. NPM1/B23: A Multifunctional Chaperone in Ribosome Biogenesis and Chromatin Remodeling. *Biochem Res Int* **2011**, 195209, doi:10.1155/2011/195209 (2011).
301 Szebeni, A. & Olson, M. O. Nucleolar protein B23 has molecular chaperone activities. *Protein Sci* **8**, 905-912, doi:10.1110/ps.8.4.905 (1999).
302 Yung, B. Y., Busch, H. & Chan, P. K. Translocation of nucleolar phosphoprotein B23 (37 kDa/pI 5.1) induced by selective inhibitors of ribosome synthesis. *Biochim Biophys Acta* **826**, 167-173, doi:10.1016/0167-4781(85)90002-8 (1985).
303 Yu, Y. *et al.* Nucleophosmin is essential for ribosomal protein L5 nuclear export. *Mol Cell Biol* **26**, 3798-3809, doi:10.1128/MCB.26.10.3798-3809.2006 (2006).
304 Muro, E., Hoang, T. Q., Jobart-Malfait, A. & Hernandez-Verdun, D. In nucleoli, the steady state of nucleolar proteins is leptomycin B-sensitive. *Biol Cell* **100**, 303-313, doi:10.1042/BC20070117 (2008).
305 Borer, R. A., Lehner, C. F., Eppenberger, H. M. & Nigg, E. A. Major nucleolar proteins shuttle between nucleus and cytoplasm. *Cell* **56**, 379-390, doi:10.1016/0092-8674(89)90241-9 (1989).
306 Grisendi, S., Mecucci, C., Falini, B. & Pandolfi, P. P. Nucleophosmin and cancer. *Nat Rev Cancer* **6**, 493-505, doi:10.1038/nrc1885 (2006).
307 Lindstrom, M. S. & Zhang, Y. B23 and ARF: friends or foes? *Cell Biochem Biophys* **46**, 79-90, doi:10.1385/CBB:46:1:79 (2006).
308 Colombo, E., Alcalay, M. & Pelicci, P. G. Nucleophosmin and its complex network: a possible therapeutic target in hematological diseases. *Oncogene* **30**, 2595-2609, doi:10.1038/onc.2010.646 (2011).

309 Itahana, K. *et al.* Tumor suppressor ARF degrades B23, a nucleolar protein involved in ribosome biogenesis and cell proliferation. *Mol Cell* **12**, 1151-1164, doi:10.1016/s1097-2765(03)00431-3 (2003).
310 Chan, P. K., Aldrich, M. & Busch, H. Alterations in immunolocalization of the phosphoprotein B23 in HeLa cells during serum starvation. *Exp Cell Res* **161**, 101-110, doi:10.1016/0014-4827(85)90494-x (1985).
311 Chan, P. K. & Chan, F. Y. A study of correlation between NPM-translocation and apoptosis in cells induced by daunomycin. *Biochem Pharmacol* **57**, 1265-1273, doi:10.1016/s0006-2952(99)00043-x (1999).
312 Kurki, S. *et al.* Nucleolar protein NPM interacts with HDM2 and protects tumor suppressor protein p53 from HDM2-mediated degradation. *Cancer Cell* **5**, 465-475, doi:10.1016/s1535-6108(04)00110-2 (2004).
313 Yang, K. *et al.* A redox mechanism underlying nucleolar stress sensing by nucleophosmin. *Nat Commun* **7**, 13599, doi:10.1038/ncomms13599 (2016).
314 Takemura, M. *et al.* Nucleolar protein B23.1 binds to retinoblastoma protein and synergistically stimulates DNA polymerase alpha activity. *J Biochem* **125**, 904-909, doi:10.1093/oxfordjournals.jbchem.a022367 (1999).
315 Kerr, L. E. *et al.* Nucleophosmin is a novel Bax chaperone that regulates apoptotic cell death. *Oncogene* **26**, 2554-2562, doi:10.1038/sj.onc.1210044 (2007).
316 Derenzini, M. *et al.* Quantitative changes of the two major AgNOR proteins, nucleolin and protein B23, related to stimulation of rDNA transcription. *Exp Cell Res* **219**, 276-282, doi:10.1006/excr.1995.1228 (1995).
317 Derenzini, M., Sirri, V., Trere, D. & Ochs, R. L. The quantity of nucleolar proteins nucleolin and protein B23 is related to cell doubling time in human cancer cells. *Lab Invest* **73**, 497-502 (1995).
318 Henras, A. K., Plisson-Chastang, C., O'Donohue, M. F., Chakraborty, A. & Gleizes, P. E. An overview of pre-ribosomal RNA processing in eukaryotes. *Wiley Interdiscip Rev RNA* **6**, 225-242, doi:10.1002/wrna.1269 (2015).
319 Politz, J. C., Polena, I., Trask, I., Bazett-Jones, D. P. & Pederson, T. A nonribosomal landscape in the nucleolus revealed by the stem cell protein nucleostemin. *Mol Biol Cell* **16**, 3401-3410, doi:10.1091/mbc.e05-02-0106 (2005).
320 Finkbeiner, E., Haindl, M. & Muller, S. The SUMO system controls nucleolar partitioning of a novel mammalian ribosome biogenesis complex. *EMBO J* **30**, 1067-1078, doi:10.1038/emboj.2011.33 (2011).
321 Finkbeiner, E., Haindl, M., Raman, N. & Muller, S. SUMO routes ribosome maturation. *Nucleus* **2**, 527-532, doi:10.4161/nucl.2.6.17604 (2011).
322 Poortinga, G. *et al.* MAD1 and c-MYC regulate UBF and rDNA transcription during granulocyte differentiation. *EMBO J* **23**, 3325-3335, doi:10.1038/sj.emboj.7600335 (2004).
323 Dai, M. S., Arnold, H., Sun, X. X., Sears, R. & Lu, H. Inhibition of c-Myc activity by ribosomal protein L11. *EMBO J* **26**, 3332-3345, doi:10.1038/sj.emboj.7601776 (2007).
324 Russo, A. *et al.* Human rpL3 induces G(1)/S arrest or apoptosis by modulating p21 (waf1/cip1) levels in a p53-independent manner. *Cell Cycle* **12**, 76-87, doi:10.4161/cc.22963 (2013).

325 Hein, N., Hannan, K. M., George, A. J., Sanij, E. & Hannan, R. D. The nucleolus: an emerging target for cancer therapy. *Trends Mol Med* **19**, 643-654, doi:10.1016/j.molmed.2013.07.005 (2013).
326 Hernandez-Verdun, D. Assembly and disassembly of the nucleolus during the cell cycle. *Nucleus* **2**, 189-194, doi:10.4161/nucl.2.3.16246 (2011).
327 Andrews, W. J. *et al.* Old drug, new target: ellipticines selectively inhibit RNA polymerase I transcription. *J Biol Chem* **288**, 4567-4582, doi:10.1074/jbc.M112.411611 (2013).
328 Drygin, D. *et al.* Anticancer activity of CX-3543: a direct inhibitor of rRNA biogenesis. *Cancer Res* **69**, 7653-7661, doi:10.1158/0008-5472.CAN-09-1304 (2009).
329 Drygin, D. *et al.* Targeting RNA polymerase I with an oral small molecule CX-5461 inhibits ribosomal RNA synthesis and solid tumor growth. *Cancer Res* **71**, 1418-1430, doi:10.1158/0008-5472.CAN-10-1728 (2011).
330 Genesca, E. *et al.* Frequency and clinical impact of CDKN2A/ARF/CDKN2B gene deletions as assessed by in-depth genetic analyses in adult T cell acute lymphoblastic leukemia. *J Hematol Oncol* **11**, 96, doi:10.1186/s13045-018-0639-8 (2018).
331 Sulong, S. *et al.* A comprehensive analysis of the CDKN2A gene in childhood acute lymphoblastic leukemia reveals genomic deletion, copy number neutral loss of heterozygosity, and association with specific cytogenetic subgroups. *Blood* **113**, 100-107, doi:10.1182/blood-2008-07-166801 (2009).
332 Holmes, R. & Zuniga-Pflucker, J. C. The OP9-DL1 system: generation of T-lymphocytes from embryonic or hematopoietic stem cells in vitro. *Cold Spring Harb Protoc* **2009**, pdb prot5156, doi:10.1101/pdb.prot5156 (2009).
333 Mohtashami, M., Shah, D. K., Kianizad, K., Awong, G. & Zuniga-Pflucker, J. C. Induction of T-cell development by Delta-like 4-expressing fibroblasts. *Int Immunol* **25**, 601-611, doi:10.1093/intimm/dxt027 (2013).
334 Weng, A. P. *et al.* Growth suppression of pre-T acute lymphoblastic leukemia cells by inhibition of notch signaling. *Mol Cell Biol* **23**, 655-664, doi:10.1128/MCB.23.2.655-664.2003 (2003).
335 Li, H. Aligning sequence reads, clone sequences and assembly contigs with BWA-MEM. doi:10.6084/M9.FIGSHARE.963153.V1 (2013).
336 Chen, X. *et al.* Manta: rapid detection of structural variants and indels for germline and cancer sequencing applications. *Bioinformatics* **32**, 1220-1222, doi:10.1093/bioinformatics/btv710 (2016).
337 Koboldt, D. C. *et al.* VarScan 2: somatic mutation and copy number alteration discovery in cancer by exome sequencing. *Genome Res* **22**, 568-576, doi:10.1101/gr.129684.111 (2012).
338 Kim, S. *et al.* Strelka2: fast and accurate calling of germline and somatic variants. *Nat Methods* **15**, 591-594, doi:10.1038/s41592-018-0051-x (2018).
339 Cibulskis, K. *et al.* Sensitive detection of somatic point mutations in impure and heterogeneous cancer samples. *Nat Biotechnol* **31**, 213-219, doi:10.1038/nbt.2514 (2013).
340 McLaren, W. *et al.* The Ensembl Variant Effect Predictor. *Genome Biol* **17**, 122, doi:10.1186/s13059-016-0974-4 (2016).
341 Talevich, E., Shain, A. H., Botton, T. & Bastian, B. C. CNVkit: Genome-Wide Copy Number Detection and Visualization from Targeted DNA Sequencing. *PLoS Comput Biol* **12**, e1004873, doi:10.1371/journal.pcbi.1004873 (2016).

342 Foulkes, W. D., Flanders, T. Y., Pollock, P. M. & Hayward, N. K. The CDKN2A (p16) gene and human cancer. *Mol Med* **3**, 5-20 (1997).
343 Sugimoto, M., Kuo, M. L., Roussel, M. F. & Sherr, C. J. Nucleolar Arf tumor suppressor inhibits ribosomal RNA processing. *Mol Cell* **11**, 415-424, doi:10.1016/s1097-2765(03)00057-1 (2003).
344 Brady, S. N., Yu, Y., Maggi, L. B., Jr. & Weber, J. D. ARF impedes NPM/B23 shuttling in an Mdm2-sensitive tumor suppressor pathway. *Mol Cell Biol* **24**, 9327-9338, doi:10.1128/MCB.24.21.9327-9338.2004 (2004).
345 Bachoo, R. M. *et al.* Epidermal growth factor receptor and Ink4a/Arf: convergent mechanisms governing terminal differentiation and transformation along the neural stem cell to astrocyte axis. *Cancer Cell* **1**, 269-277, doi:10.1016/s1535-6108(02)00046-6 (2002).
346 Randle, D. H., Zindy, F., Sherr, C. J. & Roussel, M. F. Differential effects of p19(Arf) and p16(Ink4a) loss on senescence of murine bone marrow-derived preB cells and macrophages. *Proc Natl Acad Sci U S A* **98**, 9654-9659, doi:10.1073/pnas.171217498 (2001).
347 Sachs, Z., Sharpless, N. E., DePinho, R. A. & Rosenberg, N. p16(Ink4a) interferes with Abelson virus transformation by enhancing apoptosis. *J Virol* **78**, 3304-3311, doi:10.1128/jvi.78.7.3304-3311.2004 (2004).
348 Fang, H. *et al.* Reducing INDEL calling errors in whole genome and exome sequencing data. *Genome Med* **6**, 89, doi:10.1186/s13073-014-0089-z (2014).